Flame retardancy of EVM-based polymers with low smoke emission

Présentée et soutenue publiquement à
L'UNIVERSITE LILLE 1 SCIENCES ET TECHNOLOGIES

pour obtenir le grade de
DOCTEUR
Spécialité : Molécules et Matière Condensée

par
Carmen Hoffendahl
Master of Science (Condensed Materials and Soft Matter), Universität Regensburg

Thèse dirigée par **Prof. Serge Bourbigot** et **Dr. Gaëlle Fontaine**

Soutenue le **11 Juillet 2014** devant la Commission d'Examen composée de :

Prof.	Sophie DUQUESNE	ENSCL	Président
Prof.	Manfred DÖRING	Fraunhofer-Institut Darmstadt	Rapporteur
Prof.	Richard HULL	University of Central Lancashire	Rapporteur
Mr.	Frank TASCHNER	LANXESS	Examinateur
Dr.	Martin MEZGER	LANXESS	Examinateur
Prof.	Serge BOURBIGOT	ENSCL	Directeur
Dr.	Gaëlle FONTAINE	ENSCL	Co-directrice

For Günter Hoffendahl

Acknowledgements

First, I would like to thank Prof. Alexandre Legris, head of the UMET laboratory, and Prof. Jean-Marc Lefebvre, leader of ISP group for welcoming me in their laboratory and for giving me the opportunity to carry out my PhD thesis in Lille. I extend my thanks to Mr. Bernard Fontaine, head of the Ecole Nationale Supérieure de Chimie de Lille (ENSCL), where the laboratory is located.

I would like to express my deepest appreciation to Serge, Sophie and Gaëlle who gave me the possibility to work with them and to pass my PhD thesis in the R_2Fire lab. Working with them was a great pleasure throughout the whole project. Their encouragement and faith in me helped me to progress. I appreciated their scientific knowledge, their suggestions and their availability, whenever it was needed.

I also want to acknowledge LANXESS for their financial support. Especially, I express my gratitude to Frank and Martin for their help and support as well as for answering all my questions during the last three years. Moreover, I would like to thank Pete and Uwe for help with processing of materials.

I am very grateful to Prof. Richard Hull and Prof. Manfred Döring, who accepted to be examiner for this PhD thesis and to bring their expertise to assess this manuscript.

Further, I would like to thank everyone in the lab for just being their selves and for the wonderful atmosphere in the lab: Anil, Andrea, Fabienne, Bastien, Ben, Brigitte, Fouad, Mathilde, Marion, Maude, Marianne, Michel, Nico L., Nico R., Girardini, Gwen, Pierre, Renaud, Séverine, Trang. Especially, I want knowledge three persons. First of all, Maryska who helped me a lot at the beginning of my life in France. Without her I would perhaps still live in a flat without water. Of course, I have to mention Pauline and Mathieu who enriched my everyday life in the last years. Thank you so much for this friendship and I hope we will pass a lot of wonderful moments together in future.

I have to name the persons being part of my life outside the lab, too. I gratefully thank Marion for being my best friend and for sharing all the good and bad moments since we met first over a decade ago. I extend my thanks to Käs for the great time we are spending

Table of contents

Abbreviations

ATH	Aluminum trihydroxide
APP	Ammonium polyphosphate
a.u.	Arbitrary units
CNT	Carbon nanotubes
$D_s i$	Maximum optical density
EAB	Elongation-at-break
EG	Expanded graphite
EVA	Ethylene vinyl acetate
EVM	Ethylene vinyl acetate (VA content 60 wt%)
LDH	Layered double hydroxides
LOI	Limiting oxygen index
MAPP	Microencapsulated ammonium polyphosphate
MB	Melamine borate
MDH	Magnesium dihydroxide
ML	Mass loss
MMT	Montmorillonite
MRP	Microencapsulated red phosphorus
MWCNT	Multiwalled carbon nanotubes
OD_{total}	Total optical denisty
PA6	Polyamide 6
PE	Polyether
PER	Pentaerythritol
pHRR	Peak of heat release rate
PVA	Polyvinyl acetate
PP	Polypropylene
RP	Red phosphorus
THR	Total heat release rate
TS	Tensile strength
TTI	Time to ignition
VA	Vinyl acetate

General Introduction

Polymers are quantitatively the most important products of the chemical industry used worldwide in everyday life. They are used in medicine, in textiles, for packaging, building industry etc. However, one of the main drawbacks of polymeric materials is their high flammability and it is necessary to flame retard materials for many of the named applications. In the last decade, it was already possible to decrease the total number of fire deaths thanks to concentrated use of fire retarded materials. The number of fire death was decreased from 4013 persons in 2001 to 3445 persons in 2010 in the USA [1]. Nevertheless, it is necessary to further improve the fire retardancy of polymeric materials to avoid a fire and/or to avoid fast propagation of fire in the goal to further decrease the number of fire deaths. At the same time, it is essential to reduce smoke release in case of fire. Indeed, about fifty percent of the fire casualties are due to smoke and gases produced in a fire.

This study deals with the fire retardancy and the smoke release of ethylene vinyl acetate (EVA), a copolymer made of ethylene and vinyl acetate. Possible variation of the vinyl acetate (VA) content in the polymer and the resulting control of the mechanical properties leads to a huge range of applications. EVA is used in electronic devices, electrical engineering, wire and cables, buildings, transportation (for example aircraft and cars), photovoltaics, shoe industry etc. Due to its huge range of applications, EVA is getting more important for research and industry in the last years. The increased demand of EVA is represented by the increasing number of patents dealing with EVA in the last six decades (**Figure 1**). It is found that the number of patents increase from 423 patents from 1950 to 1960 up to 14795 patents (between 2000 and 2010).
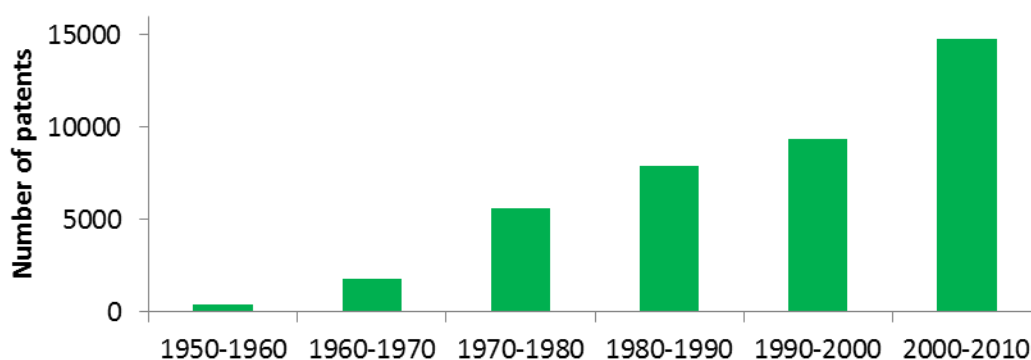
Figure 1: Patents containing the concept "Ethylene Vinyl Acetate"; Source: Scifinder 2012

As mentioned above, for many of the applications of EVA, high fire retardant properties are required. A commonly used method to improve the fire retardant properties of polymeric

materials is the incorporation of flame retardant additives into the polymeric matrix. As shown in **Figure 2**, the global flame retardant market in Asia-Pacific (47.7 %) is the largest, whereas the European market is the second largest one (25.2 %).
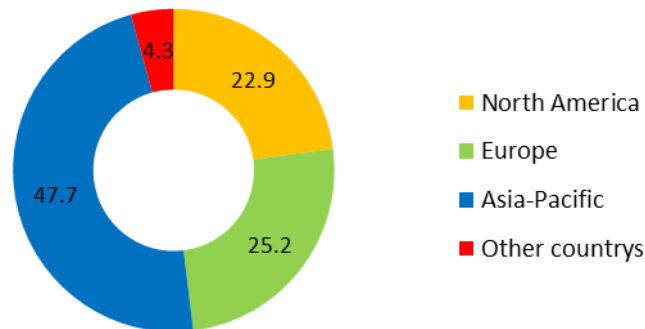
Figure 2: Global Flame retardant market in 2011 in [%] [2]

A flame retardant in general should meet different specifications: high fire retardant effect, low cost, good processability, low environmental impact and low toxicity. The complete set of those specifications is very challenging for research. This study is focused on the incorporation of additives in EVA to improve the fire retardant properties and to reduce smoke release when materials are exposed to fire. Here, in particular, the combination of mineral fillers with conventional flame retardants based on nitrogen and/or phosphorous is proposed. The EVA-polymer used in this study contains 60 wt% VA and has therefore elastomeric properties.

The PhD thesis is divided into five different chapters. The first chapter gives a general background about EVA, the fire retardancy and the smoke suppression in EVA materials. The dependence of material properties on the VA content, polymerization, vulcanization and thermal decomposition in thermo-oxidative and pyrolytic conditions is investigated. Then, the first chapter details a literature review of the mode of action of different classes of flame retardants as well as their effect in EVA. The last section gives a short overview of the development of smoke, the mode of action of smoke suppressants and their use in EVA.

The second chapter presents the materials used in this study. The polymer and flame retardant additives as well as the material preparation are described. Then, characterization methods will be presented. Tests to evaluate mechanical properties, fire retardancy and smoke release as well as experimental techniques to investigate the fire retardant mechanism and smoke release will be depicted.

The third chapter presents the screening of different additives in the polymeric matrix. The objective of this chapter is to find a material exhibiting acceptable mechanical properties, high fire retardancy and low smoke release. First, the best ratio of mineral filler and melamine as fire retardant additive is investigated. Afterwards, materials containing aluminum trihydroxide (ATH) in combination with phosphorous and/or melamine based additives is analyzed regarding mechanical properties, fire retardancy and smoke release.

Chapter four is dedicated to the investigation of the fire retardant mechanism of reference materials, i.e. EVM-ATH and EVM-ATH-MEL. Gas phase in pyrolytic and thermo-oxidative conditions as well as condensed phase mechanism is analyzed. Furthermore, dispersion of the additives and behavior of the materials versus hydrothermal aging is evaluated.

In chapter five, the role of melamine borate (MB) is investigated. At first, the decomposition mechanism of MB in pyrolytic and thermo-oxidative conditions is evaluated. Then, fire retardant mechanism of EVM-ATH-MB is investigated in the gas and condensed phase. Moreover, influence of vinyl acetate content of EVA materials containing combination of ATH and MB on mechanical properties, fire retardancy and smoke release is evaluated. After wards, a decomposition mechanism is proposed.

At the end of this work a general conclusion is given and proposal for future studies on this subject are made.

Chapter I: State of the Art

In research it is important to have a basic knowledge of the subject of the study. In this chapter, ethylene-vinyl acetate (EVA), the dependence of its physical properties on the vinyl acetate (VA) content, its polymerization and vulcanization reaction as well as its thermal decomposition is discussed in detail. Moreover, the mode of action of different classes of flame retardants and their use in EVA is described. At the end of this chapter, the formation of smoke, the mode of action of smoke suppressants and some examples of smoke suppressants used in EVA is presented.

1. Ethylene Vinyl Acetate Copolymer (EVA)

The first patent on ethylene vinyl acetate copolymer (EVA) was granted in 1938 [3]. It is a copolymer made through copolymerization of ethylene and vinyl acetate (VA). Its structure is presented in **Figure 3**. EVA-polymers can have, depending on the content of the monomers in the polymer, thermoplastic or elastomeric properties (**Table 1**). EVA copolymers with a VA content up to 40 % and from 80 to 100 % are thermoplastics (semi-crystalline), whereas EVA polymers having a VA content between 40 and 80 % are elastomers (rubber). In the so called "rubber region" the abbreviation EVM is often used instead of EVA [4]. Concerning the monomers themselves, it is found that polyethylene (PE) and polyvinyl acetate (PVA) are both thermoplastics.
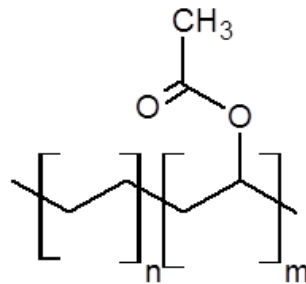
Figure 3: Structure of EVA copolymer

Table 1: Schematic classification of ethylene vinyl acetate copolymers according to their VA content

Thermoplastic EVA				Elastomers (EVM)				Thermoplastic EVA	
10	20	30	40	50	60	70	80	90	100

VA content [%]

1.1. Change of material properties with the vinyl acetate content

It is well known that the physical properties of EVA depend on the VA content in the material [5, 6]. **Table 2** summarizes the change of the physical properties with increasing VA content. It is seen that transparency, flexibility, density, glass transition temperature, weather resistance, stickiness and the filler acceptance of the EVA material increase with increasing VA content. On the other side, hardness, stiffness, melting point, chemical resistance, yield stress, stability of shape and crystallinity decrease with increasing VA content.

Table 2: Change of physical properties with increasing VA content in EVA [7]

Increase	Decrease
Transparence	Hardness
Glass transition temperature	Stiffness
Flexibility	Melting point
Density	Chemical persistence
Weather resistance	Yield stress
Stickiness	Stability of shape in warmth
Polarity	Crystallinity

The changes of the glass transition temperature, the melting point and the crystallinity as a function of the VA content in the polymer are illustrated in **Figure 4**. As it can be seen, the glass transition temperature changes from nearly -40 °C for EVA having 20 % VA to around 28 °C for pure polyvinyl acetate (PVA). In the case of the melting point, a decrease from 85 °C (20 % VA) to 10 °C (50 % VA) is observed. The crystallinity decreases from around 30 % (20 % VA) to around 7 % for EVA containing 50 % VA. Further, increasing VA content leads to increased polarity but lower crystallinity [8]. The increasing polarity with increasing VA content is useful in imparting a high degree of polymer-filler surface interaction, which is very important for polymer composites with high filler loading.
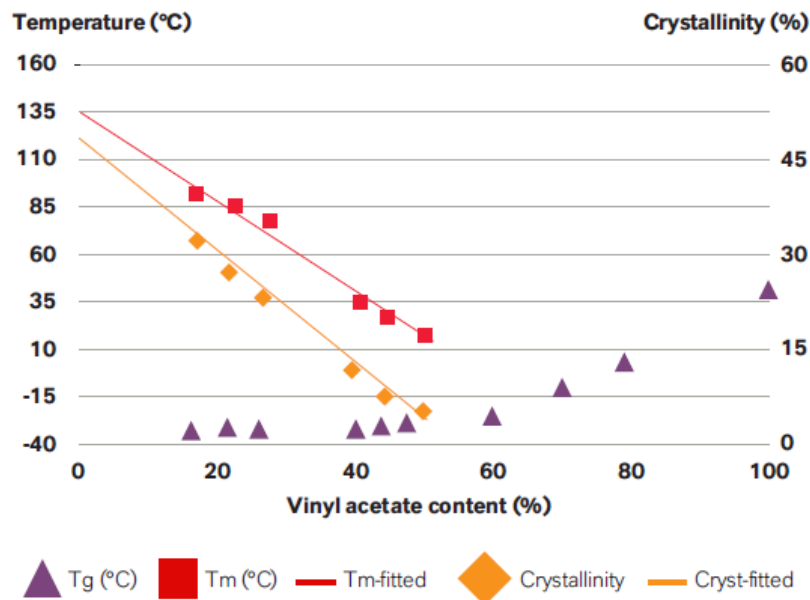
Figure 4: Influence of the VA content in Levapren (EVA polymer) on thermophysical properties and morphology [9]

1.2. Polymerization

The copolymerization of EVA was first described by Perrin in 1940 [10]. Since that date, a lot of patents concerning the polymerization of EVA can be found in literature [11-15]. Generally, EVA is obtained via radical copolymerization of ethylene and vinyl acetate (**Figure 5**). The polymerization is initiated by e.g. azocompounds or high energy radiation. The reaction can be carried out in every ratio of the comonomers as the reactivity ratios are close to 1 [4]. As a consequence the distribution of the comonomers in the chain is random. One occurring problem of the polymerization reaction is the low water solubility of ethylene (3.5 mg/100 mL at 17 °C). Vinyl acetate on the contrary has a better one (2 g/100 mL at 20 °C). Another solvent than water is therefore necessary for the polymerization reaction of EVA. Toluene, benzene, heptane or *tert*-butanol are often used as solvents instead of water. Commonly the polymerization reaction is catalyzed using e.g. trialkylaluminum-Lewis base-peroxide mixture [16] or a tenary catalyst consisting of equimolar amounts of $AlEt_3$, $ZnCl_2$ and CCl_4 [17].

ethylene   vinyl acetate   ethylene vinyl acetate
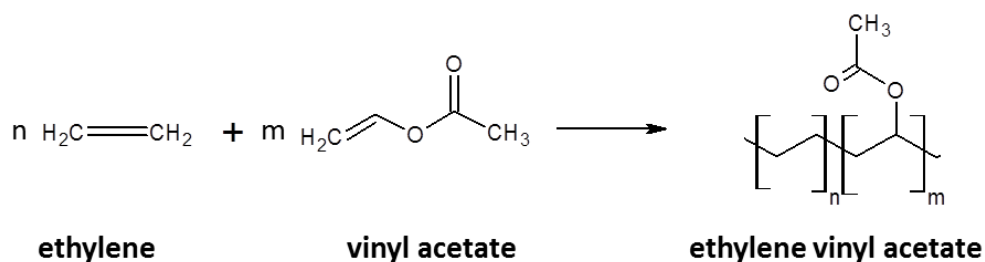
Figure 5: Copolymerization of ethylene and vinyl acetate

Three different methods for the polymerization of EVA are known (**Table 3**) [4, 18]: the high pressure method, the solution and the emulsion process. The choice of the method depends on the desired VA content in the polymer. EVA-materials having a low VA content (0 – 45 %) are made using the high pressure method. The solution process is applied on the production of EVA polymers having VA contents between 30 and 100 %. Materials with a VA content between 45 and 100 % are produced using the emulsion process. The high pressure method is carried out in bulk at a pressure between 1000 and 3000 bars and temperatures between 150 and 350 °C. The maximum molecular weight obtained using this method is relatively low due to high chain transfer activity of the vinyl acetate which limits the VA content in the polymer. The limited molecular weight using the high pressure method can be overcome by using the solution process. Often *tert*-butanol is used due to its low chain terminating

properties. The solution process is carried out under medium pressure and temperatures between 50 and 120 °C. An example for the solution method is the polymerization of ethylene and vinyl acetate in *tert*-butanol at around 34 bars at 62 °C [19]. The disadvantage of the solution process is the high amount of solvent that is required. The third method is the emulsion process. The used pressure is between 1 and 200 bars, whereas the temperature lies between 30 and 70 °C. The emulsion polymerization is carried out in water containing a surfactant. The water soluble radical initiator initiates the polymerization of the monomers whereas the polymerization reaction takes mainly place in the micelles. An example for the polymerization of EVA using the emulsion process is given by Schork et al. [20]. They polymerized EVA using miniemulsions. The advantage of miniemulsions is that the monomer transport through the water phase is not relevant (in comparison to the emulsion polymerization) and ethylene can be effectively incorporated in the micelles. In general, the emulsion process is rarely used in the rubber industry, but rather used in the case of thermoplastic applications as impact modifier.

Table 3: Overview of the different methods for the polymerization of EVA

		Solution process 200 – 1000 bar 50- 120 °C						
			Emulsion process 1 – 200 bar 30 – 70 °C					
High pressure method 1000 – 3000 bar 150 – 350 °C								
10	20	30	40	50	60	70	80	90	100

VA content [%]

1.3. Vulcanization

The first commercial method for vulcanization of natural rubber is attributed to Charles Goodyear who vulcanized natural rubber with sulfur in 1841. In the case of EVA, no sulfur-curable sites are present in the polymer structure which leads to the fact that EVA is vulcanized radically with peroxides or high energy radiation [21]. Crosslinking with peroxides was first performed by Ostromyslenski [22] for natural rubbers. However, there was little interest in peroxide crosslinking until the early 1970s. Generally, vulcanization is used in

rubber industry to make materials more resistant against physical and chemical impact. Therefore, curing is only relevant for rubber like EVA, the so-called EVM, having a VA content between 40 and 80 %. During the vulcanization process, chemical crosslinks connecting the polymer chains are formed (*Figure 6*) which leads to increased elasticity and decreased plasticity [23]. The mechanism of the vulcanization reaction starts with abstraction of a hydrogen atom by the peroxy radical from the polymer chain leading to the formation of a reactive radical chain [24]. Then, two radical polymeric chains can combine forming an irregular network. A more regular network can be formed using activators such as triallylcyanurate or triallyisocanurate. The radical polymer chains are transferred to the activator. The crosslink network is then formed from the transferred radical to another chain. In general the recommended quantities of peroxide and activator are between 2-7 phr for the peroxide and between 0.5 to 5 phr in the case of the activator [4]. It has to be noted that the vulcanization process does not change the original shape of the material. One of the main drawbacks of peroxides is their instability and the therefore resulting storage problems. Moreover, peroxides have to decompose fast at the used curing temperature. To overcome those problems, peroxides containing tertiary carbon atoms are used nowadays, because peroxy groups bonded to primary and secondary carbon atoms are less stable. In general, symmetrical and asymmetrical peroxides are used as curing agents [25].
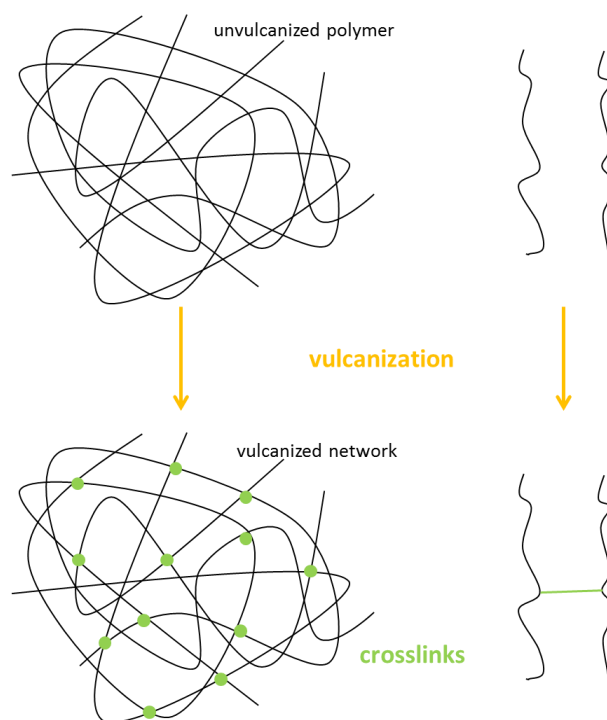
Figure 6: Network formation during vulcanization of rubbers

1.4. Thermal decomposition

The thermal decomposition of EVA is already well reported in literature [26-32]. As in the case of the physical properties, the thermal decomposition of EVA depends on the VA content in the polymer. The pyrolytic and thermo-oxidative decomposition of EVA is discussed in detail in the following part.

1.4.1. Pyrolytic decomposition

The pyrolytic decomposition of EVA is a two steps process for all grades of EVA (**Figure 7**). The first pyrolysis step occurs between 300 and 400 °C. In this temperature range, the decomposition starts with some chain scission reactions, corresponding to the cleavage of the bridged acetate groups that present the weakest cross-linking bonds (**Figure 8**) [26]. At the same time the deacetylation of the polymer takes place.
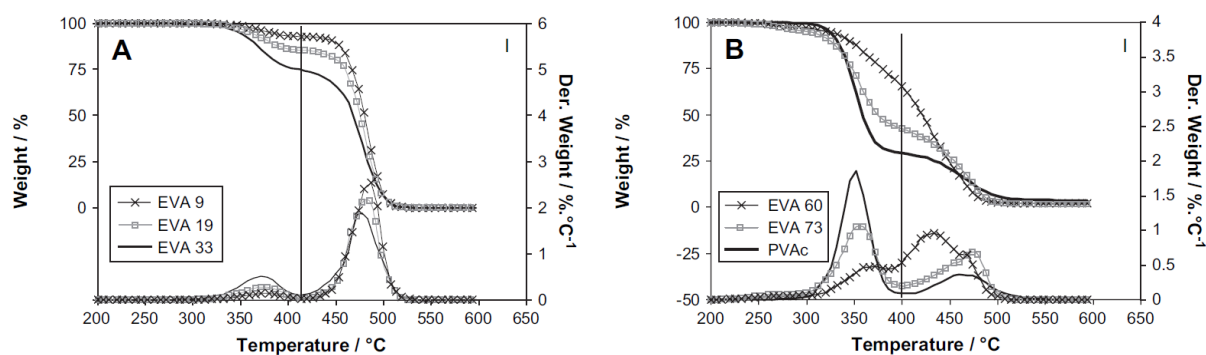
Figure 7: TGA curves of EVA polymers containing different VA content: 9, 13, 33 (A), 60, 73,100 (B), nitrogen, 20°C/min [27]

The deacetylation occurs through the β-elimination of the vinyl acetate groups of the polymer and leads to a polyene network [33]. During this step, acetic acid is evolved. If two or more VA monomer units undergo the deacetylation process, an autocatalytic effect is observed. The autocatalytic effect of the deacetylation increases with increasing VA content. The deacetylation reactions are catalyzed by the conjugation of the π-system of the double bond formed by deacetylation [34]. At the end of the first decomposition step, a polyene network remains which is then completely decomposed into unsaturated and aromatic compounds in the second decomposition step taking place from 400 to 500 °C. It has to be noted that the formation of aromatic products becomes more important than the formation of aliphatic ones with increasing VA content in the polymer.
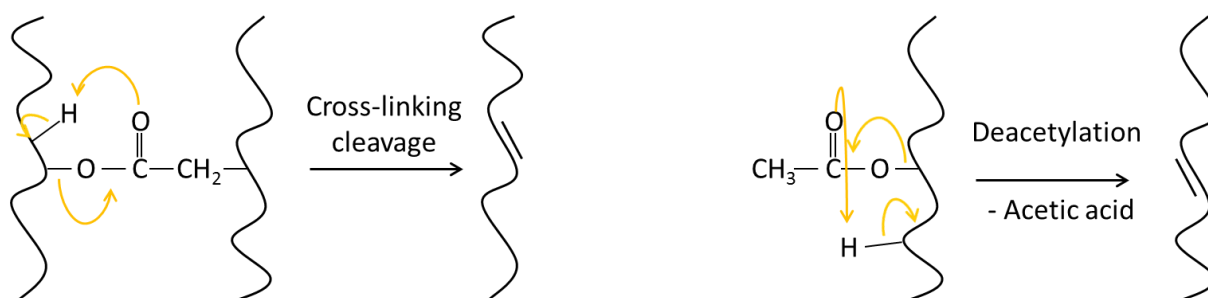
Figure 8: Schematic presentation of the cross-linking bond cleavage and deacetylation of the polymer

The pyrolysis of unvulcanized and vulcanized rubber like EVA (EVM, 60 wt% VA) is similar (**Figure 9**), even if the weight loss of vulcanized EVM is slightly less important than that of pure EVM. A small amount of char is left after the decomposition of vulcanized EVM, whereas unvulcanized EVM is fully degraded. This is explained by the fact that the crosslinks in the cured system favor the condensation of carbonaceous species and thus the formation of an aromatic charred structure.

Figure 9: TG curves for pure (unvulcanized) and vulcanized EVM and the corresponding DTG curve of vulcanized EVM, nitrogen, 10 °C/min [26]

The schematic presentation of the pyrolysis of vulcanized EVM is presented in **Figure 10**. The deacetylation takes place from 300 to 375 °C. Up to 450 °C, aliphatic carbonaceous species are evolved and unsaturated compounds are formed. From 400 to 500 °C some aromatization of the residue occurs, leading to a residue made of unsaturated and aromatic compounds.
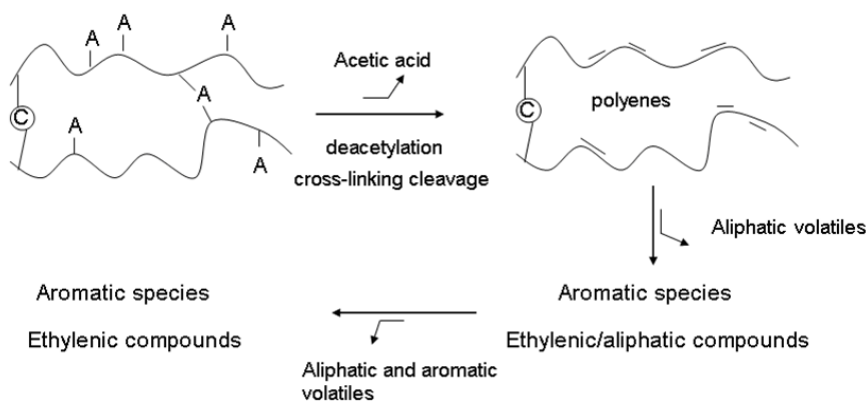
Figure 10: pyrolytic decomposition of EVM; (A = acetate, C = cross-linking) [26]

1.4.2. Thermo-oxidative decomposition

Under oxidative conditions (**Figure 11**), the decomposition of EVA with a VA content lower than 60 % (semi-crystalline EVA) is a two-step process, whereas for higher VA content (rubber like EVA, (B)), three steps are observed.
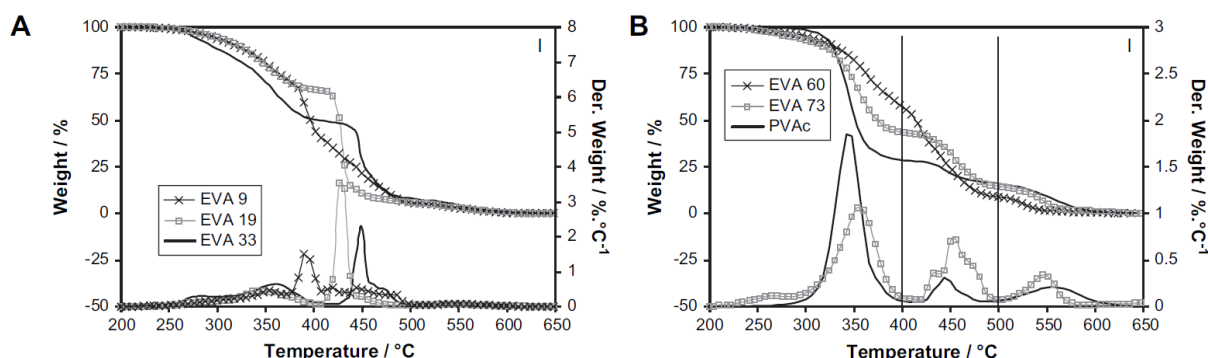
Figure 11: TGA curves of EVA polymers containing different contents of VA: 9, 19, 33 (A), 60, 73,100 (B), air, 20°C/min [27]

The first decomposition step in both cases occurs between 300 and 400 °C, as found in pyrolytic conditions. This step is attributed to the deacetylation of the polymer. At the end of the first decomposition step, a highly unsaturated residue or polyene is obtained. The second step of decomposition takes place between 400 and 550 °C. The polyene residue formed in the first decomposition step is degraded by chain scissions. These reactions lead to the formation of a carbonaceous char in the case of rubber like EVA, whereas for semi-crystalline EVA, a stabilized aromatic structure or char is not formed. The third decomposition step of rubber like EVA is obtained at temperature higher than 500 °C. During this step, the formed char oxidizes forming aliphatic and aromatic volatiles. Moreover,

carbon dioxide and water are released. It shows therefore that oxygen plays an important role in the thermo-oxidative decomposition of EVA.

The comparison of the thermo-oxidative decomposition of unvulcanized, rubber like EVM (EVM, 60 % VA) and vulcanized, rubber like EVM shows that the thermo-oxidative decomposition of the vulcanized polymer is more complex than that of the unvulcanized EVM (**Figure 12**). Vulcanized EVM degrades following a five step process. The first decomposition step is observed from 200 to 220 °C having a small weight loss of 6 wt%. The second occurs between 220 and 305 °C and the third decomposition step from 305 to 405 °C. Up to 300 °C, deacetylation of the polymer is completed leading to the formation of a polyene network which decomposes up to 350 °C. The fourth decomposition step occurs from 405 – 455 °C and the fifth one up to 525 °C. These steps correspond to the decomposition of the char layer formed before evolving carbon dioxide, aliphatic and/or ethylenic products. The schematic presentation of the five-step, thermo-oxidative decomposition of rubber like EVM is presented in **Figure 13**.
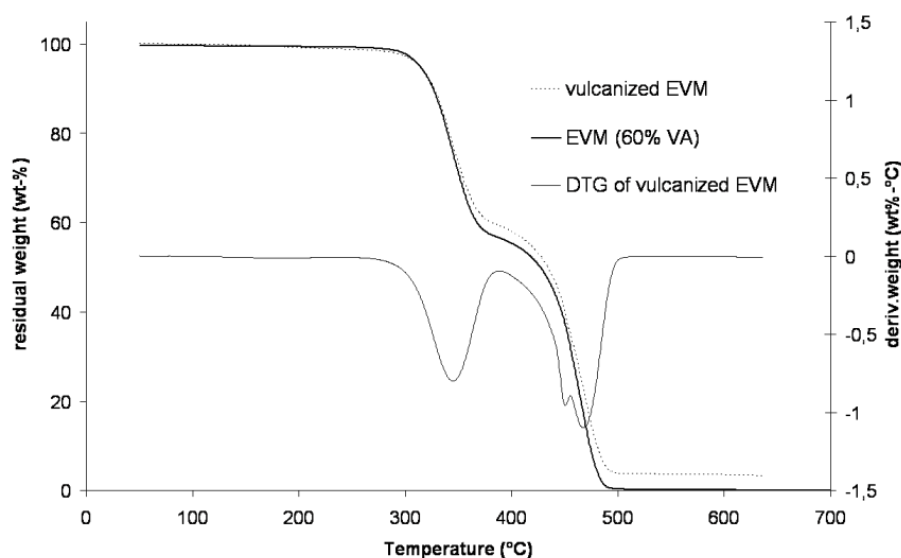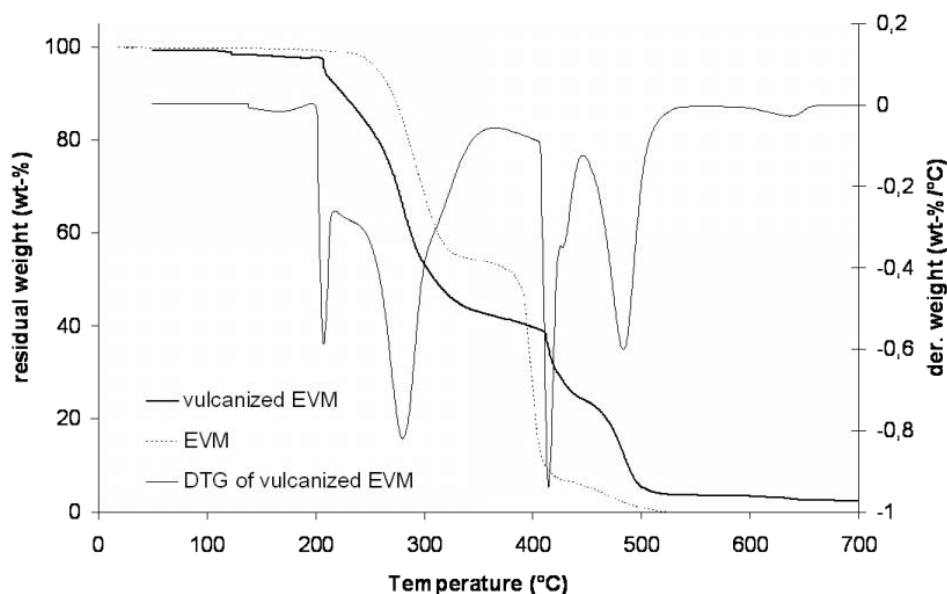

Figure 12: TG curves of pure EVM and vulcanized EVM and the corresponding DTG curve of vulcanized EVM, air, 10 °C/min [26]
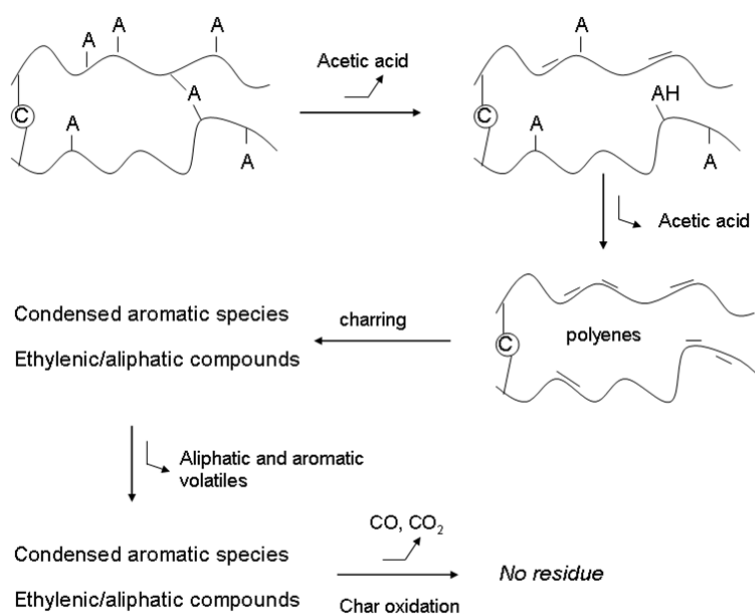
Figure 13: Thermo-oxidative decomposition scheme of vulcanized EVA (A = acetate, C = cross-linking) [26]

1.5. Conclusion

In this part, it was seen that the main advantage of EVA materials is the adaptability of desired mechanical properties and the thermal decomposition thanks to variation of the VA content in the polymer. Polymerization process was shown to be varied mainly in temperature and pressure to obtain the desired VA grade. Moreover, it is possible to vulcanize EVA materials increasing especially thermal and mechanical stability of the materials.

The next part is dedicated to the fire retardancy of EVA and the different types of additives used to enhance fire retardant properties when submitted to fire.

2. Flame retardancy of EVA

As it was already mentioned above, EVA-materials have a huge range of application; they are used for cables, flooring, solar cells, sporting goods, packaging, as insulating materials and as adhesives. For many of these applications, it is important that EVA-materials perform high fire retardancy. Previously, it was demonstrated that physical properties and thermal decomposition of EVA depend on the VA content of the polymer. The same is observed for fire retardancy of EVA. As an example, it is known that the limiting oxygen index (LOI) of EVA increases with increasing VA content. For EVA containing 190 phr of aluminum trihydroxide (ATH) (**Figure 14**) it is observed that LOI increases from 36 vol%O_2 for EVA having 40 % VA to 50 vol%O_2 for the EVA material having a vinyl acetate content of 80 %.
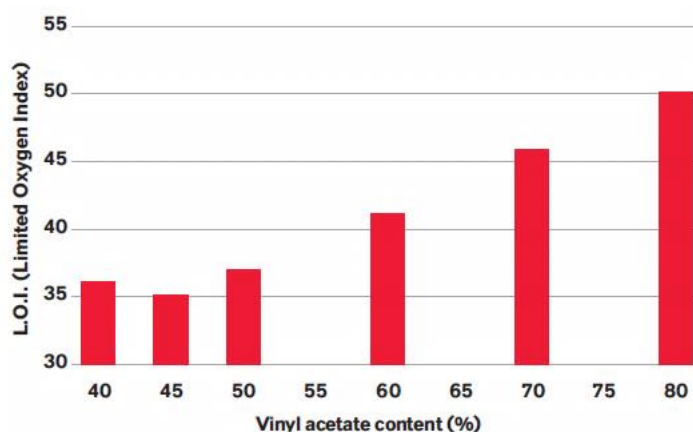
Figure 14: Dependence of the LOI values on the VA content on formulations containing EVA and ATH (190 phr) [9]

Besides ATH, a mineral filler, other flame retardant additives are used as fire retardant in EVA: halogenated compounds, mineral fillers, phosphorus and nitrogen compounds, silicone additives, nanoadditives and combinations of the different flame retardants. In this part, the mode of action of the different fire retardant additives as well as their use in EVA is discussed. The EVA grade used in this study contains 60 wt% VA (EVM). Due to the fact that flame retardancy of EVM, i.e. elastomeric ethylene vinyl acetate, is not well reported in literature [35-40], the discussion hereafter also includes literature regarding EVA materials having low acetate content (18 - 40 % VA).

2.1.   What is fire retardancy?

When materials are submitted to an external heat source (fire), they start to decompose. To inhibit the combustion process of polymeric materials against the attack of fire, various methods are possible. One possibility is the chemical modification of the polymer itself. For example, it is possible to copolymerize the flame retardant with the polymer monomers [41, 42]. The flame retardant additive is then directly present in the polymeric chain. Another possibility is the use of inherently flame retardant polymers, e.g. poly(tetrafluoroethylene) or polyimides [43, 44]. It is also possible to protect polymeric materials against fire using a surface coating [45-48]. The application of a coating has the advantage that the material itself is not modified; the coating protects the material against the influence of the external heat source. The last possibility to protect polymers against the attack of fire is the incorporation of flame retardants into the polymer during its processing (e.g. extrusion). Due to the fact that this study is focused on the direct incorporation of the flame retardant into the polymer, the state of the art is focused on this method. Consequently, the other methods are not further discussed.

In general, fire retardant additives can have a physical and/or chemical mode of action in the gas and/or condensed phase. The physical action takes place through formation of a protective layer, by cooling and/or by dilution. In the first case, a protective layer with a low thermal conductivity is formed when the material is submitted to an external heat source and protects the material through reduction of the heat and mass transfer between the external heat source and the material. Materials can also be protected by cooling through the endothermically decomposition of fire retardant additives (usually dehydration) leading to a decrease in temperature by absorbing the external heat. The protection by dilution takes place through the addition of compounds releasing inert gases, such as carbon dioxide or water, upon decomposition. These additives dilute the fuel in the solid and in the gaseous phase and thus lower the concentration of combustible gases in the surrounding atmosphere.

The other possibility by which materials can be protected is the chemical mode of action which takes place in the condensed and/or gas phase. In the condensed phase, two types of reactions can occur. First, the formation of a carbon layer (charring) on the polymer surface

limiting the volatilization of the fuel. It also limits oxygen diffusion and insulates the polymer underneath from the external heat. The second possibility is the acceleration of the polymer decomposition which causes a pronounced flow of the polymer and, hence, a withdrawal from the sphere of influence of the flame that breaks away. The chemical mode of action of flame retardants in the gas phase takes place through interruption of the radical mechanism of the combustion process by flame retardants or by their decomposition products. As a result, the exothermic processes that occur in the flame are stopped and the system cools down. Consequential, the supply of flammable gases is reduced or even completely suppressed.

It is possible that fire retardants (e.g. aluminum hydroxide and magnesium hydroxide) show exclusively a physical mode of action, but flame retardants acting exclusively through a chemical mode of action are rare. Chemical mechanisms are often accompanied by one or several physical mechanisms, most commonly endothermic dissociation or dilution of fuel. Charring is the most common condensed phase mechanism [49, 50].

2.2.   Halogenated compounds

The effectiveness of halogen containing flame retardants increases in the following order F < Cl < Br < I. Iodine and fluorine containing flame retardants are not used. Iodine compounds, on the one hand are too expensive and on the other hand the I-C bond is too weak and therefore the compounds are relatively unstable against heat and light. Fluorine containing compounds are ineffective as flame retardants due to its breakdown product (HF) which is too stable to interfere in the flame. Nevertheless, fluorine plays an important role in flame retardancy. For example, it is used in non-combustible fluoropolymers like e.g. Teflon (poly(tetrafluorethylene)) and FEP (fluorine containing elastomer). The most effective halogen containing flame retardants are those containing bromine and then chlorine. Brominated fire retardants are classified in two classes: aliphatic and aromatic compounds. The aliphatic ones are known to be more effective, because they are easier to break down than the aromatic ones. In the case of chlorine, chlorinated hydrocarbons or chlorinated cycloaliphatics are used as flame retardants which is due to their high light stability. Often antimony oxide is used as synergist for halogen containing flame retardants. The presence of

antimony oxide and halogenated compounds leads to the formation of antimony trihalide which acts in the gas phase as flame-quenching compound [51, 52].

2.2.1. Mode of action

Halogen containing flame retardants act in general by interfering in the radical chain reaction that takes place in the gas phase. The flame retardant (RX) breaks down in the flame (**Equation 1**) and the halogen radical (X$^\bullet$) reacts with the polymeric chain to form the hydrogen halide (HX) that is used to trap the high-energy radicals (H$^\bullet$ and OH$^\bullet$) present in the flame (**Equation 2**).

$$RX \quad \rightarrow R^\bullet + X^\bullet$$

Equation 1: Break down of the flame retardant

$$X^\bullet + RH \rightarrow R^\bullet + HX$$

$$HX + H^\bullet \rightarrow H_2 + X^\bullet$$

$$HX + OH^\bullet \rightarrow H_2O + X^\bullet$$
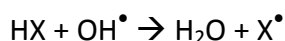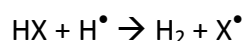
Equation 2: Reaction of HX with high-energy OH and H radicals; X = Cl or Br, R = polymer chain

Regarding the effectiveness of the hydrogen halides, it appears that hydrogen bromide (HBr) has a higher fire retardant effect than hydrogen chloride (HCl). HBr is evolved over a narrow temperature range at high concentrations. HCl instead is evolved over a wider temperature range. Consequently, a lower concentration is available in the flame zone. Moreover, higher quantities of chlorine compounds are required to reach the same fire retardant effect as bromine containing compounds [51].

2.2.2. Halogenated flame retardants in EVA

There is not a lot reported in literature about halogenated flame retardants in EVA. Yang et al. [53] investigated the influence of tetrabromo-*p*-cresol and pentabromophenol on the flame retardancy of EVA. The incorporation of decabromodiphenyl oxide (35 phr) in combination with antimony oxide as synergist shows a good fire retardant effect [52]. V-0 classification was reached in EVA with a VA content of 18%,. To get the same effect in EVA having a VA content of 28%, a loading of only 30 phr was required. It can therefore be

concluded that the higher the VA content in the polymer, the lower the amount of flame retardant is needed to reach the same fire retardant properties.

2.3.   Mineral fillers

The second class of fire retardants is mineral fillers. In general, mineral fillers such as aluminum hydroxide (ATH) or magnesium hydroxide (MDH) are widely used as fire retardant additives in EVA. To achieve good fire retardant properties, high loadings (higher than 50 wt%) are required. However, high loadings drastically change the mechanical properties of the material [54, 55]. To overcome this disadvantage, several solutions are possible. The surface of the mineral fillers can be treated to improve lack of mechanical properties. Another possibility is the use of processing aids which change mechanical properties of the material. Finally, the combination of mineral fillers with other conventional flame retardants to develop synergist effects can also be investigated.

2.3.1.   Mode of action

Mineral fillers have three different fire retardant effects, which can occur alone or in combination [56].

1. They decompose endothermically and so absorb heat. This phenomenon leads to a "cooling effect", which cools down the surrounding polymer.
2. Mineral fillers generally release inert gases during the combustion process. These gases, e.g. water or carbon dioxide dilute the fuel and thus reduce the concentration of the flammable gases.
3. They built an inert protective layer at the surface of the decomposing polymer and thus protect the material from the external heat. Moreover, this layer acts as barrier preventing the diffusion of gases and heat from the material to the fuel and otherwise.

Hull et al. [56] estimated the contribution of those different effects for various mineral fillers determining the heat absorption due to the filler, the residue, the evolved gas, i.e. water and carbon dioxide, and to the endotherm decomposition (**Figure 15**). It is seen that for the studied mineral fillers most of the energy is absorbed by endotherm decomposition

reactions. The following discussion on the contribution of the mineral to heat absorption and its decomposition reaction is focused on ATH and MDH due to the fact that these two fillers are the most common ones. It can be seen that for ATH the heat capacity absorbed by the condensed phase (filler) is smaller than that absorbed by the gas phase. In the case of MDH instead, the opposite is observed: the filler absorbs more energy than the gas phase. Moreover, the absorbed energy by the filler is two times greater for MDH than for ATH. **Table 4** presents additional information about ATH and MDH: chemical composition, decomposition temperature, standard enthalpy of dehydration, decomposition reaction and the remaining residue at 800 °C. Both mineral fillers decompose forming the corresponding oxide through the release of water. MDH decomposes at around 300 °C whereas ATH decomposes at around 200 °C. Moreover, MDH has a slightly higher enthalpy of dehydration (1202 J/g)) than ATH (1190 J/g) and thus can absorb more heat during the combustion process.
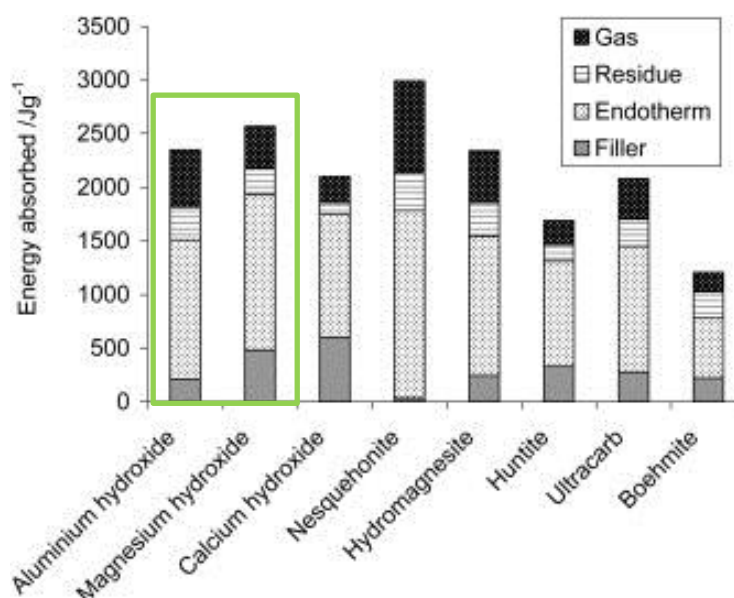
Figure 15: Comparison of the absorbed energy of different mineral fillers [56]

Table 4: Comparison of ATH and MDH characteristic data

	ATH	MDH
Formula	$Al(OH)_3$	$Mg(OH)_2$
Decomposition temperature [°C]	180-200	300-320
Enthalpy [J/g]	1190	1202
Decomposition reaction	$Al(OH)_3$ (s)$\rightarrow$ Al_2O_3 (s) + 3 H_2O (g)	$Mg(OH)_2$ (s)$\rightarrow$ MgO (s) + H_2O (g)
Residue at 800 °C [%]	65	69

2.3.2. Mineral fillers in EVA

2.3.2.1.   Mineral fillers used as fire retardants in EVA

The most commonly used mineral fillers in EVA are ATH and MDH due to low cost of the additives. The incorporation of hydrotalcite ($Mg_6Al_2(OH)_{16}(CO_3)*4H_2O$ is also widely reported [54, 57], leading to better fire retardant properties of EVA materials (higher LOI and lower pHRR) than the incorporation of ATH or MDH. Basfar et al. [58] compared EVA-materials containing MDH or huntite hydromagnesite ($Mg_3(Ca(CO_3)_4)$) at different ratios. It was found that both mineral filler have comparable fire retardant effects in EVA. Moreover, the influence of polymer cross-linking (dicumyl peroxide) was investigated demonstrating that cross-linked samples possess lower fire retardancy than uncross-linked samples. Morgan et al. [59] compared the fire retardancy of materials containing EVA and different magnesium carbonates. It was found that at a loading of 50 wt% only the material containing hydromagnesite reached comparable results in cone calorimetry like the material containing MDH. Laoutid et al. [60] compared fire retardant properties of EVA containing hydrated lime ($Ca(OH)_2$) or MDH. The materials containing 60 wt% of hydrated lime had better reduction in pHRR than the material containing the same quantity of MDH, whereas the lime containing material ignited at shorter time. Moreover, it was shown that the use of semi hydrated dolime, which is a sort of combination of lime and MDH, as fire retardant combined the lower pHRR of lime and the higher TTI of MDH, whereas char residues were less cohesive.

It is known that fire retardant properties as well as smoke release of EVA depend on the nature of the incorporated mineral filler such as particle size, morphology or surface treatment of the additive. Those effects are investigated in the following. Moreover, synergism of different mineral fillers with conventional fire retardants is discussed.

2.3.2.2.   Effect of the particle size of mineral fillers

It is reported that material properties depend on the particle size of the mineral filler. For example, Huang et al. [61] showed that the fire retardancy and mechanical properties of EVA-materials containing MDH depend on the particle size and on the loading of the filler. Three different particles sizes were used. EVA-materials containing 55 wt% of filler are evaluated in terms of fire retardancy and mechanical properties. It was found that best

enhancement of flame retardant properties was achieved for the material containing the smallest particles. LOI is 37.7 vol%O_2 for the material containing the largest particles and 34.6 vol%O_2 for that with the smallest MDH particles. Regarding the mechanical properties it was found that the highest tensile strength (13.1 MPa) and the highest elongation-at-break (124 %) were found for the material containing MDH particles of medium size. Moreover, it was shown that the effect of the particle size of MDH is less important when filler loading (35 and 45 wt% MDH) decreases or increases (75 wt%). Another study on the effect of the particle size of mineral fillers (ATH and MDH) on material properties of EVA was published by Camino et al. [62]. It was demonstrated that with decreasing MDH particle size, the LOI value decreases. In the case of ATH instead, smaller particles led to a slightly increase in LOI. Concerning mechanical properties, it was found that elongation-at-break and tensile strength decrease with decreasing particle size of both fillers. Férnandez et al. [63] reported the fire retardancy of MDH with a particle size of above 200 µm. The addition of 60 wt% MDH to EVA enhanced the fire retardant properties. The comparison with an EVA material containing MDH showed that the materials containing the smaller MDH particles had better fire retardant properties than those with the bigger particles. Moreover, it is reported that the incorporation of nano-MDH shows better fire retardant properties than micro-MDH [61, 64]. Jiao et al. [65] compared the fire retardant properties for materials containing nano-MDH or nano-hydrotalcite. They observed that the fire retardancy increased with increasing filler content, whereas the materials containing nano-hydrotalcite showed better fire retardant properties (obtained by cone calorimetry and UL-94 test) than the materials containing nano-MDH. V-0 classification was only reached for the material containing 150 phr of nano-hydrotalcite. Another study [60] showed the dependence of the particle size of hydrated lime (Ca(OH)$_2$) on mechanical and fire retardant properties. It was found that with increasing particle size, stress-at-break and pHRR increases.

In summary, a general tendency of the effect of the particle size of mineral fillers on fire retardant properties on EVA materials is controversy. Generally, dispersion of additives in the polymeric matrix is known to play an important role on mechanical as well as fire retardant properties. However, dispersion of the additives is rarely discussed in context with the effect of particle size on material properties. Especially in the case of additives having a small particle size, agglomeration has to be taken into account.

2.3.2.3.   Modification of mineral fillers

Besides the effect of the particle size of mineral fillers on fire retardancy and mechanical properties, the surface treatment of the additives plays an important role concerning material properties. It was found that the use of coated metal hydroxides leads to a further improvement of the flammability properties in comparison to the uncoated filler.

The incorporation of zinc hydroxystannate ($Zn[Sn(OH)_6]$,ZHS) coated ATH and MDH into EVA led to improved fire retardant properties in comparison to the material containing the uncoated filler [66]. It has to be noted, that in this study, the incorporation of ATH showed better fire retardant results than the incorporation of MDH. Moreover, smoke production during combustion was decreased from 210 MW/kg for the virgin polymer to 27 MW/kg for the material containing 50 wt% of the coated ATH and to 40 a.u. for that containing 50 wt% of the coated MDH. Haurie et al. [67] incorporated hydromagnesite ($MgO_4CO_2*5H_2O$) coated with stearic acid into a LDPE/EVA blend, which lead to improved fire retardancy of the materials. Moreover, elongation-at-break, tensile strength and hardness Shore D were also improved.

2.3.2.4.   Layered double hydroxides as mineral fillers in EVA

In addition to the previously described mineral fillers and to their combinations with conventional flame retardants, it is also possible to enhance fire retardancy of EVA using positively charged layered double hydroxides (LDH). The modification of LDH with a phosphorous-nitrogen compound, PAHPA (N-(2-(5,5-dimethyl-1,3,2-dioxaphosphinyl-2-ylamino)-hexylacetamine-2-propyl acid) [68], nickel containing compounds [69-71], rare earth ions (La, Ce, Nd) [72] or boric anions [73] led, when incorporated in EVA, to improved thermal stability and fire retardant properties in comparison to the virgin polymer. Further the intercalation of phosphonates into LDH [74] or into hydrocalcite [75, 76] enhanced the fire retardant properties of EVA. In the case of LDH, pHRR was decreased from 1680 kW/m² for the virgin polymer to 669 kW/m², whereas TTI was decreased from 65 s to 29 s. At the opposite, the use of α-zirconium phosphonate nanoparticles in LDH did not lead to a significant improvement of the fire retardancy of EVA [77]. The comparison of nano-LDH with nano-MDH showed that nano-LDH in EVA improves the fire retardant properties more than nano-MDH alone in EVA [65, 78]. Regarding the mechanical properties of EVA

containing nano-MDH or nano-LDH, it appeared that the elongation-at-break and the tensile strength for all tested materials was lower than for the virgin polymer. Moreover slight synergistic effects for LDH were detected when hyperfine MDH is additionally present in the polymeric matrix [79]. Li et al. [80] investigated the fire retardancy, smoke release and thermal decomposition of EVA materials containing LDH in combination with melamine (MEL). It was demonstrated that a ratio of LDH:MEL of 9:1 exhibits the best fire retardant properties (investigated using cone calorimeter, LOI and UL-94), lowest smoke release and best thermal stability. A lower or higher content of MEL in the matrix leads to worse material properties. The effect of the MEL content on material properties was explained by the char formed during burning; the char for the best formulation is more cohesive than the others.

2.3.2.5. Combination of mineral fillers with other flame retardant additives

Like it was mentioned before, it is possible to combine mineral fillers with conventional flame retardants. In the case of ATH, a synergistic effect was found for its combination with Fe-montmorillonite (Fe-MMT) [81] and organomodified MMT [82], as well as for zinc borate [83] and SiO_2 [84]. Ramirez-Vargas et al. [85] tested different organomodified MMT clays in combination with ATH in LDPE/EVA materials. Clays were modified with the following chemicals: N-octadecyl trimetyl amine chloride and dimethyl di(hydrogenated tallow) alkyl ammonium chloride. A synergistic effect between ATH and the organomodified clays could not be found. Cérin et al [86] investigated mechanical properties and fire retardancy of EVM (rubber like EVA, 60 % VA) containing ATH in combination with different phosphorous additives. It was shown that combining ATH with OP1230 (aluminum phosphinate) at a ratio of 2 to 1 exhibited the best fire retardant properties in terms of LOI, UL-94 and MLC test. A LOI value of 40 vol%O_2 and a V-0 classification in UL-94 was reached using this ratio. Moreover, pHRR was decreased from 500 kW/m² for the virgin polymer to 123 kW/m².

Synergistic effects for MDH in EVA were observed with fumed silica (SiO_2) [87, 88], silicone rubber (Second chemical factory), silicone powder (Dow Corning Corp.) [89], boroxo siloxanes [90], MWNT [91], zinc borate [83, 92], sepiolite [93], talc [94] and organomodified MMT [82, 95-98].

2.4. Melamine derivatives

Besides halogenated compounds and mineral fillers, it is possible to fire retard EVA adding nitrogen-containing compounds. The advantage of nitrogen based compounds is their ability to act in all stages of the combustion process. The most commonly used nitrogen-containing flame retardants are melamine and its derivatives. The chemical structure of melamine, melamine cyanurate, melamine sulfate, melamine borate, melamine nitrate and melamine phosphates, i.e. melamine phosphate, melamine pyrophosphate and melamine polyphosphate is presented in **Figure 16**.
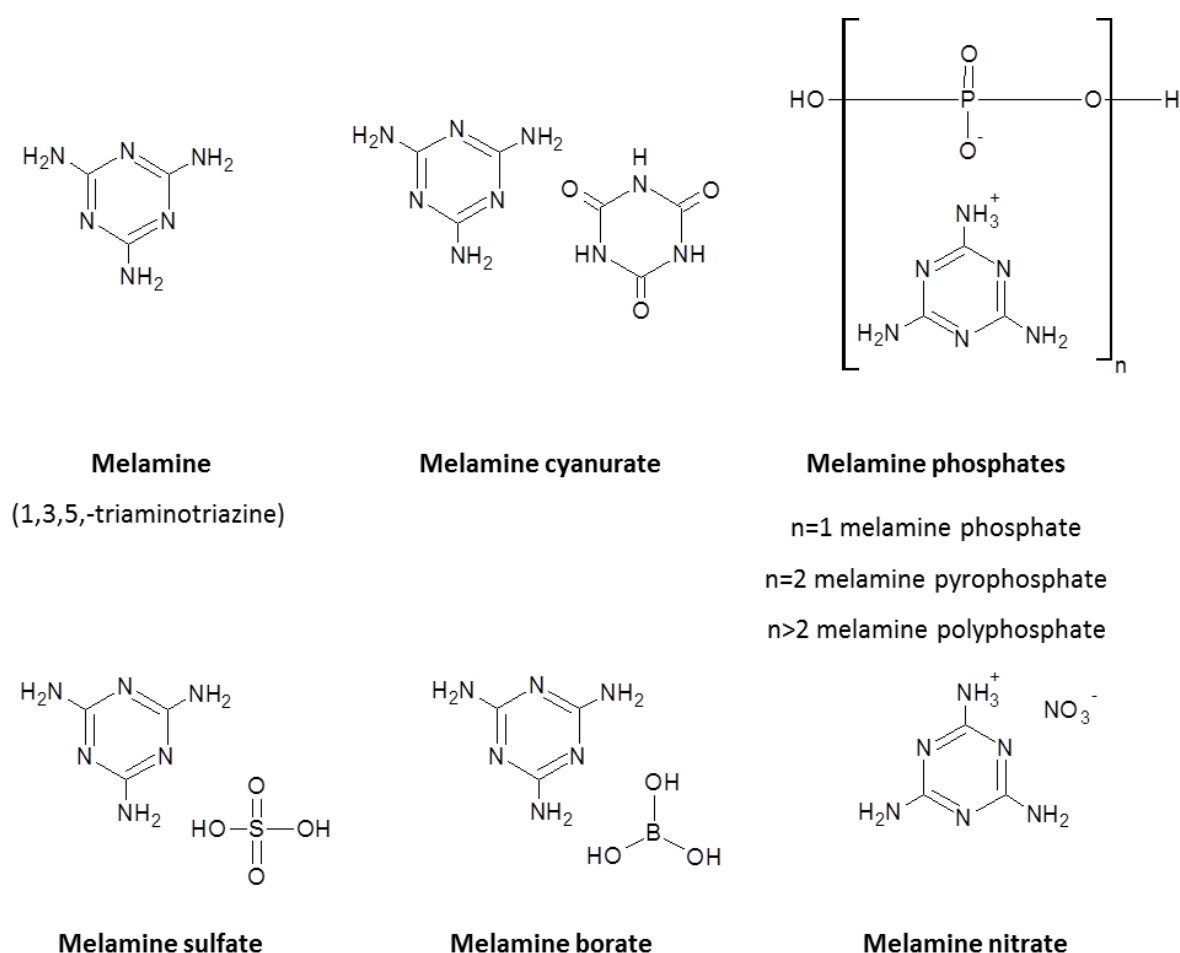

Figure 16: Chemical structure of melamine and melamine derivatives

2.4.1. Mode of action of melamine and its derivatives

Melamine is known to act in both phase, the gas and the condensed phase. It sublimates endothermically at around 200 °C and is nearly decomposed at 375 °C. It can decompose into low volatile condensation products named melam, melem and melon (**Figure 17**). These

three compounds are stable up to 350, 450 and 600 °C respectively [99, 100]. Melamine derivatives promote in general an additional fire retardant effect which is due to the activity of the additional molecule, e.g. nitrate, cyanurate or borate. This leads to a more important condensed phase action of melamine salts in comparison to melamine.

Melam

(*N2*(4,6-diamino-1,3,5-triazin-2-yl-1,3,5-triazine-2,4,6-triamine))

Melem

(2,5,8-triamino 1,3,4,6,7,9,9b - Heptaazaphenalene)

Melon

(poly[8-amino-1,3,4,6,7,9,9b-Heptaazaphenalene-2,5-diyl)imino])
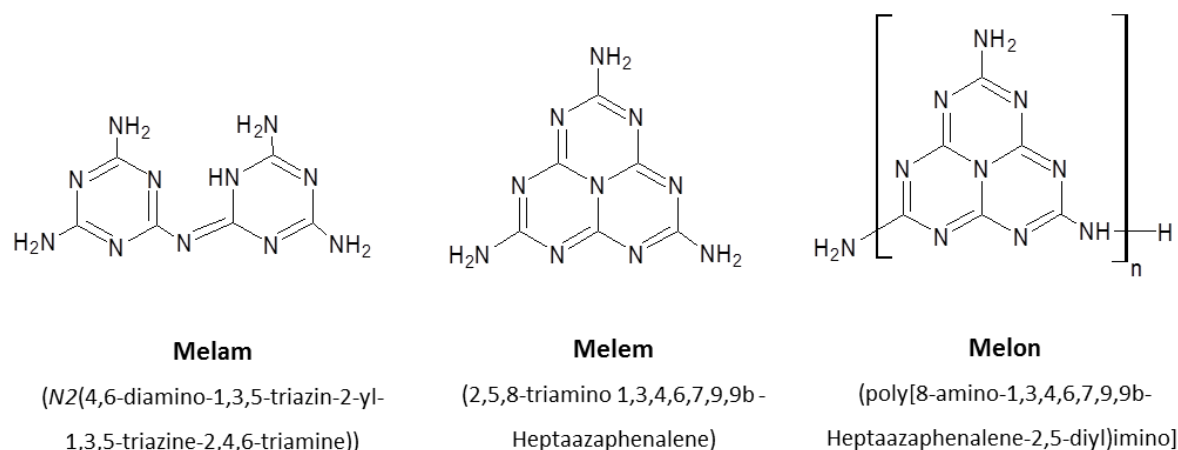
Figure 17: Chemical structure of melamine condensation products (melam, melem, melon)

2.4.2. Melamine and its derivatives as flame retardants in EVA

Few works report the use of melamine or its derivatives as flame retardants in EVA. Zilberman et al. [101] showed that the incorporation of 60 wt% of melamine into EVA led to comparable fire retardant properties in terms of pHRR as the virgin polymer. Comparison to EVA containing 60 % ATH showed that EVA-MEL ignited at shorter time than EVA-ATH. The total smoke release was increased from 236 a.u. (for virgin EVA) to 393 a.u. in the case of EVA-MEL, whereas a smoke release of 505 was observed for EVA-ATH. The substitution of 20 and 40 wt% melamine respectively by ATH instead enhanced the flammability properties (reduction pHRR, higher TTI), but total smoke production was increased to 852 and 589. Comparison of EVA-ATH-MEL and EVA-ATH indicated that combination of ATH and MEL led to decreased fire retardancy and increased smoke release. The combination of 40 wt% melamine and 20 wt% APP in EVA resulted in a further reduction in pHRR but ignition at shorter time than EVA-ATH. Moreover, the smoke production rate and the carbon monoxide production of EVA-ATH-APP were reduced in comparison to EVA-ATH. These results showed that a combination of melamine with a mineral filler or a phosphorous containing compound significantly improves fire retardant properties in comparison to the material containing EVA and ATH and can decrease smoke production in some cases.

A study on the fire retardancy of EVA/nitrile rubber containing 60 phr or 80 phr of MDH or 50 phr of melamine cyanurate (MC) was published by Rybinski et al. [102]. Fire retardancy measured by cone calorimetry is improved for EVA/NBR containing MDH or MC, whereas it was found that MC had similar effectiveness than MDH for enhancing fire retardancy of EVA/NBR rubbers. Fire retarded materials ignited at longer times, i.e. 123 and 126 s respectively than the virgin blend (TTI = 76 s). Moreover, pHRR was decreased from 362.kW/m² for the virgin blend to 119 kW/m² for EVA/NBR containing MC.

2.5. Phosphorous compounds

Phosphorous containing flame retardants are widely used as alternative solution of halogenated fire retardants. This section shows the mode of action of this kind of fire retardant additive and gives examples of their use in EVA. The class of phosphorous compounds includes ammonium polyphosphate (APP) and red phosphorus as well as phosphinate, phosphonate, phosphate ester (pyrophosphate and polyphosphate) (**Figure 18**), whereas the phosphorus content in the phosphorus containing flame retardants can vary from few percent to 100 % (red phosphorus) [103].
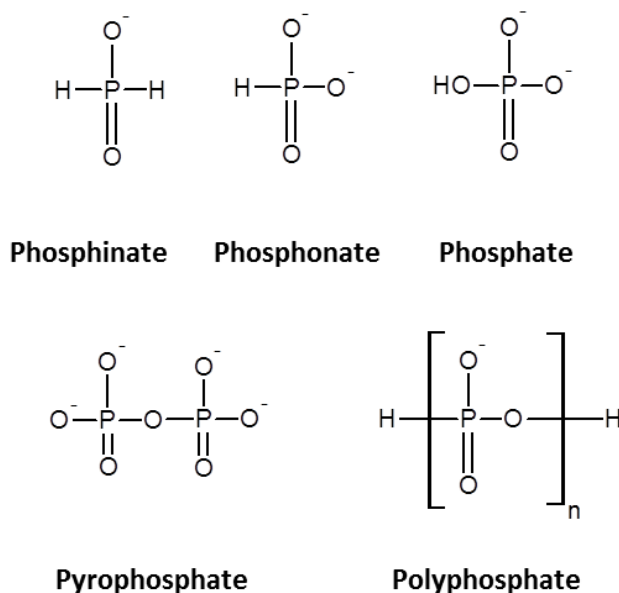

Figure 18: Different structures for organophosphorus flame retardants
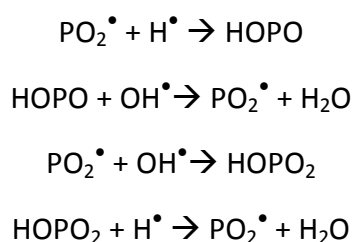
Nguyen et al. [104] investigated a relationship between the structure and the fire retardant effect of different phosphorus based additives as well as the mode of action of the different organic phosphorous compounds. It was postulated that compounds containing P-CH$_3$ or P-H

bonds have a fire retardant action in the gas phase due to the generation of small phosphorus containing species arising from the weak bond to the P atom. Moreover, it was found that in this study a phosphorus content of about 4 % is needed in EVA to reach a V-0 classification.

Due to the fact that phosphorus containing compounds are usually not chemically bonded to the final products they are considered by regulators to have potential to leach out of the polymer. Phosphorus compounds containing also halogens were already found in indoor air, house dust, drinking water, sediment and biota, whereas non-halogenated phosphorus compounds were only found in indoor environments, like offices, hospitals or schools [103].

2.5.1. Mode of action

Phosphorus containing flame retardants can have a condensed and/or a gas phase action. A condensed phase action can be obtained when a phosphate compound is heated in combination with a carbon containing compound. A protective char layer is formed at the sample surface due to the reaction of phosphoric acid formed by decomposition of the phosphorous compound with the carbon source. In the gas phase, phosphorus compounds have a flame extinguishing effect similar to that of halogenated flame retardants [103]. The mechanisms taking place in the gas phase are well reported in literature [105-108]. **Equation 3** presents reaction of $PO_2^\bullet$ with $H^\bullet$ forming HOPO which reacts with $OH^\bullet$ to form $PO_2^\bullet$ and H_2O. $PO_2^\bullet$ can also react with $OH^\bullet$ forming $HOPO_2$ which then reacts with $H^\bullet$ to form $PO_2^\bullet$ and H_2O. Recombinations like $H^\bullet + H^\bullet$, $O^\bullet + H^\bullet$, $OH^\bullet + H^\bullet$ and recombination of these atoms with phosphorus species are also possible [109].

$$PO_2^\bullet + H^\bullet \rightarrow HOPO$$
$$HOPO + OH^\bullet \rightarrow PO_2^\bullet + H_2O$$
$$PO_2^\bullet + OH^\bullet \rightarrow HOPO_2$$
$$HOPO_2 + H^\bullet \rightarrow PO_2^\bullet + H_2O$$

Equation 3: Inhibition cycles of phosphorus compounds

2.5.2. Phosphorous containing additives in EVA

Phosphorus containing flame retardants are widely used in EVA to improve its fire retardancy. The most common phosphorous compound used to enhance its fire retardant

properties is ammonium polyphosphate (APP). The incorporation of APP and microencapsulated APP (MAPP) led to an improvement of fire retardant properties of the polymer [110-114]. Moreover, the incorporation of MAPP exhibits better water resistance, a better thermal stability and a higher char yield than with APP. A synergistic effect (measured by LOI and UL-94 test) is observed using APP or MAPP in combination with expandable graphite (EG) [115].

Furthermore, EVA can be fire retarded through the incorporation of red phosphorus (RP) [116] or microencapsulated red phosphorous (MRP) [57, 117, 118]. MRP can be used in combination with talcite [118] hydrotalcite [57] or layered double hydroxides (LDH) [119] to improve the flammability properties of EVA. Moreover, an improvement of the fire retardancy is obtained when MRP is incorporated into cyclodextrin nanosponges [117].

An intumescent system is observed when APP and polyamide-6 (PA) are incorporated together in the EVA copolymer [120]. APP acts as acid source and PA as carbonization agent. This system has improved fire retardant properties in comparison to the virgin polymer. Combining APP and pentaerythriol (PER) forms an intumescent system in EVA. The pHRR is decreased to around 400 kW/m² in comparison to that of the virgin polymer (pHRR = 1800 kW/m²). The thermal stability as well as the fire retardant properties of a material containing EVA/APP/PER can be enhanced through the addition of zeolite [121], lanthanum ferrite (LaFeO$_3$) [122], nickel phosphide [123] and ferrous disulfide (FeS$_2$) [124]. Moreover, an intumescent system containing MAPP and a nitrogen compound (**Figure 19**) as char forming agent shows improved fire retardant and thermal stability when ferric pyrophosphate is added as co-agent [125].
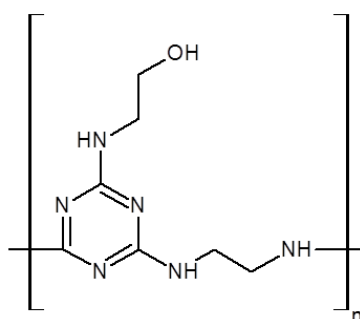
Figure 19: Nitrogen containing char forming agent

Another study concerning the combination EVA and PA6 is based on the incorporation of APP and MDH [126]. It was demonstrated that the material containing MDH and APP has lower flammability properties (measured by UL-94 and LOI) than the material containing only APP (30 wt%). When combined with MDH, higher loadings of APP are required to reach the same fire retardancy than the material containing only APP.

On the other hand, it is common to synthesize molecules containing phosphorous functions. Nguyen et al. [104] and Wang et al. [127] synthesized different phosphorous compounds (analogous of phosphinic and phosphonic acid as well as a DOPO (10-(2,5-dihydroxyphenyl)-9,10-dihydro-9-oxa-10-phosphaphenanthrene-10-oxide10-(2,5-dihydroxyphenyl)-9,10-dihydro-9-oxa-10-phosphaphenanthrene-10-oxide) compounds) and showed that they reduce the flammability of EVA-materials. Phosphorus-nitrogen compounds are often used to reduce flammability of EVA materials. Zhu et al. [128] observed a phosphorus-phosphorus synergism by using melamine pyrophosphate (MPP) in combination with 5,5,5',5',5",5"-hexamethyltri (1,3,2-dioxaphosphorinanemethan) amine 2,2',2"-trioxide (XPM-1000, **Figure 20**). The combination of XPM-1000 and melamine polyphosphate allows the formation of an intumescent system which improves the fire retardant properties of the polymer [129].
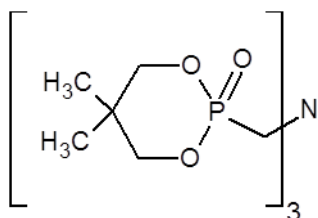
Figure 20: Chemical structure of XPM-1000

Another phosphorus-nitrogen compound, synthesized by Nguyen and Kim, is diphenyl piperazine-1,4-diylbis(methylphosphinate) (DPPMP, **Figure 21**) [130]. When incorporated in EVA, fire retardancy (LOI and UL-94 test) is enhanced. LOI value is increased from 18.7 for virgin EVA to 25 vol%O_2 for EVA containing 30 wt% of the fire retardant compound. Moreover, the fire retarded material is V-0 classified in UL-94 test.
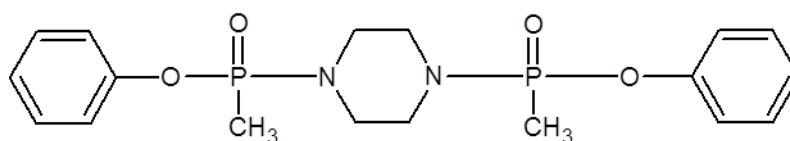
Figure 21: Chemical Structure of DPPMP

Wang et al. synthesized a phosphorous-silicone compound which shows improved fire retardant properties when used in combination with MDH [131] or when multiwalled carbon nanotubes (MWCNT) are modified with this compound [132].

Moreover, an improvement of the fire retardant properties (measured by cone calorimeter) of EVA is found for the incorporation of Diethylphosphato-ethyltriethoxysilane (SiP) [133]. Peak of heat release rate (pHRR) is reduced from 1302 kW/m² for the virgin polymer to 842 kW/m² for the fire retarded material, whereas time to ignition (TTI) decreases from 76 to 46 s as well.

Besides the named compounds, some other phosphorous-nitrogen containing compounds are reported to increase fire retardancy of EVA. For example, NP 28, a compound containing 15.6 wt% of phosphorous and 27.5 wt% of nitrogen (Weizheng Fine Chemical Inc.), enhances its fire retardant properties. EVA containing 28 wt% of NP28 reaches a V-0 classification in UL-94 test. Further, the LOI jumps from 18 to 33 vol%O_2 in comparison to the virgin polymer when 30.6 wt% NP28 are incorporated [134]. Furthermore, Liu et al. [54, 135-137] synthesized different nitrogen-phosphorous additives which increase the thermal stability as well as the fire retardancy (LOI, UL-94 and/or microscale combustion calorimeter (MCC)) of EVA.

2.6. Conclusion – Fire retardancy of EVA

Fire retardant action in the gas and condensed phase as well as addition of different fire retardant additives used in EVA was investigated in this part. It was shown that fire retardancy of EVA is mainly enhanced using mineral filler, phosphorous or nitrogen containing compounds. The most commonly used flame retardants are mineral fillers even if they require high loadings which degrade the mechanical properties. It was further demonstrated that phosphorous compounds are widely incorporated to EVA to increase its fire retardant properties. Besides APP, synthesized phosphorous compounds are widely reported as flame retardant in EVA. Melamine derivatives could provide interesting fire retardant effects in EVA, but are not enough studied up to now. Moreover, melamine was found to increase smoke release in case of fire.

3. Smoke release of EVA materials

Besides high fire retardant properties, polymeric materials have to exhibit low smoke release in the case of fire. This part of Chapter I is dedicated to the description and discussion of smoke production and the different ways to suppress smoke release of EVA materials when exposed to an external heat source.

3.1. What is smoke?

In general, it is difficult to get an overall adapted definition of smoke. According to ASTM E176, smoke is defined as the airborne solid and liquid particulates and gases evolved when a material undergoes pyrolysis or combustion [50]. Smoke is also considered to be the gaseous products of burning organic materials in which solid and liquid particles are dispersed. Another definition limits smoke to solid particles, such as carbon and ash, suspended in air [138]. Besides the question "what is smoke", the development of smoke is complex. It depends on numerous factors such as source of ignition, oxygen availability, constitution and properties of the combustible material, regime of the flame, buoyancy of the luminous flame environment, the location of the fire, etc. Further, the size distribution of the smoke particles is not predictable; it depends on the nature of the flame retardant, the composition of the material and on morphology of the soot particles of the burning polymer [50].

3.2. Toxicity of combustion products

One of the major drawbacks of smoke is its toxicity. Toxic combustion products generated by fires can be in the form of gases, vapor, aerosols, fumes and coated particles [139]. About fifty percent of the fire casualties are due to smoke and gases produced in a fire. For example, carbon monoxide is responsible for the death of 80 % of the persons who die in a fire [103, 140]. Regarding the toxicity of smoke, it is important not only to consider the acute toxicity but also the gases with environmental impact and long-term effects [141]. Fire retarded materials containing nitrogen compounds are known to evolve hydrogen cyanide, nitrogen monoxide and nitrogen dioxide when strongly heated or incompletely burned. In the case of melamine, the presence of air reduces the hydrogen cyanide yield [142]. Stec et
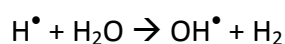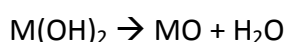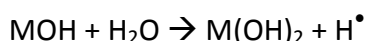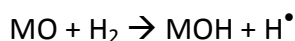
al. [143] investigated the carbon monoxide yield, hydrocarbon evolution and smoke production according to the environment for polypropylene (PP) and polyamide 6 (PA6) materials containing APP and nanoclay. Tests were performed in well ventilated, small under-ventilated and large under-ventilated conditions. It was found that carbon monoxide evolution for PP and PA6 materials is smaller in well ventilated conditions. Smoke release and hydrocarbon evolution are higher in large under ventilated conditions.

Another well-known disadvantage of smoke release is the presence of soot particles formed during combustion of a material. These particles can accumulate in the respiratory system of human beings and animals or can be found in devices surrounding the fire. Particles in fire surrounding devices can led to even bigger damage than the fire itself; for example when particles are accumulated in electrical devices. An important parameter of soot particles is their size, due to the fact that toxicity is supposed to be increased with decreasing particle size. Smaller particles are known to accumulate easier in the human respiratory system. It is reported that PP and PA6 materials containing flame retardant additives (APP and nanoclay) produce more smoke than the polymer itself [144]. Moreover, it was shown that size distribution of soot particles of PA6 and PP materials (virgin polymer and fire retarded materials) seems to be unaffected by the ventilation condition.

3.3. How to suppress smoke?

To reduce smoke release of materials in the case of fire, smoke suppressant additives can be added to the polymeric matrix. Like for the fire retardancy, the smoke suppressant effect can occur in the gas and in the condensed phase [50], whereas smoke suppressant effects are a combination of different mode of actions. In the gas phase, the smoke density due to the release of combustion gases can be reduced by chemical and physical mode of action. Smoke is reduced chemically by the elimination of smoke precursors or smoke particles. Aromatic smoke precursors can be removed by oxidation, which takes place through the presence of transition metal complexes. Removal of soot particles can occur through oxidation by high energy radicals ($OH^\bullet$) coming from the catalytic action of metal oxides or hydroxides. The reaction of the $OH^\bullet$ formation through the presence of metal oxides or hydroxide is presented in **Equation 4**. It is assumed that they catalyze the breakdown of hydrogen and water to molecular hydrogen forming metal hydroxides or metal dihydroxides.

Equation 5 presents the reaction taking place to remove soot particles with high-energy $OH^\bullet$ forming CO and $H^\bullet$. Metal hydroxides can also have another smoke suppressant effect: Ionization of the nuclei which is necessary to form soot. Further, some transition metal oxides can cause flocculation of the soot particles. The smoke release may also be reduced through dilution of the combustion gases.

$$MO + H_2 \rightarrow MOH + H^\bullet$$

$$MOH + H_2O \rightarrow M(OH)_2 + H^\bullet$$

$$M(OH)_2 \rightarrow MO + H_2O$$

$$H^\bullet + H_2O \rightarrow OH^\bullet + H_2$$

Equation 4: Reaction of the formation of $OH^\bullet$ through the presence of metal oxides or hydroxides; M presents metal

$$C_{solid} + OH^\bullet \rightarrow CO + H^\bullet$$
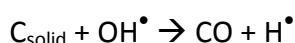
Equation 5: Removal of soot particles by high-energy $OH^\bullet$

In the condensed phase, both modes of action, i.e. physical and chemical mode of action are possible. The physical mode of action is similar to that of the fire retardants: a glassy or intumescent coating is formed to avoid the liberation of the gases and soot. Another possibility is the dilution of the evolved gases through the addition of inert fillers. The chemical reduction of smoke in the condensed phase occurs through the reduction of the extent to which smoke precursor species escape to the gas phase. This takes place through reaction with acidic pyrolysis products or through affection of the cross-linking process.

Smoke suppressants often act through a combination of different mechanisms. When smoke suppressants are incorporated into a polymer in combination with a fire retardant the effectiveness of one or even both additives can be worsened. Often the additives have contrary mechanism. For example, fire retardants may act through the removal of radicals, i.e. $OH^\bullet$, $H^\bullet$ or $O^\bullet$ in the gas phase. This reaction is the contrary of the reaction of the smoke suppressant that act through the formation of these radicals. When the fire retardant removes the radicals, soot particles are not removed and more smoke will be released. Another phenomenon of the combination of smoke suppressants and fire retardants is that

smoke suppressants often act by activating the combustion process which is the opposite effect of the fire retardant. To overcome the problem of the contrary effect of smoke suppressants and fire retardants, often a system forming a protective char layer is used. With this system the amount of fuel is reduced, as well as, the amount of carbon available to form soot particles.

3.4. Smoke suppressants in EVA

The most known and studied smoke suppressants in EVA are zinc additives: Zn-layered double hydroxides [145], zinc borate [146, 147] and zinc hydroxystannate [148]. The use of zinc borate even reduces the toxicity of the evolved decomposition products. In most cases, the presence of zinc containing additives leads to a formation of a char that inhibits smoke release.

The incorporation of SiO_2 into EVA-MDH system led to a decrease of smoke production and a decrease in carbon monoxide emission during the combustion [87]. For example, total smoke release was decreased from a value of 1118 a.u. for EVA-MDH to 553 a.u. for EVA-MDH- SiO_2 (40-52-8 wt%). For the same materials, carbon monoxide yield decreased from 0.0122 kg/kg to 0.0082 kg/kg for the material containing SiO_2. This was explained by the fact that SiO_2 forms together with MDH a barrier that avoids the migration of volatile products to the sample surface. Another possibility to decrease smoke of EVA/MDH materials was the additional incorporation of sepiolite [93]. Moreover, a reduction of the smoke release during combustion was obtained for the combination of ATH or MDH with modified MMT [82].

Zilberman et al. [101] showed that smoke release (measured by cone calorimetry) of EVA-ATH materials was reduced by addition of APP to the material. Further, it was demonstrated that when APP and MEL are incorporated into EVA, total smoke release (no units) increased to a value of 975 in comparison to the material containing ATH (Total smoke release = 505). On the other side, carbon monoxide yield was smaller for the material containing MEL and APP. EVA-ATH releases 0.018 kg/kg and EVA-MEL-APP 0.007 kg/kg. EVA-ATH-MEL (40-40-20 wt%) exhibited a total smoke release of 852, whereas carbon monoxide yield was 11.7 kg/kg. Bugajny et al. [149] showed that the addition of APP in combination with tris(2-hydroxyethyl) isocyanurate to EVA (without ATH) reduced smoke release by forming a protective shield.

The use of graphene-based compounds as smoke suppressants is also well reported in literature. Smoke production can be decreased through the incorporation of different graphites (expanded, natural and graphite oxide) in combination with zinc borate and zinc stannate, whereas expanded graphite showed the best smoke reduction of the tested graphites [150]. The smoke suppressant effect of the graphites is explained by the formation of an intumescent char which traps gases and soot particles. Furthermore, the addition of MWCNT and modified MWCNT to EVA also reduced the smoke production [8].

4. Conclusion

Ethylene vinyl acetate (EVA) is a versatile polymer made from copolymerization of ethylene and vinyl acetate (VA). Its versatility is due to the adaption of the VA content on the desired polymer properties. In function of the VA content, mechanical properties, fire retardancy and thermal properties of the EVA materials change. For many of its applications wire and cable industry, transportation, buildings etc.) high fire retardant properties, low smoke release and acceptable mechanical properties are required. In this chapter, it was demonstrated that there are many possibilities to fire retard EVA. An overview was given about the use of mineral fillers, halogenated compounds, nitrogen- and phosphorus-containing compounds as fire retardants in EVA. Moreover, it was demonstrated how smoke release can be reduced for EVA materials.

The goal of this study is the enhancement of fire retardant properties and reduction of smoke release of EVA materials containing 60 wt% VA (hereafter called EVM). The material has therefore rubber properties. Up to now there is not a lot reported in literature about the enhancement of fire retardancy and reduction of smoke release of elastomeric EVM. The strategy of this work is to incorporate additives to improve fire retardancy and to decrease smoke release of EVA materials. The most commonly used compounds are mineral fillers due to their high efficiency and their low costs. However, the use of mineral fillers requires high loadings which often decrease mechanical properties. In this study, mineral fillers is combined with classical flame retardant compounds to maintain low costs but to overcome the lack of mechanical properties. It was demonstrated that in EVA in general the incorporation of phosphorus and/or nitrogen (especially melamine) containing compounds results in promising material properties. Due to the fact that little is known about the fire retardant effect and smoke release of EVA materials containing a mineral filler in combination with different melamine derivatives, it is decided to work with these systems in this study. Furthermore, it was shown that phosphorous containing additives in EVA have good fire retardant properties. Therefore, melamine derivatives containing phosphorous and phosphorous-free melamine derivatives are used in combination with a mineral filler. ATH is chosen as mineral filler, due to its low price and high efficiency as fire retardant in EVM.

The next chapter, Chapter II, is dedicated to the materials that are used in this study. Moreover, the experimental techniques used are discussed in detail.

Chapter II: Materials and Methods

This chapter is dedicated to the presentation of the polymer and the additives used in this study. Moreover, the preparation method of the samples is discussed. Then, test methods to investigate mechanical properties, fire retardancy and smoke release of materials are presented. Furthermore, experimental techniques used to characterize thermal decomposition, gas and condensed phase are illustrated.

1. Materials

This part is dedicated to the materials used in this study, that is to say the polymer, the fire retardant compounds and the processing additives. Processing of the materials is then described. In the second section characterization methods are discussed.

1.1. Polymer

The polymer used in this study is Levapren® 600 (hereafter called EVM), an ethylene-vinyl acetate copolymer containing 60% vinyl acetate. Thanks to its rubber properties, Levapren® 600 can be used as sporting goods and in the following industrial sectors: automotive, machinery, construction and wire and cable industry. Levapren® 600 is supplied in almost colorless granules which are dusted with silica and talc to avoid agglomeration. Product specifications of Levapren® 600 are presented in **Table 5**.

Table 5: Product specifications for Levapren® 600

	Property	Nominal Value
Unvulcanized Levapren® 600	Mooney Viscosity UML (1+4) 100 °C	27 ± 4 MU
	Vinyl acetate content	60 ± 1.5 wt%
	Volatile matter (6 h at 105 °C)	≤ 0.6 wt%
	Total Ash	≤ 0.8 wt%
	Specific gravity	approx. 1.04
	Solubility	Soluble in chlorinated and aromatic hydrocarbons
Vulcanized Levapren® 600	Tensile strength	Up to 24 MPa
	Hardness Shore A	50-90 Shore A

In comparison to other commercial available elastomers, Levapren® 600 often shows superior properties (**Figure 22**). First of all, it can be seen that Levapren® 600 has a higher filler acceptance, a higher scorch safety and a higher performance cost ratio than the other tested elastomers. Moreover, it has better (or comparable) oil, heat and hot tear resistance. In terms of low temperature behavior it shows comparable results to the other elastomers.

To improve chemical and physical resistance of Levapren® 600, materials are vulcanized adding peroxide (bis(*tert*-butyldioxyisopropyl)benzene) and activator (triallylcyanurate) to the polymeric matrix. The vulcanized polymer is also known to have a high stability against ozone, UV radiation, rain and industrial waste gases. Performing an outdoor weathering test

over a two-year-period demonstrated that even after two years samples were still usable [9]. Positive results were also obtained concerning UV stability of the polymer in laboratory tests.
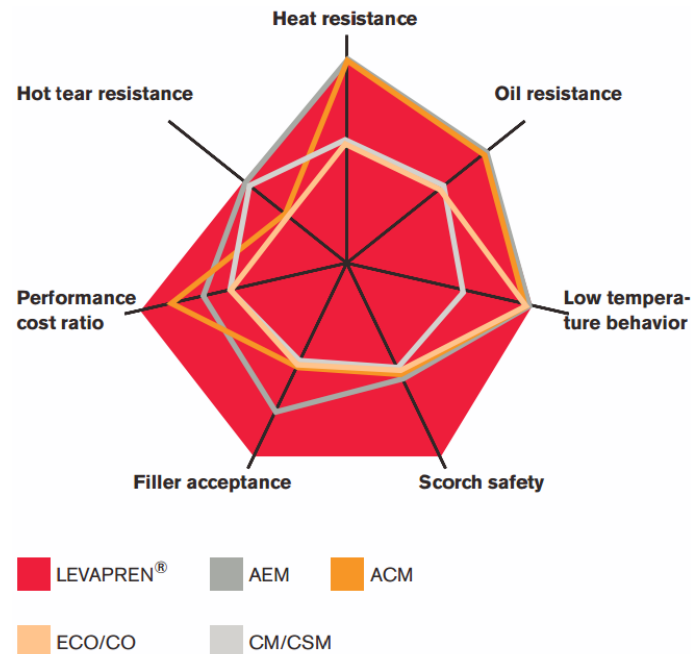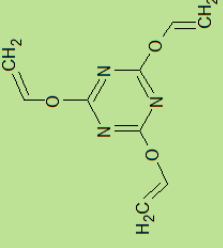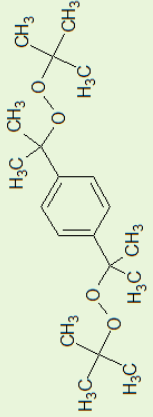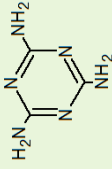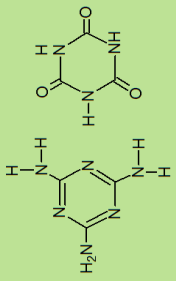
Figure 22: Comparison of Levapren® 600 with other elastomers; AEM = ethylene-acrylic elastomer, ACM = acrylate elastomer, ECO/CO = epichlorohydrin, CM/CSM = chlorinated/chlorosulfonated polyethylene [9]
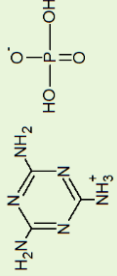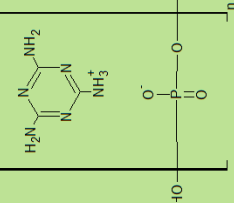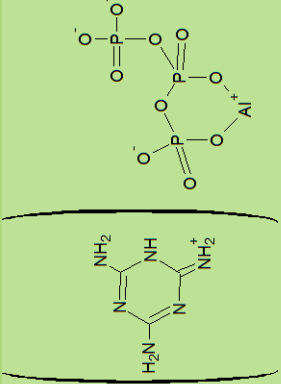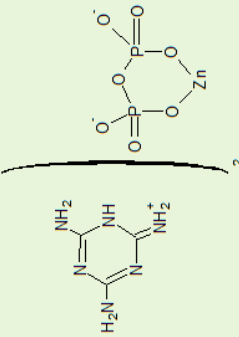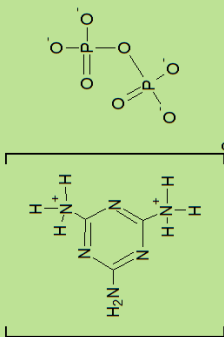
1.2. Additives

As mentioned before, this study is based on the improvement of fire retardant properties and reduction of smoke release of EVM materials maintaining (or improving) mechanical properties of the polymer. A combination of ATH (Apyral 120E) and different melamine derivatives is incorporated to the polymer to reach the objectives of this work. ***Table 6*** summarized all additives that are used in this study, their supplier and their chemical nature.

The ATH particles have a particle size of 0.9 μm (D_{50}) and a specific surface area of 11 m²/g. Additives used in combination with ATH are: melamine, PPM Triazine ("poly-melamine" structure), melamine borate, melamine cyanurate, melamine orthophosphate, melamine polyphosphate, melamine-poly(aluminum phosphate), melamine poly(zinc phosphate) and di-melamine pyrophosphate. As it can be seen, nitrogen as well as nitrogen and phosphorous containing additives are tested in EVM.

Table 6: Summary of additives used

Chemical	Abbrevation	Supplier	Composition	Chemical structure
Rhenofit TAC/S	-	LANXESS	Triallyl cyanurate	
Perkadox 14-40B-PD	-	AkzoNobel	40 wt% Bis(*tert*-butyldioxyisopropyl) benzene	
Apyral 120E	ATH	Nabaltec	Aluminum trihydroxide	$Al(OH)_3$
PMN500	MEL	Thor	Melamine	
PPM-Triazine	PPM	MCA Technologies	Poly-[2,4-(piperazine-1,4-yl)-6-(morpholine-4-yl)-1,3,5-triazine]/Piperazin	$[C_{11}H_{16}N_6O]n.C_4H_9NO$
Melagard MB	MB	Italmatch	Melamine borate	$C_6H_6N_6$ H_3BO_3
Melagard MC 25	MC	Italmatch	Melamine cyanurate	

Trade name	Product code	Manufacturer	Chemical name	Structure
Melagard MP	MP	Italmatch	Melamine orthophosphate	
Melapur 200	MP 200	BASF	Melamine polyphosphate	
Melapur 200-70	MP 200-70	BASF	Melamine polyphosphate	Like above, different particle size
Safire 200	SF200	Catena – Floridienne Chimie	Melamine-poly(aluminum phosphate)	
Safire 400	SF400	Catena – Floridienne Chimie	Melamine-poly(zinc phosphate)	
Budit 311	B311	Budenheim	Di-melamine pyrophosphate	

1.3. Preparation of materials

All samples (**Table 7**) are prepared following an upside down process in an internal mixer (GK 1.5L from Werner & Pfleiderer). Mixing is performed at 20 °C with a rotation speed of 40 rpm for 4 min. First, additives are added into the mixing chamber then the polymer. After mixing, the materials are further dispersed on an open two roll mill at 20 °C. During this step, the peroxide and the co-agent (Perkadox TAC/s and Rhenofit respectively) are added to the material. After batch off and 24h relaxation time, the materials are treated a second time on the two roll mill. Later the compounds are pressed into plates and vulcanized at 180 °C for 12 min. Specimens for mechanical testing, fire tests and smoke test are cut out after vulcanization.

Table 7: Composition of materials

Compound	Loading [phr]
Levapren 600	100
Fire retardant additives	130
Rhenofit TAC/S	1
Perkadox 14-40	6

2. Methods

This section presents the methods that are used to evaluate the mechanical properties, the fire retardancy and the smoke release of materials used in this study. Moreover, techniques to further characterize materials are presented. Methods to characterize thermal behavior, gas and condensed phase of materials are detailed afterwards.

2.1. Mechanical properties

The knowledge of the physical properties of materials is essential for the commercial use of materials. The mechanical properties are obtained by the stress-strain test and by the measurement of the Hardness Shore A.

2.1.1. Stress-strain test

The stress-strain test is performed according to ASTM D412 standard (DIN53504) on a Zwick ZO10 tensile tester (**Figure 23**). Two values are measured with this test method: the elongation-at-break (EAB) and the tensile strength (TS). The EAB is the strain on the sample when it breaks and is expressed in percent. It is calculated using **Equation 6**. The TS is the stress which is needed to break the sample and is expressed in MPa.

Figure 23: Zwick Z010 stress-strain device

The specimens (**Figure 24**) are brought into the device and a strain rate of 200 mm/min is applied until the sample breaks. All measurements were carried out at room temperature

(23 °C). Margin of error of elongation-at-break is ± 25% and ± 1.5 MPa in the case of tensile strength.
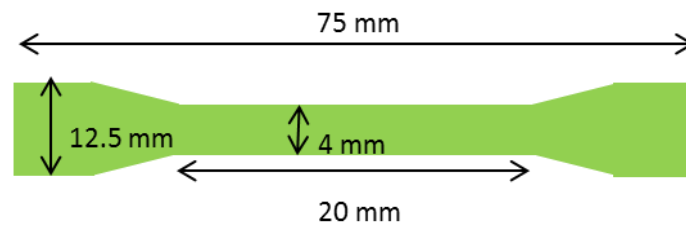
Figure 24: Specimen used in stress-strain test; thickness 2mm

$$EAB = \frac{l}{l_0} * 100$$

Equation 6: Calculation of elongation-at-break (EAB); whereas l_0 is the origin length of the sample and l that obtained after test

2.1.2. Hardness Shore A

The Hardness Shore A is measured according to the standard test ASTM D2240 (DIN53505). This test method is based on the penetration of a specific type of indenter into a material. The indentation hardness is inversely related to the penetration and is dependent on the elastic modulus and viscoelastic behavior of the material. The hardness measurement is performed on a Digitest Durometer from Bareiss (**Figure 25**). The intender used in the experiment is shown in **Figure 26**; it consists of a hard steel rod (diameter 1.25 mm) with a truncated cone (35 °, diameter 0.79 mm).

Figure 25: Hardness Shore A durometer
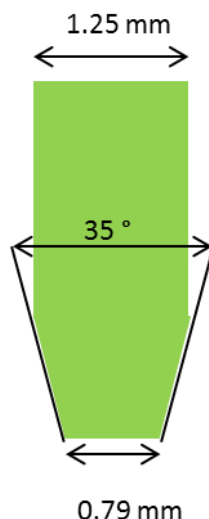
Figure 26: Intender used in Hardness Shore A test

Values can be observed from 0 to 100 Shore A, where 0 Shore A corresponds to a penetration depth of 2.5 mm and 100 Shore A of 0 mm. A change in hardness of one Shore A corresponds to a penetration depth of 0.0025mm. Some typical Shore A values are presented in **Table 8**. The test is performed with specimens of 6.3 mm thickness and a diameter of 36 mm. Each material is tested three times at room temperature (23 °C ± 2 °C). The value presented in this report is the average of the three measurements, whereas the margin of error is ±1 Shore A.

Table 8: Examples of Hardness Shore A values for different materials

Materials	Hardness [Shore A]
Rubber band	25
Door seal	55
Automotive tire tread	70
Soft wheel of roller skates	98
Ebonite rubber	100

2.1.3. Hydrothermal aging

Hydrothermal aging of materials is performed according to DIN ISO 181. In our case, two different test configurations are used (**Table 9**). Materials are immersed in distilled water for 70 h at 70 °C or in artificial sea water for 168 h at 40 °C, whereas the composition of the artificial sea water is given in **Table 10**. Water swelling tests are carried out with the same specimen size as used for the stress strain test (**Figure 24**). Hardness, TS and EAB are

measured before and after the water swelling test. Moreover, the changes in volume (ΔV) and mass (Δm) are given, with a margin of error of change of mass and volume of 10 %.

Table 9: Configurations used for the water swelling test

Configuration	Type of water	Temperature [°C]	Time [h]
1	Distilled water	70	70
2	Artificial sea water	40	168

Table 10: Composition of artificial seawater, compounds are dissolved in 985 mL distilled water

Chemical	Chemical Structure	Mass [g]
Sodium chloride	$NaCl$	28
Magnesium sulfate heptahydrate	$MgSO_4 * 7H_2O$	7
Magnesium chloride hexahydrate	$MgCl_2 * 6H_2O$	5
Calcium chloride hexahydrate	$CaCl_2 * 6 H_2O$	2.4
Sodium bicarbonate	$NaHCO_3$	0.2

2.2. Fire tests

Depending on the application of materials, different fire tests are used to evaluate the flammability of materials. This part presents the different fire tests used in this work: UL-94, limiting oxygen index (LOI) and mass loss calorimeter (MLC).

2.2.1. UL-94

The set of UL-94 tests, "Test of Flammability of Plastic Materials for Parts in Devices and Appliances", is an example for small heat-source ignition tests that is approved by the Underwriters Laboratories Inc. The most common and widely used test is the UL-94 V (IEC 60695-11-10) that describes the tendency of a material to extinguish or to spread the flame after ignition of the material. It classifies specimens from NC (not classified),V-2, V-1 to V-0, whereas V-0 is the best rating. The different criteria for the classifications are presented in **Table 11**. The experimental set-up for the UL-94 test can be seen in **Figure 27**.

A blue flame with a 20 mm high central cone is applied for 10 s to the bottom edge of the vertical specimen. After 10 s the flame is removed and the afterflame time required to extinguish the flame is recorded. The flame is reapplied for another 10 s and removed again. After the second burning, the time to extinguish and the afterglow time are noted. It is

possible that during the burning the barrels begin to drop and the burning drops inflame the piece of cotton that is below the specimen. For each material a set of 5 bars was tested. The specimens have a size of 127 x 13 x 1.5 mm³.

Table 11: Classification of materials for the UL-94 V

Criteria	V-0	V-1	V-2
Afterflame time for each individual flaming	≤ 10 s	≤30 s	≤30 s
Afterflame and glow time for each individual specimen, after second flaming	≤30 s	≤60 s	≤60 s
Total afterflame time for any condition set (5 flamings)	≤50 s	≤250 s	≤250 s
Cotton indicator ignited by flaming drops	No	No	Yes
Afterflame or afterglow of any specimen up to the holding clamp	No	No	No
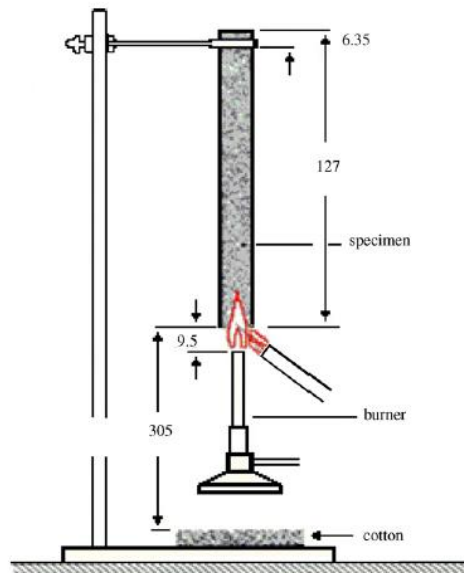
Figure 27: Experimental set-up for UL-94 V

2.2.2. Limiting Oxygen Index

Like the UL-94, the limiting oxygen index (LOI) is a small heat source ignition test. With the LOI test (ISO 4589-2), the relative flammability of materials, their ignitability and inflammation can be described. The experimental set-up of the LOI device is shown in **Figure 28.** LOI measurements are performed on a Fire Testing Technology device with barrels of 100 x 10 x 0.3 mm³ at room temperature. The specimen is clamped vertically into a glass cylinder in a controlled oxygen-nitrogen mixture atmosphere. The measured LOI value corresponds to the minimal oxygen concentration required to sustain the combustion of a

material. It is expressed as the percentage of oxygen in an oxygen-nitrogen mixture (**Equation 7**), whereas the error of measurement is $\pm$ 1 vol%O_2.

$$\text{LOI} = 100 \times \frac{[O_2]}{[O_2] + [N_2]}$$

Equation 7: Calculation of the LOI value, [O_2] and [N_2] concentrations of oxygen and nitrogen

Materials having a LOI value below 21 vol%O_2 are called combustible, those with a LOI value above 21 vol%O_2 are flame retarded. Thus, the higher the LOI value, the better the fire retardancy of the material. The materials presented in this report should have a LOI value above 21 vol%O_2.
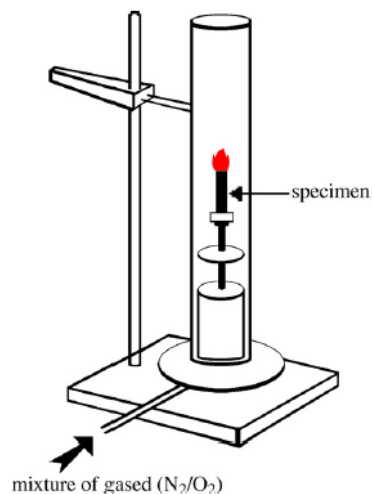
Figure 28: Experimental set-up of the LOI test

2.2.3. Mass loss calorimeter

Mass loss calorimetry (MLC) is a bench-scale reaction-to-fire test which provides a forced-flaming combustion scenario that is typical of developing or developed fires. The measurements were carried out on a Fire Testing Technology mass loss calorimeter device (ISO 13927, ASTM E906). The schematic representation of the device is shown in ***Figure 29***. The sample (100 x 100 x 3 mm³) is covered by a grid (100 x 100 mm³) to avoid contact between the material and the spark igniter due to bloating of the sample before ignition (grid not mentioned in ISO 13927). The distance between the sample holder and the heat source was 25 mm. An external heat flux (35 kW/m²) produced by a conical heater element

is applied to the sample. The temperature of the gaseous combustion products is measured at the top of the chimney with a thermopile.
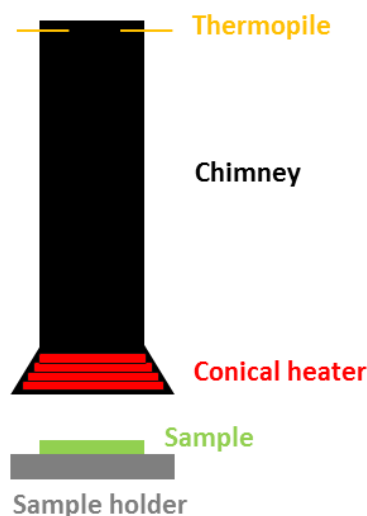
Figure 29: Schematic representation of the mass loss calorimeter

The values measured by mass loss calorimeter are: the heat release rate (HRR), the peak of heat release rate (pHRR), the total heat release (THR), the time to ignition (TTI) and the mass loss of the sample during combustion (ML). All measurements were performed twice. The presented curves are the worst case of repeatable results. The acceptable error of measurement is estimated at 10 % for all values.

2.3.   Smoke opacity test

The smoke opacity test (**Figure 30**) is a homemade test that had been developed to evaluate the smoke release during combustion. The goal is the development of a test method which is comparable to existing normalized test methods. As it is seen, the structure is similar to that of the mass loss cone calorimeter. An external heat flux of 35 kW/m² produced by a conical heater is applied on a horizontal sample (100 x 100 x 3 mm³). The distance between the heating element and the sample is fixed at 35 mm (instead of 25 mm for MLC) which permits to remove the grid (used in MLC experiment) on the sample surface. Samples were ignited by a spark igniter. The generated smoke is measured at the top of the chimney with a smoke density analyzer TRDA 302 from Taurus Instrument. A light source (halogen point light source) emits light (intensity I_0) and the transmitted light (intensity I) is measured by a light sensor (Silizium Photoempfänger). Calculation of optical density is presented in **Equation 8**.

$$OD = -\log\left(\frac{I}{I_0}\right)$$

Equation 8: Calculation of optical density

The values measured during the test are the time to ignition (TTI), the total optical density (OD_{total}) and the VOF4, i.e. the summation of the optical density (OD) over the first four minutes. Moreover, the maximum optical density during the experiment (D_s1 and D_s2) and the maximum optical density during the four minutes (D_s4) are measured. All measurements are performed twice. Presented curves (time vs. optical density) are the worst case of the repeatable curves. The error is estimated at 10 % for all values.
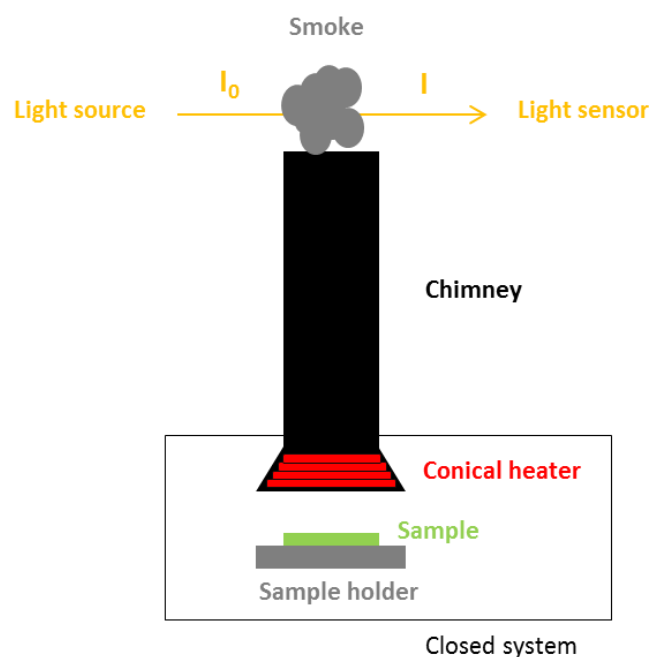
Figure 30: Smoke opacity test device

2.4. Thermal analysis

The thermogravimetric analysis are performed on a TA Instrument TGA Q5000IR with alumina crucibles under air and nitrogen to mimic thermo-oxidative and pyrolytic decomposition respectively. The balance purge flow is set to 15 mL/min, whereas the purge flow is fixed to 25 mL/min nitrogen. All samples (5 -7 mg) underwent an isotherm at 50°C for 10 minutes followed by a heating ramp from 50 to 800°C at a chosen heating ramp (10 to 500 °C/min). All experiments are performed two times to ensure the repeatability.

2.5. Gas phase analysis

The analysis of the gas phase gives information about the nature of the evolved gases during the decomposition process. The gas phase is analyzed using three different methods: thermogravimetric analysis coupled with Fourier transform infra-red (TGA-FTIR), pyrolyzer gas chromatography-mass spectrometry (py-GCMS) and mass loss calorimeter coupled with Fourier transform infra-red (MLC-FTIR).

2.5.1. Thermogravimetric analysis coupled with Fourier transform infra-red (TGA-FTIR)

Thermogravimetric analysis coupled with Fourier transform infra-red (TGA-FTIR) is performed on a TA Instrument TGA Q5000IR coupled with a Thermo Scientific Nicolet iS10 spectrometer. Analyses are carried out in air in alumina crucibles. The balance flow is set to 15 mL/min whereas the purge flow is fixed to 100 mL/min. Samples are heated up from 50 to 800 °C (10 °C/min) after an isothermal of 10 min at 50 °C. Gases evolved during the TGA experiment are detected continuously by the FTIR device. The spectra are recorded every 10 seconds with the OMNIC® software in a range from 400-4000 cm^{-1}. The number of scans is fixed at 8 and the resolution at 4. The temperature of the transfer line between the TGA and the FTIR instrument is set to 225 °C to avoid condensation of the evolved gases.

Problems occurred performing TGA-FTIR experiments for materials containing melamine or its derivatives. To detect melamine in the gas phase using TGA-FTIR, a high amount of melamine or its derivatives has to be present in the material. However, high contents of melamine or its derivatives lead to blockage of the interphase and the transfer line located between TGA and FTIR device. Further, blockage leads to bad results for FTIR spectra. After some tests it was found that the best results are obtained using around 5 mg of sample. This sample amount does not block the connection between TGA and FTIR and permits analysis of decomposition gases except of melamine or its condensation products which condensate in the transfer line.

2.5.2. Mass Loss Calorimeter coupled with Fourier transform infra-red

Mass loss calorimeter coupled with Fourier transform infra-red (MLC-FTIR) is performed on the mass loss calorimeter described above (**Figure 31**), whereas MLC experiment is

performed as described above at 35 kW/m², with a distance between resistance and sample of 25 mm, using plates of 100x100x3 mm³ size covered by a grid.

Gas picking pistol and transfer line are provided by M&C Tech Group. FTIR, Antaris™ Industrial Gas System, is provided by ThermoFisher. The transfer line between MLC and FTIR is 2 m long and is heated up to 200 °C. To assure constant temperature of the transfer line, two temperature controllers are installed. Before analyzing the gases by FTIR, soot particles are filtered by two different filters (2 and 0.1 µm). Filters consist of glass fibers and ceramic respectively. The FTIR gas cell is set to 185 °C and 652 Torr. The optical pathway is 2 m long and the chamber of the spectrometer is filled with dry air. FTIR spectra obtained using MLC-FTIR are treated using OMNIC software. To quantify gases, spectra have to be recorded at different concentrations for targeted gases and a quantification method has to be created using TQ Analyst. Creating a method, representative regions in the spectra of the selected gas have to be chosen and interactions with other gases have to be taken into account. Using MLC-FTIR the following gases can be quantified: water, carbon monoxide, carbon dioxide, acetic acid, ammonia, methane, nitrogen monoxide, nitrogen dioxide, hydrogen cyanide. Quantification is reproducible within 10 %.
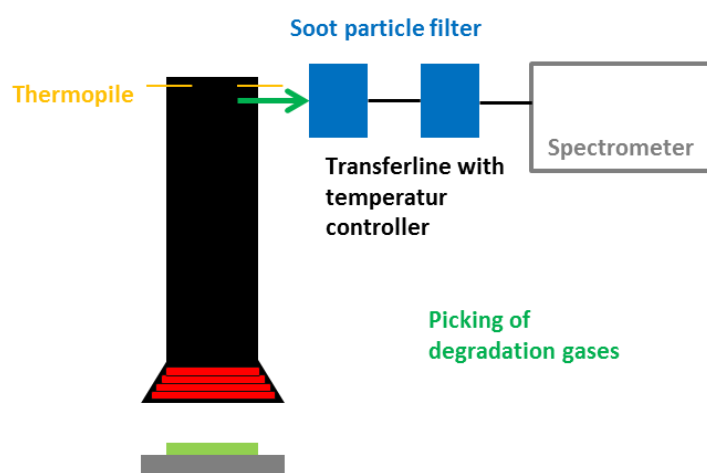
Figure 31: Schematic presentation of MLC-FTIR test

2.5.3. Pyrolysis-Gas chromatography-mass spectrometry

Pyrolysis-gas chromatography-mass spectrometry (py-GCMS) analyses are performed on a device provided by Shimadzu (**Figure 32**). The device consists of a micro-furnace pyrolyzer

(Frontier Lab PY-2020iD) coupled with a GCMS (Shimadzu GCMS QP2010 SE). Experiments are performed under inert conditions using helium. Sample size is about 200 µg.
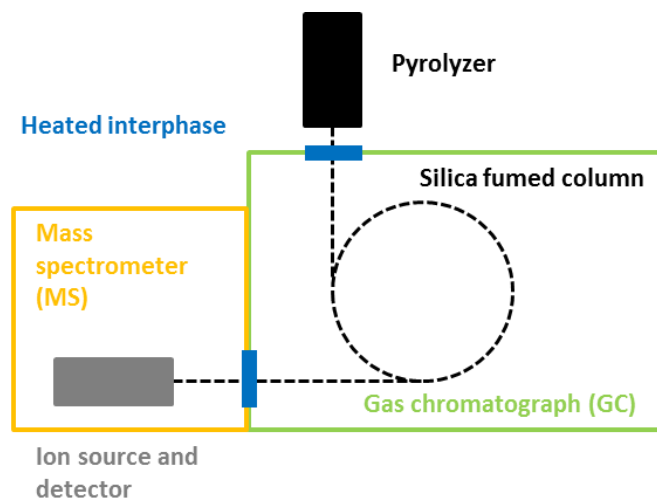
Figure 32: Schematic presentation of the Py-GCMS device

Samples (in a stainless steel cup) are heated up from 50 to 800 ° with a heating ramp of 10 °C/min. After the decomposition process evolved gases are introduced into the GCMS system whereas a part of the gases is split to avoid blockage in the column or saturation of the detector. Released decomposition gases are separated using a 30 m long fused silica capillary column. The temperature of the column is set to 35 °C during the desorption process. The column is then heated up to 300 °C with a heating rate of 10 °C/min followed by an isotherm at 300 °C for 30 min. The linear velocity of the carrier gas helium is set to 40 cm/s. The separated gases and fragments are then analyzed with the quadrupole mass spectrometer with an Electron-Impact (IE) ionization source. The IE spectra are recorded at 70 eV with a mass scan of 2 scans per second. The interface between the pyrolyzer and the GC is heated up to 320 °C; the interface GC-MS to 280 °C. The temperature of the ion source is set to 230 °C. After the experiments data is analyzed using the GCMS post-run analysis from Shimadzu and F-Search from Frontier lab, whereas products are identified using NIST database.

To mimic the decomposition of materials obtained by TGA experiments a so called step wise desorption process is used (**Figure 33**).Materials are degraded at a given heating ramp to their first decomposition step. Then, evolved gases are separated and analyzed by GCMS. Afterwards the remaining material is heated up to the end temperature of the second

decomposition step and the evolved gases are again analyzed. This desorption process is continued until 800 °C following the different decomposition steps.

Besides the step wise desorption process, flash pyrolysis is performed. Therefore, materials are given for ten minutes into the pyrolyzer which is heated to a temperature of 800 °C. Released gases are analyzed directly by the GC-MS system.
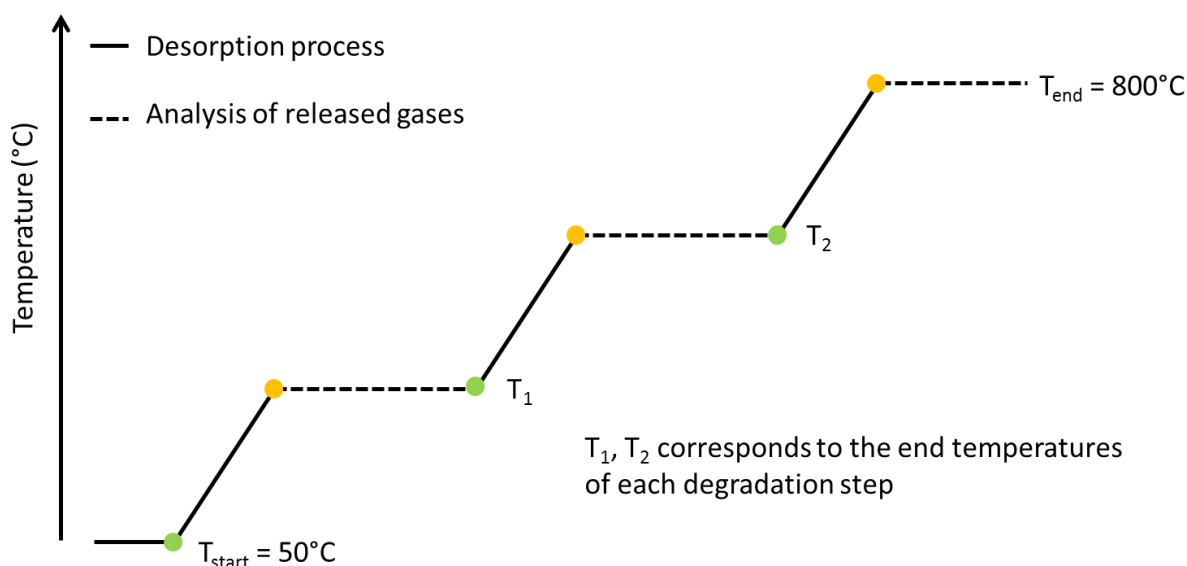
Figure 33: Schematic presentation of step wise desorption process

2.6. Condensed phase analysis

Besides an action in the gas phase, fire retardant additives can also have a condensed phase mechanism. In the following section, experimental techniques (microscopy, X-ray photoelectron spectroscopy, rheology, infrared spectroscopy, thermal treatments and solid state NMR) used to analyze the condensed phase of a material are described in details.

2.6.1. Microscopy

Scanning electron microscopy (SEM) images were taken at various levels of magnification using a Hitachi S4700 SEM at 6 kV. All samples were ultra microtomed with a diamond knife on a Leica UltraCut microtome at cryo temperature (−120 °C) to obtain smooth surfaces.

2.6.2. X-ray photoelectron spectroscopy

X-ray photoelectron spectroscopy (XPS) measurements are carried out on an AXIS Ultra^{DLD} under vacuum (p = 10^{-9} Torr). XPS is an analytical technique permitting to quantify the

amount of targeted elements and to identify their chemical or electronic state to get detailed information about the bonding of elements at the sample surface. Samples are irradiated by an X-ray beam (E = hv) generated by an high power aluminum monochromator. The energy of the X-rays is adsorbed by an atom leading to emission of a core photoelectron. The emitted photoelectron exhibits a kinetic energy ($E_{kinetic}$) depending on the incident X-ray and the binding energy ($E_{binding}$) of the atomic orbital (**Equation 9**). A constant analyzer pass energy of 40 eV is used. The kinetic energy of the emitted photoelectrons is detected by a photoelectron detector, whereas accuracy is ± 0.1 eV. Simulation of the experimental peaks was carried out using the Gaussian-Lorentzian mixture from CasaXPS software. Quantification took into account a linear background subtraction. The core level binding energies are referenced to the C 1s line of carbon contamination at 285.00 eV.

$$hv = E_{kinetic} + E_{binding}$$

Equation 9: Calculation of binding energy

2.6.3. Infrared spectroscopy

FTIR spectra are recorded between 500 and 4000 cm^{-1} on Nicolet impact 400D spectrometer. The final spectra result from 64 scans and are processed by OMNIC software with a resolution of 4 cm^{-1}.

2.6.4. Thermal treatments

Thermal treatments are carried out under in a tubular furnace in air and/or nitrogen at characteristic temperatures determined by TGA. Samples are heated up to the desired temperatures with a heating ramp of about 10 °C/min followed by an isotherm of two hours. Residues are analyzed afterwards by solid state NMR.

2.6.5. Solid state NMR

Solid state NMR is a powerful tool for determining the surrounding of a given nucleus. However, because of the low abundance of some nuclei, the radiofrequency pulse is poorly absorbed in some cases. To overcome this limitation, protons of the sample can be excited at the place of the nucleus. A dedicated sequence called crossed polarization (CP) permits to transfer this energy to atoms of lower abundance. On the other hand, the large number of

protons in the sample interferes with the decay of the isolated nucleus due to weak interactions of the spins. This results in a broadening of the signal. This drawback can be overcome by the use of a 1H dipolar decoupling (DD): a strong radio frequency signal holds the protons in a highly resonating state so that they are not able to absorb resonance from the nuclei. Finally in solid state, existence of chemical shift anisotropy has a strong effect on the spectra: peaks are broadened. When spinning at the magic angle (MAS), a minimization of the broadening is observed. All NMR data were collected and analyzed at room temperature with the TopSpin software (Bruker).

^{13}C solid state NMR spectra are recorded at 100.6 MHz (B_0 = 9.4 T) on Bruker Avance II 400 using a 4 mm standard probe. The conditions are cross-polarization (CP) ^{1}H-^{13}C (contact time of 1 ms) with dipolar decoupling (DD) and magic angle spinning (MAS) at 10 kHz. The recycle delay between two pulses is 5 s. The number of scans is 1024 and ^{13}C chemical shifts are referenced to tetramethylsilane (TMS).

^{27}Al NMR measurements are carried out at a frequency of 104.2 MHz on a Bruker Avance II 400 (B_0 = 9.4 T) with a probe head of 4 mm using MAS at 12.5 kHz. The repetition time is fixed at 1 s for all samples. The number of scans is set to 128. The reference used is 1 M solution of aluminum nitrate.

^{11}B NMR acquisitions are performed at 256.81 MHz on a Bruker Avance 800 (18.8 T) spectrometer with a probe head of 3.2 mm using MAS at 20 kHz. The number of scans is set to 256, whereas recycle delay between two pulses is 4 s. Sodium borohydride is used as reference. Signal coming from the BN stator (probe background signal) is removed by running the same experiment without the sample, then calculating the spectrum difference between the two experiments. BO_3/BO_4 ratios are estimated using Dmfit software [151].

2.6.6. Thermal conductivity

Thermal conductivity measurements are carried using Hot Disk thermal constants analyzer (TPS 2500 S) from Thermoconcept, which is based on the transient plane source method [152]. Thereby, the transient plane source element is used as a heat source and a temperature sensor at the same time. It consists of a thin layer of an electrically conducting material. During the experiment, a current passes through a Nickel spiral which leads to an

increase in temperature. The generated heat dissipates then through the sample depending on the thermal characteristic of the tested material.

Hence, the device permits to measure the change of thermal conductivity of materials versus the temperature. The thermal conductivity of a material generally describes the transport of energy in form of heat through a material. The sensor (warmth emitter) and the thermocouple are placed in between sample plates (25 x 25 x 3 mm²), whereas the sensor (r=3.189mm in mica to resist at high temperatures) is in the middle of four stacked plates (**Figure 34**). The stacked sample is put into a furnace which is directly connected to a nitrogen flow. Experiments are carried out in inert atmosphere to prevent oxidation of the sensor. Samples are heated up from 100 to 600 °C, whereas temperature is stabilized each 50 °C with less than 0.1 °C deviation. Conductivity measurements are performed by applying a power of 40 or 50 mW for 20 and 40 s respectively. For each parameter, the experiment is realized five times. The presented results are the arithmetical average of the obtained values at each temperature.

Figure 34: Arrangement of sample plates and sensor for thermal conductivity measurement

3. Conclusion

In Chapter II, the polymer and the additives as well as the preparation of the materials used in this study were presented in the first part. Afterwards, methods to evaluate mechanical properties, fire retardancy and smoke release were described. Experimental techniques used to investigate the decomposition mechanism in the gas and condensed phase, as well as methods to investigate thermal decomposition of the materials were discussed.

The following chapters describe the development of a new flame retarded EVA based material containing ATH in combination with melamine or its derivatives. Moreover, the fire retardant mechanism of selected material is investigated using the experimental techniques presented in this chapter. Chapter III is dedicated to a screening of different materials comparing their mechanical and fire retardant properties and their smoke release. Chapter IV and V are dealing with the comprehension of the mechanisms going on when EVM-materials containing ATH and melamine or its derivatives are exposed to fire.

Chapter III: Material-screening

This chapter deals with the development of a new flame retarded EVM material containing ATH in combination with melamine or its derivatives. The tested materials have to reach targeted mechanical and fire retardant properties and have to release less smoke than the virgin polymer. First, the influence of the ratio of the fillers (ATH and melamine) on mechanical properties, fire retardancy and smoke release is evaluated. Then, different phosphorous-free and phosphorous-containing melamine derivatives (in combination with ATH) are screened concerning their impact on mechanical properties, fire retardancy and smoke release in EVM materials. At the end of this chapter, promising materials are selected and their fire retardant mechanism is analyzed in details in Chapter IV and V.

1. Investigation of ratio of ATH and melamine

Literature research [54, 66, 81-84] and preliminary studies (**Appendix 1**) showed that the use of ATH as fire retardant is a promising candidate to improve fire retardant properties and to reduce smoke release of EVM materials. Due to required high loadings of ATH and the therefore resulting change of mechanical properties, ATH is combined with different conventional fire retardants. According to the literature review, it was shown that the combination of ATH with melamine (MEL) or its derivatives could lead to promising material properties concerning fire retardancy and smoke release. In this part, the effect of the ratio of ATH:MEL on mechanical properties, fire retardancy and smoke release of EVM materials is investigated. Therefore, the amount of additive is kept constant at 130 phr, whereas the ratio of ATH and melamine is varied. The following ratios of ATH:MEL are evaluated: 5:1, 10:1 and 25:1. These ratios are chosen taking into account the efficiency of the additives and the price of final material. A higher amount of melamine is not tested due to high costs of the additive and the therefore increasing price of materials with increasing melamine content.

1.1. Mechanical properties

Mechanical properties of virgin polymer, EVM-ATH and EVM-ATH-MEL materials are presented in **Table 12**. Thinking of potential applications of EVM materials, i.e. in cable and wire industry, it is important that at this stage of the study, materials exhibit a high elongation-at-break (EAB) (higher than 120 %), a tensile strength (TS) higher than 8.5 MPa and a hardness between 70 and 80 Shore A. Margin of error of EAB is ± 25 %, ± 1.5 MPa for TS and ± 1 Shore A in the case of hardness.

Virgin EVM reaches desired EAB, whereas desired TS and hardness are not reached. EVM has EAB of 209 %, a TS of 2.6 MPa and a hardness of 46 Shore A. Addition of 130 phr ATH to EVM leads to an increase in TS and hardness, which is explained by the fact that ATH is harder than the virgin polymer. The increase of the TS by adding ATH to EVM, indicates that the filler and the polymeric matrix exhibit a good compatibility leading to a propagation of the stress in the material. Moreover, it is reported that fillers act as stress concentrators in elastomers, whereas the smaller the particle size, the more efficient is the transfer of the

applied stress from the rubber matrix to the filler [153]. EVM-ATH exhibits a TS of 7.1 MPa and a hardness of 78 Shore A. EAB values of EVM and EVM-ATH are comparable (209 and 239 % respectively), the difference between the values lies in the margin of error.

Table 12: Mechanical properties of EVM materials containing ATH and MEL at different ratios

	EAB [%] ± 25	TS [MPa] ± 1.5	Hardness [Shore A] ± 1
EVM	209	2.6	46
EVM-ATH	238	7.1	78
EVM-ATH-MEL (5:1)	284	8.8	74
EVM-ATH-MEL (10:1)	287	9.3	75
EVM-ATH-MEL (25:1)	252	8.0	79

Partial replacement of ATH by MEL leads to decreased hardness values with increasing melamine content in the material possibly indicating that melamine is softer than ATH. Regarding EAB and TS of EVM-ATH-MEL materials observed values lie in the margin of error of those found for EVM-ATH. An influence of melamine on the stress transfer and elongation properties is therefore excluded.

1.2.   Fire retardancy

Fire retardant properties of EVM-ATH-MEL are investigated using MLC, LOI and UL-94 test. Results of these tests are presented in **Figure 35** and **Table 13**. Virgin EVM exhibits a peak of heat release rate (pHRR) of 510 kW/m², a total heat release rate (THR) of 97 MJ/m², a mass loss (ML) of 96 % and a time to ignition (TTI) of 67 s. EVM is not classified (NC) in UL-94 test and exhibits a LOI value of 19 vol%O_2. Addition of 130 phr of ATH to EVM (EVM-ATH) leads to significant improvement of fire retardant properties. Firstly, LOI value is increased to 33 vol%O_2 and a V-0 classification is reached for EVM-ATH. Secondly, regarding results obtained for EVM-ATH using MLC it is found that pHRR is reduced by 71% to a value of 146 kW/m² and THR is reduced by 38 % to a value of 60 MJ/m² in comparison to the virgin polymer.

Looking at MLC results for EVM-ATH-MEL materials, it is observed that partial replacement of ATH by MEL leads to ignition at shorter time of the material in comparison to EVM-ATH. The longest TTI of materials containing ATH and MEL is found for the material having a ratio of ATH:MEL of 25:1 (180 s). Concerning reduction of pHRR and THR for EVM-ATH-MEL (25:1), an improvement of fire retardant properties obtained using MLC is not found in comparison

to EVM-ATH. EVM-ATH-MEL (5:1) and EVM-ATH-MEL (10:1) exhibit both similar results in MLC experiment. Both materials have decreased pHRR and decreased TTI in comparison to EVM-ATH. EVM-ATH-MEL (5:1) has a $pHRR_1$ 118 of kW/m², a $pHRR_2$ of 89 kW/m², a THR of 60 MJ/m² and a ML of 63 %. EVM-ATH-MEL (10:1) has a $pHRR_1$ of 109 kW/m², a $pHRR_2$ of 88 kW/m², a THR of 51 MJ/m² and a ML of 61 %. In LOI test same LOI values, i.e. 33 vol%O_2, are measured for EVM-ATH-MEL materials whatever the ATH:MEL ratio. Hence, LOI values are independent of the amount of MEL in the material. UL-94 classification at the opposite depends on the ratio ATH:MEL: EVM-ATH-MEL (5:1) reaches V-0 classification, whereas V-2 classification is observed for EVM-ATH-MEL (10:1) and EVM-ATH-MEL (25:1).
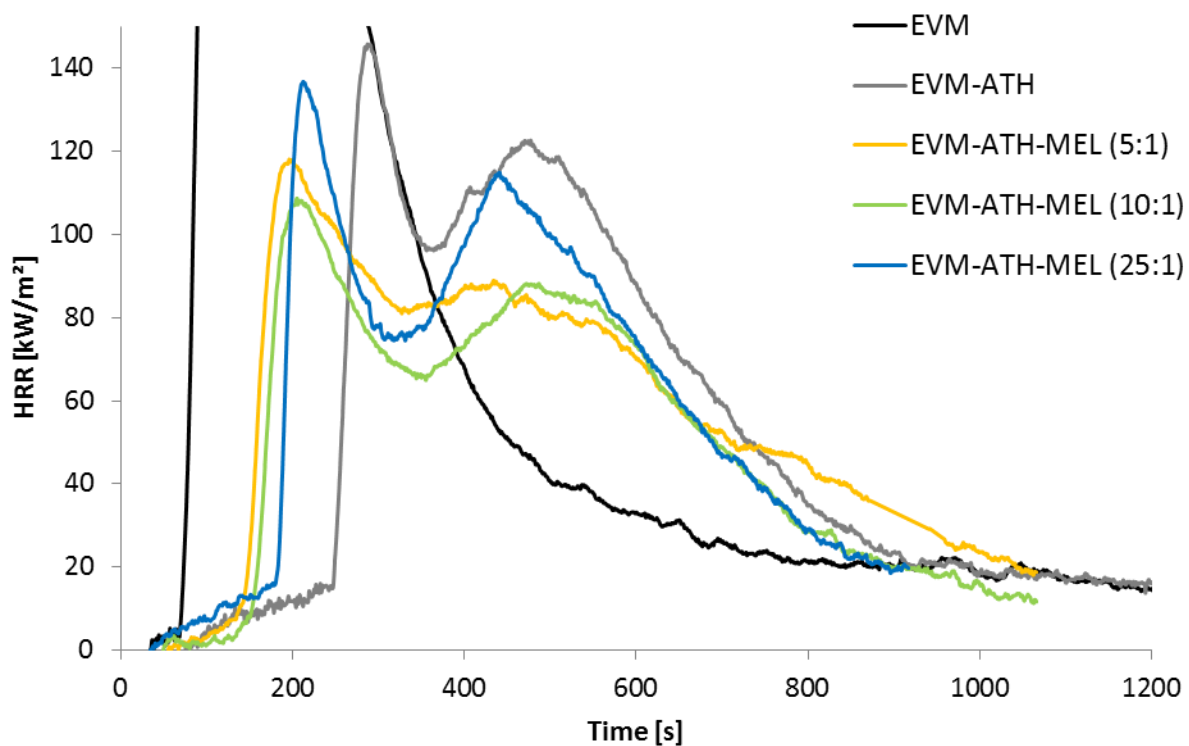
Figure 35: HRR curves for EVM materials containing ATH and MEL at different ratios

Table 13: Fire retardant properties of EVM materials containing ATH and MEL at different ratios; margin of error for MLC ± 10 %, LOI ±1 vol%O_2

	$pHRR_1$ [kw/m²]	$pHRR_2$ [kw/m²]	THR [MJ/m²]	TTI [s]	ML [%]	LOI [vol%O_2]	UL-94
EVM	510	-	97	67	96	19	NC
EVM-ATH	146	123	60	245	61	33	V-0
EVM-ATH-MEL (5:1)	118	89	60	145	63	33	V-0
EVM-ATH-MEL (10:1)	109	88	51	152	61	33	V-2
EVM-ATH-MEL (25:1)	137	115	53	180	60	33	V-2

1.3. Smoke release

Optical density curves and corresponding smoke release values are presented in **Figure 36** and **Table 14**. Virgin EVM has an total optical density (OD_{total}) of 114, a VOF4 (summation of the optical density over the first four minutes) of 87, a highest optical density value in the first four minutes (D_s4) of 1.1 and a first local maximum of optical density (D_s1) of 1.1. In smoke test, EVM ignites at 86 s. Differences in TTI of EVM in MLC and smoke test is explained by the different boundaries conditions (see **page 64** and **65**). Both experiments are carried out using an external heat flux of 35 kW/m², but the distance between the sample and the heat source is different. In smoke test the distance between the sample and the radiative heat flux is 35 mm, whereas in MLC test it is 25 mm. Moreover, in MLC test, a grid is put at the sample surface to avoid contact between the sample and the spark igniter.
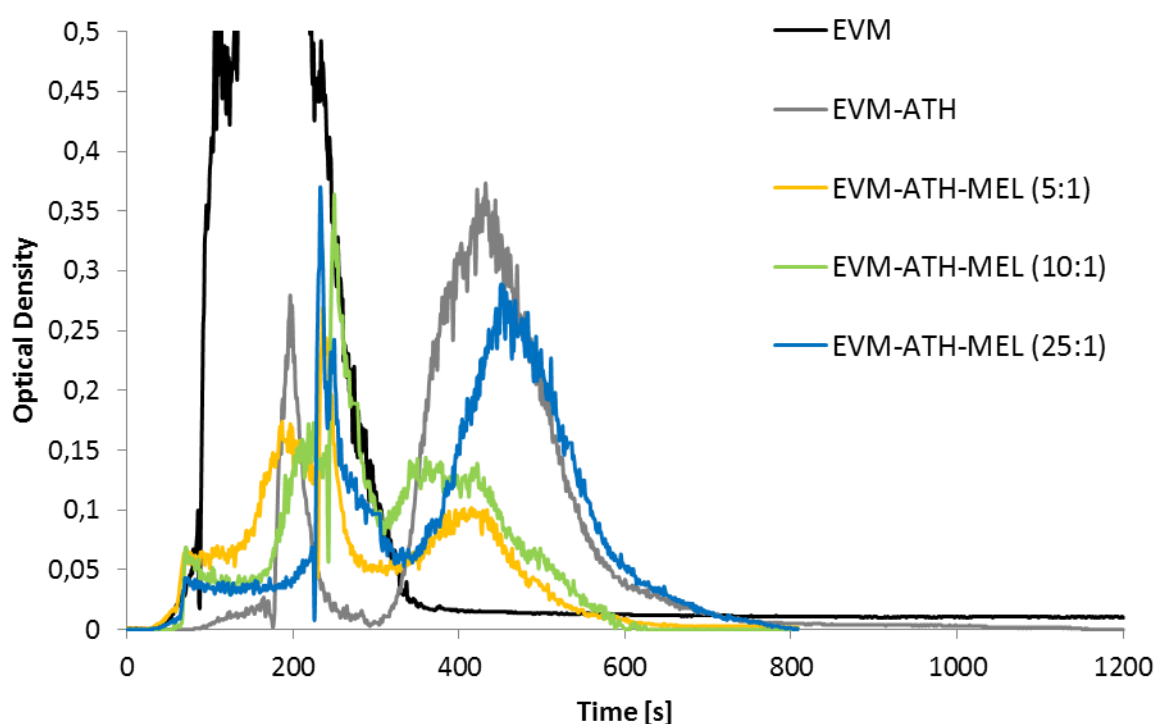
Figure 36: Smoke release curves for EVM materials containing ATH and MEL at different ratios

Addition of 130 phr ATH (EVM-ATH) results in a decrease of smoke production in comparison to the virgin polymer. EVM-ATH exhibits an OD_{total} of 67, a VOF4 of 9, a D_s4 and D_s1 of 0.3 and a D_s2 of 0.4. It is found that for EVM-ATH OD_{total} is decreased by half and VOF4 value by a factor of 10 in comparison to the virgin polymer. D_s4 and D_s1 values are decreased by a

factor of three. Moreover, TTI (176 s) of EVM-ATH is increased in comparison to the virgin polymer. Inter alia, the reduced smoke production of EVM-ATH could be explained by the lower amount of polymer. In EVM-ATH, about half of the material weight is due to the presence of the polymer. Therefore, reduction by half of the total optical density is not surprising. Nevertheless, reduction of VOF4 by a factor of 10 and decrease of the D_s values is counted as reduced smoke release.

Table 14: Smoke release of EVM materials containing ATH and MEL at different ratios; margin of error for observed values ± 10 %

	OD_{total}	VOF 4	D_s4	D_s1	D_s2	TTI [s]
EVM	114	87	1.1	1.1	-	86
EVM-ATH	67	9	0.3	0.3	0.4	176
EVM-ATH-MEL (5:1)	41	19	0.3	0.3	0.1	228
EVM-ATH-MEL (10:1)	48	13	0.3	0.4	0.1	243
EVM-ATH-MEL (25:1)	65	10	0.4	0.4	0.3	224

Partial replacement of ATH by MEL results in a change of smoke production. First of all, it is observed that TTI of EVM-ATH-MEL materials increase in comparison to EVM and EVM-ATH. It has to be noted that is the contrary to the results found during MLC experiment. Differences in TTI are due to different configurations of the two tests. In smoke test, the observed TTI values for EVM-ATH-MEL materials lie in the same range (224 – 243 s). Thus, an influence of the melamine content on TTI is not observed. Concerning total smoke production during experiment, it is found that OD_{total} for ratio ATH:MEL of 5:1 and 10:1 is decreased (OD_{total} = 41 and 48 respectively) in comparison to EVM-ATH. EVM-ATH-MEL (25:1) instead has a total optical density value of 65 which is comparable to that of EVM-ATH. Hence, partial replacement of ATH by melamine reduces the smoke production during experiment, whereas the amount of melamine in EVM-ATH-MEL (25:1) is too low to reduce smoke production efficiently. In the case of the VOF4 value, it is observed that EVM-ATH-MEL (25:1) has a VOF4 of 10 which is similar to that found for EVM-ATH (VOF4 = 9). Concerning EVM-ATH-MEL (10:1) and EVM-ATH-MEL (5:1), VOF4 values (13 and 19 respectively) are increased in comparison to EVM-ATH. This indicates that with increasing melamine content in the material, the VOF4 increases. D_s4 and D_s1 values for EVM-ATH-MEL materials are comparable to those observed for EVM-ATH, whereas D_s2 is decreased to 0.1 for EVM-ATH-MEL (10:1) and EVM-ATH-MEL (5:1). In general, partial replacement of ATH by

melamine leads to lower smoke production, whereas smoke is released earlier but total density of smoke is lower than for EVM-ATH. In the case of EVM-ATH no smoke is released before ignition of the material. For EVM-ATH-MEL materials instead smoke is already evolved before ignition.

1.4. Conclusion

The influence of the melamine content on material properties of EVM-ATH-MEL materials was investigated in this part. Moreover, material properties of EVM-ATH-MEL were compared to those of EVM-ATH. It was found that addition of ATH to the polymeric matrix enhances fire retardancy and reduces smoke production, whereas reduction seems only to be due to reduced amount of polymer in the material. Smoke was released at longer times and over a longer period of time for EVM-ATH.

Partial replacement of ATH by melamine led to comparable fire retardant properties in MLC and LOI test as found for EVM-ATH. V-0 classification was only reached for the ratio of 5:1. Smoke production of EVM-ATH-MEL materials was significantly decreased in comparison to EVM-ATH when a sufficient amount of melamine is present in the material. A ratio of ATH and MEL of 25:1 is found to be too low to reduce smoke production, whereas a ratio of 10:1 and 5:1 is sufficient to reduce smoke successfully. It has to be noted that the combination of ATH and melamine in EVM led to reduced smoke production but also to ignition at shorter time in comparison to EVM-ATH in MLC experiment.

Comparing the different ATH-MEL ratios it was found that 5:1 seems to be most promising. EVM-ATH-MEL (5:1) was the only material that reaches V-0 classification. Smoke production of the ATH:MEL based material including ratio of 5:1 and 10:1 was found to be reduced in comparison to EVM-ATH. From now the following screening is performed with a ratio of 5:1 of ATH and another fire retardant additive. In the next step, ATH is combined with different melamine derivatives to overcome the main drawback of EVM-ATH-MEL, its early ignition in MLC test. First phosphorous free melamine derivatives in combination with ATH are tested evaluating their mechanical and fire retardant properties as well as smoke release. Then, phosphorous-containing melamine derivatives are considered.

2. Combination of ATH with phosphorous-free derivatives

In this part, EVM materials containing ATH in combination with melamine or its phosphorous-free derivatives are screened according to their mechanical properties, fire retardancy and release of smoke in case of fire. The amount of additive, i.e. 130 phr and ratio of ATH and compound X, is kept constant (5:1). The properties of the combination of ATH with PPM, a poly-melamine compound, melamine cyanurate (MC) or melamine borate (MB) are investigated and compared to those obtained for EVM-ATH-MEL. The choice of PPM, MC and MB is explained by their known fire retardant activity or by the fact that these additives are relatively new on the market and thus their fire retardant effect is not well reported yet. PPM is a new fire retardant compound which is known to enhance fire retardancy of PP [154] but has not been tested in EVM materials up to now. Due to its poly-melamine structure it is supposed to have similar or even enhanced fire retardant effects as melamine. In the case of MB, fire retardant effect is reported in literature [155-157]. Bodzay et al. [158] investigated release of gases of EVA (28 %VA) containing ATH and MB whereas fire retardancy is not discussed in this work. MC as fire retardant additive is mainly used in polyamide [159-161]. The use of MC in combination with MDH in EVA materials is also reported [102], whereas ratio of MDH and MC is 50:1.

2.1. Mechanical properties

Mechanical properties of materials tested in this part are presented in **Table 15**. Tested materials reach all the desired mechanical properties. In comparison to EVM-ATH-MEL, the material containing the "poly-melamine" compound PPM (EVM-ATH-PPM), has an increased hardness and a decreased EAB whereas the difference of the TS lies in the margin of error. EVM-ATH-PPM, has an EAB of 216 %, a TS of 10.1 MPa and a hardness of 78 Shore A. In the case of EVM-ATH-MC and EVM-ATH-MB, EAB and TS are comparable to results observed for EVM-ATH-MEL. Hardness of EVM-ATH-MB is comparable to that found for EVM-ATH-MEL, whereas hardness of EVM-ATH-MC is increased in comparison to EVM-ATH-MEL. EVM-ATH-MC has an EAB of 251 %, a TS of 7.7 MPa and hardness of 80 Shore A. EVM-ATH-MB has an EAB of 243 %, a TS of 6.6 MPa and a hardness of 75 Shore A.

Increased hardness of EVM-ATH-MC and EVM-ATH-PPM is due to the fact the MC and PPM are harder than MEL leading to an increase of hardness in comparison to EVM-ATH-MEL. Increase of TS for EVM-ATH-PPM indicates that PPM has better stress transfer properties than MEL in EVM-ATH-MEL, whereas interaction with EVM leads to lower EAB.

Table 15: Mechanical properties of EVM materials containing ATH in combination with melamine or its phosphorous-free derivatives

	EAB [%] ± 25	TS [MPa] ± 1.5	Hardness [Shore A] ± 1
EVM	209	2.6	46
EVM-ATH	238	7.1	78
EVM-ATH-MEL	284	8.8	74
EVM-ATH-PPM	216	10.1	78
EVM-ATH-MC	251	7.7	80
EVM-ATH-MB	243	6.6	75

2.2. Fire retardancy

Fire retardant properties obtained using MLC, LOI and UL-94 test for EVM materials containing ATH in combination with melamine or its phosphorous-free derivatives are presented in **Table 16** and **Figure 37**. At a first glance, it is found that EVM-ATH-PPM, EVM-ATH-MC and EVM-ATH-MB exhibit similar values like EVM-ATH-MEL in terms of pHRR, THR and ML. It is found that materials containing phosphorous-free melamine derivatives exhibit longer TTI than EVM-ATH-MEL, whereas observed times are similar to that of EVM-ATH. EVM-ATH-PPM has a TTI of 276 s which is a longer time than observed for EVM-ATH-MC and EVM-ATH-MB which ignite at 201 and 195 s respectively.

Table 16: Fire retardant properties of EVM materials containing ATH in combination with melamine or its phosphorous-free derivatives; margin of error for MLC ± 10 %, LOI ±1 vol%O$_2$

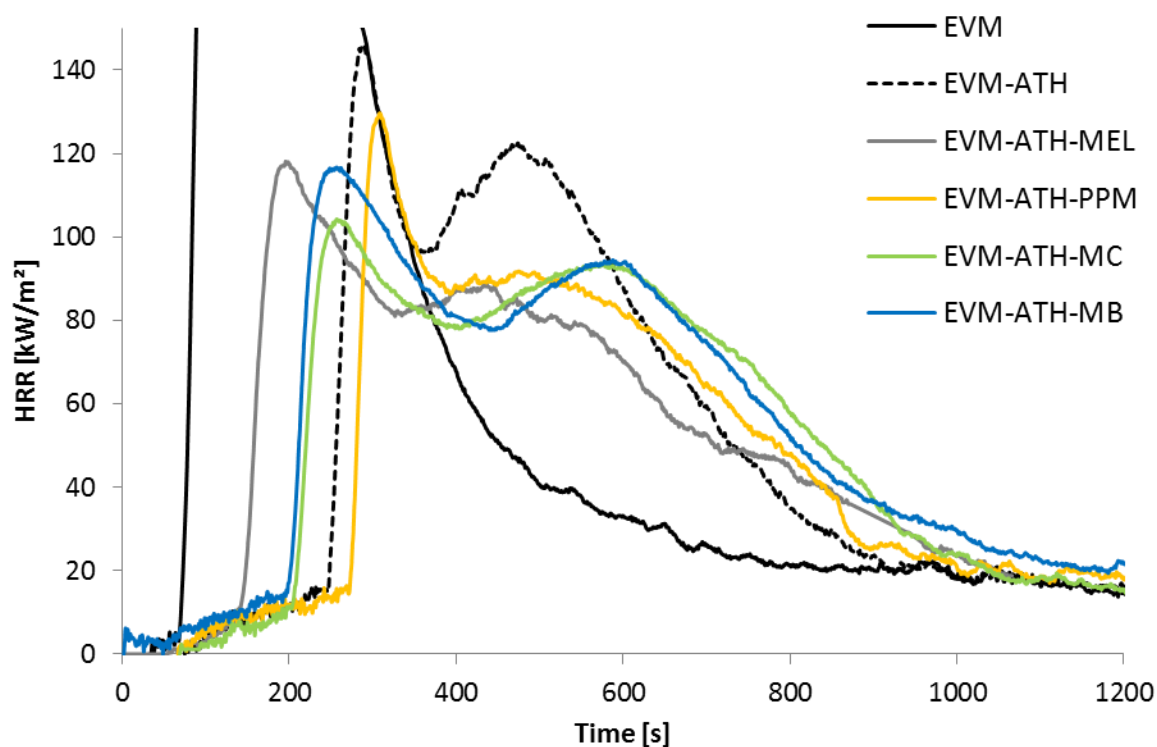|	pHRR$_1$ [kW/m²]	pHRR$_2$ [kW/m²]	THR [MJ/m²]	TTI [s]	ML [%]	LOI [vol%O$_2$]	UL-94
EVM	510	-	97	67	96	19	NC
EVM-ATH	146	123	60	245	61	33	V-0
EVM-ATH-MEL	118	89	60	145	63	33	V-0
EVM-ATH-PPM	125	92	55	276	64	30	V-0
EVM-ATH-MC	104	94	61	201	66	31	V-0
EVM-ATH-MB	117	94	65	195	64	35	V-0

Figure 37: HRR curves for EVM materials containing ATH in combination with melamine or its

phosphorous-free derivatives

Regarding UL-94 test, it is found that all materials are classified V-0. LOI values obtained for EVM-ATH-PPM (30 vol%O_2) and EVM-ATH-MC (31 vol%O_2) are comparable to those found for EVM-ATH-MEL and EVM-ATH (33 vol%O_2). In the case of EVM-ATH-MB instead, a higher LOI of 35 vol%O_2 is observed.

2.3. Smoke release

The results obtained with the smoke test for materials containing ATH in combination with melamine or its derivatives are presented in **Figure 38** and **Table 17**. In general, it is found that combination of ATH with PPM, MC or MB leads to comparable results in terms of smoke release during experiment as observed for EVM-ATH-MEL. EVM-ATH-PPM has an OD_{total} of 54, a VOF4 of 10, a D_s4 of 0.3, a D_s1 of 0.3 and a D_s2 of 0.2. EVM-ATH-MC has an OD_{total} value of 55, a VOF4 of 12, a D_s4, D_s1 and D_s2 of 0.2. EVM-ATH-MB has a total OD_{total} of 49, a VOF 4 of 14, a $Ds4$ of 0.2 and the D_s1 and D_s2 values lie at 0.4 and 0.1 respectively. As it is found during MLC experiment, the most significant difference between the tested materials is their TTI. Longest TTI of 302 s is detected for EVM-ATH-MB which is increased in comparison to EVM-ATH and EVM-ATH-MEL. TTI observed for EVM-ATH-MC (197 s) lies in the margin of

error of the TTI observed for EVM-ATH-MEL (228 s). In the case of EVM-ATH-PPM a TTI of 148 s is observed indicating that the material ignite at shorter times than EVM-ATH-MEL. As mentioned above, TTI values detected using MLC and smoke test are different due to the different test conditions (see **page 64** and **65**). Therefore, it is not surprising that tendencies of TTI evolution are different in MLC and smoke test. EVM-ATH-PPM for example exhibits earliest TTI in smoke test but longest TTI in MLC experiment.
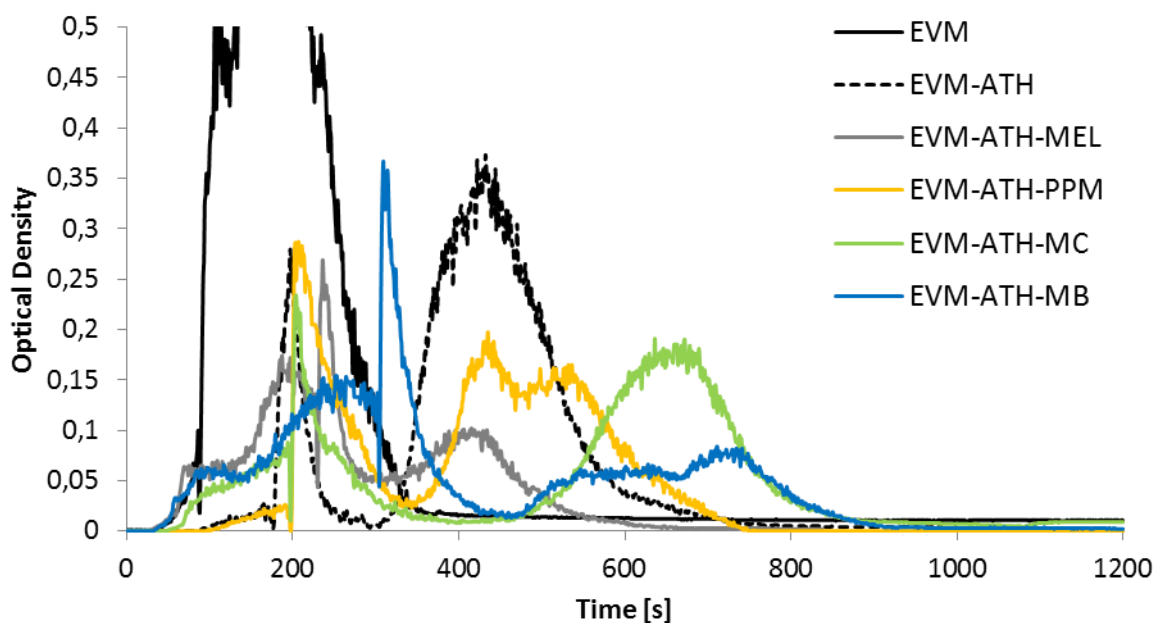

Figure 38: Smoke release curves for EVM materials containing ATH in combination with melamine or its phosphorous-free derivatives

Table 17: Smoke release of EVM materials containing ATH in combination with melamine or its phosphorous-free derivatives; margin of error for observed values ± 10 %

	OD_{total}	VOF 4	D_s4	D_s1	D_s2	TTI [s]
EVM	114	87	1.1	1.1	-	86
EVM-ATH	67	9	0.3	0.3	0.4	176
EVM-ATH-MEL	45	19	0.3	0.3	0.1	228
EVM-ATH-PPM	54	10	0.3	0.3	0.2	148
EVM-ATH-MC	55	12	0.2	0.2	0.2	197
EVM-ATH-MB	49	14	0.2	0.4	0.1	302

2.4. Conclusion

Investigation of the mechanical properties, fire retardancy and smoke release of EVM materials containing ATH in combination with phosphorous-free melamine derivatives (ratio

5:1) showed that replacement of melamine by melamine borate (MB) leads to better fire retardant properties than observed for EVM-ATH-MEL. The main drawback of EVM-ATH-MEL, its shorter ignition compared to EVM-ATH, was reduced using MB instead of melamine. EVM-ATH-MB ignited at longer time than EVM-ATH-MEL and this was observed for both MLC and smoke release experiment. Mechanical properties and smoke release of EVM-ATH-MB were found to be comparable to that of EVM-ATH-MEL. The use of EVM-ATH-PPM and EVM-ATH-MC as fire retarded material was excluded due to the fact that both materials exhibit reduced fire retardancy (lower LOI values) in comparison to EVM-ATH-MEL, whereas smoke release was comparable to EVM-ATH.

In the next part, ATH is combined with phosphorous-containing melamine derivatives.

3. Combination of ATH with phosphorous-containing melamine derivatives

This part of the screening deals with combination of ATH with phosphorous containing melamine derivatives. EVM materials contain 130 phr of additives, whereas the ratio of ATH and the derivative is set to 5:1. Materials are screened according their mechanical properties, fire retardancy and smoke release. Here, the following phosphorous-containing melamine derivatives are considered: melamine orthophosphate (MP), two melamine polyphosphate (MP200, MP200-70), melamine pyrophosphate (B311), melamine-poly (aluminum phosphate) (SF200) and melamine-poly (zinc phosphate) (SF400). These phosphorous-containing melamine derivatives are chosen, because most of them, i.e. MP, MP200 and B311 are known to enhance fire retardant properties of EVA materials [86]. SF200 and SF400 instead are relatively new fire retardant additives known to enhance the flame retardancy of PA66 [162] and have not been tested in EVM yet.

Due to the fact that the particle size of fire retardant additives plays a role on material properties, two different melamine polyphosphate compounds are tested. **Table 18** presents particle sizes of all additives used in this part. As it is seen, except from MP200-70 having a D_{99} value of 70 µm, the tested compounds have a major particle size of around 25 µm.

Table 18: Particle size of phosphorous containing melamine derivatives

Additive	Particle size
MP	$D_{98} = 25$ µm
MP200	$D_{98} = 25$ µm
MP200-70	$D_{99} = 70$ µm
B311	$D_{50} = 10$ µm
SF200	$D_{90} < 30$ µm
SF400	$D_{90} < 30$ µm

3.1. Mechanical properties

Mechanical properties of EVM materials containing ATH in combination with phosphorous-containing melamine derivatives are presented in **Table 19**. As it is seen, all tested materials reach desired mechanical properties. It is found that hardness of tested materials is comparable for all tested materials (76 - 79 Shore A). The observed hardness values are

comparable to that found for EVM-ATH but increased in comparison to EVM-ATH-MEL. This indicates that phosphorous-containing melamine additives exhibit higher hardness than melamine itself. In the case of TS, observed values are also comparable to that of EVM-ATH-MEL. For EAB values, instead only EVM-ATH-MP (EAB = 248 %) and EVM-ATH-B311 (EAB = 255 %) reach values lying in the margin of error of that of EVM-ATH-MEL (EAB = 284 %). The other materials exhibit lower EAB values. Concerning materials containing MP200 and MP200-70, it is found that mechanical properties do not depend on the particle size of the additive.

Table 19: Mechanical properties of EVM materials containing ATH in combination with different phosphorous-containing melamine derivatives

	EAB [%] ± 25	TS [MPa] ± 1.5	Hardness [Shore A] ± 1
EVM	209	2.6	46
EVM-ATH	238	7.1	78
EVM-ATH-MEL	284	8.8	74
EVM-ATH-MP	248	7.4	77
EVM-ATH-MP200	197	8.3	78
EVM-ATH-MP200-70	216	8.4	76
EVM-ATH-B311	255	7.5	78
EVM-ATH-SF200	199	8.9	79
EVM-ATH-SF400	200	9.1	78

3.2. Fire retardancy

Fire retardant properties are presented in **Figure 39** and **Table 20**. As it is seen, MLC results of EVM materials containing ATH in combination with different phosphorous-containing melamine compounds exhibit similar results concerning pHRR, THR and ML as EVM-ATH-MEL. $PHRR_1$ is around 124 kW/m² and $PHRR_2$ around 80 kW/m², whereas observed THR values are between 54 and 62 MJ/m². Most significant differences concern the TTI. Materials containing phosphorous-containing melamine derivatives have comparable TTI as observed for EVM-ATH-MEL (TTI = 145 s) except EVM-ATH-B311 (TTI = 192 s) which ignites at longer times. Nevertheless, this material does not reach the TTI of EVM-ATH of 245 s. All materials expect EVM-ATH-SF200 (not classified) are classified V-0 in UL-94 test. Looking at LOI values of materials, it is found that partial replacement of ATH by phosphorous-containing melamine derivatives leads to an increase in LOI in comparison to EVM-ATH or EVM-ATH-

MEL (33 vol%O_2). The LOI values are comparable for the different phosphorous containing materials (LOI is 37 and 38 vol%O_2 respectively). Influence of the particle size of melamine polyphosphate on fire retardant properties was not detected.
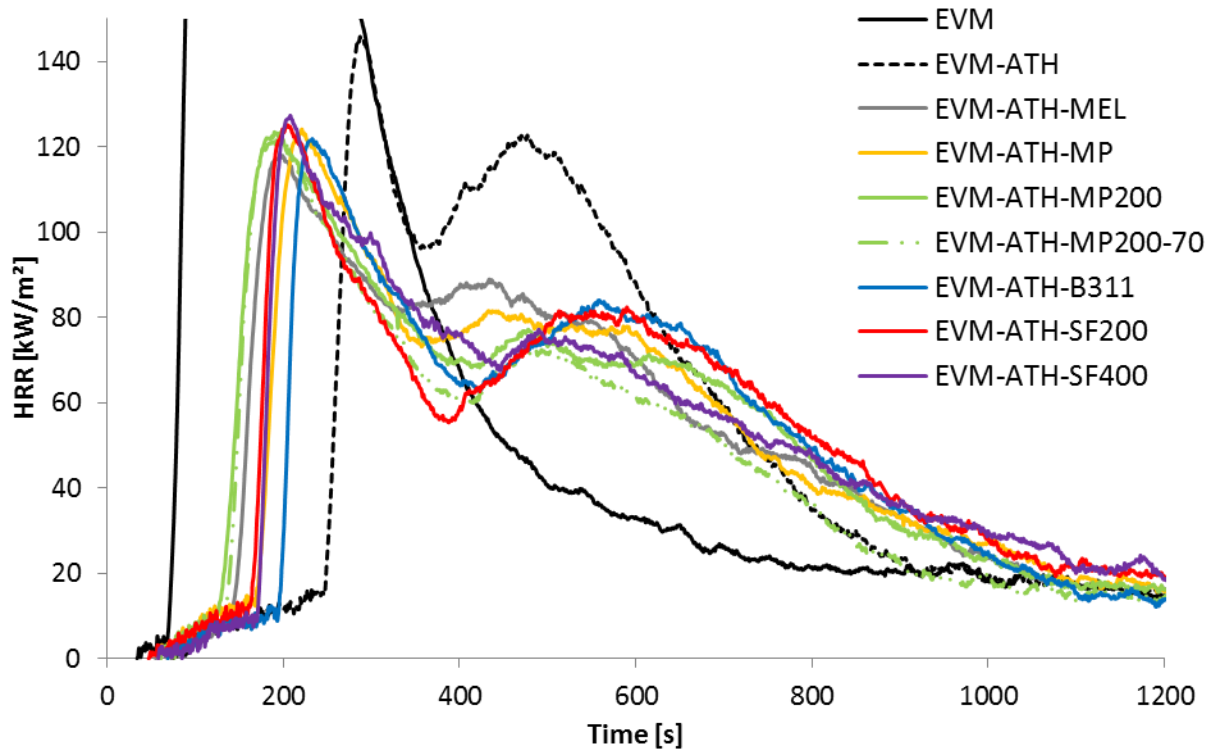

Figure 39: HRR curves for EVM materials containing ATH in combination with different phosphorous-containing melamine derivatives

Table 20: Fire retardant properties of EVM materials containing ATH in combination with different phosphorous-containing melamine derivatives; margin of error for MLC ± 10 %, LOI ±1 vol%O_2

	pHRR$_1$ [kW/m²]	pHRR$_2$ [kW/m²]	THR [MJ/m²]	TTI [s]	ML [%]	LOI [vol%O_2]	UL-94
EVM	510	-	97	67	96	19	NC
EVM-ATH	146	123	60	245	61	33	V-0
EVM-ATH-MEL	118	89	60	145	63	33	V-0
EVM-ATH-MP	124	78	60	167	64	38	V-0
EVM-ATH-MP200	123	77	62	128	63	38	V-0
EVM-ATH-MP200-70	122	72	54	132	62	38	V-0
EVM-ATH-B311	122	84	58	192	64	37	V-0
EVM-ATH-SF200	125	82	61	163	60	38	NC
EVM-ATH-SF400	127	77	60	171	60	37	V-0

3.3. Smoke release

Smoke release curves and corresponding values are presented in **Figure 40** and **Table 21**. Comparing the total smoke production (OD_{total}) of tested materials during smoke test it is seen that only EVM-ATH-MP and EVM-ATH-B311 exhibit comparable smoke production as observed for EVM-ATH-MEL, i.e. lower smoke production than EVM-ATH. The other tested materials produce more smoke than EVM-ATH-MEL during the experiment. Therefore, only the results of latter materials is discussed in this part even if some of the other materials exhibit significantly longer TTI than EVM-ATH-MEL. VOF4 and Ds values of EVM-ATH-MP and EVM-ATH-B311 are comparable to those of EVM-ATH-MEL. TTI at the opposite is different, EVM-ATH-MP ignites at 578 s and EVM-ATH-B311 at 475 s which is at significantly longer times in comparison to EVM-ATH-MEL (228 s). TTI found in smoke test are different to that observed using MLC due to different test configurations (see **page 64** and **65**).

Materials containing MP200 and MP200-70 exhibit comparable results in smoke test. As observed for mechanical properties and fire retardancy, an influence of the particle size on smoke production is not found.
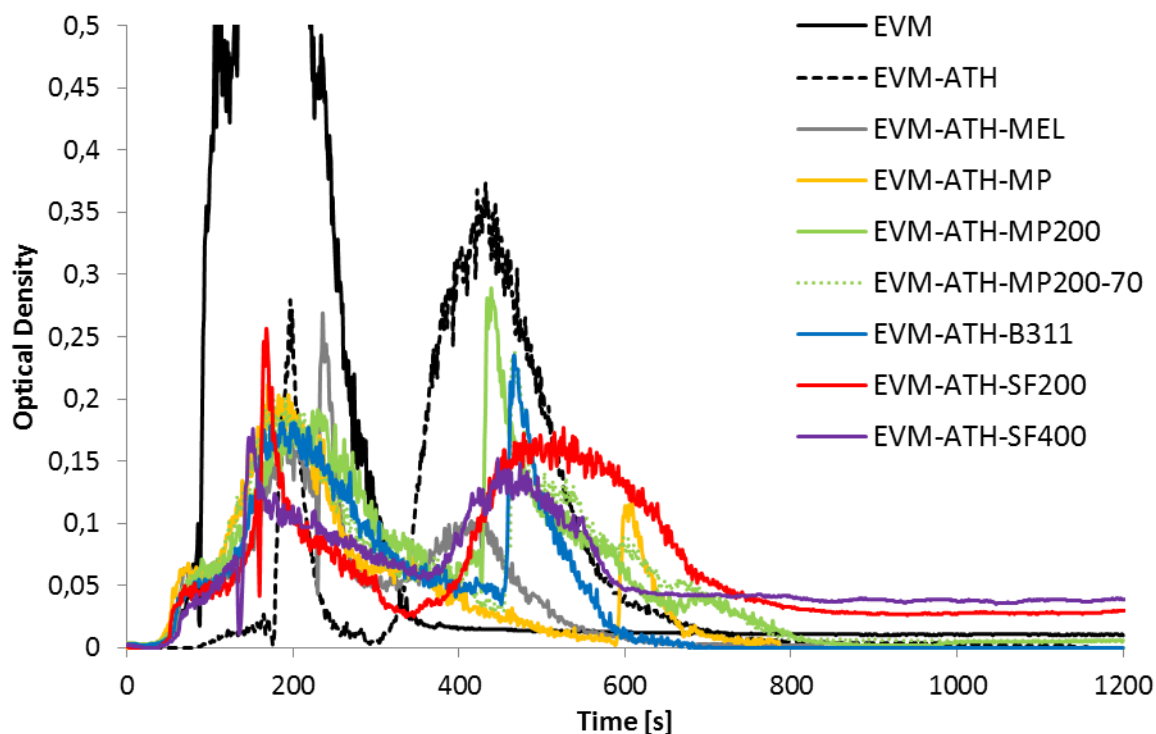

Figure 40: Smoke release curves for EVM materials containing ATH in combination with different phosphorous-containing melamine derivatives

Table 21: Smoke release of EVM materials containing ATH in combination with different phosphorous-containing melamine derivatives; margin of error for observed values ± 10 %

	OD$_{total}$	VOF 4	D$_s$4	D$_s$1	D$_s$2	TTI [s]
EVM	114	87	1.1	1.1	-	86
EVM-ATH	67	9	0.3	0.3	0.4	176
EVM-ATH-MEL	45	19	0.3	0.3	0.1	228
EVM-ATH-MP	43	23	0.2	0.2	0.1	578
EVM-ATH-MP200	68	21	0.2	0.2	0.3	425
EVM-ATH-MP200-70	65	22	0.2	0.2	0.2	458
EVM-ATH-B311	49	20	0.2	0.2	0.2	475
EVM-ATH-SF200	76	16	0.3	0.3	0.2	158
EVM-ATH-SF400	71	15	0.2	0.2	0.2	135

3.4. Conclusion

Replacement of melamine by phosphorous-containing melamine derivatives resulted in comparable fire retardant properties obtained using MLC and UL-94 test as found for EVM-ATH-MEL except of EVM-ATH-SF200 which was none classified in UL-94. LOI values were significantly increased when phosphorous melamine derivatives are used in combination with ATH. Despite improvement of the fire retardant properties, some phosphorous-containing melamine derivatives were found to increase smoke production in comparison to EVM-ATH-MEL. Only the combination of ATH with melamine pyrophosphate (B311) and melamine orthophosphate (MP) released the same quantity of smoke as found for EVM-ATH-MEL. Moreover, EVM-ATH-MP significantly ignited at longer times than EVM-ATH and EVM-ATH-MEL in smoke test. In MLC test, EVM-ATH-B311 reached a TTI at longer times than EVM-ATH-MEL but at shorter time than EVM-ATH.

Concerning all tested material properties, a dependence of the particle size of melamine polyphosphate on mechanical and flame retardant properties as well as smoke release of EVM materials was not found.

4. Conclusion of material screening

Chapter III was dedicated to the screening of different fire retardant additives and their influence on mechanical properties, fire retardancy and smoke release of EVM materials. It was found that addition of 130 phr ATH enhances fire retardant properties of EVM materials. Smoke production of EVM-ATH was reduced in comparison to the virgin polymer due to lower polymer content in the material, whereas smoke was released later and over a longer period of time. Mechanical properties of EVM-ATH were changed in comparison to EVM due to the presence of 55 wt% filler. Partial replacement of ATH by melamine in a ratio of 5:1 resulted in similar fire retardant properties, whereas EVM-ATH-MEL ignited at shorter times in MLC experiment compared to EVM-ATH. The main advantage of the combination of ATH and melamine was its decreased smoke release in comparison to EVM-ATH. Other tested ratios of ATH and melamine, i.e. 10:1 and 25:1 were excluded due to the fact that both materials did not reach V-0 classification and smoke production was found to be reduced with increasing melamine content in the material.

Then, melamine was replaced by different phosphorous-free and phosphorous-containing melamine derivatives expecting to overcome shorter TTI in MLC test. Evaluation of material properties of EVM materials containing ATH in combination with phosphorous-free melamine derivatives showed that melamine borate (MB) is the best choice to replace MEL. EVM-ATH-MB ignites at longer time than EVM-ATH-MEL in MLC and smoke test maintaining mechanical properties, fire retardancy and smoke release of EVM-ATH-MEL. In the case of phosphorous-containing melamine derivatives, replacement of melamine by melamine pyrophosphate (B311) or melamine orthophosphate (MP) resulted firstly in increased LOI value in comparison to EVM-ATH-MEL while other fire retardant properties were comparable. Secondly, EVM-ATH-B311 and EVM-ATH-MP kept reduced smoke production of EVM-ATH-MEL in comparison to EVM-ATH. Moreover, both materials exhibited longer TTI than EVM-ATH and EVM-ATH-MEL in smoke test and EVM-ATH-B311 ignited at longer time than EVM-ATH in MLC test, but TTI value of EVM-ATH was always longer.

In the following study, a phosphorous containing and a phosphorous-free material are examined. At first, influence of melamine on reduced smoke production and shorter ignition in MLC test in comparison to EVM-ATH has to be understood. Therefore the condensed

phase and the gas phase mechanism of EVM-ATH-MEL have to be investigated and compared to that of EVM-ATH. Thus, Chapter IV is dedicated to the comprehension of the influence of melamine in the flame retarded mode of action of the system EVM-ATH-MEL.

As described above, shorter ignition of EVM-ATH-MEL can be overcome by using MB, MP or B311 instead of melamine. One of the goals of this work is to design EVM material with high fire retardant properties and low smoke release in the case of fire. Due to the fact that EVM materials are often used in the cable and wire industry, materials also have to exhibit high water resistance. It is known that phosphorous containing materials can exhibit low resistance against the attack of water. Thus, EVM-ATH-MP and EVM-ATH-B311 are not further discussed in this study. Nevertheless, the fire retardant mechanism of EVM-ATH-MP is presented in Appendix 2 (**page 216**) [163] to allow comparison of different melamine derivatives in combination with ATH in EVM. It is decided to investigate the role of MB in EVM-ATH-MB in Chapter V. The reasons for the increased TTI in MLC experiment as well as the reduced smoke release of EVM-ATH-MB are analyzed in details.

Chapter IV: Mode of action of EVM-ATH and EVM-ATH-MEL

In this chapter, EVM-ATH and EVM-ATH-MEL are analyzed concerning the dispersion of the additives in the polymeric matrix, hydrothermal aging in distilled and sea water, thermal behavior and fire retardant mechanism in the gas and condensed phase.

1. Dispersion of the additives in the polymer matrix

It is known that dispersion of additives in the polymeric matrix plays an important role on mechanical properties and on fire retardancy. Therefore, the dispersion of ATH and MEL in EVM-ATH and EVM-ATH-MEL is examined using SEM. **Figure 41 (a)** shows a SEM image of the ATH particles in EVM-ATH. ATH particles are evenly dispersed in the polymeric matrix exhibiting a size lying between 0.5 and 1 µm. This corresponds to the data indicated by the supplier for the particle size of ATH (D_{50} = 0.9 µm). Dispersion of ATH and MEL particles in EVM-ATH-MEL is shown in **Figure 41 (b,c)**. It is seen that ATH particles are evenly dispersed in EVM-ATH-MEL. This shows that addition of melamine to an EVM-material containing ATH does not change the dispersion of the mineral filler. Besides to small ATH particles, bigger ones (encircled) are observed in the polymeric matrix. These particles having a size of 3 to 15 µm are evenly dispersed in the material. Due to the fact that in EVM-ATH, the big particles are not observed it is supposed that it is melamine. Moreover, particle size corresponds to that of melamine reported by the supplier.
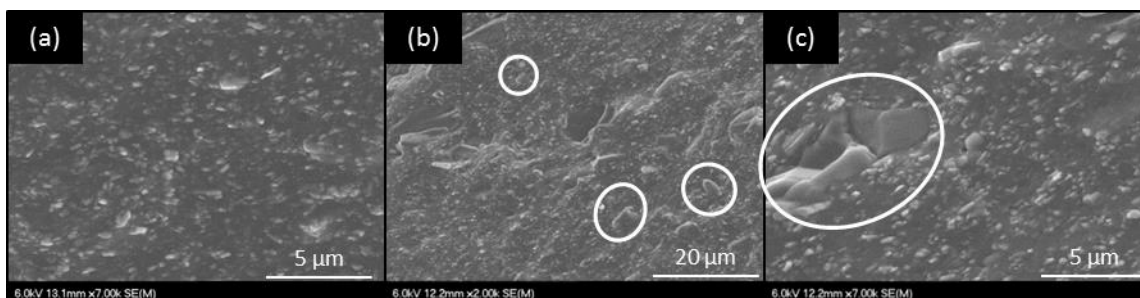

Figure 41: SEM image EVM-ATH (a) and EVM-ATH-MEL (b,c)

2. Water swelling behavior of EVM-ATH and EVM-ATH-MEL

As it was already mentioned before, it is important that besides good fire retardant properties and low smoke production, materials exhibit mechanical properties meeting the specifications of their application, especially for cable and wire industry. In this part, change of mechanical properties after immersion in distilled and sea water is investigated for EVM-ATH and EVM-ATH-MEL. Then, change of material structure after hydrothermal aging test is analyzed using FTIR and SEM.

2.1. Change of mass, volume and mechanical properties

Change of mass and volume after immersion in water of EVM-ATH and EVM-ATH-MEL is presented in **Figure 42**. After immersion of EVM-ATH in distilled water, the mass of the material increases of 6.8 % whereas volume increases of 10.2 %. Immersion in sea water results in an increase of mass of 3.0 % and an increase of volume of 4.2 %. Partial replacement of ATH by MEL leads to lower increases in mass and volume after immersion of the material in distilled water in comparison to EVM-ATH. It can be seen that for EVM-ATH-MEL in distilled water mass increases of 3.8 % and volume of 6.9 %. Concerning change of mass and volume of EVM-ATH-MEL in sea water, it is found that values are equal (marge of error) to those obtained for EVM-ATH.
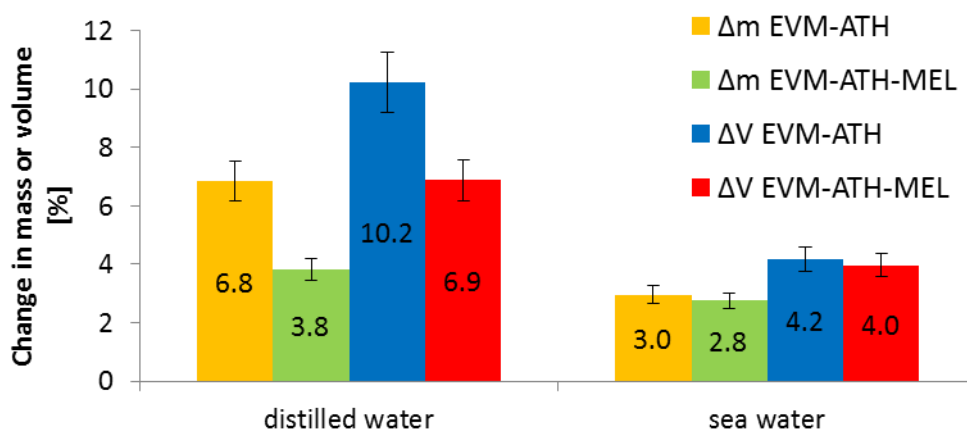

Figure 42: Change of the mass and volume during hydrothermal aging of EVM-ATH and EVM-ATH-MEL

In general, changes of mass and volume for EVM-ATH and EVM-ATH-MEL in both test configurations can be explained by penetration of water molecules into the polymeric

matrix. As it is seen, penetration of water into the material is lower for EVM-ATH-MEL than for EVM-ATH in distilled water. Moreover, changes of mass and volume are significantly lower when the materials are immersed in sea water. It is reported that the presence of ions reduces penetration capacity of water due to an increased chemical potential [164]. It is assumed that lower change of mass and volume for EVM-ATH-MEL is due to an increased ionic strength of the surrounding medium leading to limitation of water molecule penetration into the material. It is important to know that solubility of melamine depends on temperature and ionic strength of the medium. In general, melamine is not very soluble at room temperature (0.3 g per 100g water). However, its solubility increases with increasing temperature [165]. Melamine solubility increases from 0.3 g of melamine per 100 g of water at room temperature to 0.6 g at 35 °C and to 2.4 g at 75 °C. Moreover, it is reported that the lower ion concentration in the water, the more melamine solubility increases [166]. Due to the fact that EVM-ATH-MEL is immersed in distilled water (absence of ions), solubility of melamine increases additionally. Thus, ionic strength of the medium is supposed to increase which in turn decreases penetration capacity of water molecules.

Generally, the solubilization of melamine in EVM-ATH-MEL has to be taken into account for the change of mass during hydrothermal aging. Penetration of water molecules into the structure of EVM-ATH-MEL leading to increase of mass, is higher than the observed value due to mass loss by solubilization of melamine and compensation of the lost mass by penetrated water molecules. Especially for hydrothermal aging in distilled water compensation of mass lost by melamine solubilization has to be taken into account. Thus, decreased change of mass of EVM-ATH-MEL in comparison to EVM-ATH in distilled water can also be due to loss of melamine. In sea water, melamine is less soluble and thus mass compensation is less than in distilled water.

Analysis of changes of mass and volume during hydrothermal aging of EVM-ATH and EVM-ATH-MEL evidenced penetration of water into the material structure. The effect of the penetrated water molecules on the mechanical properties, i.e. tensile strength (TS), elongation-at-break (EAB) and hardness is investigated in the next step **(Figure 43)**. As it is seen, tensile strength increases for EVM-ATH and EVM-ATH-MEL after immersion in distilled and sea water in comparison to values obtained before water swelling test. TS values obtained after immersion in both water types are comparable for both tested materials.

Before immersion, a TS of 8.7 and 8.6 MPa respectively is measured for EVM-ATH and EVM-ATH-MEL. After immersion (distilled and sea water) both materials exhibit TS jumping from 8.6 to around 13 MPa. Increase of TS after hydrothermal aging is explained by the penetration of water molecules into the material structure. The applied stress is transferred from the rubber matrix to the water molecules which act as stress concentrators [153].
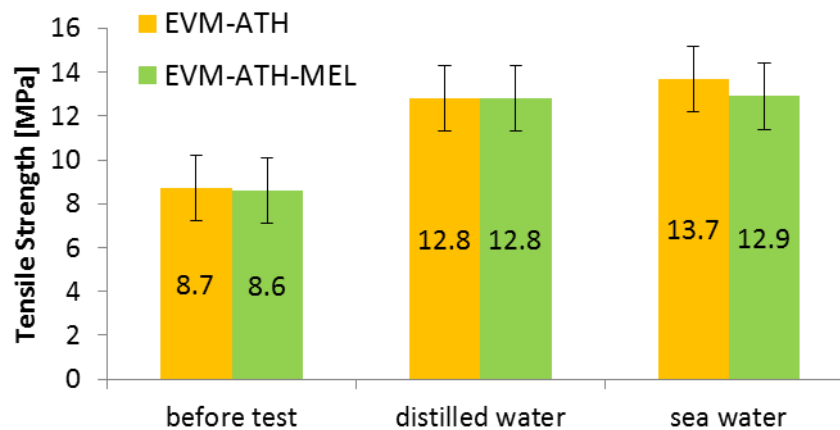

Figure 43: Tensile strength before and after hydrothermal aging for EVM-ATH and EVM-ATH-MEL

Change of EAB after immersion in water for EVM-ATH and EVM-ATH-MEL has the same tendencies like tensile strength values (**Figure 44**). EAB increases for both materials in both test configurations, moreover all values observed after immersion are comparable. Before test, elongation-at-break is 247 % for EVM-ATH and 261 % for EVM-ATH-MEL. After immersion in distilled and sea water, EAB increases to values around 350 % for both materials in both test configurations. As for TS, increase of EAB values after hydrothermal aging is assumed to be due to penetration of water molecules into the materials.

Concerning similar increase of TS and EAB for EVM-ATH and EVM-ATH-MEL after water test, it is supposed that TS and EAB are independent of the presence (or absence) of ions in water. Above, it was shown that when materials are immersed in distilled water, more water molecules penetrate into the material structure than in the case of hydrothermal aging in sea water. Concerning TS and EAB, it seems that the quantity of water in the molecule structure does not affect these mechanical properties.
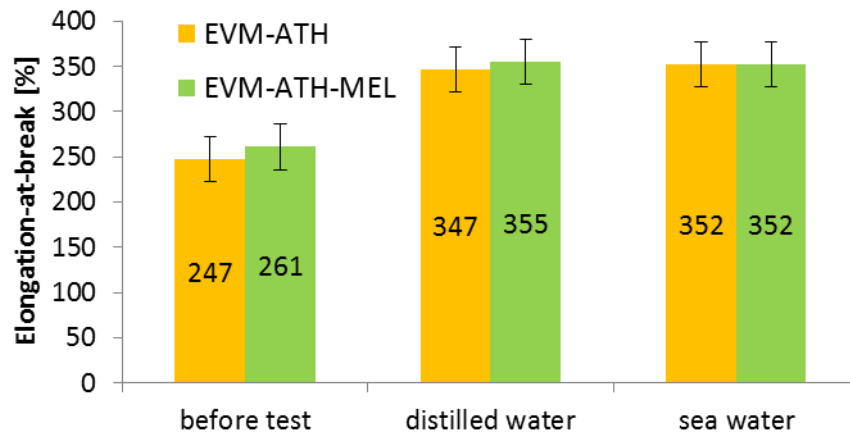
Figure 44: Elongation-at-break before and after hydrothermal aging for EVM-ATH and EVM-ATH-MEL

In the case of the hardness of EVM-ATH and EVM-ATH-MEL before and after hydrothermal aging in distilled or sea water, it is observed that hardness decreases when measured after immersion in distilled and sea water (**Figure 45**). Hardness of EVM-ATH is 75 Shore A before test, 62 Shore A after immersion in distilled water and 68 Shore after immersion in sea water. Hardness of EVM-ATH-MEL decreased from 77 Shore A before immersion to 58 (distilled water) and 63 Shore A (sea water). Beg et al. [167] evidenced that decrease of hardness after hydrothermal aging for wood fiber reinforced PP is due to penetration of water molecules into the polymeric matrix leading to softening of the material. Thus, decreased hardness in the case of EVM-ATH and EVM-ATH-MEL are explained by water molecule penetration into the polymeric matrix leading to lower hardness of the material.
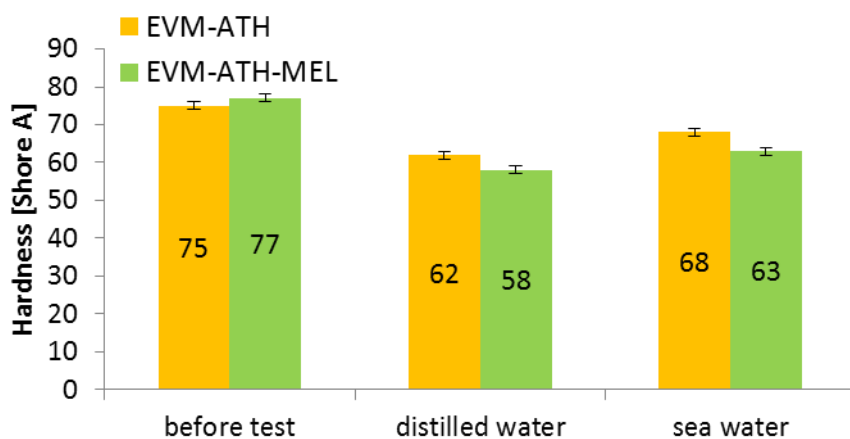

Figure 45: Hardness before and after hydrothermal aging for EVM-ATH and EVM-ATH-MEL

2.2. Material structure after hydrothermal aging

To understand the change of mass and volume as well as of the mechanical properties of EVM-ATH and EVM-ATH-MEL after hydrothermal aging in distilled and sea water, materials were analyzed after water tests using FTIR and SEM. **Figure 46** shows FTIR spectra of EVM-ATH and EVM-ATH-MEL obtained before and after immersion in distilled and sea water. Spectrum obtained for EVM-ATH before hydrothermal aging corresponds to that reported in literature (**Table 22**) [168] except the bands observed from 3619 to 3375 cm^{-1}. These additional bands are assigned to OH groups in ATH. Vibrations at 2941, 2854, 1460, 1433 and 1371 cm^{-1} are attributed to aliphatic CH_2 and CH_3 groups of the polymer. Bands corresponding to the carbonyl function of the acetate group are observed at 1732 and 1236 cm^{-1}. The vibration observed at 1014 cm^{-1} is assigned to C-O-C. Moreover, a band at 1094 cm^{-1} attributed to C-O is detected. As it can be seen, EVM-ATH-MEL exhibits the same vibrations as EVM-ATH, except of bands at 1649, 1536, 1433 and 1461 cm^{-1} which correspond to vibrations of the melamine [99, 169, 170]. It has to be noted that vibrations at 1433 and 1461 cm^{-1} are also present in EVM-ATH (assigned to C-H vibration). Nevertheless, these bands are assigned to melamine due to the fact that intensity of these peaks is higher in the case of EVM-ATH-MEL than in the case of EVM-ATH.

After immersion in distilled water (70 °C for 70h), EVM-ATH has a similar spectrum as before immersion. An observed difference is a peak at 1094 cm^{-1} assigned to C-O which is more intense after water test. This vibration is already observed before immersion in water, whereas its intensity is low. Moreover, the vibration at 2924 cm^{-1} observed before immersion in distilled water for EVM-ATH, is splitted into two peaks at 2961 and 2922 cm^{-1} indicating a change in the polymer chain consisting of aliphatic C-H bonds. Nevertheless, it can be said that no modification in the chemical structure of the polymer is detected when EVM-ATH is immersed in distilled water.

Infrared spectrum of EVM-ATH-MEL after immersion in distilled water has the same spectrum as EVM-ATH after water test concerning bands corresponding to EVM and ATH. Vibrations corresponding to melamine instead undergo a change. Intensity of vibrations at 1433 and 1461 cm^{-1} decreases significantly in comparison to the spectrum found before immersion. In the case of C=N vibration (1649 cm^{-1}), two weak bands at 1575 and 1539 cm^{-1}

are found after immersion of EVM-ATH-MEL in distilled water. Furthermore, the band at 1536 cm^{-1} (assigned to NH$_2$ group) disappears completely in the IR spectrum. The intensity of bands (1433 and 1461 cm^{-1}) for EVM-ATH-MEL after immersion in distilled water is comparable to that observed in the spectrum of EVM-ATH (after immersion in distilled water). It is therefore concluded that presence of these vibrations is only due to the presence of the polymer (C-H vibrations). It is assumed that most of melamine molecules present in EVM-ATH-MEL are solubilized during immersion in distilled water and that only a small quantity of melamine remains in the material leading to the bands at 1575 and 1539 cm^{-1}. Solubility of melamine is known to increase with increasing temperature whereas it decreases with increasing ionic strength of the surrounding medium [165, 166]. This evidences that melamine is solubilized during hydrothermal aging of EVM-ATH-MEL in distilled water carried out at 70 °C.
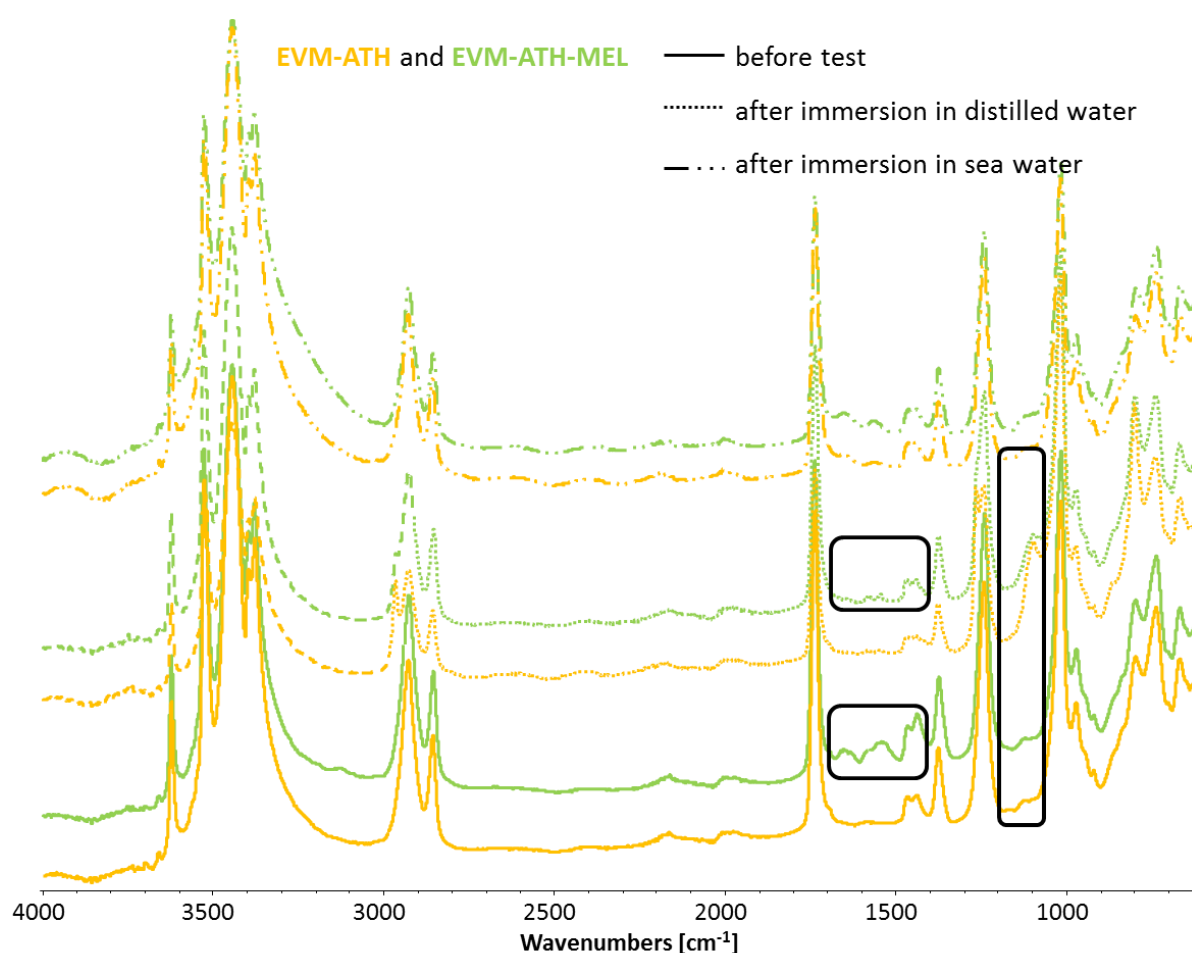

Figure 46: IR spectra of EVM-ATH and EVM-ATH-MEL before immersion and after immersion in distilled water and in sea water

Table 22: Main FTIR wavelengths obtained for EVM-ATH and EVM-ATH-MEL before and after water swelling test in distilled and sea water

Wavelength [cm^{-1}]	Corresponding chemical structure
3619, 3524, 3441, 3392 and 3375	ν (O-H) and ν (N-H)
2924, 2854	ν (C-H) (aliphatic)
1732	ν (C=O) (carbonyl)
1649	ν (C=N)
1536	δ (N-H)
1460, 1433	δ (C-H) in CH$_2$
1371	δ (C-H) in CH$_3$
1236	ν (C-O)
1094	ν (C-O)

In the case of the FTIR spectra of EVM-ATH and EVM-ATH-MEL after hydrothermal aging in sea water (40 °C for 168h), it is found that both materials display the same spectra as obtained before immersion in distilled and sea water respectively. EVM-ATH-MEL still possesses its vibrations assigned to melamine after immersion in both water types. Intensity of vibrations is slightly decreased in comparison to those observed before immersion which is explained by a partial solubilization of melamine. It is therefore assumed that less melamine is solubilized when EVM-ATH-MEL is immersed in sea water that it is the case in distilled water. Lower melamine solubility is explained by lower temperature and presence of ions in the medium. As mentioned above, solubility of melamine increases with increasing temperature and temperature is lower in the case of immersion in sea water. Further, decreased solubility is explained by the "salting out" effect of ions on melamine (lower chemical potential) which leads to lower solubility of melamine.

Samples of EVM-ATH and EVM-ATH-MEL after immersion in distilled or sea water are analyzed using SEM (**Figure 47**). It is observed that both materials exhibit cracks in the polymer structure after immersion in distilled water. It is assumed that penetration of water molecules during immersion leads to formation of cracks in the material structure. In the case of EVM-ATH-MEL, additionally to cracks, holes are observed in the material structure. It is supposed that these holes are due to partial solubilization of melamine leaving a hole in the material structure. After immersion of EVM-ATH and EVM-ATH-MEL in sea water instead, no significant damage of the matrix is found (no cracks, no holes). The absence of cracks and holes is explained by the fact that penetration of water molecules during

immersion in sea water is less important than in the case of immersion of the materials in distilled water.
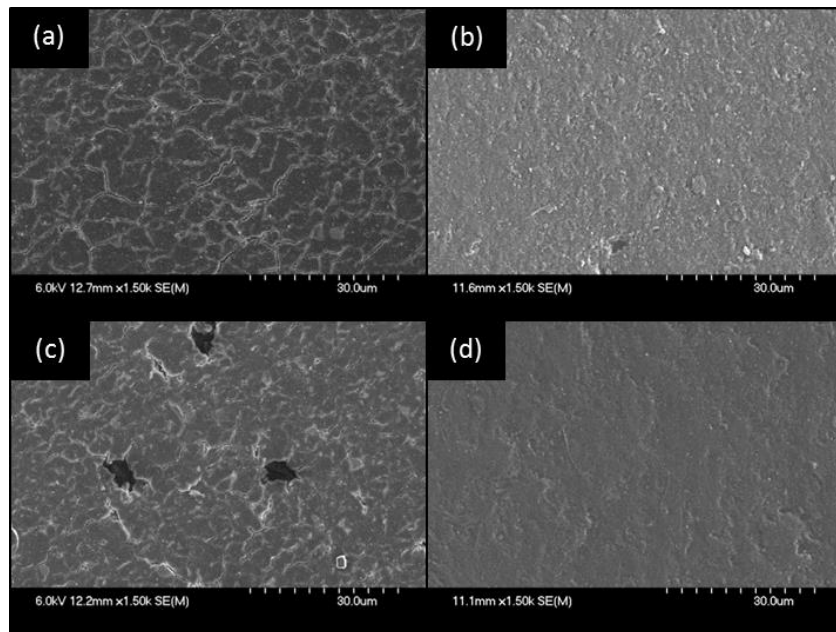

Figure 47: SEM images of EVM-ATH after immersion in distilled (a) and sea water (b) and EVM-ATH-MEL after immersion in distilled (c) and sea water (d)

2.3. Conclusion

Hydrothermal aging of EVM-ATH and EVM-ATH-MEL in distilled and sea water was investigated. It was demonstrated that in sea water, both materials exhibit the same results showing that in sea water penetration of water molecules into the material is limited in comparison to that observed in distilled water. This leads to higher stability of the materials against the attack of sea water. Change of the mechanical properties was found to be similar for both materials in both test configurations even if material structure of EVM-ATH and EVM-ATH-MEL is more damaged after hydrothermal aging in distilled water than in sea water.

In the next part, thermal decomposition of EVM-ATH and EVM-ATH-MEL is investigated. Moreover, fire retardant mechanism (gas and condensed phase) of both materials is discussed in detail.

3. Thermal analysis of additives and materials

Thermal decomposition of the additives, i.e. EVM, ATH and melamine and of the materials, i.e. EVM-ATH and EVM-ATH-MEL is discussed in this part.

3.1. Thermal decomposition of EVM, ATH and melamine

Pyrolytic and thermo-oxidative decomposition of the additives is discussed briefly, because it is already well reported in literature [26, 86, 99, 100, 169, 171]. **Table 23** summarizes observed decomposition steps and residual mass at 800 °C of EVM, ATH and melamine. Decomposition of EVM in pyrolytic conditions occurs following a three step process, whereas five steps are found in thermo-oxidative conditions. In both cases, first deacetylation of the polymer takes place evolving acetic acid and forming a polyene network which is then degraded. Deacetylation is mainly observed in the temperature range from 200 to 400 °C. Decomposition of the polyene network evolving hydrocarbon structures mainly takes place from 400 to 700 °C. In thermo-oxidative conditions, oxidation reaction occurs leading to a more complex decomposition. For example, oxidation of the polyene network is observed.

Table 23: Decomposition steps of EVM, ATH and melamine in pyrolytic and thermo-oxidative conditions, 10 °C/min

	Condition	Degradation steps [°C]					Residue at 800 °C [%]
		1	2	3	4	5	
EVM	air	200-220	220-410	410-480	480-570	570-670	0
	nitrogen	250-390	390-510	600-680	-	-	1
ATH	air and nitrogen	160-315	-	-	-	-	63
Melamine	air and nitrogen	180-360	-	-	-	-	0

Concerning decomposition of ATH and melamine, both compounds decompose in a one-step process which is similar in thermo-oxidative and pyrolytic conditions. ATH (in gibbsite form) dehydrates between 160 and 315 °C forming alumina (Al_2O_3). The remaining residue at 800°C corresponds to alumina. Melamine decomposes in the temperature range from 180 to 360 °C. Melamine is known to sublimate at around 200°C and is totally decomposed at 375 °C. Formation of melamine condensates, i.e. melam, melem and melon is generally possible

during decomposition reaction. At the end of decomposition no residue is left; melamine is completely decomposed.

3.2.   Thermal decomposition of EVM-ATH and EVM-ATH-MEL

TG curves of the materials, i.e. EVM-ATH and EVM-ATH-MEL are presented in **Figure 48**. Thermal decomposition of EVM-ATH in pyrolytic and thermo-oxidative conditions corresponds to that reported in literature [86, 172]. Therefore decomposition of EVM-ATH is discussed briefly. Pyrolytic decomposition occurs in four steps. The first decomposition step occurs from 180 to 315 °C and the second one from 315 to 400 °C. The first step is mainly due to dehydration reaction of ATH and the second one to deacetylation of the polymer. From 400 – 540 °C polyenes formed during deacetylation are vaporized. The last small decomposition step (625 – 700 °C) is attributed to decomposition of Rhenofit TAC/S used for vulcanization of the material. At the end, a residue of 35 wt% is left.
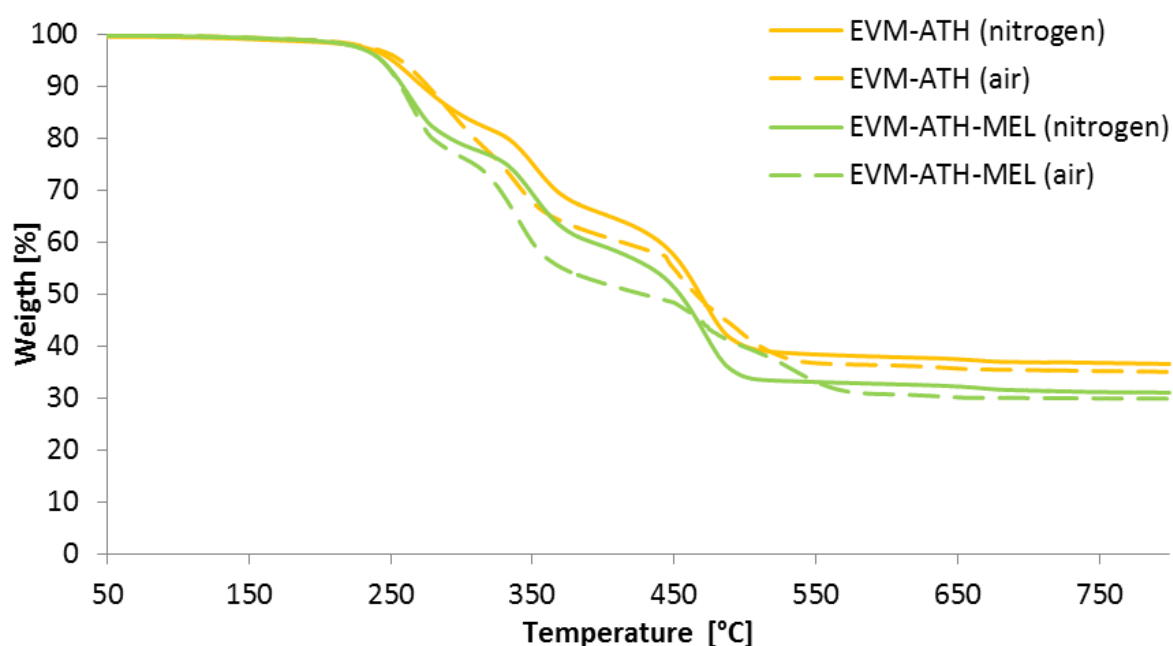
Figure 48: TG curves of EVM-ATH and EVM-ATH-MEL, 50-800°C, 10 °C/min, in air and nitrogen

Decomposition of EVM-ATH in thermo-oxidative conditions takes place following a five step process. The first and second decomposition steps are similar to those found in pyrolytic conditions. The third step takes place from 410 to 480 °C, the fourth one from 480 to 580 °C and the fifth one from 580 to 675 °C. These decomposition steps are mainly attributed to the

oxidation and the decomposition of the polyene network formed during deacetylation. At the end, a residue of 37 wt% remains.

Theoretical residual mass of EVM-ATH in pyrolytic and thermo-oxidative conditions is calculated based on theoretical residue of ATH (65 wt%). EVM-ATH contains 55 wt% of ATH leading to a theoretical residue of 36 wt % (55 wt% x 0.65 = 36 wt%). Difference of calculated residual mass and experimental residual mass of 37 (pyrolytic decomposition) and 35 wt % (thermo-oxidative decomposition) respectively lies in the margin of error. It is concluded that at the end of the decomposition of EVM-ATH, the polymer is completely degraded and the residue consists only of alumina.

In contrast to the thermal decomposition of EVM-ATH, the decomposition of EVM-ATH-MEL is not reported in literature. The pyrolytic decomposition of EVM-ATH-MEL has four steps. The first one takes place from 180 to 310 °C with a maximum mass loss rate at 260 °C and a mass loss of 21 wt%. The second decomposition step occurs from 310 to 390 °C (T_{max} = 350 °C, 18 % weight loss) and the third one from 390 to 520 °C (T_{max} = 470 °C, 26 % weight loss). During the last decomposition step (620 -685 °C, T_{max} = 670 °C) 1 wt% of the mass is lost. At the end of the pyrolytic decomposition, a residue of 31 wt% is left. In thermo-oxidative conditions EVM-ATH-MEL degrades according to a five step process. The first decomposition step takes place from 180 to 300 °C with a corresponding mass loss of 23 wt% and a maximum weight loss at 265 °C. During the second decomposition step (300 - 430 °C, T_{max} = 335 °C), 27 wt% mass are lost. From 430 to 500 °C, the third decomposition step (T_{max} = 470 °C, 9 % weight loss) takes place. The fourth decomposition step occurs from 500 to 600 °C (T_{max} = 530 °C, 9 % weight loss) and the fifth one from 600 to 665 °C (T_{max} = 635 °C, 1 % weight loss). At the end of the thermo-oxidative decomposition of EVM-ATH-MEL, a residue of 30 wt% is left. Theoretical residual mass of EVM-ATH-MEL is calculated based on theoretical residue of ATH (65 wt%) since pure melamine does not left any residue at high temperature. EVM-ATH-MEL contains 46 wt% of ATH leading to a theoretical residue of 30 wt % (46wt% x 0.65 = 29.9 wt%). As it is seen, remaining residue of 31 and 30 wt% respectively corresponds to the theoretical calculated residue leading to the assumption that only alumina is left at the end of the combustion and that the polymer is completely decomposed.

It is seen that decomposition steps of EVM-ATH-MEL are similar to those observed for EVM-ATH. Therefore, it is supposed that both materials decompose following the same decomposition pathway. At the beginning (at low temperatures) ATH dehydrates forming alumina. Furthermore, melamine is supposed to decompose or sublimate respectively at the beginning. At the same time the polymer starts to decompose and deacetylation takes place forming a polyene network which is degraded at higher temperatures. In thermo-oxidative conditions, the polyene residue is oxidized. Due to the fact that mass of remaining residues correspond to that of calculated alumina, it is further supposed that melamine is acting in the gas phase and is not left in the residue and does not lead to formation of more stable residue during decomposition.

Thermal decomposition in pyrolytic and thermo-oxidative conditions of the additives and the formulations EVM-ATH and EVM-ATH-MEL was studied. Due to the fact that decomposition of EVM-ATH-MEL is not understood in detail, its fire retardant mechanism is investigated in the next part using solid state NMR, py-GCMS and MLC-FTIR. Moreover, fire retardant mechanism of EVM-ATH is analyzed using the same methods to understand the role of melamine in EVM-ATH-MEL.

4. Gas phase analysis

In this part, gases released during decomposition of EVM-ATH and EVM-ATH-MEL are analyzed. Investigation of gases released during decomposition of EVM-ATH is already reported in literature [172, 173] (**Appendix 2: Fire retardant mechanism of ethylene vinyl acetate elastomer (EVM) containing aluminium trihydroxide and melamine phosphate** on **page 216**). Thus, gas phase of EVM-ATH is discussed rapidly. Investigation of the gas phase of EVM-ATH-MEL is not reported in literature up to now and is therefore analyzed in details using the same methods, i.e. py-GCMS and MLC-FTIR.

4.1. Investigation of the gas phase of EVM-ATH

The gas phase of EVM-ATH is analyzed using py-GCMS and MLC-FTIR. In pyrolytic conditions (py-GCMS), the material decomposition starts around 180 °C with the deacetylation process of the polymer evolving acetic acid and acetone which is formed by catalytic transformation of acetic acid through presence of alumina in the condensed phase. At the same time, dehydration reaction of ATH is taking place releasing water to the gas phase which dilutes the fuel and prevents early ignition. The polyene network formed during deacetylation is decomposed at higher temperatures (300 -500 °C) releasing hydrocarbons. The structure of evolved hydrocarbons depends on the applied heating ramp. At low heating ramp (10 °C/min) formation of saturated and monounsaturated linear hydrocarbons is favored. At high heating ramps (flash pyrolysis) in contrast benzene and its homologues are mainly formed. Studies on gases evolved during flash pyrolysis (T = 700 – 900 °C) of n-decane, 1,7-octadiene, 1,3 butadiene and different polymers (polyethylene, polypropylene and polystyrene) showed that amount of aromatic hydrocarbons in the gas phase increases with increasing temperature and contact time [174-177]. Results of these studies can be compared to our system, EVM-ATH, due to the fact that the polyene residue obtained after deacetylation of the polymer has a similar chemical nature as the compounds investigated in these studies. For EVM-ATH both parameters, i.e. high temperature and long contact time (ten minutes at 800 °C instead of some seconds), favoring formation of aromatic hydrocarbons over formation of saturated hydrocarbons are achieved.

Analysis of gases released in a fire scenario (MLC-FTIR) revealed that before ignition of EVM-ATH mainly three gases are detected in the gas phase: acetic acid (evolved during

deacetylation), water (coming from dehydration of alumina) and a low quantity methane (indicating material decomposition). The material ignites when concentration of water is not high enough to dilute the fuel sufficiently to prevent ignition. At the ignition of the material, deacetylation of the polymer is nearly completed. After ignition, concentration of carbon dioxide and water increase rapidly indicating complete combustion. At the $pHRR_2$, additional release of carbon monoxide, water and acetic acid is observed leading to the assumption that the protective layer formed at $pHRR_1$ cracks. This leads to release of gases trapped underneath. Towards end of the material combustion, concentration of carbon monoxide (detected after ignition for the first time) is increased until flameout. It has to be noted that complete combustion dominates incomplete one during the whole combustion process.

4.2. Investigation of the gas phase of EVM-ATH-MEL

The gas phase mechanism of EVM-ATH-MEL is investigated in pyrolytic conditions using py-GCMS (low and high heating ramp). Moreover, MLC-FTIR is carried out to get information about gases released during a fire test.

4.2.1. Release of gases in pyrolytic conditions of EVM-ATH-MEL

Py-GCMS experiments (10 °C/min) are based on thermal decomposition of EVM-ATH-MEL obtained using TGA. Gases are analyzed after each decomposition step (**Figure 49**). First of all, it has to be mentioned that the peak "air" present in the mass spectra corresponds to air that is left in the interface between the pyrolyzer and the GCMS, which is evolved into the column after the heating ramp of the material. From 50 to 180 °C, evolved gases are attributed to presence of vulcanization agent (Rhenofit) which is known to decompose before 180 °C (similar to results for EVM-ATH). Additionally, a peak corresponding to melamine (1) is detected. During investigation of thermal decomposition of melamine, it was found that melamine starts to degrade at 180 °C. Therefore, the presence of melamine in the gas phase before 180 °C is explained by the fact that melamine starts to sublimate before 180 °C.

From 180 to 310 °C (corresponding to the first decomposition step of EVM-ATH-MEL), the following molecules are detected in the gas phase: water (2), acetic acid (3) and melamine (4). Presence of water indicates decomposition of ATH forming alumina and evolving water. Acetic acid is known to be released during deacetylation of the polymer. This shows that the polymer

starts to degrade during the first decomposition step. Besides water and acetic acid, melamine is detected in the gas phase between 180 and 310 °C.
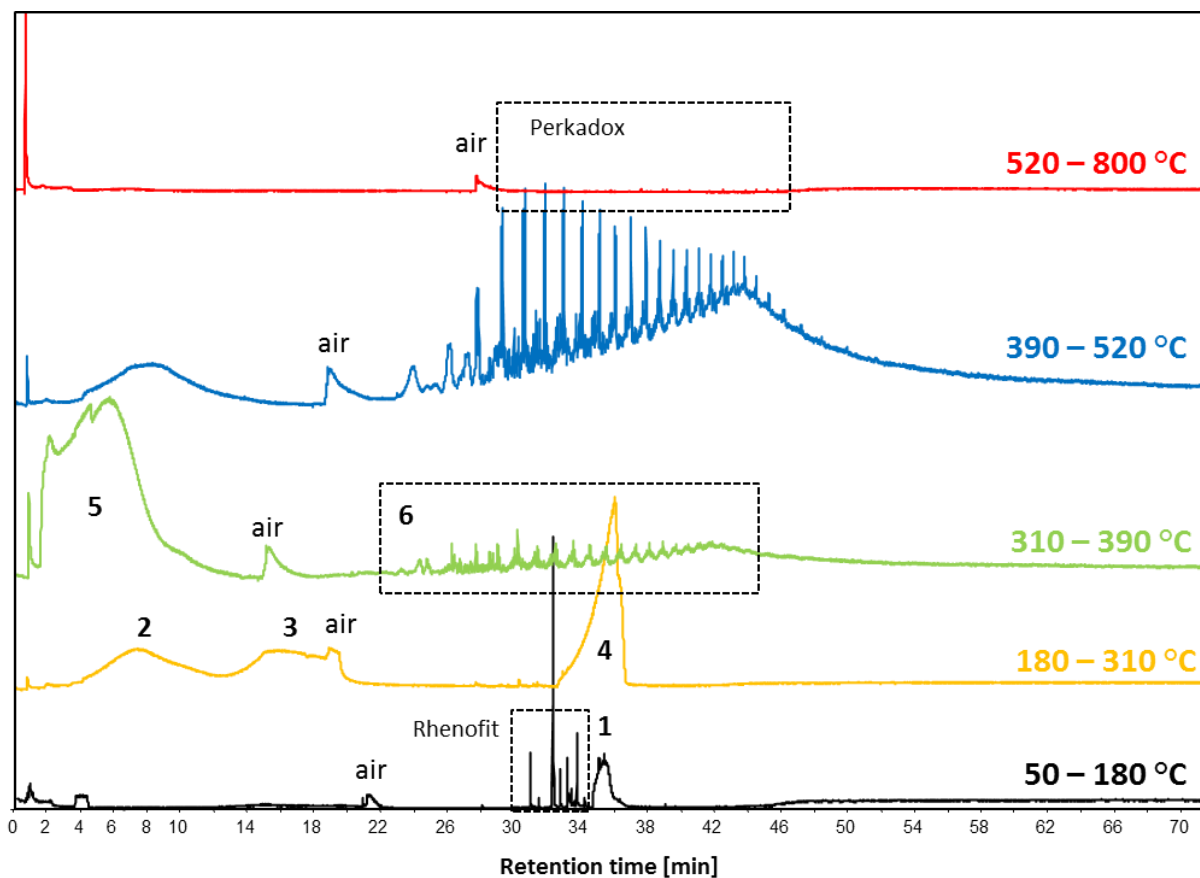

Figure 49: Chromatograms of EVM-ATH-MEL obtained by py-GCMS, 10°C/min

Chromatograms observed for the second (310 – 390 °C), third (390 - 520 °C) and fourth (520 - 800 °C) decomposition step of EVM-ATH-MEL correspond to those obtained for EVM-ATH. Between 310 and 390 °C a broad peak (5) at early retention time, indicating the presence of acetic acid, acetone and acetonitrile, is observed. Formation of acetone is explained through catalytic transformation of acetic acid due to the presence of alumina in the condensed phase [173, 178]. Detection of acetonitrile is due to decomposition of melamine. Moreover, peaks corresponding to mono-unsaturated and saturated hydrocarbons having between 8 to 34 carbon atoms are present in the chromatogram. It can therefore be said that during the third decomposition step (310 – 390 °C), deacetylation of the polymer still takes place leading to formation of a polyene network. At the same time, the formed polyenes start to decompose.

From 390 to 520 °C only saturated and mono-unsaturated hydrocarbons (C8 – C34) are found in the gas phase of EVM-ATH-MEL. During the last decomposition step (520 – 800 °C) molecules due to decomposition of Perkadox are detected in the gas phase.

Decomposition of EVM-ATH-MEL at high heating ramps (flash pyrolysis at 800 °C for 10 min) induce a change in the structure of evolved hydrocarbons (**Figure 50**). The following molecules are detected: water (1), butene (2), acetonitrile (3), isocyanic acid (3), pentadiene (4), 1,3 cyclopentadiene (5), cyclopentene (6), 1-hexene (7), methylcyclopentadiene (8), acetic acid (8), 1-methyl-3-cyclopentene (9), benzene (10), 1,3-cyclohexadiene (11), cyclohexene (12), 1-heptene (13), 2-hydroxyethyl acetate (14), toluene (15), xylene (16), styrene (17), ketene (18), n-propylbenzene (18), isopropylbenzene (19), methylstyrene (20), indane (21), indene (21), butylbenzene (22), benzonitrile (22), methylindene (23), naphthalene (24), methylnaphthalene (25), biphenyl (26) and melamine (27).
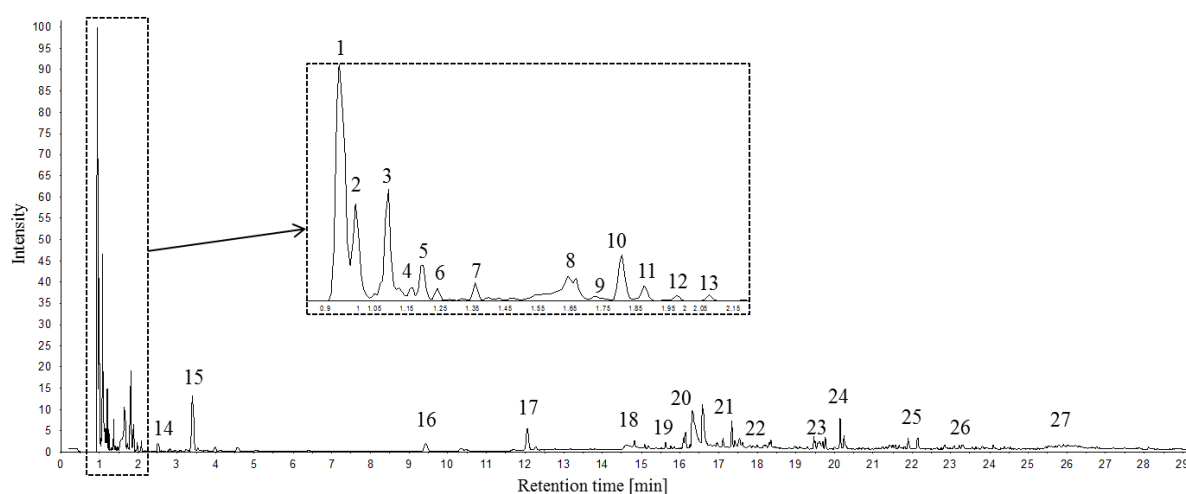
Figure 50: Chromatogram of EVM-ATH-MEL obtained by py-GCMS, flash pyrolysis (10 min at 800 °C)

In general, chemical natures of released gases evolved from EVM-ATH-MEL are similar to those obtained for EVM-ATH at high heating rate. In addition, molecules indicating decomposition of melamine, i.e. isocyanic acid, benzonitrile and melamine are detected in the gas phase. Regarding decomposition of ATH, change of heating rate does not change decomposition pathway of ATH. ATH is degraded forming alumina and evolving water. Concerning decomposition of EVM, it is found that at first deacetylation of the polymer is taking place evolving acetic acid (acetone is not detected). Polyenes formed from deacetylation decompose forming benzene and its homologues rather than linear saturated and mono-unsaturated hydrocarbons (low heating rate, 10 °C/min). As for EVM-ATH favored formation of benzene and its homologues is due to high temperature and long contact time [174-177].

4.2.2. Release of gases during a fire test (MLC-FTIR) of EVM-ATH-MEL

The gas phase of EVM-ATH-MEL in a fire scenario is investigated using MLC-FTIR (**Figure 51** and **Table 24**). Before ignition (145 s), mainly four gases are released in the gas phase: water, acetic acid, ammonia and methane, whereas concentration of methane is very low. Presence of water before ignition is attributed to decomposition of ATH releasing water. It is seen that release of water has a local maximum around one minute, corresponding to 11% of its total release.
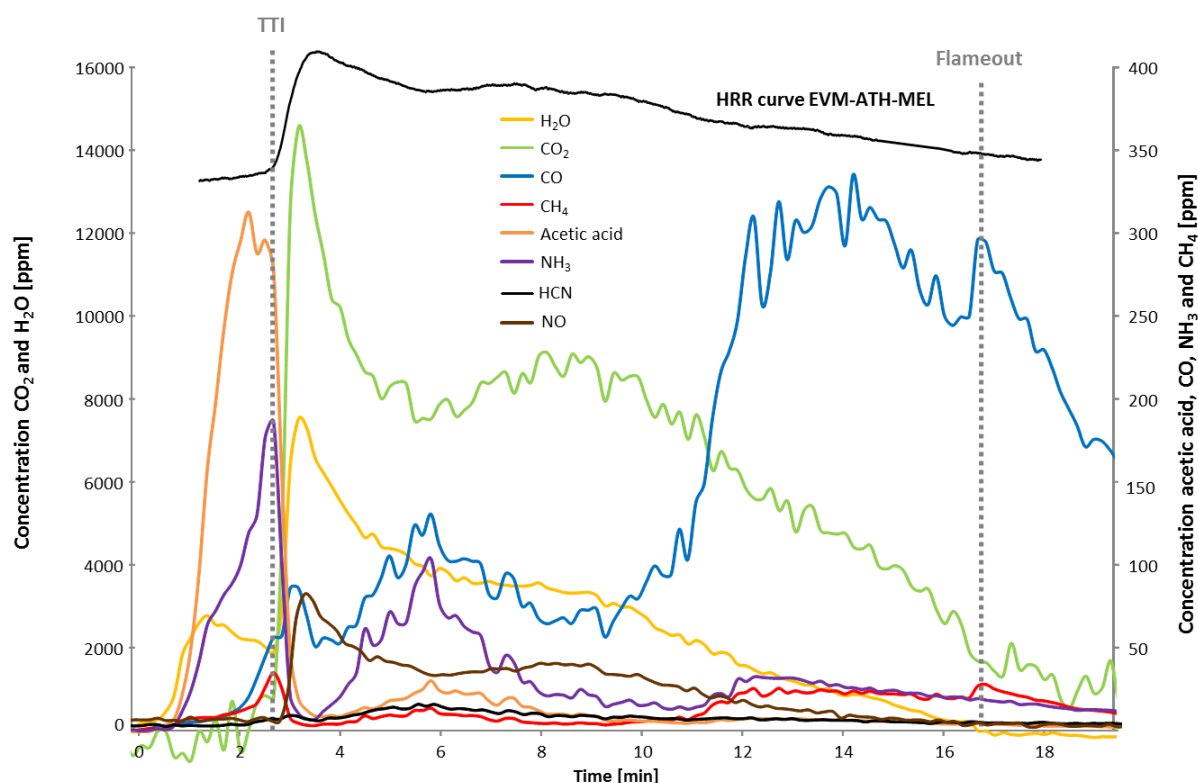
Figure 51: Evolution of gases versus time obtained by MLC-FTIR for EVM-ATH-MEL

Table 24: Quantification of released gases during MLC-FTIR experiment for EVM-ATH-MEL

Gas	Total quantity released [ppm]	Released before ignition [ppm]	Released before ignition [%]
H_2O	258427	29652	11
CO_2	619409	2390	0
CO	17750	230	1
CH_4	1578	173	11
Acetic acid	3629	2517	69
NH_3	4078	1101	27
NO	2427	79	3
HCN	566	20	3

Release of acetic acid (2517 ppm, 69 % of total release of acetic acid) is due to deacetylation of the polymer. It is found that concentration of acetic acid shows a local maximum around two

minutes and that concentration of acetic acid in the gas mixture starts to decrease. This indicates that deacetylation process is not complete before ignition of the material. Besides acetic acid, presence of methane (173 ppm) also demonstrates that decomposition of the polymer takes place before ignition. It is assumed that methane comes from decomposition of polyene structures formed during deacetylation. Moreover, 1101 ppm of ammonia (27 % of total release of ammonia) is detected in the gas phase before ignition. Presence of ammonia is attributed to decomposition of melamine [169]. It has to be noted that in pyrolytic conditions, melamine is partially sublimated and at the same time decomposed evolving acetonitrile. In a fire scenario instead melamine is found to decompose into ammonia (detected before ignition) and hydrogen cyanide which is detected in the gas phase after ignition of the material. Directly after ignition, ammonia is not detected due to its complete combustion into nitrogen monoxide (**Equation 10**). At $pHRR_2$, additional release of ammonia is observed. Afterwards, concentration of ammonia decreases constantly until flame out. As a consequence, after ignition, 2427 ppm of nitrogen monoxide are found in the gas phase. Nitrogen dioxide was not detected in the gas phase which is explained by the combustion reaction of ammonia [179]. Moreover, nitrogen dioxide is known to be decomposed into nitrogen monoxide at 150 °C [180]. Hydrogen cyanide (from melamine decomposition) is also detected after ignition. During the whole combustion process, 566 ppm of hydrogen cyanide is released, whereas concentration never exceeds 15 ppm.

$$4\ NH_3 + 5\ O_2 \rightarrow 4\ NO + 6\ H_2O$$

Equation 10: Combustion reaction of ammonia

After ignition of EVM-ATH-MEL concentration of water and carbon dioxide indicating complete combustion, increase sharply and reach their maxima of 7525 ppm and 14568 ppm respectively around 227 s (3.8 min). Afterwards, concentration of both gases decreases constantly until flame out, whereas local maxima are observed around the $pHHR_2$. Concentration of carbon monoxide (17750 ppm in total) due to incomplete combustion of the material, increases after ignition and reaches its maximum of 350 ppm after $pHRR_2$ (local maximum before $pHRR_2$). This observation is explained by the fact that at the end of combustion process, most of the material is already decomposed and the remaining material burns with small flames on the material surface (visual observation). Smoldering is not observed during experiment. After flame out, concentration of carbon monoxide decreases.

Concentration of methane decreases after ignition of EVM-ATH-MEL. Its concentration never exceeds 30 ppm during the whole experiment. This indicates that not all methane molecules are burned during experiment. In the case of acetic acid, it is found, that a small quantity of acetic acid (local maximum at 32 ppm) is found before $pHRR_2$, at the same time as ammonia and carbon monoxide have exhibit their local maxima.

The local maxima of concentrations of carbon monoxide, ammonia and acetic acid before $pHRR_2$ and local maxima of carbon dioxide and water concentration at $pHRR_2$, suggests formation of a protective layer at the beginning of the experiment which cracks after $pHRR_1$ leading to an additional release of gases trapped underneath the layer (as for EVM-ATH). It can be clearly seen that increase of gas concentration is significantly lower in the presence of melamine. It can therefore be assumed that the protective layer formed at the material surface is more stable and accordingly more effective in the case of EVM-ATH-MEL than it is the case of EVM-ATH. A higher barrier effect explains reduced $pHRR_2$ and reduced smoke release at $pHRR_2$ in comparison to EVM-ATH.

Using MLC-FTIR experiment, presence of acetone cannot be clearly evidenced. On the one hand, the device was not calibrated for acetone and thus a quantification of its release is not possible. On the other hand, obtained FTIR spectra do not permit to confirm presence of acetone in the gas phase. Nevertheless, it is assumed that acetic acid is transformed to acetone through catalytic reaction with alumina during MLC-FTIR experiment. First, conditions for formation of acetone are met: alumina formed during dehydration of ATH and acetic acid was shown to be evolved during combustion of EVM-ATH-MEL. Moreover, presence of acetone was confirmed by py-GCMS experiment.

4.2.3. Conclusion of gas phase analysis of EVM-ATH-MEL

Investigation of the gas phase of EVM-ATH-MEL in pyrolytic conditions and during a fire test revealed that decomposition of the polymer is equal to that of EVM-ATH. Partial replacement of ATH by melamine (ratio 5:1) was found to lead to shorter ignition during MLC test, which is explained firstly by the lower amount of ATH in EVM-ATH-MEL in comparison to EVM-ATH. Lower amount of ATH leads to lower release of water into the gas phase and lower dilution of the fuel. Secondly, during combustion of EVM-ATH-MEL, ammonia is released. Thus, the fuel consists of more flammable gases (acetic acid and ammonia) than it is the case for EVM-ATH.

Concentration of released water is not high enough to dilute the fuel sufficiently to prevent ignition and EVM-ATH-MEL ignites at shorter time than EVM-ATH. Moreover, partial replacement of ATH by melamine leads to release of higher concentrations of toxic gases, i.e. nitrogen monoxide, isocyanic acid and carbon monoxide.

To complete the understanding of the mechanism of action during decomposition of EVM-ATH and EVM-ATH-MEL, the condensed phase of both materials is analysed using solid state NMR in the next part.

5. Condensed phase analysis

The condensed phase of EVM-ATH and EVM-ATH-MEL is investigated using a method in which the combustion process is stopped at characteristic times during the cone calorimeter experiment. The resulting materials afterwards are analyzed by solid state NMR (^{13}C and ^{27}Al). The top of the sample and the bottom are analyzed.

5.1. Investigation of condensed phase of EVM-ATH

For EVM-ATH, the combustion was stopped at six characteristic points: before the ignition (230 s), just after ignition at the increase (245 s), at the $pHRR_1$ (275 s), at the $pHRR_2$ (444 s), during decrease of the HRR curve (700 s) and at the end of combustion (1200 s). Due to the fact that the condensed phase of EVM-ATH was already investigated in details [86, 172], results observed here are briefly discussed. Generally, results obtained in this study correspond to those reported in literature. This validates the solid state NMR as a method to characterize the condensed phase of materials.

^{13}C NMR spectra obtained at the different stages of combustion are presented in **Figure 52**. The spectrum of the unburned material shows several peaks (attribution of observed chemical shifts presented in **Table 25**). The spectrum corresponds to data already reported in literature for pure EVM [26, 181-185].

Table 25: Attribution of chemical shifts obtained for EVM-ATH and EVM-ATH-MEL

Chemical Shift [ppm]	Attribution
21	CH_3
25, 30, 35 and ~ 42	CH_2
69, 71 and 73, 76	CH
130	Unsaturated hydrocarbons
169	C=O in acetate/C=N in melamine
182, 181, 180 and 179	C=O (carbonyl)

The peak at 21 ppm corresponds to methyl-group (CH_3) of the acetic acid of the polymer [183]. Those at 25, 30 and 35 ppm are attributed to methylene–groups (CH_2) in the polymer backbone [182, 186]. The multiplicity of the peaks is due to the fact that when VA monomer copolymerizes with ethylene, a random copolymer is obtained leading to several different monomer sequences in the chain. According to Delfini et al. [187], the chemical shift

depends on the position of the carbon in a monomer. However, this work was carried out in liquid state NMR, and thus does not take into account structural effects. But, since all the reported bands are present on our solid state NMR spectrum, it can be assumed that the assignments are transposable. Peaks assigned to CH bonds in the polymer chain are detected around 70 ppm. The multiplicity of this chemical shift is also explained by the sequence distribution of pentads in the polymer [187]. The chemical shift at 170 ppm corresponding to C=O in the acetate group is not observed for the virgin material EVM-ATH. Due to the fact that this peak is obtained for the virgin EVM, it can be said that the absence of the C=O peak in unburnt EVM-ATH is due to the large anisotropy of the chemical shift tensor of C=O [188].
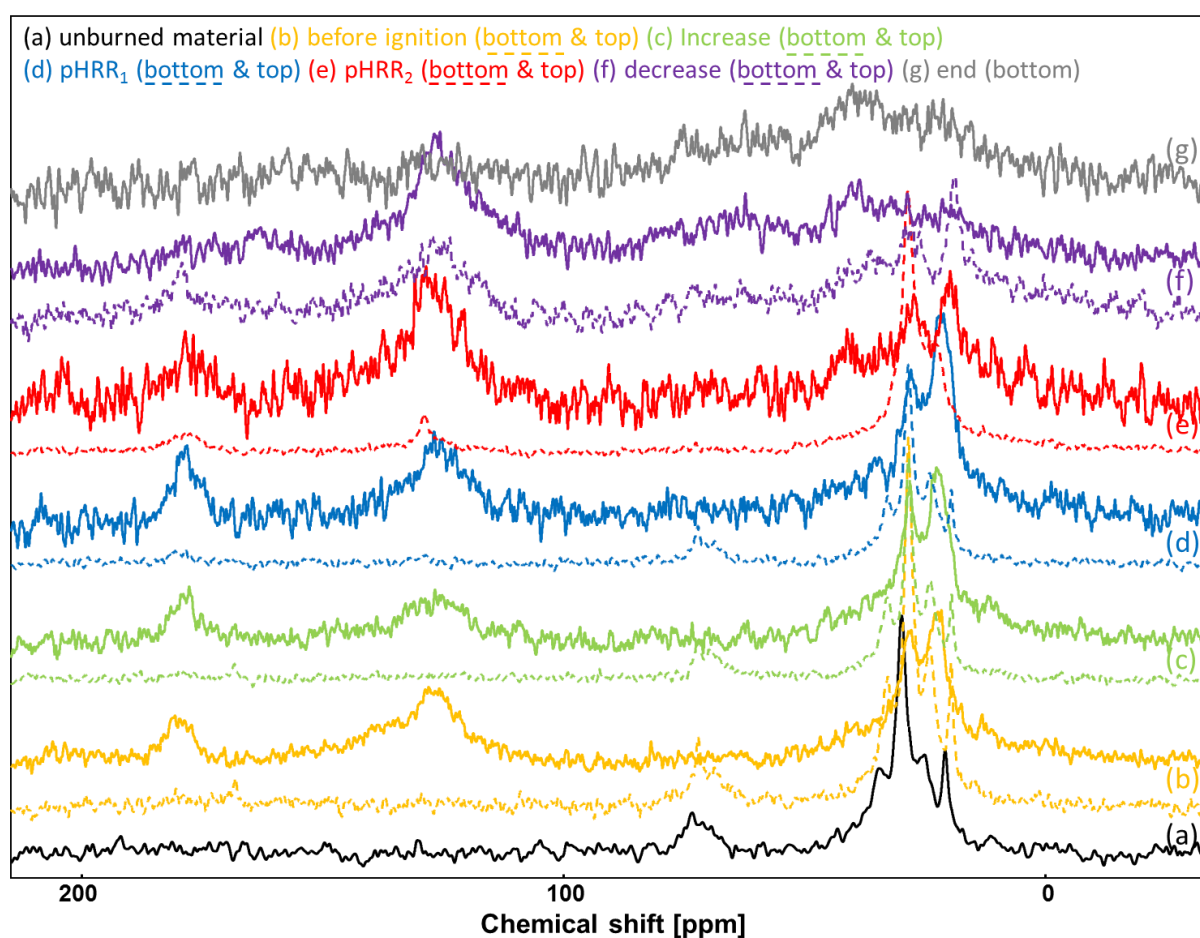
Figure 52: ^{13}C spectra obtained for different stages of combustion of EVM-ATH (MLC experiment at 35 kW/m²)

When EVM-ATH is exposed to an external heat source, it starts to decompose at the surface, and then the decomposition penetrates the whole material with ongoing decomposition process. The resonance corresponding to the acetate group disappears before ignition at the top of the plaque and at the pHRR$_2$ at the bottom of the plate. This indicates that

deacetylation of the polymer is not complete until $pHRR_2$. It was previously found that around the $pHRR_2$ acetic acid is again present in the gas phase. It was assumed that presence of acetic acid is only due to crack of the protective layer releasing gases trapped underneath. Detection of acetic acid in the gas phase shows that not all molecules are burned. High quantity of acetic acid is explained by release of trapped gases. Deacetylation of the polymer leads to formation of aliphatic (20 – 70 ppm) and aromatic (130 ppm) hydrocarbons which form a char layer at the sample surface. It has to be noted that the char layer is oxidized due to presence of oxygen in the surrounding atmosphere. At the end of the combustion of EVM-ATH a ^{13}C signal is not detected indicating that all carbon containing material is decomposed. This corresponds to the result obtained using TGA, i.e. the remaining residue consist only of alumina.

^{27}Al spectra of the residues of EVM-ATH are presented in **Figure 53**. The unburnt material exhibits a peak at 8 ppm corresponding to octahedral coordinated aluminum [189]. An additional site is observed at -3 ppm. The recorded spectrum corresponds to the spectrum for gibbsite ($Al(OH)_3$) found in literature [190, 191]. The spectrum starts to change before ignition at the surface. Additionally to the resonance found for the unburnt material, a chemical shift at 65.0 ppm attributed to tetrahedral coordinated aluminum indicating formation of alumina, is observed. The ratio of AlO_4/AlO_6 estimated using Dmfit [151] is 1:4. The observed spectrum is the same at the surface for all stages of the decomposition process. The underlying material is protected until the $pHRR_1$, where a small peak corresponding to tetrahedral coordinated Al is found (ratio AlO_4/AlO_6 = 7/100). It can therefore be concluded that only a small part of ATH is degraded at this stage of the combustion. Afterwards, spectra recorded of the bottom of the plates are similar to those found for the top of the plates.

It has further to be noted that water detected after ignition of EVM-ATH during MLC-FTIR experiment, is not only due to complete combustion but also to the dehydration of ATH occurring until the $pHRR_1$. Presence of a "char" protecting the material at its surface can be evidenced through the fact that ^{27}Al NMR showed that ATH is not fully degraded until $pHRR_1$, the underlying material is protected through a layer formed at the sample surface consisting of alumina and saturated and unsaturated hydrocarbons. This result is different to the results found in previous studies [146], where an ethylene vinyl acetate polymer having a VA

content of 24 % was studied. It was shown that when 65 wt% ATH are incorporated into the polymeric matrix, ATH is completely degraded into alumina oxide before ignition of the material. The difference between the results found in this study and in our present study is explained by the different conditions used. First, the VA content of the polymer in our study is much higher. Secondly, residues were obtained stopping MLC experiment carried at 50 kW/m², whereas 35 kW/m² is used in our case.
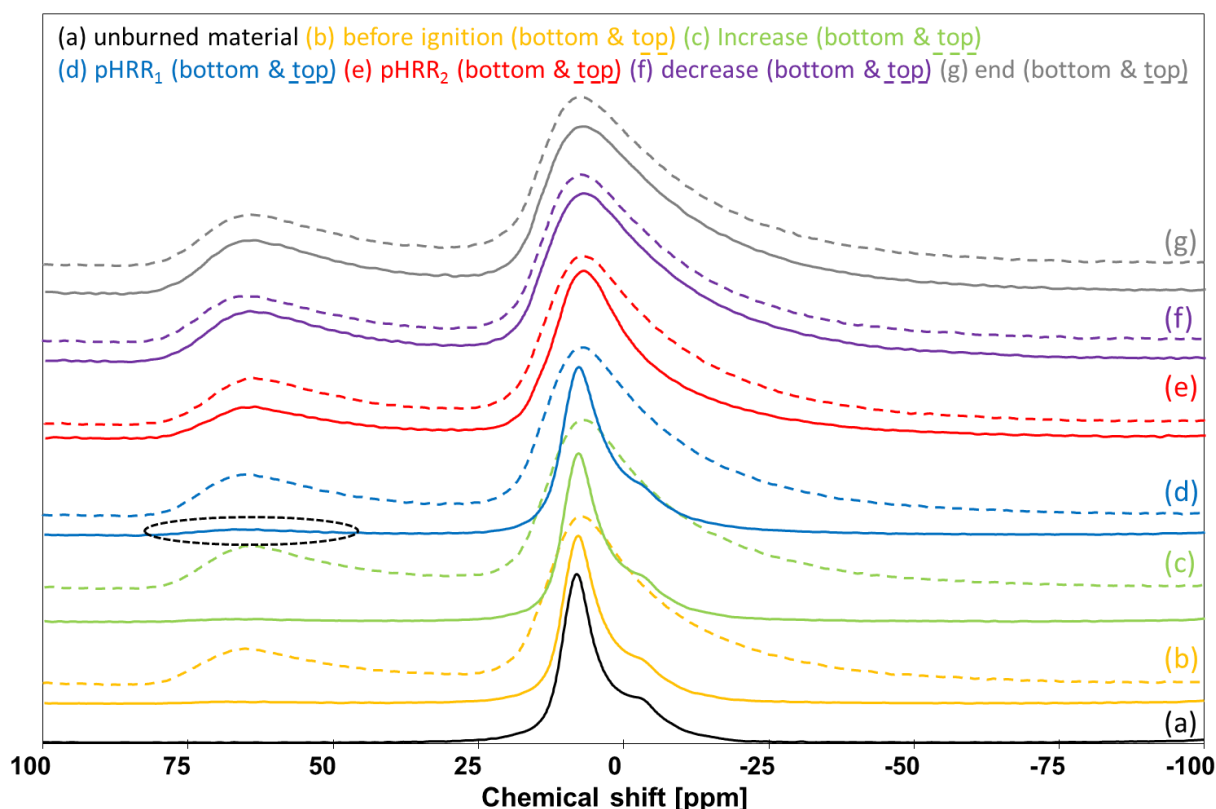

Figure 53: ^{27}Al spectra obtained for different stages of combustion of EVM-ATH (MLC experiment at 35 kW/m²)

As short conclusion of the analysis of the condensed phase of EVM-ATH, it can be said that the material is protected by the formation of a protective layer consisting of saturated and unsaturated (oxidized) hydrocarbons and alumina which starts to form before ignition of the material and persist until decrease of pHRR curve.

5.2.   Investigation of condensed phase of EVM-ATH-MEL

MLC experiment of EVM-ATH-MEL (100-108-22) was stopped at six characteristic points: before the ignition (154 s), during increase of the HRR (184 s), at the pHRR$_1$ (230 s), at the pHRR$_2$ (486 s), during decrease of the HRR curve (700 s) and end of combustion (1200 s). The

residues (**Figure 54**) were analyzed by ^{13}C and ^{27}Al solid state NMR. In the ongoing combustion process, EVM-ATH-MEL is decomposed forming a loose black char layer at the surface. At the end of the combustion, additionally a white residue is observed at the sample surface.
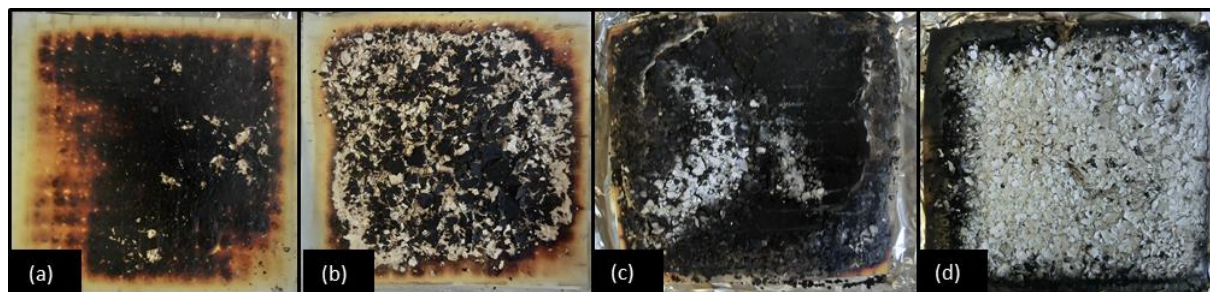
Figure 54: Residues of EVM-ATH-MEL (a) before ignition, (b) at the pHRR1, (c) during the decrease of HRR curve and (d) at the end of combustion

^{13}C NMR spectra of the residues at different stages of combustion are presented in **Figure 55**. Virgin EVM-ATH-MEL exhibits the same chemical shift as virgin EVM-ATH. Peaks attributed to CH_3 (21 ppm), CH_2 (26, 30 and 34 ppm), and CH (73 ppm) are observed. Additionally, two peaks at 157 and 165 ppm coming from melamine are detected [99, 192]. These chemical shifts could also be due to the quaternary C atom connecting the vinyl acetate groups to the polymer backbone. Nevertheless, this possibility is excluded due to the fact that the peak is not present in the case of EVM-ATH. Before ignition, the spectrum recorded from the residue at the bottom of the plate is identical to that of virgin EVM-ATH-MEL.

At the top of the plate before ignition, the peak corresponding to the methyl group of vinyl acetate decreases and additional peaks at 130 ppm (unsaturated hydrocarbons) and 180 ppm (carbonyl) are observed. These peaks indicate the presence of an oxidized, carbonaceous char. The spectrum of the bottom of the sample taken at the increase is similar to that obtained before ignition (bottom). The top of the plate at this stage of the combustion process exhibits chemical shifts corresponding to CH_2-groups (around 40 ppm), unsaturated hydrocarbons (130 ppm) and carbonyl functions (180 ppm) indicating the presence of oxidized carbonaceous char at the surface of the material. Moreover, a peak at 167 ppm corresponding to melamine [99] is observed. The absence of the methyl peak in the

spectrum taken of the top during increase of the HRR curve, indicates that deacetylation of the polymer is completed at the surface.
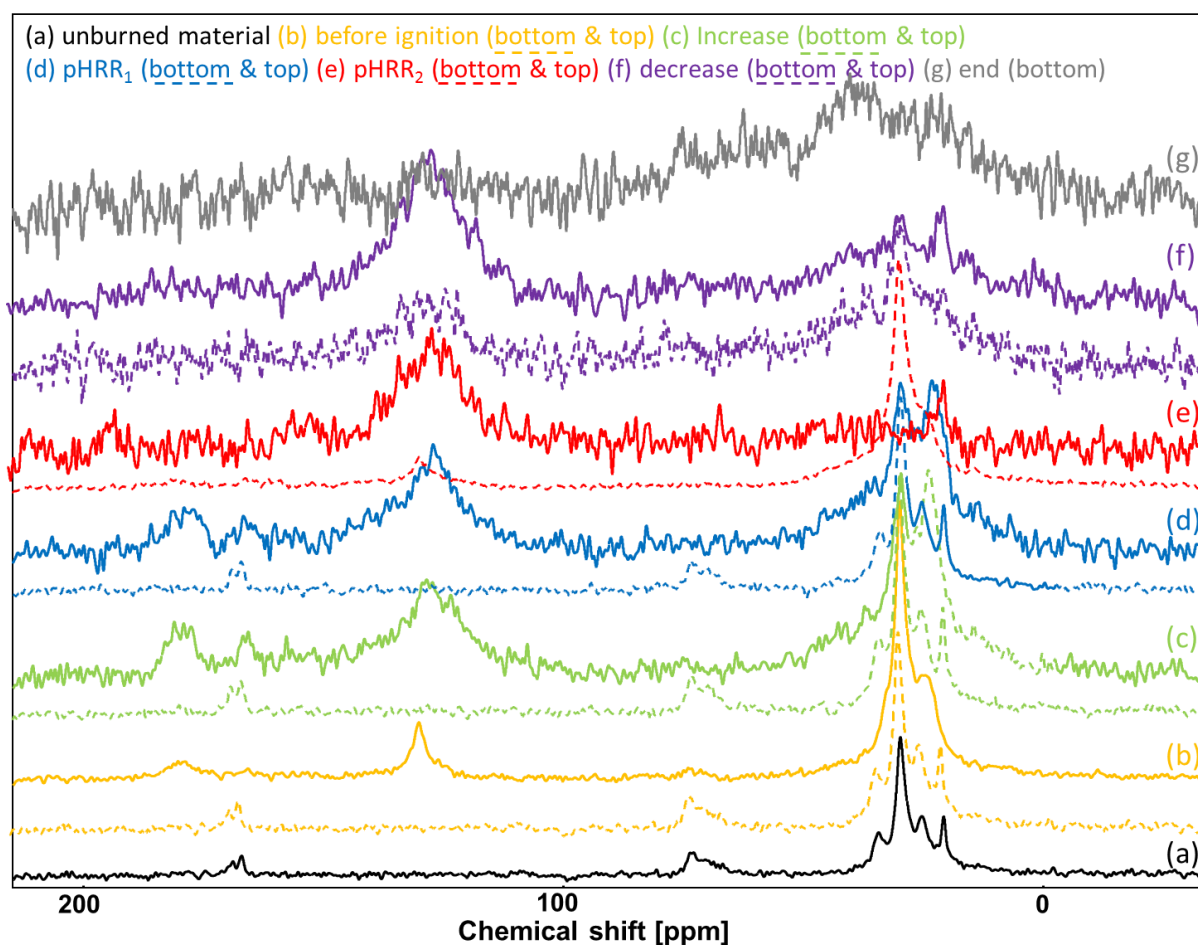
Figure 55: ^{13}C spectra obtained at different stages of combustion of EVM-ATH-MEL (MLC experiment at 35 kW/m²)

Spectra recorded for the bottom and the top of the plate at pHRR$_1$ are similar to those obtained at increase (bottom and top). At the pHRR$_2$, at the bottom of the plate only peaks corresponding to saturated (40 ppm) and unsaturated (130 ppm) hydrocarbons are observed. The chemical shift attributed to carbonyl (180 ppm), indicating oxidation of the char, found before is no longer present at this stage of the combustion. The spectrum recorded of the top of the plate at pHRR$_2$ exhibits only a chemical shift at 130 ppm (unsaturated hydrocarbons). During decrease of the HRR curve, spectra obtained for the bottom and the top of the plate are similar: peaks corresponding to saturated (40 ppm) and unsaturated (130 ppm) hydrocarbons are found. At the end of the combustion (bottom) only a broad peak attributed to saturated hydrocarbons is detected. The spectrum of the residue at the top of the plate left at the end of the experiment give no signal. ^{13}C solid state NMR

spectrum of EVM-ATH-MEL at the end of combustion confirms the absence of carbon structures in the residue postulated during analysis of TGA experiment. Thus, the remaining residue consists only of alumina.

^{27}Al NMR spectra of the residues of EVM-ATH-MEL are presented in **Figure 56**. The spectrum obtained for unburnt EVM-ATH-MEL is similar to that obtained for unburnt EVM-ATH. The chemical shift at 7.9 ppm with a small shoulder at -2.0 ppm is attributed to octahedral coordinated Al^{3+} [189]. At the top of the plate taken before the ignition a peak at 64 ppm assigned to tetrahedral coordination of aluminum indicating the dehydration of ATH forming an aluminum oxide is detected.
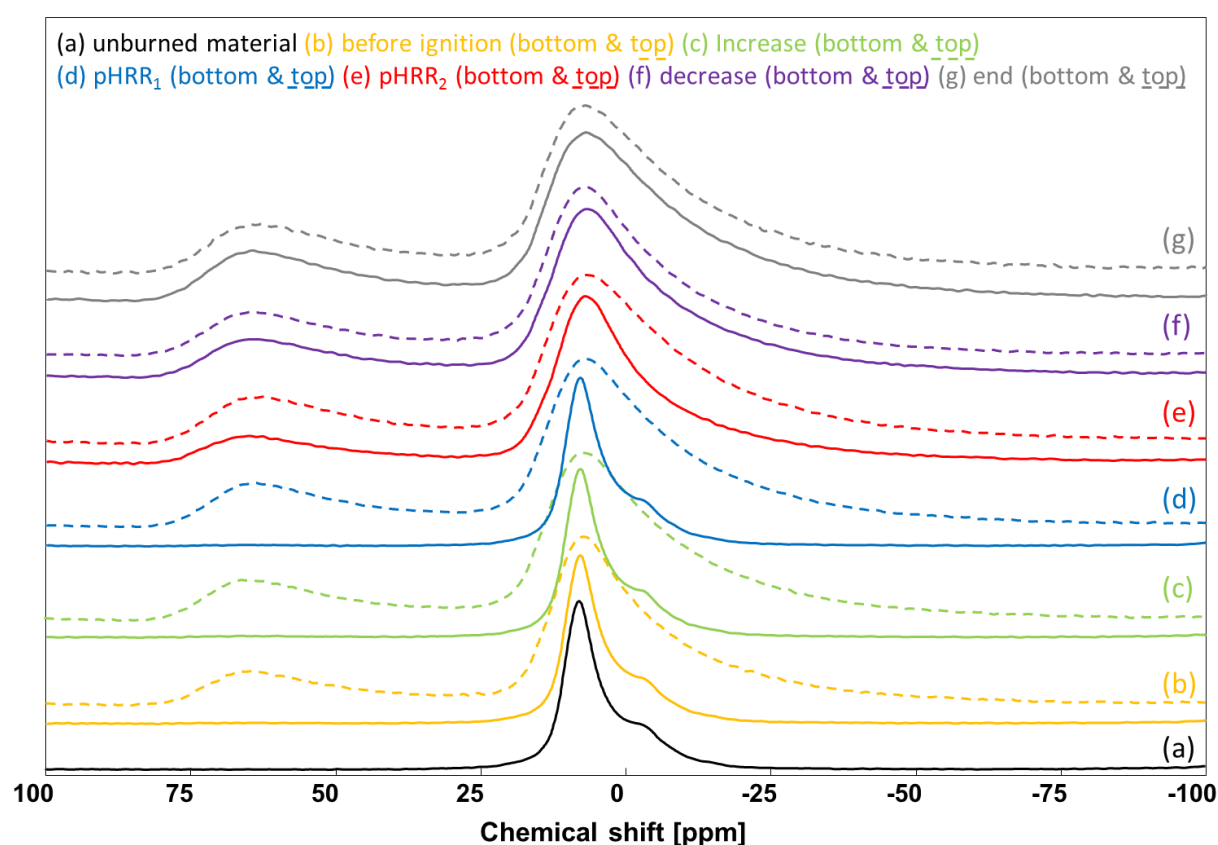
Figure 56: [27]Al spectra obtained at different stages of combustion of EVM-ATH-MEL (MLC experiment at 35 kW/m²)

The underlying material (bottom of the plates) has the same spectra like unburnt EVM-ATH-MEL until $pHRR_2$. Top of the plates always show chemical shifts corresponding to tetrahedral and octahedral coordinated aluminum. As for EVM-ATH, the peak corresponding to octahedral coordinated Al is getting broader with progressed combustion process. It has to be noted that decomposition of ATH is not completed before $pHRR_2$.

In summary, the protection mechanism of EVM-ATH-MEL is similar to that of EVM-ATH. The material is protected by formation of a char layer consisting of saturated and unsaturated (oxidized) hydrocarbons and alumina. The protective layer starts to be formed before ignition of the material and persist until decrease of HRR curve. The formed protective layer acts as barrier avoiding/reducing transfer of gases, heat and smoke. A condensed phase action of melamine is not observed.

It is supposed that decreased $pHRR_2$ of EVM-ATH-MEL in comparison to EVM-ATH is due to a higher stability of the char. It was shown that melamine or its condensation products are not present in the residue at the end of the combustion. Thus, higher barrier effect is not due to the presence of these compounds in the condensed phase. However, it is supposed that the morphology of the char consisting of alumina is changed due to presence of melamine and its condensation products, which leads to a better barrier effect of EVM-ATH-MEL than EVM-ATH.

6. Decomposition mechanism of EVM-ATH and EVM-ATH-MEL

Based on thermal analysis and investigation of the gas and the condensed phase of EVM-ATH and EVM-ATH-MEL a decomposition mechanism for both materials could be proposed. As supposed during thermal analysis of EVM-ATH and EVM-ATH-MEL, both materials decompose following the same pathway. **Figure 57** presents schematic decomposition mechanism of both materials.

When EVM-ATH or EVM-ATH-MEL is exposed to an external heating source, e.g. fire, the material starts to decompose. At first, deacetylation of the polymer takes place evolving acetic acid by forming a polyene network. At the same time, ATH degrades to alumina evolving water. Released water dilutes the fuel and thus protects the material in the gas phase. Furthermore, presence of alumina in the condensed phase leads to catalytic transformation of acetic acid to acetone. Before ignition of the material, the polyene network formed by deacetylation of the polymer starts to decompose evolving hydrocarbons. The chemical structure of evolved hydrocarbons depends on the applied heating ramp. A low heating ramps (10 °C/min) leads to formation of saturated and monounsaturated linear hydrocarbons. With a high heating ramp (flash pyrolysis) at the opposite formation of benzene and its homologues is favored. During material decomposition a char layer is formed at the material surface consisting of alumina and saturated and unsaturated hydrocarbons. This layer protects the material in the condensed phase and acts like a barrier limiting transfer of mass. It has to be noted that before ignition the protective layer is not fully developed and therefore gas transport to the fuel is still possible. The material ignites when concentration of water is not high enough to dilute the fuel sufficiently to prevent ignition. At the ignition of the material, deacetylation of the polymer is still taking place. The main reaction taking place at this stage is the decomposition of the polyene network, whereas complete and incomplete combustion take place. Going on further in the decomposition, the protective layer cracks evolving gases trapped underneath. Moreover, incomplete combustion dominates complete combustion at this stage. At the end of material decomposition, a residue consisting of alumina is left.

Presence of melamine in the material leads to release of additional gases to the gas phase. Before ignition, melamine and ammonia are evolved due to sublimation and/or

decomposition of melamine or its condensation products. EVM-ATH-MEL ignites at shorter time than EVM-ATH due to higher concentration of flammable gases in the gas phase before ignition. After ignition, nitrogen oxide and hydrogen cyanide are detected in addition to hydrocarbons.
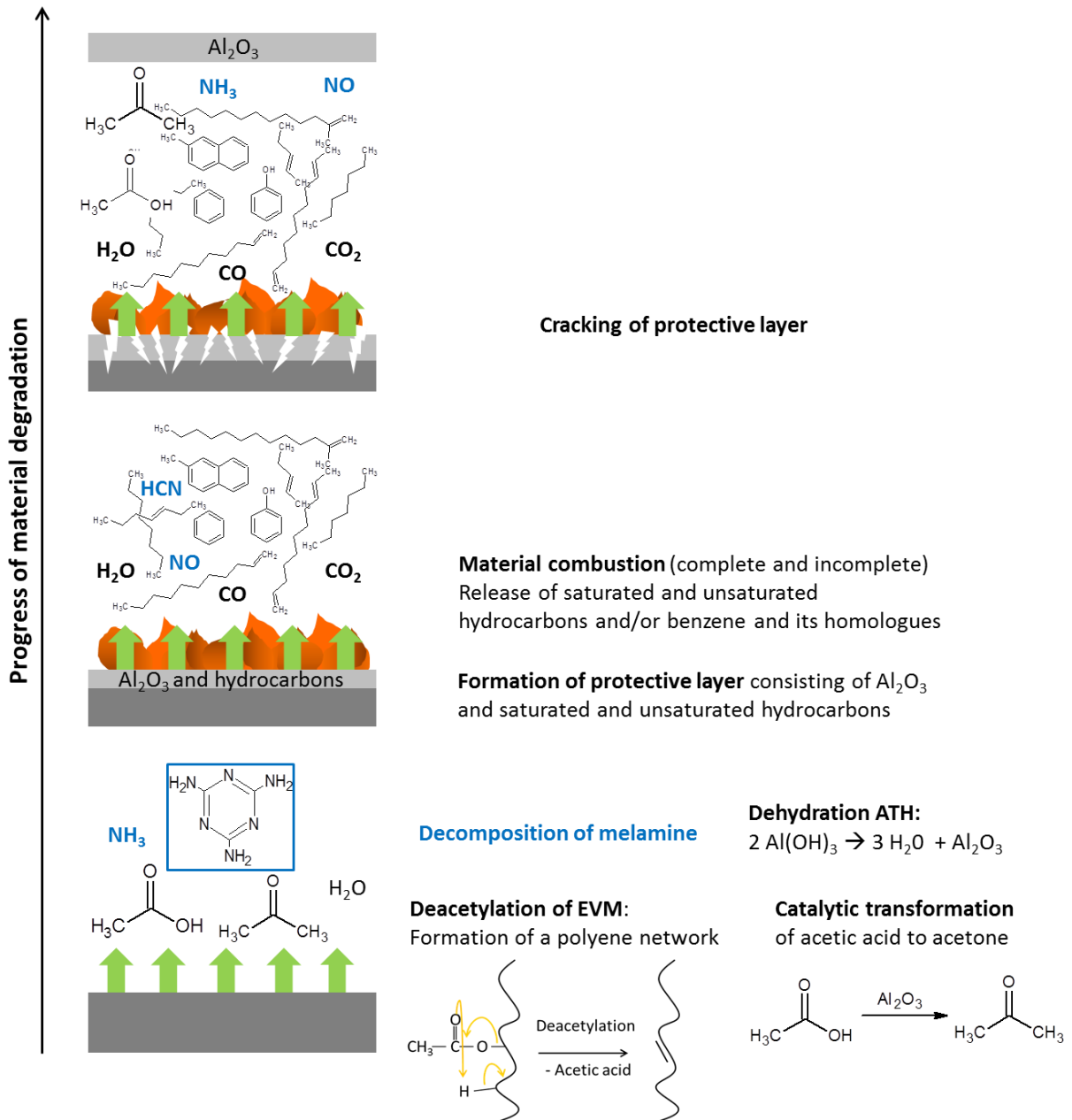
Figure 57: Decomposition mechanism of EVM-ATH and EVM-ATH-MEL

7. Conclusion

Chapter IV was dedicated to the comprehension of the fire retardant mechanism of EVM-ATH-MEL and to the comparison with EVM-ATH to understand the role of melamine on shorter ignition of EVM-ATH-MEL in case of fire. Thermal analysis of the additives and of the materials was carried out showing that decomposition in pyrolytic and thermo-oxidative conditions of EVM-ATH and EVM-ATH-MEL is similar. Analysis of the gas and of the condensed phase demonstrated that degradation pathway of the polymer is not affected when ATH is partially replaced by melamine. Nevertheless, presence of melamine results to a higher concentration of flammable and toxic gases, i.e. ammonia and acetic acid in the gas phase leading to shorter ignition of EVM-ATH-MEL in comparison to EVM-ATH.

Additionally, the dispersion of the additives in the polymeric matrix and hydrothermal aging of EVM-ATH and EVM-ATH-MEL was investigated. It was demonstrated that additives are evenly dispersed in the material and that partial replacement of ATH by melamine has no influence on the ATH dispersion in the polymeric matrix. Hydrothermal aging in distilled and sea water of EVM-ATH and EVM-ATH-MEL showed that modification of the mechanical properties is generally higher in sea water than in distilled water. Moreover, EVM-ATH-MEL exhibits higher stability than EVM-ATH in distilled water.

In the next part, the role of MB in EVM-ATH-MB is evaluated. As for EVM-ATH and EVM-ATH-MEL, the dispersion of the additives in the polymeric matrix, the behavior in distilled and sea water, its thermal decomposition and fire retardant mechanism of EVM-ATH-MB is investigated.

Chapter V: Investigation of the role of MB in EVM-ATH-MB

Chapter V is dedicated to the decomposition mechanism of MB in pyrolytic and thermo-oxidative conditions. The role of MB in EVM-ATH-MB regarding hydrothermal aging and fire retardant mechanism is also investigated. Afterwards, combination of ATH and MB is evaluated in different ethylene vinyl acetate polymers having different vinyl acetate (VA) contents in order to evaluate the VA effect on their mechanical properties, fire retardancy and smoke release.

1. Hydrothermal aging

As for EVM-ATH and EVM-ATH-MEL, the change of mass and volume as well as change of mechanical properties of EVM-ATH-MB after immersion in distilled and sea water is investigated. First, change of mass and volume, then change of mechanical properties after hydrothermal aging in distilled and sea water for EVM-ATH-MB is presented hereafter.

1.1. Change of mass and volume

Regarding change of mass and volume (**Figure 58**) in distilled water, it is seen that in comparison to EVM-ATH and EVM-ATH-MEL, EVM-ATH-MB exhibits less changes after the test. Change of volume after immersion in distilled water is as low as 3 %, whereas a change of mass is not detected. It is known that change of mass and volume can be due to penetration of water molecules into the material and/or solubilization of additives whereas penetration depends on ionic strength and temperature of the surrounding medium. Presence of ions leads to reduced penetration of water molecules due to decreased chemical potential [164]. Moreover, it is known that increased temperature leads to change solubility of the additives. In the case of melamine, it was found that its solubility is increased with increasing temperature. A dependence of the solubility of MB on temperature is not reported in literature. Solubility of melamine borate is 0.67g/100g water at room temperature which is two times higher than that of melamine (0.3g/100g water) [165]. Therefore, melamine borate is more soluble when EVM-ATH-MB is immersed in water than melamine when EVM-ATH-MEL is immersed in water in the same conditions.
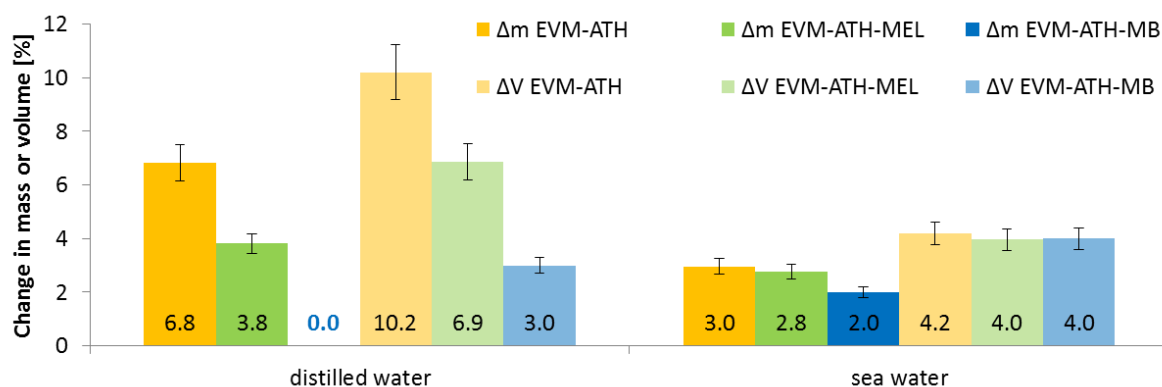
Figure 58: Change of the mass and volume during the water swelling test for EVM-ATH-MB

On one side, melamine borate is more soluble than melamine but on the other side, change of mass and volume after hydrothermal aging in distilled water is lower for EVM-ATH-MB than for EVM-ATH-MEL. It is supposed that in the case of EVM-ATH-MB more additive is solubilized due to higher solubility but less water molecules penetrate into the polymeric structure. Thus, change of mass during hydrothermal aging of EVM-ATH-MB is lower than that of EVM-ATH-MEL. It is assumed that solubilization of melamine borate leads to higher ionic strength of the medium than it is in the case of EVM-ATH-MEL. Consequently, penetration capacity of water molecules is lower and results in to lower change in mass and volume of EVM-ATH-MB after immersion in distilled water. Change of mass of 0 % in distilled water is explained by compensation of mass loss due to solubilization through penetration of water molecules into the polymeric matrix.

Concerning hydrothermal aging in sea water, similar results of EVM-ATH-MB and EVM-ATH-MEL concerning change of mass and volume are found. For EVM-ATH-MEL, it was found that high ionic strength leads to decreased solubility of melamine [166]. Nothing is reported about the solubility of MB in sea water. Nevertheless, it is assumed that MB conducts the same way as melamine in sea water. Increased ionic strength of the medium is therefore supposed to lead to lower MB solubility. At the same time penetration of water molecules is limited due to the high ionic strength.

Figure 59 presents FTIR spectra of EVM-ATH-MB before and after immersion in distilled and sea water. Before test, EVM-ATH-MB exhibits the same spectra as EVM-ATH (and EVM-ATH-MEL) (**chapter 4, page 101**) indicating that presence of melamine borate does not change the chemical nature of the polymeric matrix. After hydrothermal aging in distilled and sea water, EVM-ATH-MB exhibits the same spectra as EVM-ATH-MEL after aging. FTIR spectrum of EVM-ATH-MB after immersion in distilled water exhibits vibrations (1649, 1536, 1433 and 1461 cm^{-1}) corresponding to melamine indicating that melamine borate is still present in the material. It is therefore concluded that melamine borate is partially solubilized. As discussed above, lower solubility of MB in sea water is due to higher ionic strength and lower temperature of the medium in comparison to the test in distilled water. Vibrations corresponding to EVM and ATH are detected in the spectra after immersion in distilled and sea water. This indicates that the chemical structure of the polymeric matrix is not changed during hydrothermal aging.
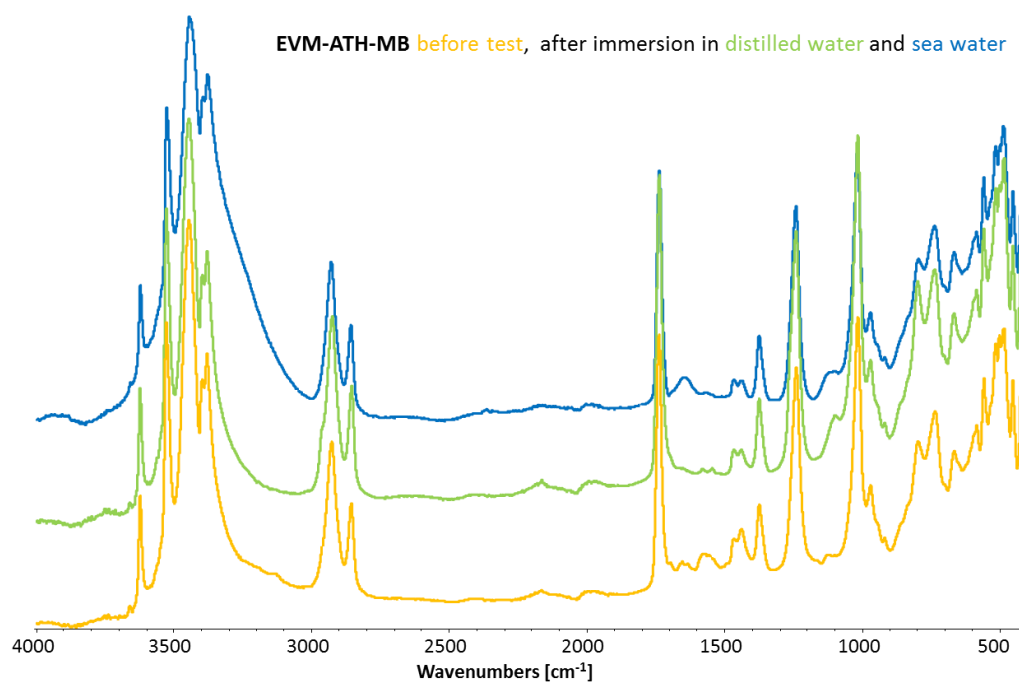
Figure 59: IR spectra of EVM-ATH-MB before test and after immersion in distilled water and in sea water

SEM images of EVM-ATH-MB after hydrothermal aging are presented in **Figure 60**. As it is seen, after immersion in distilled water (**Figure 60 (a)**) the material exhibits cracks indicating physical damage of the material. Moreover, holes are observed which is supposed to be due to solubilization of melamine borate. EVM-ATH-MB exhibits fewer holes as EVM-ATH-MEL (**page 101**) indicating that less physical damage is present. As it was discussed in chapter 4, physical damage of material is supposed to be due to penetration of water molecules into the polymer. Assumption made above that lower change of mass and volume of EVM-ATH-MB after immersion in distilled water is due to reduced penetration of water molecules is confirmed by SEM.
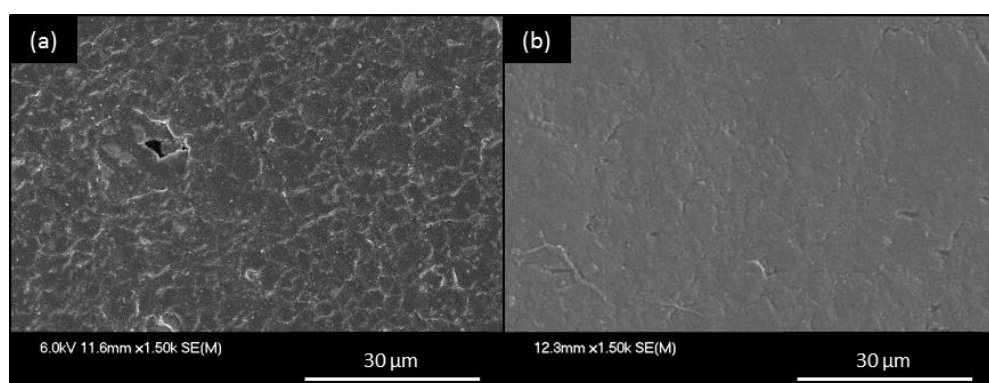
Figure 60: SEM images of EVM-ATH-MB after immersion in distilled (a) and sea water (b)

In the case of the material structure after immersion in sea water (**Figure 60 (b)**), it is found that EVM-ATH-MB exhibits less cracks than after immersion in distilled water. As mentioned before, lower temperature and higher ionic strength during hydrothermal aging in sea water lead to lower penetration of water molecules into the polymeric matrix in comparison to immersion in distilled water. It has to be noted that a difference between EVM-ATH-MB and EVM-ATH-MEL after immersion in sea water is not observed.

1.2. Change of mechanical properties

Results of stress-strain test before and after hydrothermal aging are presented in **Figure 61** and **Figure 62**. Tensile strength (TS) and elongation-at-break (EAB) of materials increase slightly after immersion in distilled and sea water, whereas increase is similar for both water types. TS increases from 8.0 MPa before test to 13.0 and 14.0 MPa after immersion in distilled and sea water respectively. EAB increases from 244 % to 343 and 347 % respectively. A difference of the EAB and the TS after hydrothermal aging between EVM-ATH-MEL and EVM-ATH-MB is not observed neither in distilled nor in sea water.

Figure 63 presents change of hardness after immersion in distilled and sea water. After hydrothermal aging, hardness of EVM-ATH-MB is decreased in comparison to the value obtained before test. Hardness decreases from 79 Shore A before test to 44 Shore A after immersion in distilled water and 48 Shore A after immersion in sea water. Decrease of hardness after hydrothermal aging is explained by penetration of water into the polymeric matrix leading to softening of the material [167]. Due to the fact that decrease of hardness is smaller after immersion in sea water than after immersion in distilled water it is supposed that penetration of water molecules is less favorable in sea water. This corresponds to results discussed before that during immersion of EVM-ATH-MB in sea water MB is less soluble than in comparison to immersion in distilled water (higher ionic strength and lower temperature).

Comparison of the results obtained for EVM-ATH-MB to those of EVM-ATH-MEL, shows that EVM-ATH-MB exhibits lower hardness after hydrothermal aging than EVM-ATH-MEL. It is known that MB is more soluble than MEL but increases ionic strength of the medium which leads to lower penetration capacity of water molecules. Penetration of water molecules in turn is known to decrease hardness. It is supposed that in the case of EVM-ATH-MB the

amount of water molecules penetrated in the polymer matrix is lower but the local concentration of water is higher at the surface leading to lower hardness Shore A values.
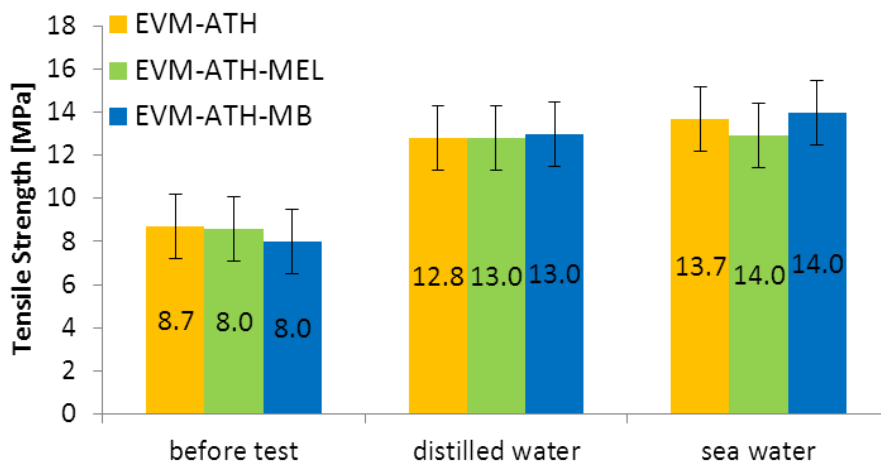
Figure 61: Change of tensile strength after the water swelling test for EVM-ATH, EVM-ATH-MEL and EVM-ATH-MB
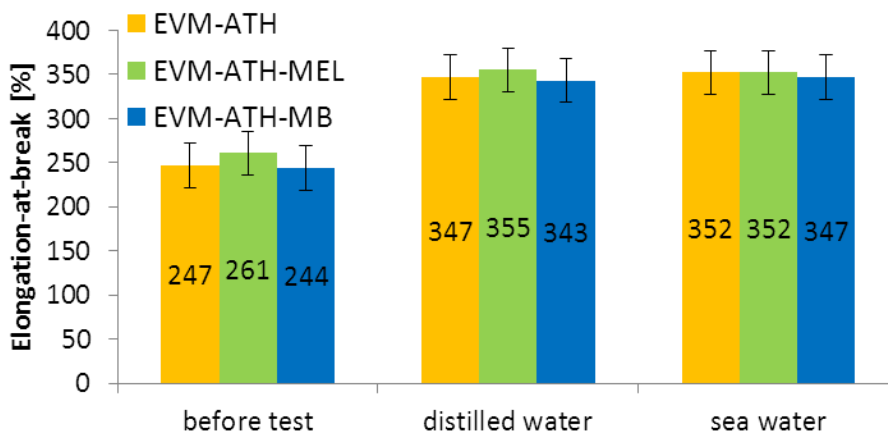
Figure 62: Change of elongation-at-break after the water swelling test for EVM-ATH, EVM-ATH-MEL and EVM-ATH-MB
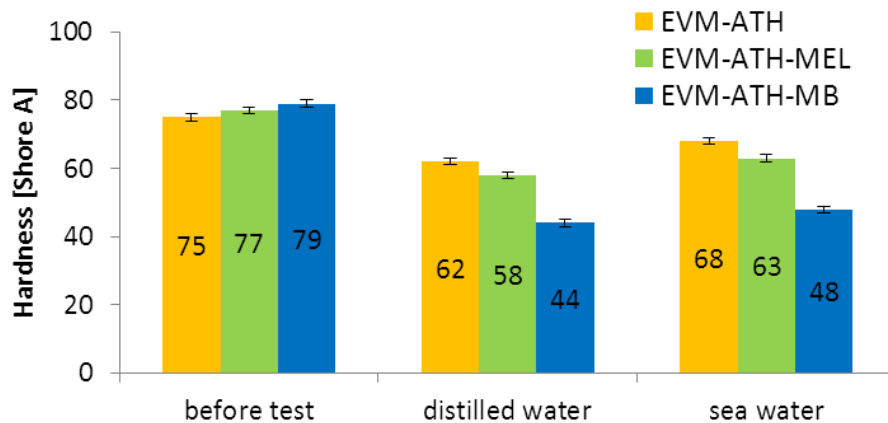

Figure 63: Change of hardness after the water swelling test for EVM-ATH, EVM-ATH-MEL and EVM-ATH-MB

1.3. Conclusion

It was found that replacement of melamine by melamine borate has an influence on the material behavior during hydrothermal aging in distilled water whereas a difference between EVM-ATH-MEL and EVM-ATH-MB in sea water was not observed for TS and EAB. Melamine borate is more soluble leading to higher ionic strength of the medium and therefore to lower penetration of water molecules into the matrix. Moreover, EVM-ATH-MB exhibits less physical damage after immersion in distilled water than EVM-ATH-MEL. Elongation-at-break and tensile strength were found to be similar for EVM-ATH-MB and EVM-ATH-MEL in both test configurations. Hardness of EVM-ATH-MB after testing at the opposite has lower values than EVM-ATH-MEL. Generally, replacement of melamine by MB leads to improved material resistance during hydrothermal aging in distilled water.

In the next part, the dispersion of the additives in the polymeric matrix is investigated. Then, the influence of MB on fire retardant properties and smoke release is investigated. Additionally, the decomposition mechanism of MB is analyzed in details.

2. Dispersion of the additives

Concerning fire retardant and mechanical properties, even dispersion of the additives is indispensable. **Figure 64** presents SEM images of EVM-ATH-MB. It is found that ATH particles are evenly dispersed in the polymeric matrix (as for EVM-ATH and EVM-ATH-MEL on **page 96**). It is therefore concluded that the presence of MB in the polymeric matrix has no effect on dispersion of ATH particles. Moreover, agglomerates (encircled) having of around 7 to 13 µm in size are detected. These agglomerates are supposed to be due to the presence of MB in the polymeric matrix, because in EVM-ATH, these agglomerates are not detected.
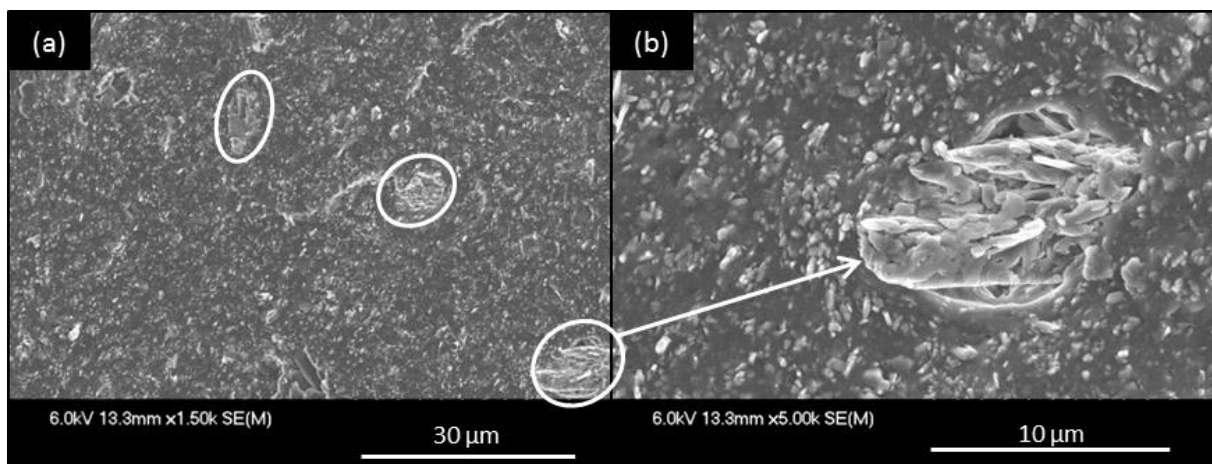
Figure 64: SEM pictures of EVM-ATH-MB

3. Fire retardant mechanism of EVM-ATH-MB

This part is dedicated to the decomposition mechanism of MB and its influence on the fire retardant properties of EVM-ATH-MB. Decomposition mechanisms in pyrolytic and thermo-oxidative conditions are investigated using TGA, solid state NMR, py-GCMS, TGA-FTIR and MLC-FTIR. Furthermore, influence of MB on fire retardant mechanism is compared to that of melamine and melamine phosphate.

3.1. Investigation of the decomposition mechanism of melamine borate

Costa et al. [193] investigated decomposition of MB (**Figure 65**) in pyrolytic conditions using FTIR analysis in the 90's. They proposed that melamine borate dehydrates between 130 and 270 °C evolving water and forming boric anhydrate with melamine. In the second step (270 – 350 °C) melamine is evolved and unidentified melamine-boric anhydride structures are formed. From 350 to 950 °C a loss of melamine structures is observed and it is proposed that molecules containing B-N bonds, such as for example boron nitride are formed.
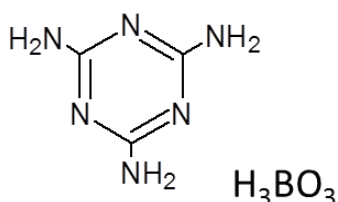
Figure 65: Chemical structure of melamine borate

Since the decomposition mechanism of MB was not further investigated in literature, it was decided to examine the decomposition of MB in pyrolytic and thermo-oxidative conditions in details. For investigation of the condensed phase, thermal treatments of MB are performed in air and nitrogen. Therefore, MB is heated according to its decomposition temperatures found using TGA. MB was heated up to 100, 200, 270, 350, 425, 750 and 850 °C. Afterwards, residues are analyzed using ^{13}C and ^{11}B solid state NMR. Moreover, gas phase of MB is analyzed using py-GCMS (pyrolytic condition) and TGA-FTIR (thermo-oxidative conditions).

3.1.1. Thermal decomposition of melamine borate

Figure 66 presents the thermal decomposition of MB in pyrolytic and thermo-oxidative conditions. It is seen that decomposition in both conditions takes place in a five step process,

whereas two steps (first and fourth one) are quite small. The principle three degradation steps (two, three and five) are reported in literature [193, 194]. The first degradation step occurs from 60 to 100 °C with a mass loss of 0.5 wt%. An attribution for this step could not be found in literature. It is assumed that this step is due to first dehydration of orthoboric acid [180]. Uptake of environmental water is excluded, because MB was dried over night before TGA experiment. The second degradation step taking place from 100 to 200 °C (T_{max} = 140 °C) with a mass loss of 16 wt% is assigned to the dehydration of orthoboric acid forming metaboric acid (HBO_2) and boron oxide (B_2O_3) (**Equation 11**) [195]. At the end of this degradation reaction, a physical mixture or adduct of boron oxide with melamine is left.
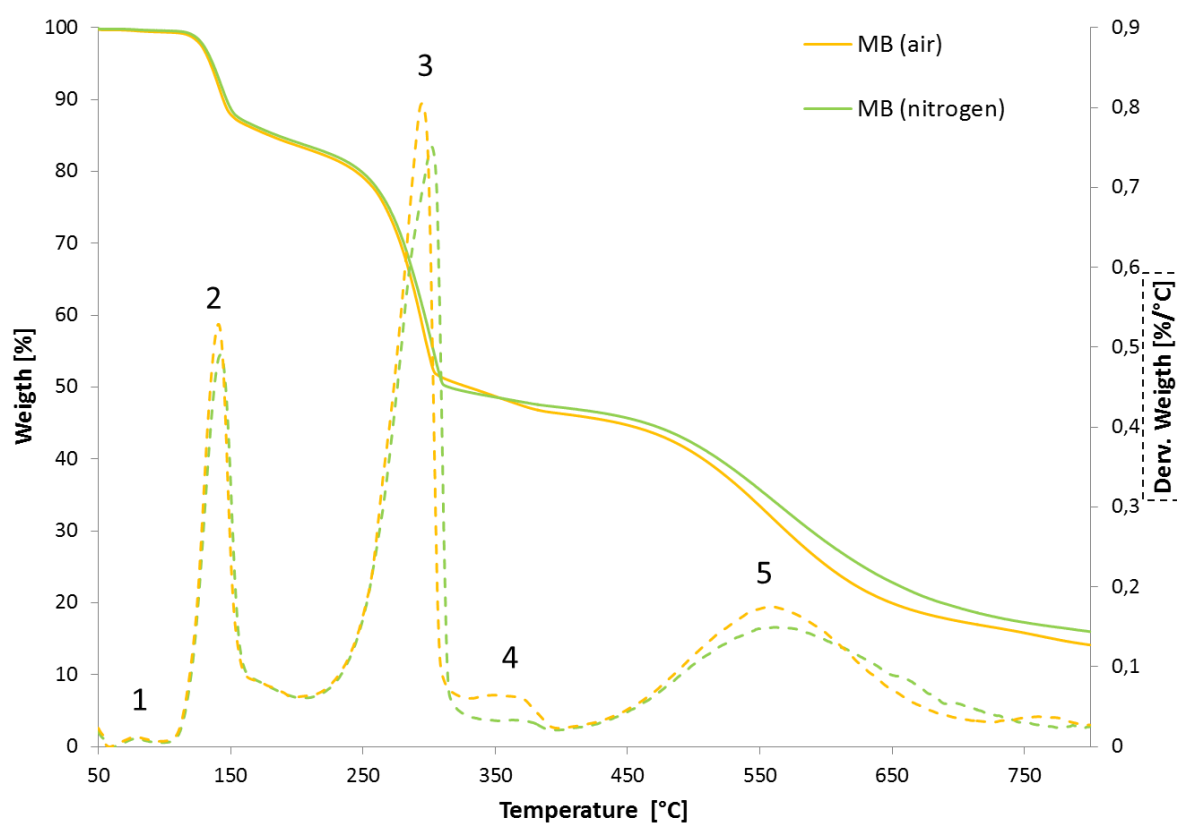
Figure 66: TG and DTG curves for MB, 50-800 °C, 10 °C/min, in air and nitrogen

During the third degradation step from 200 to 330 °C (T_{max} = 300 °C, 34 wt% mass loss), melamine is released. The residue left after this degradation step is expected to consist of a condensate of melamine and boron oxide, but its structure is not reported in literature. A fourth degradation step takes place from 330 to 390 °C (T_{max} = 370 °C, 2 wt% mass loss). As it can be seen this step is slightly more important in thermo-oxidative than in pyrolytic conditions. An attribution to this step was also not found in literature and it must be

elucidated. The last degradation step occurs over a broad temperature range. It takes place from 390 up 800 °C (T_{max} = 560 °C, 30 wt% mass loss). During this step the remaining melamine decomposed completely. At the end of pyrolytic decomposition of MB, a residue of 16 wt% is left and of 14 wt% in the case of the thermo-oxidative degradation. The structure of the residue is not completely reported in literature, but Costa et al. [193] supposed that it contains BNO and/or BN.

$$H_3BO_3 \rightarrow H_2O + HBO_2$$

$$2HBO_2 \rightarrow H_2O + B_2O_3$$
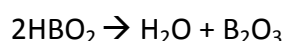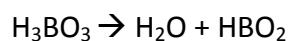
Equation 11: Dehydration of orthoboric acid to metaboric acid and boron oxide

3.1.2. Decomposition of melamine borate in pyrolytic conditions

Decomposition mechanism of MB in pyrolytic conditions is investigated in the condensed and gas phase. First, condensed phase is analyzed. Therefore, MB was treated at 100, 200, 270, 350, 425, 725 and 850 °C under nitrogen. Residues are analyzed using ^{13}C and ^{11}B solid state NMR as well as XPS. Gas phase of MB decomposition is investigated using py-GCMS.

3.1.2.1.   Condensed phase analysis

Residues obtained after thermal treatment of MB in pyrolytic conditions are of white color until 425 °C. A yellowish-brownish residue is found at 725 °C and a brown one at 850 °C (**Figure 67**).
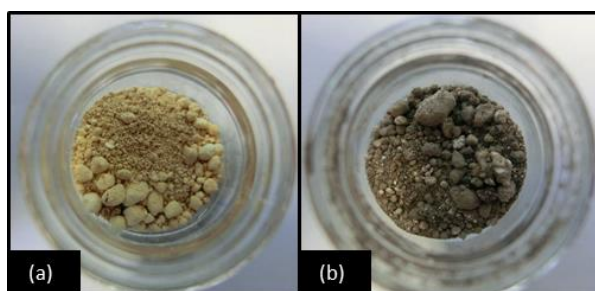
Figure 67: Residues of MB after heat treatment in nitrogen (a) at 725 °C and (b) at 850 °C

Figure 68 presents ^{13}C solid state spectra of the MB residues. As it is seen, virgin MB exhibits a chemical shift at 165, 167 and 168 ppm corresponding to carbon atoms of the melamine ring [196, 197]. At 100 °C, the peak assigned to melamine is slightly shifted to lower resonances (163 ppm). This shift can be due to the first dehydration of MB or due to

formation of melam, a condensation product of melamine, exhibiting two close signals at 164 and 167 ppm having a shoulder on the high-field side [198]. Despite the fact that melam is known as low-temperature condensation product of melamine, a temperature of 100 °C is not high enough to form melam. Thus, formation of melam is excluded and it is therefore assumed that slight shift of the melamine resonance to lower frequencies is due to first dehydration of orthoboric acid in MB leading to a change of chemical environment (structural changes) of the melamine ring.
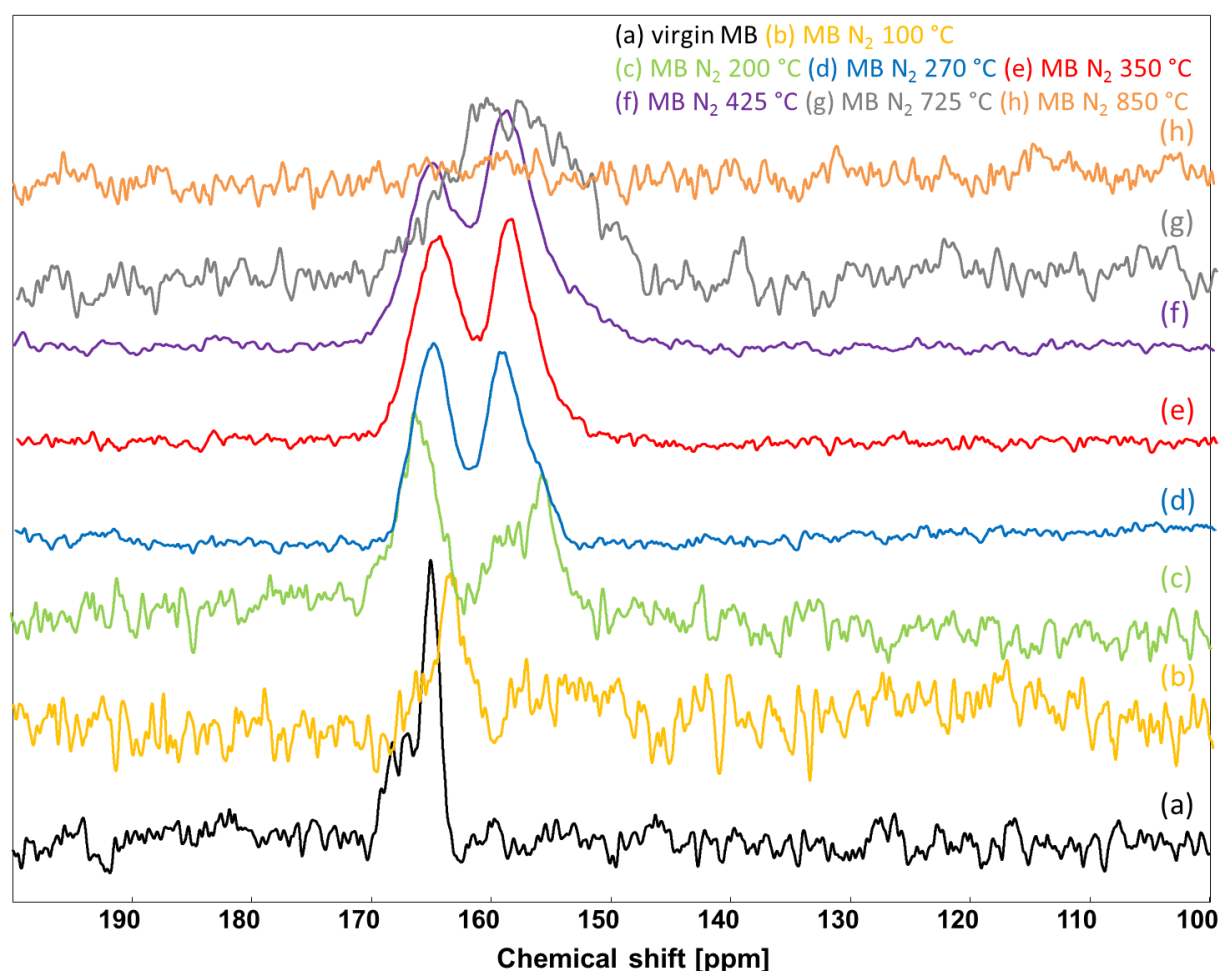
Figure 68: ^{13}C NMR spectra of different stages of MB decomposition in pyrolytic conditions

At 200 °C, two chemical shifts at 165 and 159 ppm assigned to melem are observed [199]. The resonances reveal the presence of carbon linked to the amino groups and C(N$_3$) groups of the cyameluric nucleus. Formation of melon is excluded, even if melon is known to exhibit similar chemical shifts as melem. Indeed, melon is known to be of yellowish-brownish color, whereas MB residue at 200 °C is white (visual observation). Secondly, temperature is too low for melon formation which is usually formed at around 600 °C [199]. NMR spectra taken of

the MB residues at 270, 350 and 425 °C are similar to that observed at 200 °C. It seems that melem exhibits higher ordered structures with increasing temperature due to better resolution of the spectra. At 725 °C, one broad signal around 160 ppm is found. The obtained residue is yellowish-brownish at the surface which shows that melon is formed. The ^{13}C spectrum of MB at 850 °C does not exhibit any signal, supposing that at this temperature, all melamine corresponding structures are totally degraded. This assumption is supported by the fact that melon (detected at 725 °C) is the most stable melamine condensate and is known to decompose before 850 °C. Brownish color of residue is suspected to be due to formation of B-N bonds.

Evolution of the boron structure with temperature in MB is investigated using ^{11}B solid state NMR. Generally, two types of boron environments are distinguished by ^{11}B isotropic signals. Trigonal coordinated boron atoms (B^{III}) exhibit chemical shifts between 12 and 26 ppm, whereas tetrahedral coordinated boron atoms (B^{IV}) have chemical shifts between -4 and 6 ppm. B^{III}/B^{IV} ratio is estimated using Dmfit. Evolution of B^{III}/B^{IV} ratio versus temperature in pyrolytic conditions is presented in **Figure 69**.
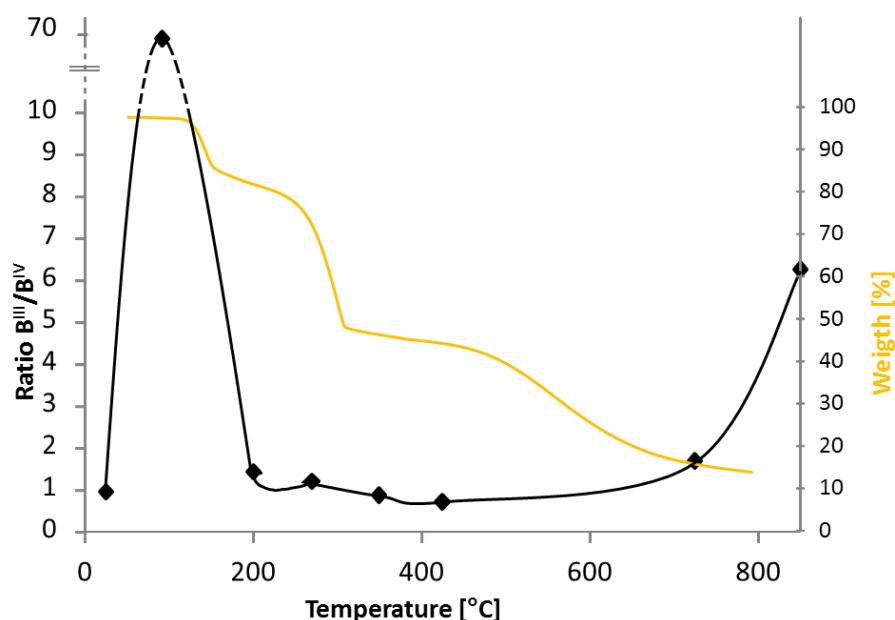
Figure 69: Evolution of B^{III}/B^{IV} ratio versus temperature and TG curve for MB (pyrolytic conditions)

^{11}B spectra of MB heated at different temperatures in pyrolytic conditions are presented in **Figure 70**. Spectrum of virgin MB at ambient temperature, exhibits a second order

quadrupolar lineshape. The observed resonance is attributed to boron in trigonal bonding configuration (B-O bond). It is known that MB consists of melamine and orthoboric acid. The detected B^{III} signal corresponds to that reported for orthoboric acid [195].

After heat treatment at 100 °C in pyrolytic conditions, spectrum of MB exhibits additionally a chemical shift at 1 ppm, which is attributed to tetrahedral coordinated boron atoms (B-O bond). Orthoboric acid is known to undergo dehydration with increasing temperature, whereas orthoboric acid dehydrates around 140 °C forming metaboric acid, which is then dehydrated forming boron oxide [200-202]. It has to be noted that boron in orthoboric acid and metaboric acid is trigonal coordinated. Therefore, it is not possible to clearly assign the signal at 18 ppm to orthoboric and/or metaboric acid. Due to the fact that dehydration reaction of orthoboric acid occurs around 140 °C, it is assumed that only a small quantity of orthoboric acid is dehydrated to metaboric acid at 100 °C. At the same time, hypothesis postulated during analysis of ^{13}C NMR spectrum of MB at 100 °C that slight shift of the ^{13}C signal attributed to melamine indicates dehydration reaction of MB is confirmed. Detection of the signal at 1 ppm is assigned to boron in tetragonal coordination (BO_4). It is reported that boron oxide can consist of BO_3 and BO_4 units or a combination of both [203, 204]. Therefore, detection of B^{IV} is assigned to the formation of boron oxide. Due to the fact that boron oxide can also consist of BO_3 units, the B^{III} signal attributed to orthoboric and/or metaboric can also be coming from BO_3 units in boron oxide. B^{III}/B^{IV} ratio at 100 °C shows that much more B^{III} than B^{IV} is present in the residue and it is concluded that only a small quantity of orthoboric acid is transformed into metaboric acid and boron oxide.

Spectra obtained at 200 and 270 °C are comparable. Both spectra exhibit signals at 16 and 0 ppm assigned to B^{III} and B^{IV} respectively. Ratio of B^{III}/B^{IV} shows that quantity of B^{III} is slightly higher than that of B^{IV}. As mentioned before B^{III} is assigned to the B-O bond in orthoboric, metaboric acid and /or boron oxide. It is supposed that at this stage of the decomposition of MB, orthoboric acid is completely dehydrated to metaboric acid and boron oxide. This is supported by the fact that temperature of dehydration reaction of orthoboric acid is around 140 °C. Presence of B^{IV} signal is assigned to BO_4 units in boron oxide.

^{11}B spectra of MB residue taken at 350 °C and 425 °C exhibit the same resonances. A broad resonance at 17 ppm indicating presence of B^{III} is detected. Broadening of peaks indicates

that crystallinity of the product is decreased. Moreover, signals attributed to B^{IV} are observed at 0 and -5 ppm. The chemical shift at 0 ppm is assigned to B-O bond in tetragonal coordination (BO_4). It is assumed that the resonance at -5 ppm assigned to tetragonal coordinated B-N bonds. Literature reports that resonance at -5 ppm can be assigned to B-H bonds in tetrahedral coordination [205], whereas this possibility is excluded due to low stability of B-H bonds at high temperatures. For example diborane (B_2H_6) which is known to consist of tetrahedral coordinated boron atoms is gaseous at room temperature and starts to decomposes at 300 °C [180]. Therefore, the presence of B-H bonds in the condensed phase at 350 and 425 °C does not make sense. Ratio of B^{III}/B^{IV} at 350 and 425 °C, i.e. 0.8 and 0.7 respectively, is smaller than that obtained at lower temperatures. This indicates that more tetragonal than trigonal coordinated boron is present in the residue. It is concluded that at this stage of the decomposition of MB, boric acid is completely dehydrated to boron oxide.
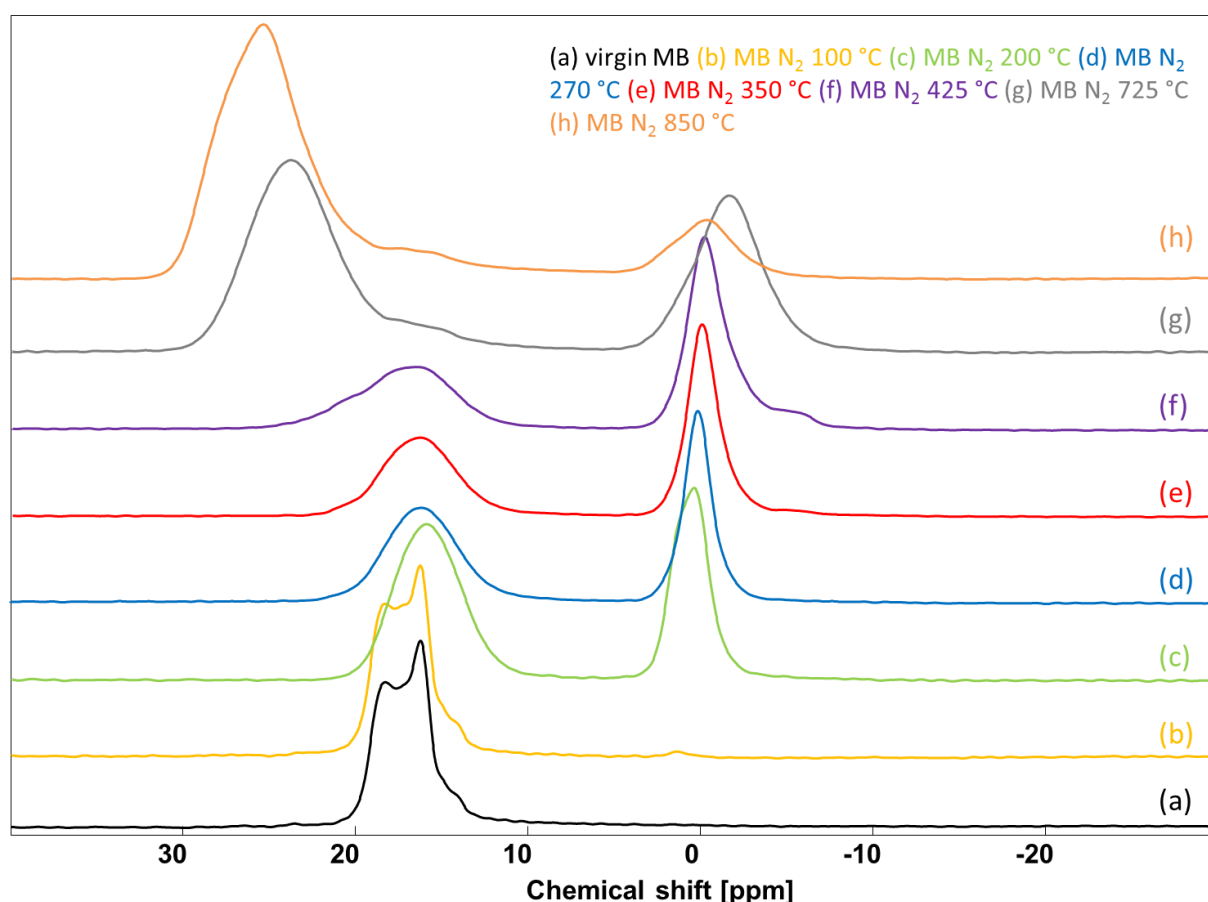
Figure 70: ^{11}B NMR spectra of different stages of MB decomposition in pyrolytic conditions

Figure 71 shows the ^{11}B NMR spectrum of boron oxide with 99.9 % purity. The spectrum exhibits one main signal at 15 ppm assigned to boron in trigonal coordination (BO_3). Besides a small resonance at 2 ppm is observed indicating presence of a small quantity of BO_4 units in boron oxide. In the spectra of MB obtained at 325 and 425 °C quantity of BO_4 units is significantly higher than observed for pure boron oxide at room temperature. It has to be noted that the spectrum of boron oxide shown in **Figure 71** is performed in boron oxide having a high purity. In MB at higher temperatures instead, boron oxide does not consist in its pure form and thus it is not surprising that the quantity of BO_4 units is higher than that of BO_3 units. Moreover, as mentioned above, boron oxide is known to consist of BO_3 and BO_4 units or a combination of both [203, 204]. Generally, presence of boron oxide in the residue of MB obtained at 325 and 425 °C is evidenced by looking at the [11]B spectrum of boron oxide in its pure form.
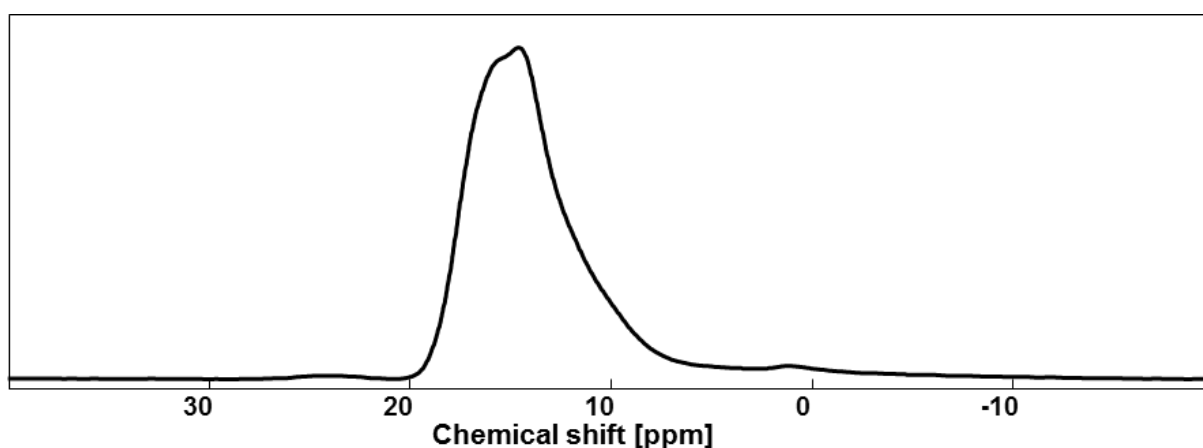
Figure 71: ^{11}B NMR spectrum of boron oxide (99.9 % purity)

At 725 °C three chemical shifts are detected in the spectrum of MB. The resonance at 24 ppm is attributed to formation of B-N bonds in trigonal coordination in the residue [206-208]. A shoulder at 18 ppm indicates presence of BO_3 units. As mentioned before, it is assumed that at this temperature metaboric acid is completely dehydrated and signal is only due to BO_3 units in boron oxide. The chemical shift at -2 ppm is due to tetragonal coordinated boron and is assigned to BO_4 units in boron oxide. At the end of decomposition of MB in pyrolytic conditions, at 850 °C, resonances assigned to BO_3 and BO_4 units as well as B-N bonds are detected. It has to be noted that Costa et al. [193] suggested formation of BN and/or BNO at the end of pyrolytic decomposition of MB. Using ^{11}B solid state NMR

presence of BN or BNO is not clearly evidenced. Presence of BO_3 and BO_4 units in the residue as well as existence of B-N bonds is proven.

Therefore, residues of MB at 725 and 850 °C are additionally analyzed using XPS to get more detailed information concerning the nature of the B-N bond detected using ^{11}B solid state NMR as well as the concentration of boron, oxygen, carbon and nitrogen (**Table 26**).

Table 26: Quantification of N, B, C and O amount in MB at 725 and 850 °C in nitrogen (XPS)

Sample	Atom orbital	Concentration
MB 725 °C	N 1s	27.49
	O 1s	26.72
	B 1s	26.00
	C 1s	19.79
MB 850 °C	N 1s	28.96
	O 1s	26.44
	B 1s	34.71
	C 1s	9.88

First of all, it has to be noted that a concentration of carbon under 10 % is due to impurities. Therefore, quantity of carbon at 850 °C is negligible. At 725 °C instead, deconvolution of the C 1s spectrum (not presented here) shows that three carbon species are present in the residue. The signals at 285.00 and 289.01 eV are assigned to impurities, whereas the signal at 286.1 eV corresponds to that of the C-N bond in melon reported in literature [209]. Moreover, N 1s spectrum (**Figure 72**) reveals presence of N-$(C)_3$ group at 399.8 eV [210]. Additionally, the peak at 398.7 eV is assigned to BN [211]. Results obtained by XPS, correspond to that obtained by ^{13}C NMR indicating that at 725 °C melon is present in the condensed phase and at 850 °C it is decomposed.

Figure 73 presents B 1s spectra of MB at 725 and 850 °C. Both residues exhibit a peak at 191.1 eV assigned to boron nitride (BN) [211]. Formation of boron nitride is explained by reaction of ammonia (evolved during MB decomposition) and boron oxide which is known to take place at high temperatures [180] (**Equation 12**).

$$2\ NH_3 + B_2O_3 \rightarrow 2\ BN + 3\ H_2O$$
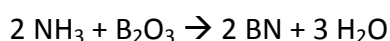
Equation 12: Formation of boron nitride

Presence of boron trinitride (BN$_3$) in the residue is excluded due to the fact that B 1s binding energy of this compound is known to be lower (190.4 eV) than that of boron nitride [212, 213]. A second peak at 192.4 eV is observed at 725 and 850 °C. This signal is assigned to BO$_x$N$_y$ [214], an intermediate state between boron nitride and boron oxide. Thus, presence of BN and BNO is evidenced. Boron oxide is found to be present at 725 °C indicated by a peak at 193.7 eV [215]. At 850 °C, boron oxide is not detected. It is supposed that boron oxide detected at 725 °C is transformed into BNO structures due to presence of ammonia coming from decomposition of melon. Moreover, as seen during analysis of ^{11}B spectra of the MB residues at 725 and 850 °C, B-H bindings are not detected using XPS since binding energy of B-H should be detected in B 1s spectra at 187.8 eV [215].
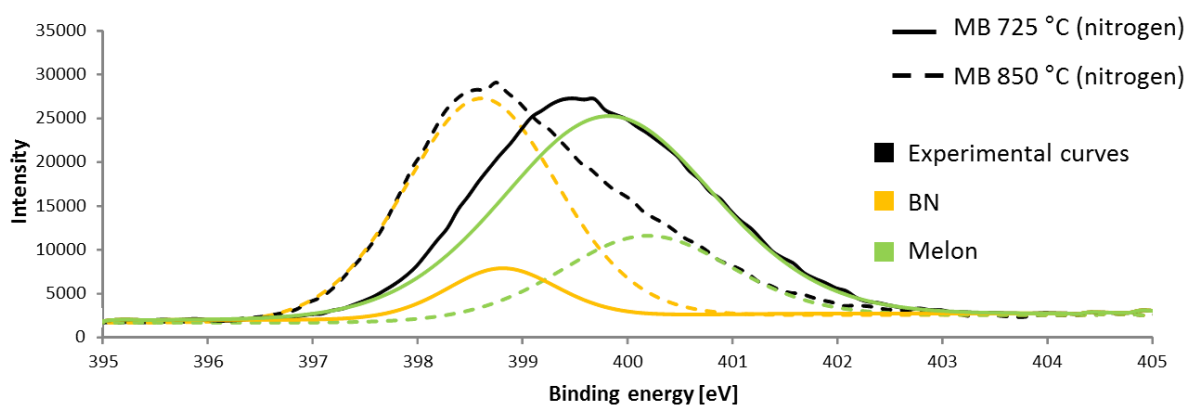
Figure 72: N 1s spectrum of MB at 725 and 850 °C in nitrogen

Comparing the concentrations of nitrogen, oxygen and boron at 725 and 850 °C, it is seen that at 850 °C more boron is detected than at 725 °C. Concentration of oxygen and nitrogen are similar at both temperatures. Amount of boron is 26 % at 725 °C and 35 % at 850 °C. Concentration of oxygen is 26 % at 725 and 850 °C, whereas concentration of nitrogen is 28 %. Unchanged nitrogen concentration at 725 and 850 °C despite the fact that melon is completely decomposed at 850 °C is explained by a favored formation of BN at higher temperatures. At 725 °C, concentration of BNO structures is ten times higher than that of boron nitride and boron oxide (**Table 27**). At 850 °C, concentration of boron nitride and BNO structures is similar and boron oxide is not detected. This indicates that boron oxide detected at 725 °C is transformed to BNO structures with increasing temperature. BNO structures in turn are transformed to boron nitride with increasing temperature.
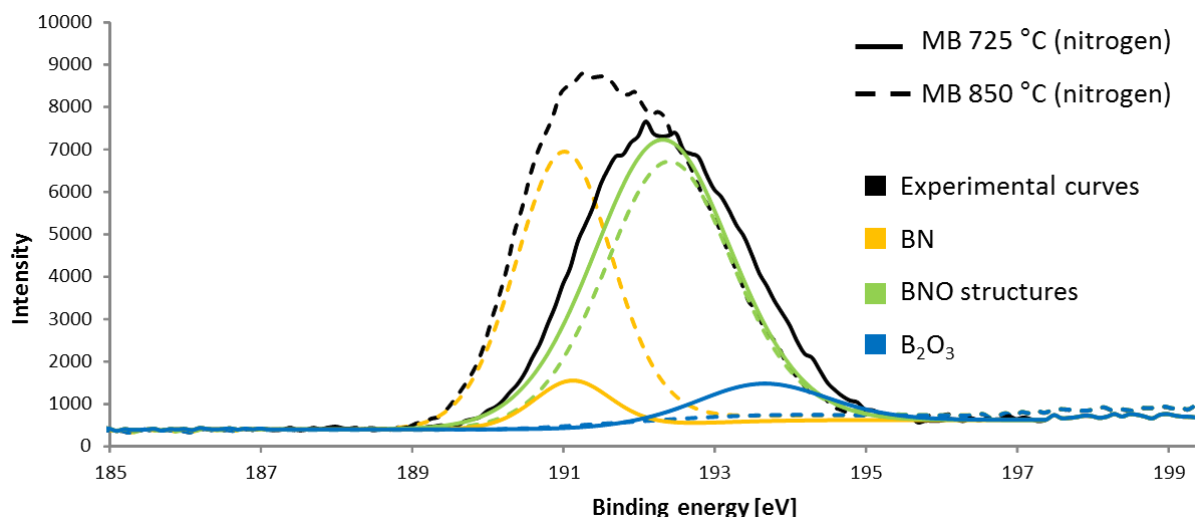
Figure 73: B 1s spectrum of MB at 725 and 850 °C in nitrogen

Table 27: Quantification (XPS) of boron species in MB at 725 and 850 °C in nitrogen

Sample	Atom orbital	Concentration
MB 725 °C	BN	7.8
	BNO structures	82.2
	B_2O_3	10
MB 850 °C	BN	44.7
	BNO structures	55.1
	B_2O_3	0.2

3.1.2.2.   Gas phase analysis

Analysis of gases evolved during pyrolytic decomposition of MB is performed using py-GCMS step wise method. Chromatograms of released gas during the different decomposition steps are presented in **Figure 74**. The presence of the peak "air" in the spectra is due to air blocked in between the pyrolyzer and the GCMS device.

From 50 to 100 °C, corresponding to the first decomposition step of MB in pyrolytic conditions, water (1) and peaks assigned to residues of the column (2) are detected. Presence of water confirms hypothesis that in this temperature range, orthoboric acid is dehydrated forming metaboric acid leading to a shift of the melamine resonance in the ^{13}C spectrum. During the second decomposition step, taking place from 100 and 200 °C, melamine (3) and water (4) are detected indicating progress in dehydration of orthoboric and metaboric acid and sublimation of melamine at the same time.

From 200 to 330 °C only melamine (5) is evolved into the gas phase. In the temperature range between 330 and 390 °C ammonia (6), cyanamide (7) and melamine (8) are detected. Release of ammonia and cyanamide is due to melamine decomposition. During the last decomposition step of MB (390 to 800 °C) a broad peak (9) is observed. Looking at the mass spectrum (**Figure 75**) at the maximum of this peak, it is seen that the obtained mass spectrum reveals the presence of several molecules.
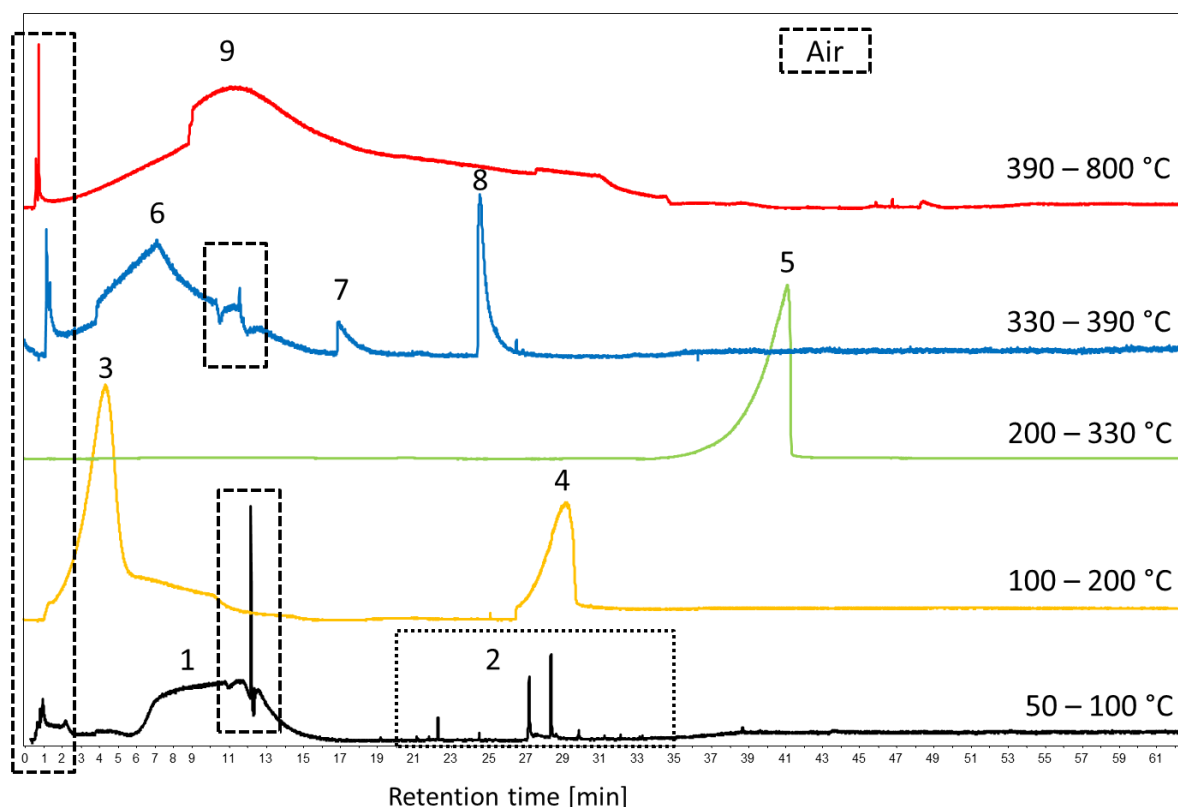
Figure 74: Analysis of gases released during pyrolytic decomposition of MB using py-GCMS
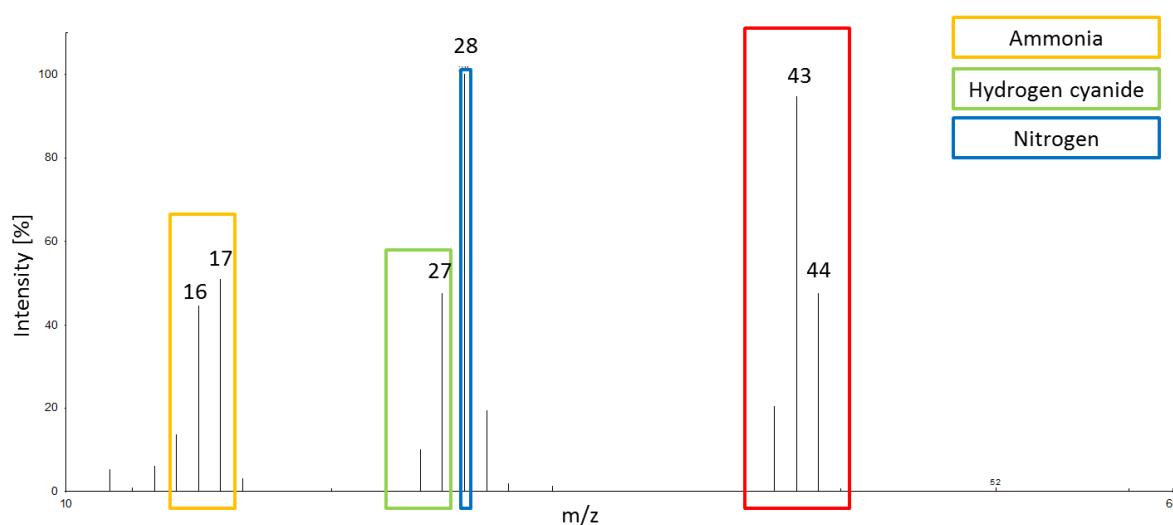
Figure 75: Mass spectrum observed from 390 – 800 °C for MB in pyrolytic conditions

After comparison with NIST library the following molecules can be identified: ammonia, hydrogen cyanide and nitrogen. Identification of the mass peaks at 43 and 44 m/z is difficult (encircled in red). During analysis of the condensed phase, it was shown that in the temperature range from 425 to 850 °C melamine degrades. It is therefore supposed that the observed mass peaks are due to melem degradation. Ju et al. [216] reported that a mass peak at 43 m/z corresponds to $CN_2H_3^+$ which corresponds to assumption that mass peaks (encircled in red) are due to decomposition of melamine condensates. Furthermore, detection of nitrogen, ammonia and hydrogen cyanide indicate that decomposition of melem is taking place.

3.1.3. Decomposition of melamine borate in thermo-oxidative conditions

As for decomposition of MB in pyrolytic conditions, decomposition in thermo-oxidative conditions is investigated in the condensed and gas phase. First, condensed phase is analyzed. Therefore, MB is treated at the same temperatures as in pyrolytic conditions and residues are analyzed afterwards using XPS, ^{13}C and ^{11}B solid state NMR. Then, gas phase of MB decomposition is investigated using TGA-FTIR.

3.1.3.1. *Condensed phase analysis*

Figure 76 presents ^{13}C solid state NMR spectra recorded for MB at different temperatures. After heat treatment all residues have a white color. Formation of melon which is known to be of yellow color is therefore already excluded or at least very limited. Spectrum found for virgin MB at room temperature indicating presence of melamine was already discussed above (**page 139**).

At 100 °C, MB exhibits a chemical shift at 164 ppm with two shoulders at 167 and 168 ppm. These resonances are similar to those obtained for MB at room temperature, whereas the peak corresponding to melamine is slightly shifted to lower resonances (-1 ppm). As it was discussed for MB decomposition in pyrolytic conditions, a shift to lower resonances is attributed to dehydration of MB.

At 200 °C, ^{13}C NMR spectrum exhibits chemical shifts at 167 and 156 ppm having a shoulder at 159 ppm. These peaks are attributed to melem [199]. Formation of melon known to be of yellow color is excluded due to white color of the residue. The spectrum recorded at 270 °C

exhibits the same resonances as observed at 200 °C. ^{13}C NMR spectra of MB at 350 and 425 °C exhibit the same signals at 166 and 160 ppm. As for lower temperatures, the observed resonances are assigned to melem. Formation of melon is again excluded due to white color of the residues. At 750 °C, ^{13}C spectrum is flat and no signal can be recorded because of complete decomposition of melamine and of its condensation products.
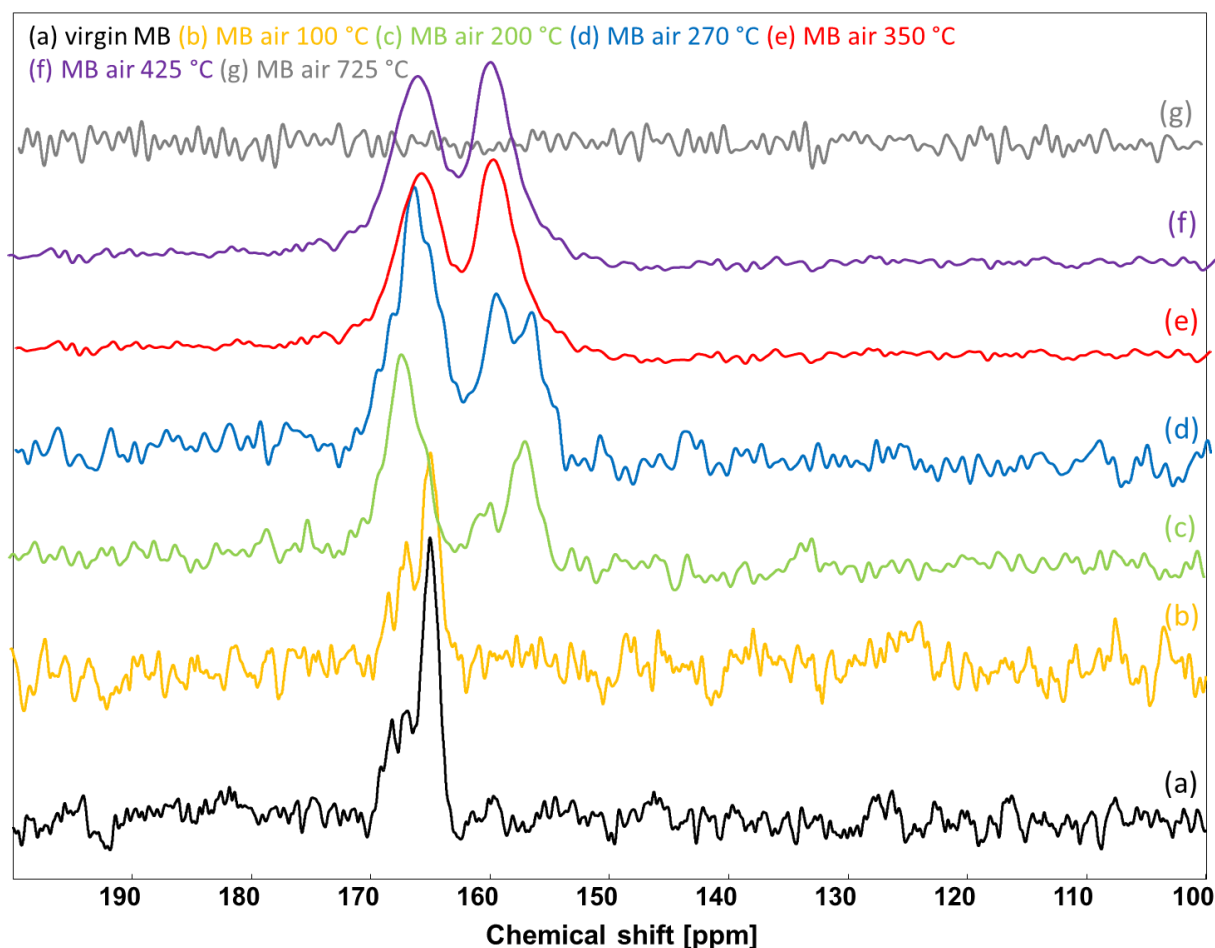

Figure 76: ^{13}C NMR spectra of different stages of MB decomposition in thermo-oxidative conditions

^{11}B NMR spectra at different stages of MB decomposition in thermo-oxidative conditions are presented in **Figure 77**. The spectrum of the MB at room temperature indicating presence of orthoboric acid was already discussed (**page 139**).

At 100 °C, the obtained spectrum is similar to that found at room temperature. The chemical shift at 17/16 ppm is assigned to trigonal coordinated boron atoms which are known to be present in orthoboric acid, metaboric acid and boron oxide. As it was discussed for the spectrum collected after heat treatment in pyrolytic conditions, this resonance is mainly

attributed to orthoboric acid. Only a small quantity of metaboric acid is supposed to be present. The result found at 100 °C in thermo-oxidative conditions is different to that found in pyrolytic conditions where at 100 °C a small quantity of boron oxide (B^{IV} signal) was detected besides the B^{III} signal attributed to orthoboric and metaboric acid.
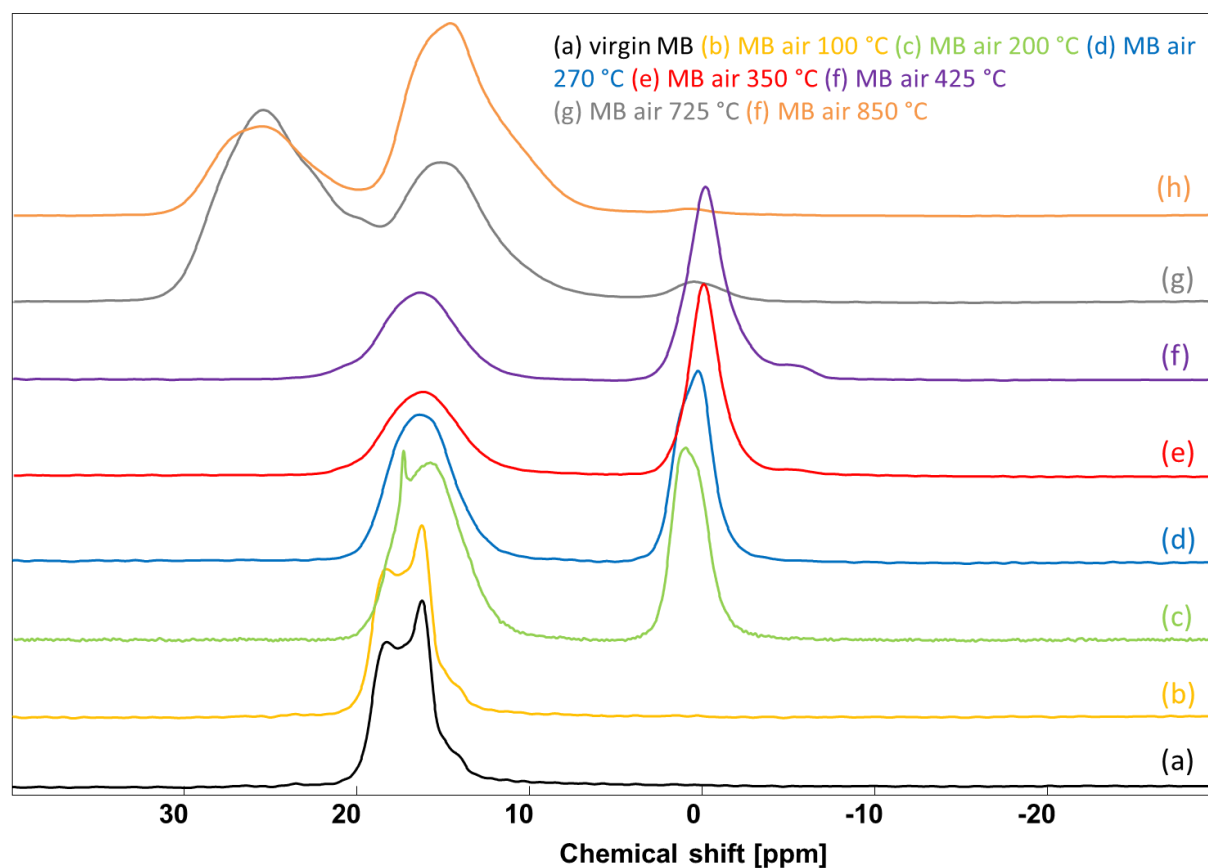
Figure 77: ^{11}B NMR spectra of different stages of MB decomposition in thermo-oxidative conditions

The spectrum of MB in thermo-oxidative conditions at 200 °C exhibits signals indicating presence of B^{III} (17 and 16 ppm) and B^{IV} (1 ppm) in the residue whereas ratio B^{III}/B^{IV} is 1.74. Signal at 17 and 16 ppm is assigned to trigonal coordinated boron found in metaboric acid and/or boron oxide. Presence of orthoboric acid is excluded due to the fact that dehydration reaction forming metaboric acid is known to take place at 140 °C. The signal at 1 ppm is due to BO_4 units in boron oxide. Residues at 270 and 350 °C exhibit the same signals as those found for MB at 200 °C. The chemical shift corresponding to B^{III} is detected around 16 ppm, whereas the signal attributed to B^{IV} is found around 0 ppm. The B^{III}/B^{IV} ratio decreases with increasing temperature indicating that dehydration of metaboric acid forming boron oxide progresses. B^{III}/B^{IV} ratio is 1.31 at 270 °C and 0.98 at 325 °C. At 425 °C additionally to signals

observed at 200, 270 and 350 °C, a chemical shift at -5 ppm is found in the ^{11}B spectrum. As it was discussed before, the resonance at -5 ppm is assigned to B-N bonds in tetragonal coordination. At 425 °C, ratio of B^{III}/B^{IV} is decreased to 0.82. At 725 and 850 °C spectra exhibit signal attributed to B-N bonds (25 ppm), B-O in trigonal coordination (15 ppm) and B-O in tetragonal coordination (1 ppm).

Comparing ^{11}B spectra for MB in pyrolytic and thermo-oxidative conditions, it is seen that spectra are similar from room temperature up to 425 °C. At high temperatures i.e. 725 and 850 °C, it is observed that in pyrolytic conditions the amount of tetragonal coordinated boron (BO_4) is higher than that of trigonal coordinated boron (BO_3). In thermo-oxidative conditions at the opposite a higher amount of BO_3 than BO_4 is found. Moreover, amount of B-N in the residue is higher in pyrolytic than in thermo-oxidative conditions. It is supposed that formation of B-N bonds with nitrogen coming from melamine decomposition is favored over formation of B-O bonds due to the fact that oxygen is absent in the surrounding atmosphere. Moreover, boron oxide structure favors crystallization in trigonal coordination of the boron atoms in thermo-oxidative conditions, whereas BO_4 units are favored in pyrolytic conditions. It has to be noted that in TGA experiment, MB has similar decomposition steps in pyrolytic and thermo-oxidative conditions. Moreover, remaining residues at the end are similar in both conditions. Thus, residue of MB at 850 °C in pyrolytic and thermo-oxidative conditions have the same mass and only composition is different.

Table 28: Quantification of N, B, C and O amount in MB at 725 and 850 °C in air (XPS)

Sample	Atom orbital	Concentration
MB 725 °C	N 1s	20.78
	O 1s	35.29
	B 1s	39.73
	C 1s	4.2
MB 850 °C	N 1s	15.11
	O 1s	42.03
	B 1s	39.91
	C 1s	2.95

As mentioned during analysis of the condensed phase in pyrolytic conditions, existence of BN and/or BNO at the end of decomposition in thermo-oxidative conditions cannot be evidenced clearly using solid state NMR. Thus, additionally XPS measurements are carried

out on MB residues at 725 and 850 °C. **Table 28** presents quantification of carbon, oxygen, nitrogen and boron in the residues.

Concentrations of carbon for both samples can be attributed to impurities. At 725 °C, MB consists of 21 % nitrogen, 35 % oxygen and 40 % boron. At 850 °C, the residue consists of 15 % nitrogen, 42 % oxygen and 40 % boron. Absence of carbon in the residues supports results found using ^{13}C solid state NMR. Melamine and melamine condensates are completely decomposed before 725 °C.

B 1s spectra of MB residues at both temperatures are presented in **Figure 78**. Deconvolution of the B 1s spectra reveals the presence of three different species: boron nitride (BN) (191.1 eV), BNO structures (192.4 eV) and boron oxide (193.7 eV) [214]. In contrast to XPS results obtained for MB in pyrolytic conditions, boron oxide is still present at 850 °C. It is known that boron oxide normally is transformed into BNO structures and boron nitride respectively through presence of ammonia coming from melamine or melamine condensate decomposition products. Due to the fact that melamine and melamine condensates are completely decomposed before 725 °C in thermo-oxidative conditions, ammonia is absent and boron oxide cannot further transform to BNO structures or BN respectively.
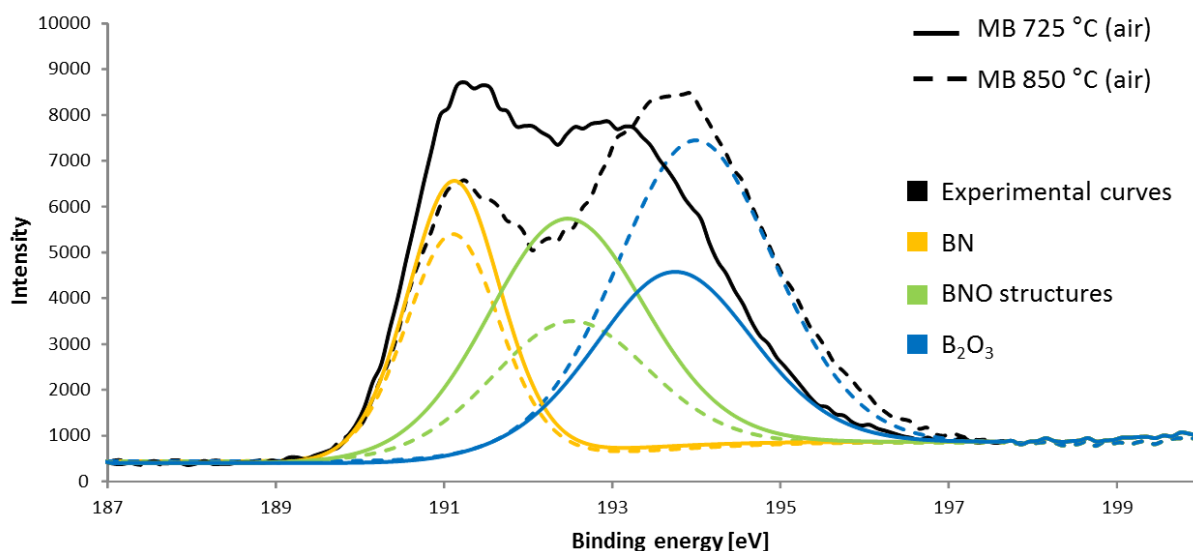
Figure 78: B 1s spectrum of MB at 725 and 850 °C in air

As seen in **Table 29**, with increasing temperature concentration of BNO structures decreases and that of boron oxide increases. This indicates that BNO structures are oxidized to boron oxide at high temperatures. At the same time, concentration of boron nitride slightly

decreases with increasing temperature indicating that boron nitride is also oxidized when temperature increases.

Table 29: Quantification (XPS) of boron species in MB at 725 and 850 °C in air

Sample	Atom orbital	Concentration
MB 725 °C	BN	28.7
	BNO structures	40.8
	B_2O_3	30.5
MB 850 °C	BN	23.2
	BNO structures	23.2
	B_2O_3	53.6

3.1.3.2.   Gas phase analysis

Gas phase analysis of MB in thermo-oxidative conditions was carried out using TGA-FTIR. Py-GCMS which is known to give more detailed information about the structure of the evolved gases can only be used in pyrolytic conditions. Therefore, TGA-FTIR experiments are carried out to investigate the gas phase of MB in thermo-oxidative conditions. The disadvantage of the TGA-FTIR device used in this study is the condensation of melamine and its condensation products in the transfer line between TGA and FTIR. Using a small amount of MB avoids blocking of the transfer line and permits analysis of decomposition gases except of melamine or its condensation products which condensate in the transfer line. **Figure 79** shows FTIR spectra as a function of time obtained at a heating ramp of 10 °C/min. The corresponding attribution of the observed vibrations is presented in **Table 30**. It has to be noted that vibrations corresponding to nitrogen monoxide and nitrogen dioxide are not detected during experiment.

From 130 to 190 °C, the typical vibrations assigned to water are observed between 3700 and 3400 cm^{-1} as well as between 1700 and 1400 cm^{-1}. Water is released during dehydration of orthoboric acid to metaboric acid. This observation supports hypothesis postulated above during analysis of the condensed phase that slight shifting of ^{13}C signal assigned to melamine at 100 °C is due to dehydration of MB. Vibrations of melamine and its condensation products are not detected. Nevertheless, release of these molecules cannot be excluded due to possible condensation in the transfer line.

In the temperature range from 190 to 310 °C, no vibrations are detected. Due to the fact that TGA curve indicates a mass loss in this temperature range (34 wt%), it is concluded that

melamine and its condensation products are evolved but condensate in the transfer line and can therefore not be detected. Moreover, analysis of the condensed phase in this temperature range showed changes in ^{13}C and [11]B spectra indicating change of chemical structure of MB.
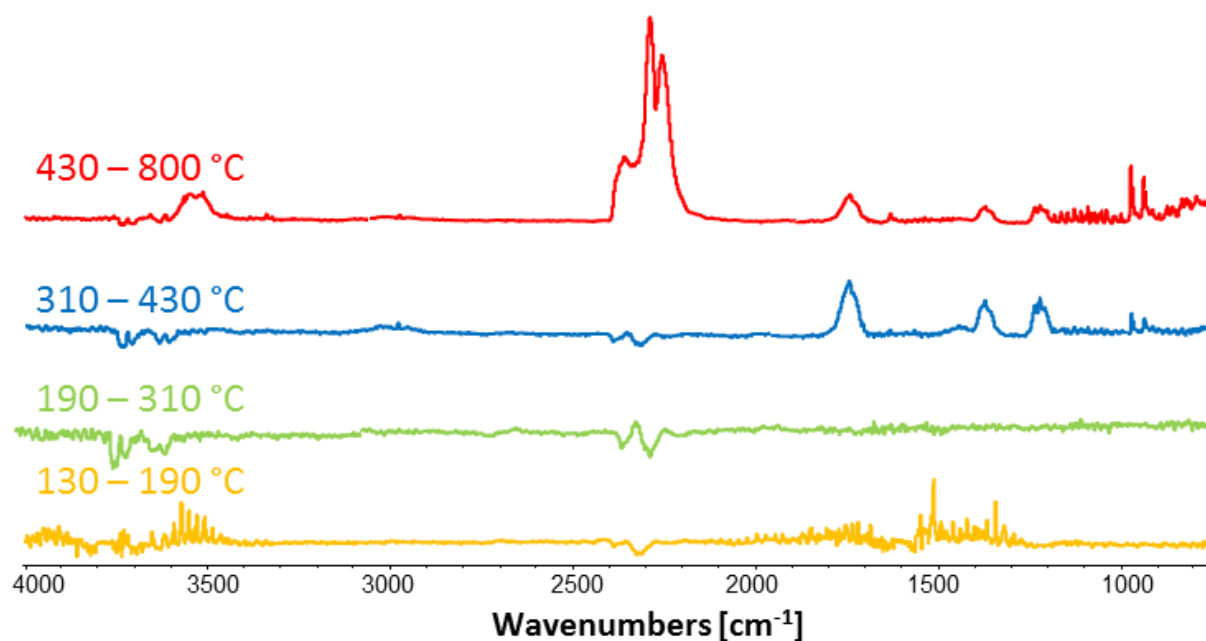
Figure 79: FTIR spectra of gases released during thermo-oxidative decomposition of MB

Table 30: Attribution of vibrations obtained by TGA-FTIR for MB in thermo-oxidative

conditions, 10 °C/min

Wavelength [cm^{-1}]	Corresponding chemical structure
3700 - 3400	ν (O-H) in H_2O
3560, 3546	CO_2 and ν (OH) in cyanic acid
2970	ν (N-H) in NH_2
2354	ν (C-O) in CO_2
2284, 2251	CO
1737	ν (C=O)
1700 - 1400	δ (O-H) in H_2O
1626	ν (N-H) in NH_3
1365	ν (C-N)
1229/1216	δ (O-H) in cyanic acid
1084	ν (C-O) in cyanic acid
965, 930	δ (N-H) in NH_3

From 310 to 430 °C, corresponding to the fourth degradation step of MB in thermo-oxidative conditions, vibrations corresponding to ammonia (1626, 965 and 930 cm^{-1}) and hydrogen cyanide (1229, 1216 and 1084 cm^{-1}) are observed. Presence of these vibrations indicates

decomposition of melamine and/or its condensation products. Besides the previously attributed vibrations, peaks attributed to C=O (1737 cm^{-1}), N-H in NH$_2$ (2970 cm^{-1}) and C-N (1365 cm^{-1}) are found. This leads to the assumption that first melamine is partially oxidized and second decomposition fragments of oxidized melamine compounds are evolved into the gas phase.

In the temperature range from 430 to 800 °C, additionally to molecules found from 310 to 430 °C, vibrations corresponding to carbon monoxide (2284 and 2251 cm^{-1}) and carbon dioxide (3560, 3564 and 2354 cm^{-1}) are detected. Presence of carbon monoxide and carbon dioxide indicates that incomplete and complete decomposition is taking place.

3.1.4. Conclusion

Decomposition mechanism of MB in thermo-oxidative and pyrolytic conditions was investigated (**Figure 80**). The decomposition mechanism of MB in pyrolytic conditions proposed by Costa et al. [193] can be extended thanks to results obtained in this work using solid state NMR, XPS, py-GCMS and TGA-FTIR. In the temperature range from 180 to 330 °C (corresponding mainly to the third decomposition step found in TGA experiment, 200 – 330 °C) orthoboric acid is dehydrated evolving water and forming metaboric acid since at 200 °C boron oxide is detected in the condensed phase. At the same time, melamine partially sublimate is released into the gas phase. Moreover, melem is formed in the condensed phase. From 330 to 390 °C (corresponding to fourth decomposition step of MB), metaboric acid is completely dehydrated into boron oxide. Furthermore, boron nitride and BNO structures are formed in the condensed phase. Melamine and melem are decomposed evolving melamine, cyanamide and ammonia. In the temperature range from 390 to 520 °C (corresponding to the fifth decomposition step detected by TGA), boron oxide, boron nitride and BNO intermediates are found in the condensed phase. Melamine and melem completely disappear from the condensed phase whereas their pyrolysis products are still detected in the gas phase. Moreover, from 425 °C, melon is formed in the condensed phase. At 850 °C, a residue consisting of boron nitride, BNO structures and melon is left.

In thermo-oxidative conditions, the decomposition mechanism is similar to that in pyrolytic conditions even if some differences are observed at high temperature. Firstly, boron oxide is already detected at 100 °C and is therefore formed at lower temperatures than in pyrolytic

conditions. Dehydration reaction of orthoboric acid is taking place at the same temperatures in both conditions. Moreover, boron nitride and BNO structures are formed at lower temperatures (ΔT = 50 °C). In contrast to pyrolytic MB decomposition, melon is not detected in the temperature range from 400 to 700 °C in thermo-oxidative conditions. Furthermore, it was found that melamine structures are oxidized in thermo-oxidative conditions. Additionally to gases observed in pyrolytic conditions, carbon monoxide and carbon dioxide are released from 400 to 800 °C. At the end of the thermo-oxidative decomposition of MB, a residue consisting of boron nitride, boron oxide and BNO intermediates is left.
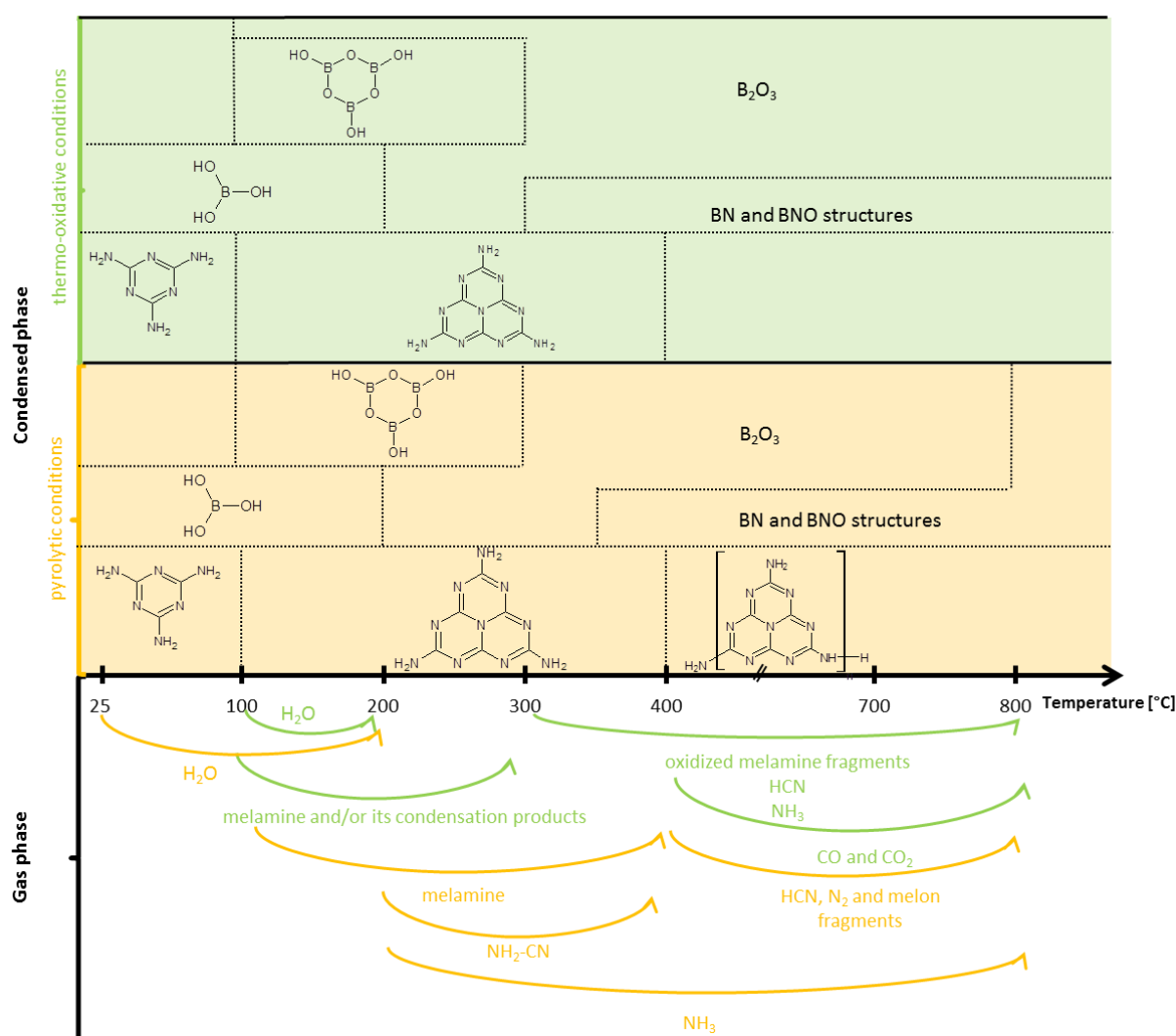
Figure 80: Decomposition mechanism of MB

The next step of this study, after comprehension of the decomposition mechanism of MB consists in the investigation of the decomposition mechanism of EVM-ATH-MB. First thermal

decomposition of EVM-ATH-MB is discussed. Then, fire retardant mechanism of EVM-ATH-MB is determined using py-GCMS, ML-FTIR and solid state NMR (^{13}C, ^{27}Al and ^{11}B).

3.2. Thermal decomposition of EVM-ATH-MB

Figure 81 presents pyrolytic and thermo-oxidative decomposition of EVM-ATH-MB. As it can be seen, the pyrolytic decomposition is a four-step process. The first decomposition step occurs from 180 to 310 °C with a maximum weight loss at 250 °C and a mass loss of 19 wt% during this step.
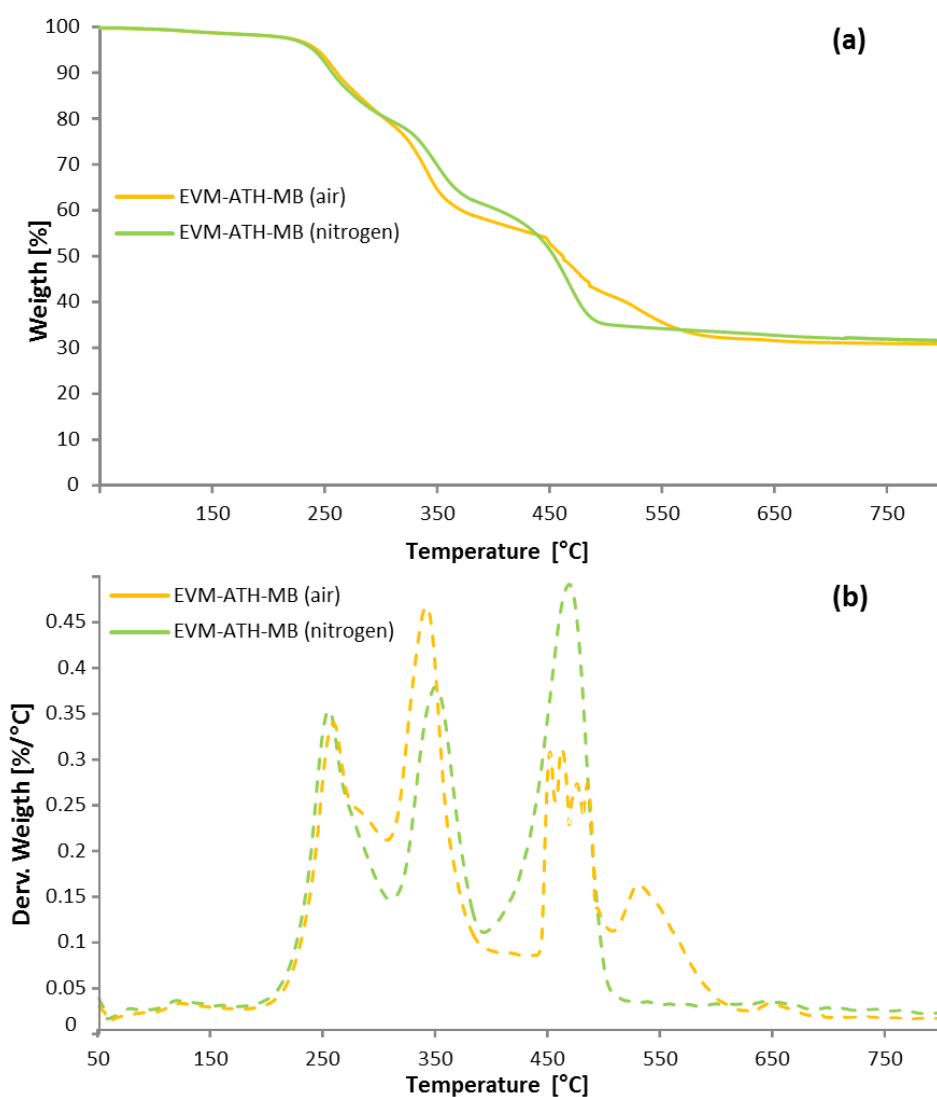
Figure 81: TG (a) and DTG (b) curves for EVM-ATH-MB, 50-800 °C, 10 °C/min, in air and nitrogen

From 310 to 390 °C the second decomposition step (T_{max} = 350 °C, 18 % weight loss) takes place. During the third decomposition step (390 – 520 °C, T_{max} = 465 °C) 26 wt% mass are lost. The last decomposition step takes place from 630 to 690 °C (1 % weight loss). A residue of 32 wt% remains after the pyrolytic decomposition of EVM-ATH-MB.

The thermo-oxidative decomposition is more complex and takes places in five steps. The first one occurs from 180-305 °C (T_{max} = 255 °C, 19 % weight loss) and the second one from 305 to 410 °C (T_{max} = 340 °C, 23 % weight loss). The third decomposition step takes place from 450 to 505 °C with a maximum weight loss at 460 °C and a total weight loss of 16 wt%. The fourth decomposition step occurs between 505 and 630 °C (T_{max} = 530 °C, 10 % weight loss) and the fifth one from 630 to 690 °C (1 % weight loss). At the end of the thermo-oxidative decomposition of EVM-ATH-MB, a residue of 31 wt% is left.

To understand the mechanisms going on during EVM-ATH-MB decomposition in pyrolytic and thermo-oxidative conditions, the gas and condensed phase of the material is investigated in the next part.

3.3. Investigation of the gas phase of EVM-ATH-MB

In this section, gases released during decomposition of EVM-ATH-MB in pyrolytic and thermo-oxidative conditions are analyzed using py-GCMS and MLC-FTIR.

3.3.1. Analysis of gases released in pyrolytic conditions of EVM-ATH-MB

To investigate the gases released during pyrolytic decomposition of EVM-ATH-MB, the material was heat treated up to 180, 310, 390, 520 and 800 °C. Those temperatures are chosen according to the decomposition steps found during TGA experiment. After reaching each temperature, evolved gases are separated and analyzed using a GCMS device. Observed chromatograms are presented in **Figure 82**.

From 50 to 180 °C water (1), molecules coming from decomposition of the vulcanization agent (Rhenofit) (2) and melamine (3) are detected in the gas phase. Presence of water is due to dehydration of orthoboric acid to metaboric acid releasing a low quantity of water in this temperature range. Possibility that presence of water is due to dehydration of ATH is

excluded due to the fact that during decomposition of EVM-ATH and EVM-ATH-MEL water is not detected in this temperature range (50 – 180 °C).

Detection of melamine in the gas phase indicates sublimation of melamine. In the temperature range from 180 to 310 °C, corresponding to the second degradation step of EVM-ATH-MB, three molecules are found. Water (4) evolved during dehydration of ATH forming alumina, acetic acid (5) evolved during deacetylation of the polymer and melamine (6) due to sublimation of melamine of MB. During the second and third degradation step (310 – 520 °C) peaks corresponding to acetic acid (7), acetone (7), acetonitrile (8) and short (9), i.e. $C_4 - C_8$, and long (10), i.e. up to C_{36}, chain of saturated und monounsaturated hydrocarbons are detected. Presence of acetic acid is as mentioned above due to deacetylation of the polymer. Alumina which is formed in the condensed phase during the second decomposition step catalyzes transformation of acetic acid into acetone [173, 178] leading to detection of acetone in the gas phase. Saturated and monounsaturated hydrocarbons are released from decomposition of the polyene structure which is formed during deacetylation of the polymer. From 520 to 800 °C (not shown), molecules coming from decomposition of the vulcanization agent (Perkadox) are found.
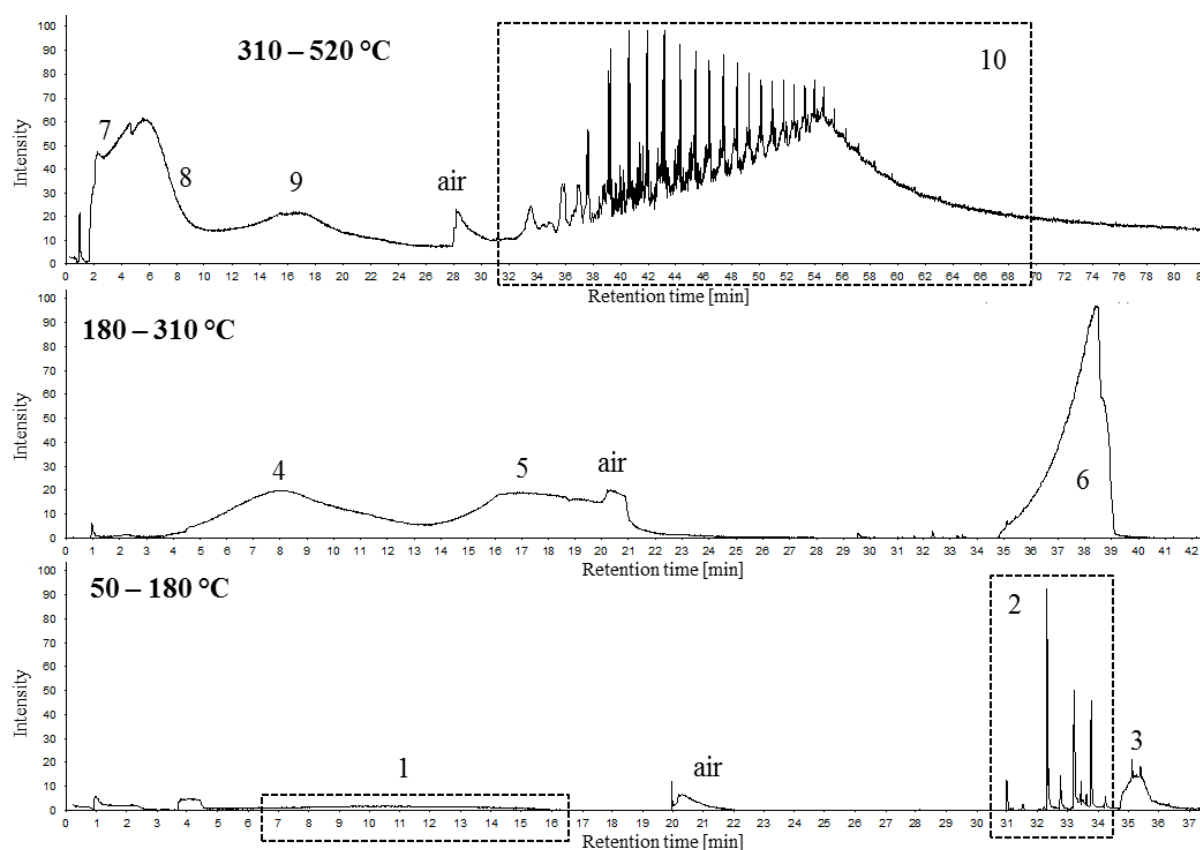
Figure 82: Chromatograms of EVM-ATH-MB obtained by py-GCMS, 10°C/min

Gases evolved during decomposition of EVM-ATH-MB at low heating ramps (10 °C/min) are similar to those found for EVM-ATH-MEL. Replacement of melamine by melamine borate and the additional presence of orthoboric acid does not change the gases evolved when the polymer decomposes. It is therefore assumed that orthoboric acid has a condensed phase mechanism.

Changing heating ramp from 10 °C/min to infinite one (flash pyrolysis at 800 °C for 10 min) leads to different structure of hydrocarbons evolved during decomposition of the polyene network formed during deacetylation of the polymer (as for EVM-ATH and EVM-ATH-MEL). **Figure 83** shows the chromatogram obtained using py-GCMS at high heating ramp. EVM-ATH-MB releases the following gases at high heating ramp: water (1), butene (2), isocyanic acid (3), acetonitile (4), 1-butene (4), pentadiene (5), 1,3-cyclopentadiene (6), cyclopentene (7), 1-hexene (8), 3-methylcyclopentene (9), methylcyclopentadiene (10), acetic acid (11), benzene (12), 1,3-cyclohexadiene (13), cyclohexene (14), 1-heptene (15), acetic anhydride (16), toluene (17), ethylbenzene (18), xylene (19), styrene (20), 1-nonene (21), benzene (22), methylstyrene (23), indane (24), indene (24), cyanobenzene (25), methylindene (26), vinylbenzoate (27), naphthalene (28), methylnaphthalene (29), biphenyl (30) and melamine (31).
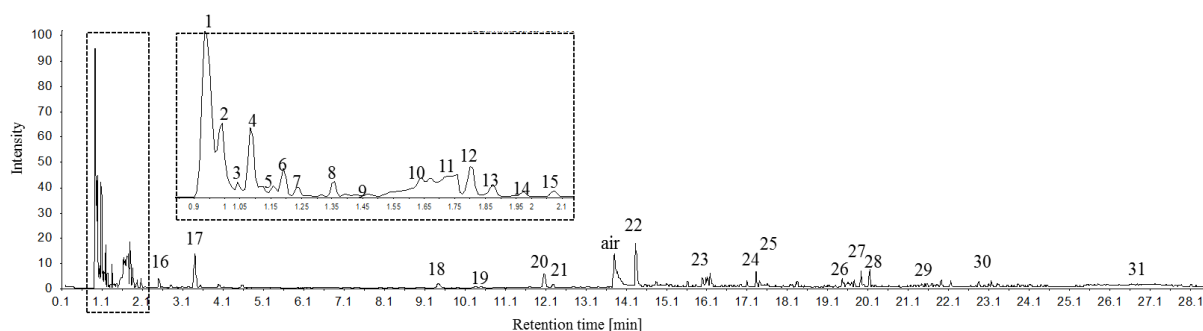
Figure 83: Chromatogram of EVM-ATH-MB obtained by py-GCMS, flash pyrolysis (10 min at 800 °C)

Detected molecules in the gas phase of EVM-ATH-MB at high heating ramps are similar to those obtained for EVM-ATH-MEL at high heating rate. Gases due to dehydration of ATH and orthoboric acid as well as decomposition of melamine are detected. Hydrocarbon structure of molecules released during decomposition of the polyene network formed during

deacetylation (release of acetic acid) is different from that obtained at low heating ramps. Formation of aromatic hydrocarbons is favored over formation of aliphatic ones. As for EVM-ATH and EVM-ATH-MEL, high quantity of aromatic hydrocarbons is due to high temperature and long contact time (ten minutes in comparison to some seconds) [174-177].

3.3.2. Analysis of gases released during decomposition of EVM-ATH-MB in a fire scenario

Release of gases when EVM-ATH-MB is submitted to an external heat source is analyzed using MLC-FTIR (**Figure 84** and **Table 31**). Before ignition (195 s) three gases are detected in the gas phase: acetic acid, water and ammonia. Before ignition, 38056 ppm of the total release of water is evolved. Presence of water is explained by dehydration reaction of ATH forming alumina and dehydration of orthoboric acid forming boron oxide. 1643 ppm ammonia, i.e. 48 % of total release is detected in the gas phase indicating decomposition of MB. Presence of acetic acid is due to deacetylation of the polymer. As it is seen, 3730 ppm of acetic acid are evolved before ignition, which corresponds to 81 % of the total release of acetic acid during decomposition of EVM-ATH-MB. Maximum release of acetic acid of 355 ppm is reached before ignition and decreases until ignition.

As for EVM-ATH-MEL, earlier ignition of EVM-ATH-MB (195 s) in comparison to EVM-ATH (245 s) is explained by presence of ammonia in the gas phase. Thus, the fuel consists of more flammable gases and concentration of released water is not high enough to dilute the fuel sufficiently to prevent ignition. In contrast to EVM-ATH-MEL (TTI = 145 s), EVM-ATH-MB ignites at longer times. The longer TTI of EVM-ATH-MB should be explained by a lower concentration of flammable gases, i.e. ammonia and acetic acid in the gas phase In order to confirm this hypothesis, the amount of gases released before ignition are compared. Regarding release of acetic acid, it appears that 3730 ppm are evolved during decomposition of EVM-ATH-MB, whereas only 2517 ppm of acetic acid are released for EVM-ATH-MEL. Comparing amount of ammonia released into the gas phase before ignition, 1101 ppm are released for EMV-ATH-MEL and 1643 ppm for EVM-ATH-MB. Thus, quantity of flammable gases in the gas phase is higher for EVM-ATH-MB than for EVM-ATH-MEL. Therefore, hypothesis postulated above that longer TTI of EVM-ATH-MB is due to less flammable gases, is not confirmed.
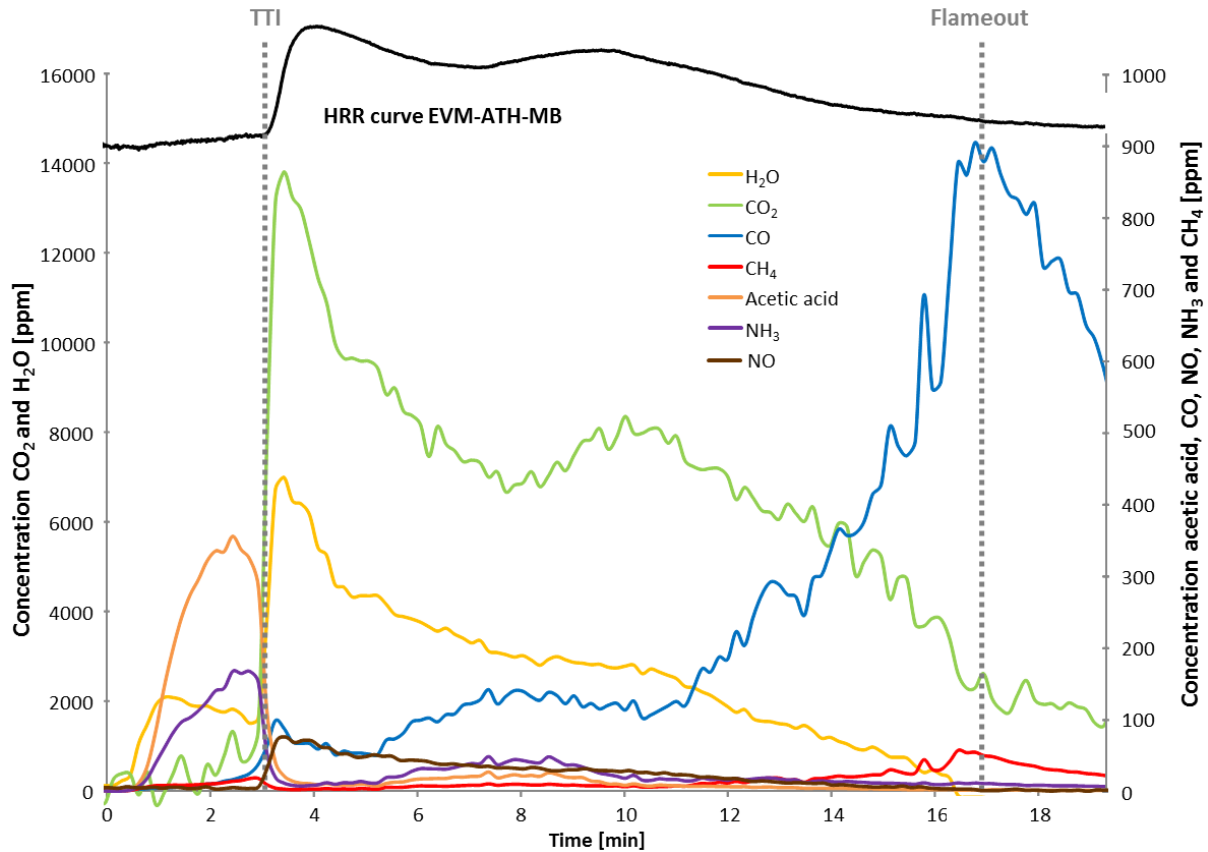
Figure 84: Evolution of gases and MLC curve versus time obtained by MLC-FTIR for EVM-ATH-MB

Table 31: Quantification of released gases during MLC-FTIR experiment for EVM-ATH-MB

Gas	Total quantity released [ppm]	Released before ignition [ppm]	Released before ignition [%]
H_2O	246435	38056	15
CO_2	649094	28337	4
CO	30604	315	1
CH_4	1754	181	10
Acetic acid	4583	3730	81
NH_3	3396	1643	48
NO	2175	102	5

Looking at the amount of water release (inert gas diluting fuel) before ignition of the materials, it is seen that more water is released in the case of EVM-ATH-MB whereas it has to be noted that it is released at longer times (longer TTI of EVM-ATH-MB). Before ignition 29652 ppm of water are released for EVM-ATH-MEL and 38056 ppm for EVM-ATH-MB. However, comparing of the quantity of water released during EVM-ATH-MB decomposition until 145 s (corresponding to TTI of EVM-ATH-MEL), a release of water of 24411 ppm is

found which is similar to that obtained for EVM-ATH-MEL before ignition. As a short conclusion, EVM-ATH-MB ignites at longer time as EVM-ATH-MEL, whereas amount of flammable gases before ignition is higher for EVM-ATH-MB and amount of water is equal for both materials. Thus, TTI at longer time of EVM-ATH-MB is not due to chemical phenomenon.

It is supposed that ignition at longer time is due to different thermal properties of EVM-ATH-MB and EVM-ATH-MEL. Both materials are tested in the same configurations. Thus, radiative exchange and view factor are similar for both materials. Moreover, emissivity is comparable due to the fact that both materials are of white color. It is assumed that thermal conductivity for EVM-ATH-MEL and EVM-ATH-MB is different. The only difference between EVM-ATH-MEL and EVM-ATH-MB is the presence of boric acid and its decomposition products, i.e. boron nitride and boron oxide at higher temperature, for EVM-ATH-MB. Indeed, literature reports that in sodium silicate glasses, the thermal conductivity increases with increasing boron oxide content [217]. Thus, presence of boron oxide formed during MB decomposition is assumed to increase the thermal conductivity of EVM-ATH-MB.

To understand the change of the thermal conductivity with increasing temperature, thermal conductivity measurements at different temperatures are carried out on EVM-ATH-MEL and EVM-ATH-MB (**Figure 85**). As it is seen, both materials exhibit comparable thermal conductivity of around 0.69 W/mK at room temperature. With increasing temperature, thermal conductivity decreases for both materials, whereas from 200 °C until 450 °C values obtained for EVM-ATH-MB are higher than those found for EVM-ATH-MEL. At 600 °C EVM-ATH-MB has a thermal conductivity of 0.27 W/mK and EVM-ATH-MEL of 0.21 W/mK. The difference between these values lies in the margin of error. Consequently, both materials have comparable thermal conductivity at the end of experiment.

Especially between 300 and 400 °C, thermal conductivity of EVM-ATH-MB is significantly higher than that of EVM-ATH-MEL. EVM-ATH-MB exhibits a thermal conductivity of 0.61 W/mK at 300 °C and of 0.38 W/mK at 400 °C. Thermal conductivity of EVM-ATH-MEL is 0.47 (at 300 °C) and 0.29 W/mK (at 400 °C) respectively. This temperature range corresponds to the ignition temperature of ethylene vinyl acetate materials [218]. Autoignition temperature is reported to be between 343 and 426 °C. Thus, especially in the range of the ignition

temperature of the polymer, the thermal conductivity of EVM-ATH-MB is increased in comparison to EVM-ATH-MEL. Increased thermal conductivity of EVM-ATH-MB leads to decreased accumulation of heat at the sample surface and so temperature at the surface is decreased as well. In the case of EVM-ATH-MEL, thermal conductivity is lower due to absence of boron oxide in the material. Hence, accumulation of heat at the sample surface is higher than for EVM-ATH-MB and the material surface of EVM-ATH-MEL is of higher temperature than that of EVM-ATH-MB. In turn, higher surface temperature leads to shorter ignition of the fuel even if concentration of flammable gases is similar for both materials.
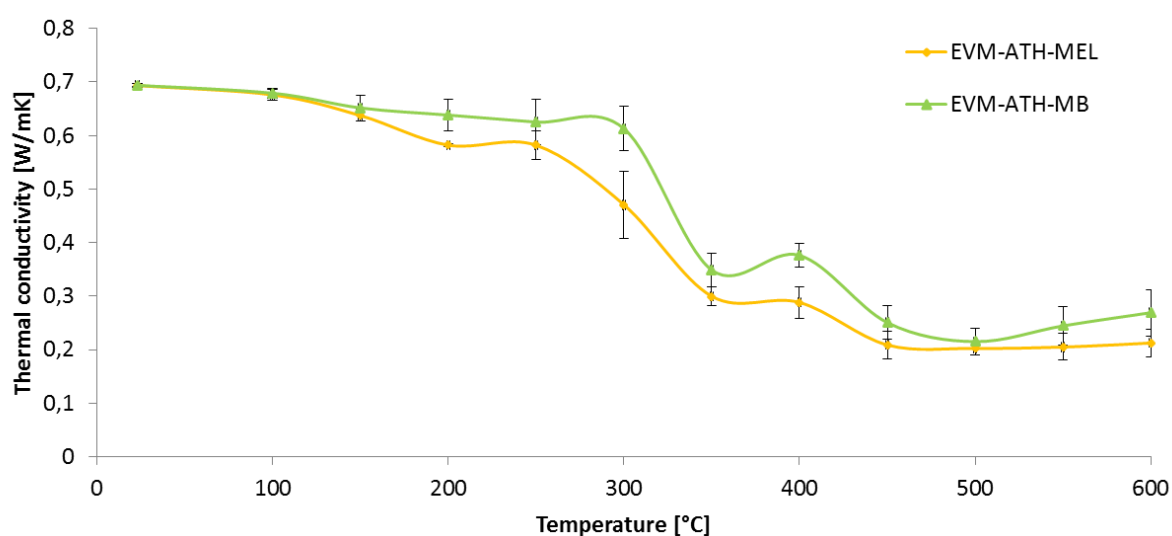
Figure 85: Thermal conductivity as function of temperature for EVM-ATH-MEL and EVM-ATH-MB

In summary, ignition at longer time for EVM-ATH-MB in comparison to EVM-ATH-MEL is explained by higher thermal conductivity at the ignition temperature due to presence of boron oxide in the polymeric matrix.

In MLC-FTIR experiment it is observed that when EVM-ATH-MB ignites, the concentrations of acetic acid and ammonia sharply decrease due to the fact that they are burning. Moreover, concentration of water and carbon dioxide increase rapidly to their maxima of 7000 and 13805 ppm respectively due to complete combustion of the material. At the same time, concentration of carbon monoxide indicating incomplete combustion increases until flameout where presence of carbon monoxide in the gas phase reaches its maximum (905 ppm). During the whole experiment, complete combustion dominates over incomplete combustion. In total, 649094 ppm of carbon dioxide and 30604 ppm of carbon monoxide are

released during experiment, leading to a ratio CO_2/CO is 21. In the case of EVM-ATH-MEL, a ratio of CO_2/CO is 35 is obtained. The comparison of the CO_2/CO ratio shows that more incomplete combustion is taking place during decomposition of EVM-ATH-MB. Looking at the evolution of carbon monoxide during decomposition of EVM-ATH-MEL and EVM-ATH-MEL, it is seen that release of carbon monoxide is taking place mainly after $pHRR_2$. After $pHRR_2$, only small flames at the boarders of the sample are observed (visual observation). It is therefore supposed that most of decomposition gases are burned at this stage of the material combustion. Presence of carbon monoxide is supposed to be due to decomposition of a char layer formed at the sample surface.

Besides water, carbon monoxide and carbon dioxide, nitrogen monoxide and methane are detected in the gas phase after ignition of EVM-ATH-MB. Release of nitrogen monoxide is due to oxidation reaction of ammonia. Nitrogen dioxide is not detected in the gas phase due to its decomposition temperature of 150 °C. Concentration of nitrogen oxide increases until its maximum of 72 ppm at the $pHRR_1$. Then, concentration decreases constantly until end of experiment. Total quantity of nitrogen oxide released during experiment is 2175 ppm. During MLC-FTIR experiment of EVM-ATH-MEL, a slightly higher quantity of nitrogen monoxide (2427 ppm) is released. Moreover, during thermo-oxidative decomposition of EVM-ATH-MEL, hydrogen cyanide coming from melamine decomposition was detected in the gas phase. Hydrogen cyanide is not found for EVM-ATH-MB. This result is in contrast to that found during investigation of MB decomposition, where it was shown that hydrogen cyanide is released in the gas phase. The absence of hydrogen cyanide can be explained by the fact that the decomposition mechanism of MB was investigated at low heating ramps (10 °C/min) and the heating rate in MLC-FTIR experiment is higher than 10 °C/min. Furthermore, in EVM-ATH-MB, MB is combined with ATH. It is possible that presence of ATH or alumina respectively suppress the formation of hydrogen cyanide.

At $pHRR_2$, additional release of acetic acid and ammonia is observed. At the same time, concentrations of water, carbon dioxide and ammonia decrease constantly after ignition until $pHRR_2$. At $pHRR_2$, a slight increase of concentrations is detected. Afterwards, concentrations decrease until end of combustion. This observation leads to the assumption that after $pHRR_1$, a protective layer is formed limiting mass transfer. At the $pHRR_2$, the

formed barrier is supposed to crack which leads to release of gases trapped under the protective layer.

From $pHRR_2$ to the end of the combustion of EVM-ATH-MB mainly carbon monoxide, carbon dioxide and water are detected.

3.4. Investigation of the condensed phase of EVM-ATH-MB

As for EVM-ATH and EVM-ATH-MEL, the condensed phase of EVM-ATH-MB is analyzed using a method in which the combustion process is stopped at characteristic times during the cone calorimeter experiment. Samples were taken out from the external heat source and flames were quenched immediately with a metal pan to prevent further decomposition. The resulting materials afterwards were analyzed by solid state NMR (^{13}C, ^{27}Al and ^{11}B). The top of the remaining plates and the bottom, i.e. the protected plate under the surface layer are analyzed separately. Combustion of EVM-ATH-MB (100-108-22) was stopped at six characteristic points: before the ignition (185 s), during increase of HRR curve (198 s), at $pHRR_1$ (254 s), at $pHRR_2$ (703 s), during decrease of HRR curve (800 s) and at end of combustion (1200 s). Pictures of selected residues are presented in **Figure 86**. As it is seen, with advancing combustion process, the material decomposition progresses and forms a black residue. Additionally, a white powder at the sample surface is observed at the end of combustion.
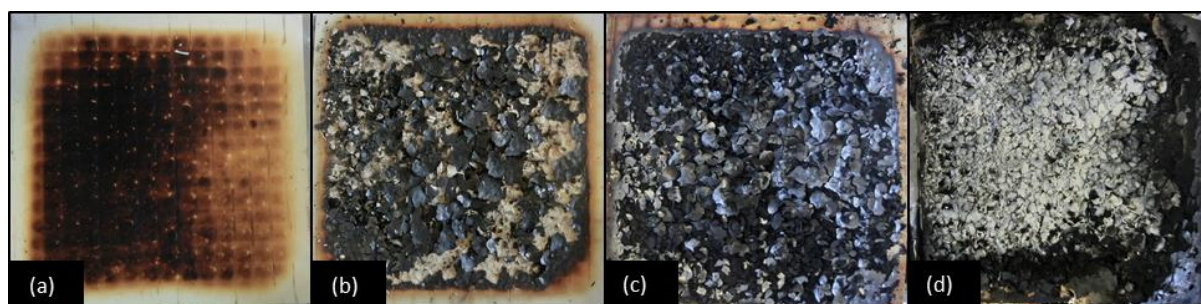
Figure 86: Residue of EVM-ATH-MB before ignition (a), at the $pHRR_1$ (b), during the decrease of HRR (c) and at the end of combustion (d)

Figure 87 presents ^{13}C solid state NMR spectra of the residues of EVM-ATH-MB at different stages of the combustion process. It is found that ^{13}C spectra of EVM-ATH-MB are similar to those observed for EVM-ATH-MEL (**page 120**). Therefore, results are not discussed in details. EVM-ATH-MB starts to degrade at the sample surface. With advancing decomposition

process, the material is decomposed until the bottom of the plate. First, deacetylation takes place forming a char layer consisting of saturated and unsaturated (oxidized) hydrocarbons. At the end of the combustion process, the whole material is decomposed and no ^{13}C signal is detected.
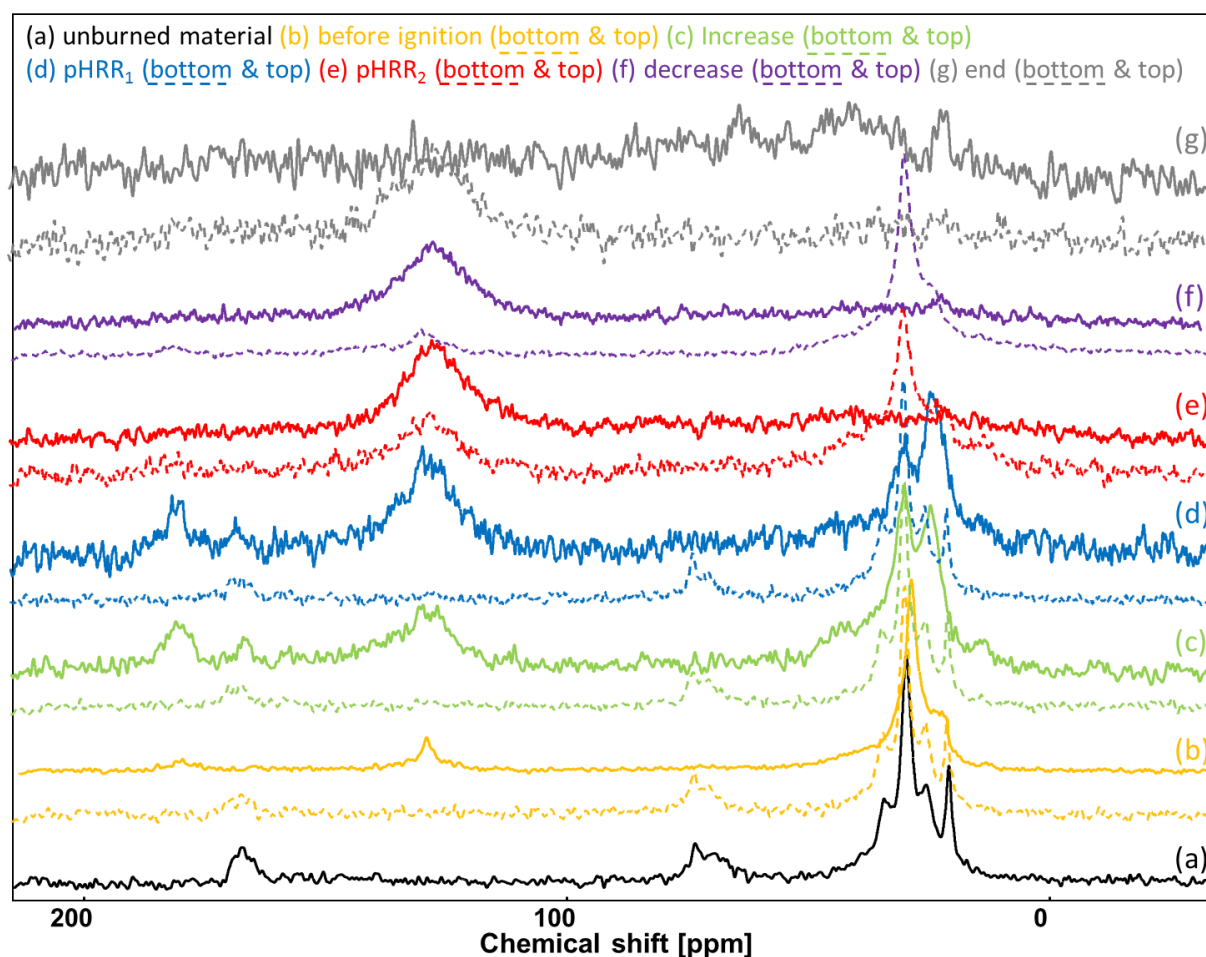
Figure 87: ^{13}C spectra obtained at different stages of combustion of EVM-ATH-MB (MLC experiment at 35 kW/m²)

As for ^{13}C NMR spectra, ^{27}Al NMR spectra for the different stages of the combustion of EVM-ATH-MB (**Figure 88**) are similar to those found for EVM-ATH-MEL (**page 120**). ^{27}Al spectra indicate dehydration of ATH into alumina, which is not completed before $pHRR_2$.

It is supposed that alumina coming from ATH decomposition as well as saturated and unsaturated (partially oxidized) hydrocarbons formed during polymer decomposition act as protective barrier. The protective layer starts to be formed before ignition of the material and remains until decrease of pHRR curve. Thereby, the formed protective layer acts as barrier avoiding/reducing transfer of gases and smoke.
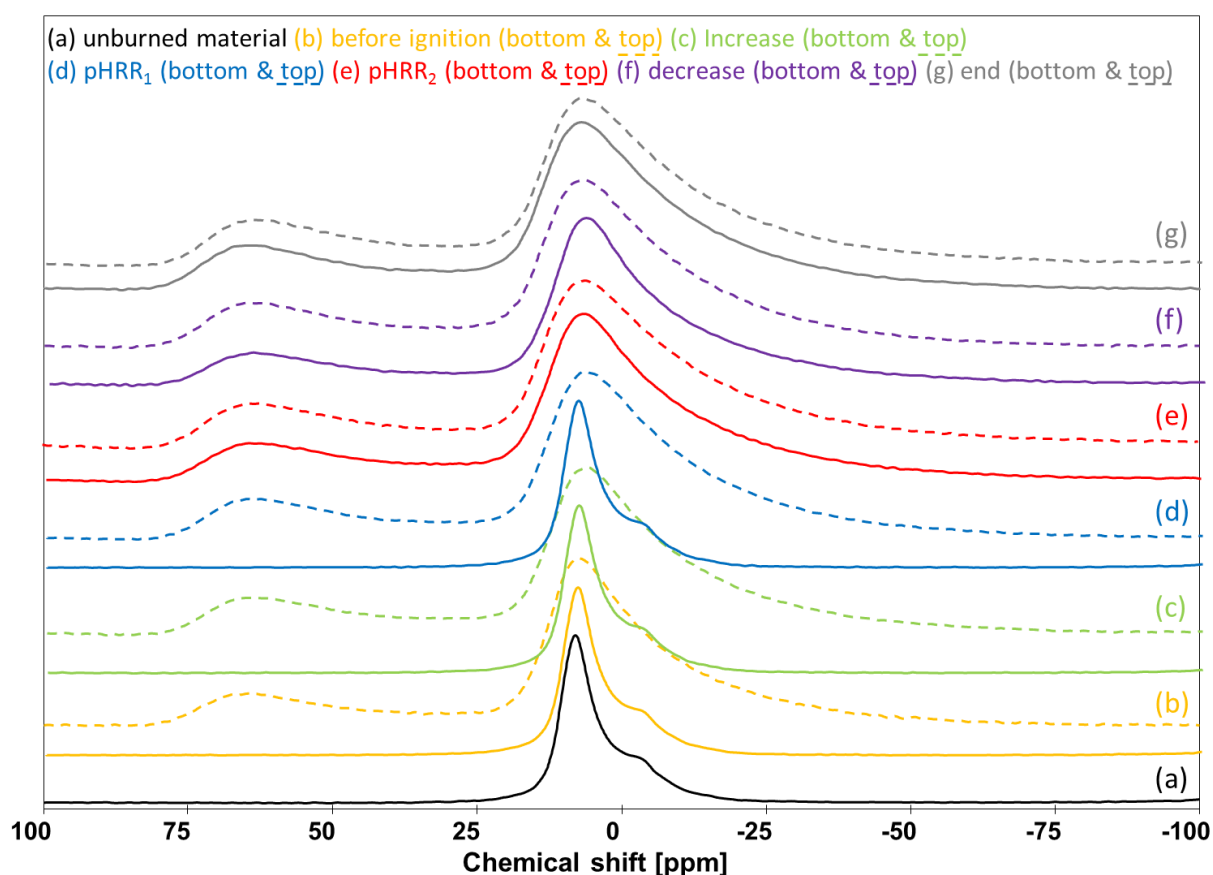
Figure 88: ^{27}Al spectra obtained at different stages of combustion of EVM-ATH-MB (MLC experiment at 35 kW/m²)

Figure 89 presents ^{11}B solid state NMR spectra of EVM-ATH-MB at different stages of the combustion. The virgin material exhibits two signals at room temperature. One resonance at 16 ppm indicating presence of BO_3 units and the other resonance at 1 ppm assigned to BO_4 units. This observation is in contrast to that observed for pure MB at room temperature. The ^{11}B NMR spectrum of virgin MB has only a signal assigned to BO_3 units in orthoboric acid. The presence of tetragonal coordinated boron atoms (BO_4) in EVM-ATH-MB demonstrates that orthoboric acid is partially dehydrated to boron oxide during the material processing. Temperature can increase up to 100 °C during processing due to the shearing forces of the material. The B^{III}/B^{IV} ratio of 8 shows that significantly more BO_3 than BO_4 units are present in the condensed phase of EVM-ATH-MB.

Signals assigned to BO_3 and BO_4 units are detected during the whole experiment. Above, it was assumed that TTI at longer times for EVM-ATH-MB in comparison to EVM-ATH-MEL is due to presence of boron oxide in the material resulting in higher thermal conductivity.

Presence of boron oxide during the whole combustion process is evidenced using ^{11}B solid state NMR.
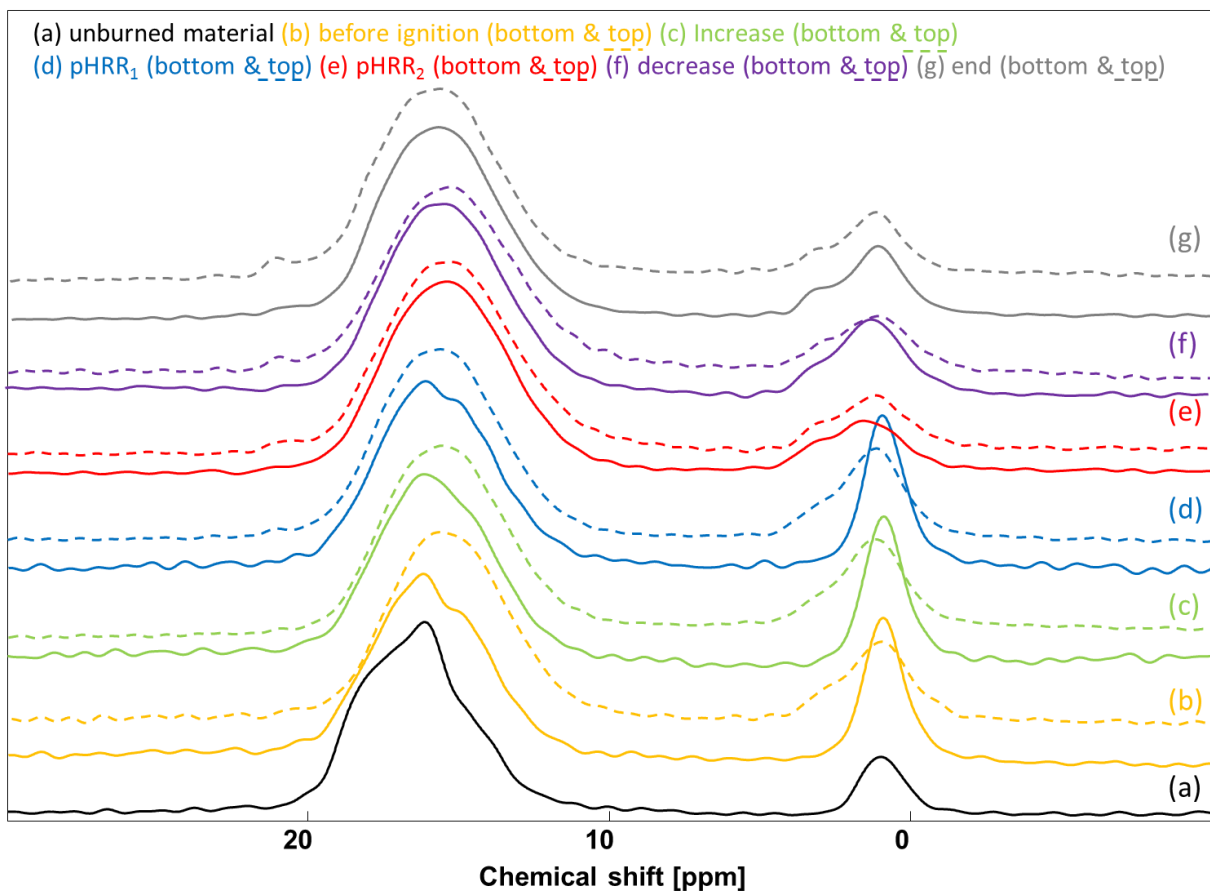
Figure 89: [11]B spectra obtained at different stages of combustion of EVM-ATH-MB (MLC experiment at 35 kW/m²)

B^{III}/B^{IV} ratio for bottom of the samples decreases to a value of 3 until the $pHHR_1$ and increases again to a value of 5 at the end of combustion. Regarding B^{III}/B^{IV} for top of the plates it appears that a value of 3 is found for samples taken until $pHRR_1$. At the $pHRR_2$ a maximum value of 6 is observed which decreases until end of combustion to a value of 4. In general, B^{III}/B^{IV} ratios indicate that until $pHHR_1$ amount of BO_4 units is higher at the sample surface than in the bulk phase. After $pHRR_1$, B^{III}/B^{IV} ratios at the surface and in the bulk phase have comparable values. Due to the fact that tetragonal coordinated boron is assigned to formation of boron oxide, it is supposed that boron oxide contributes to the formation of the protective layer which is formed at the $pHRR_1$ and cracks before $pHRR_2$. Increase of B^{III}/B^{IV} ratio at $pHRR_2$ is explained by complete dehydration of remaining metaboric acid to boron oxide whereas boron oxide coordinates in BO_3 and BO_4 units.

Additionally to the B^{III} and B^{IV} signals, the top of the residues of EVM-ATH-MB collected at the decrease and at the end of combustion, exhibit a chemical shift at 21 ppm. This resonance is attributed to B-N bonds [206-208] which are formed during MB decomposition (as discussed for MB decomposition on **page 154**). It has to be noted that B-N bonds can be present in BN and/or BNO structures.

3.5. Decomposition mechanism of EVM-ATH-MB

Decomposition mechanism of EVM-ATH-MB was investigated (**Figure 90**). Exposure of EVM-ATH-MB to an external heat source leads to decomposition of the material. As a first step, deacetylation of the polymer takes place forming a polyene network. At the same time, ATH is dehydrated to alumina evolving water into the gas phase. Released water dilutes the fuel and thus protects the material in the gas phase. During deacetylation process, acetic acid is released and partially transformed into acetone due to presence of alumina in the condensed phase. Before ignition of the material, the polyene network formed by deacetylation of the polymer starts to degrade evolving saturated and unsaturated hydrocarbons. The structure of the released hydrocarbons depends on the heating rate that is applied on the material. At low heating rates (10 °C/min) saturated and unsaturated linear hydrocarbons having a chain length of C_4 to C_{36} are released. At high heating ramp (flash pyrolysis), formation of benzene and its homologues is favored. Before ignition, melamine borate starts to decompose as well. On one hand, orthoboric acid is dehydrated forming metaboric acid and then boron oxide while water is released. On the other hand, melamine is partially sublimated whereas the remaining melamine condenses to form melem and melon. Due to condensation and decomposition of melamine, ammonia, hydrogen cyanide, nitrogen monoxide, nitrogen and melamine fragments are released into the gas phase. In thermo-oxidative conditions, molecules indicating oxidation of melamine and/or its condensates are detected. The material ignites when concentration of water is not high enough to dilute the fuel sufficiently to prevent ignition. At the ignition of the material, deacetylation of the polymer is nearly completed. The main reaction taking place after ignition is the decomposition of the polyene network whereas complete and incomplete combustion is observed. Advancing in the material decomposition leads to cracking of the protective layer formed at the sample surface resulting in release of gases trapped

underneath. At this stage of the decomposition of EVM-ATH-MB incomplete combustion dominates complete combustion. At the end of decomposition, a residue consisting of alumina, boron oxide, boron nitride and/or BNO structures is left.
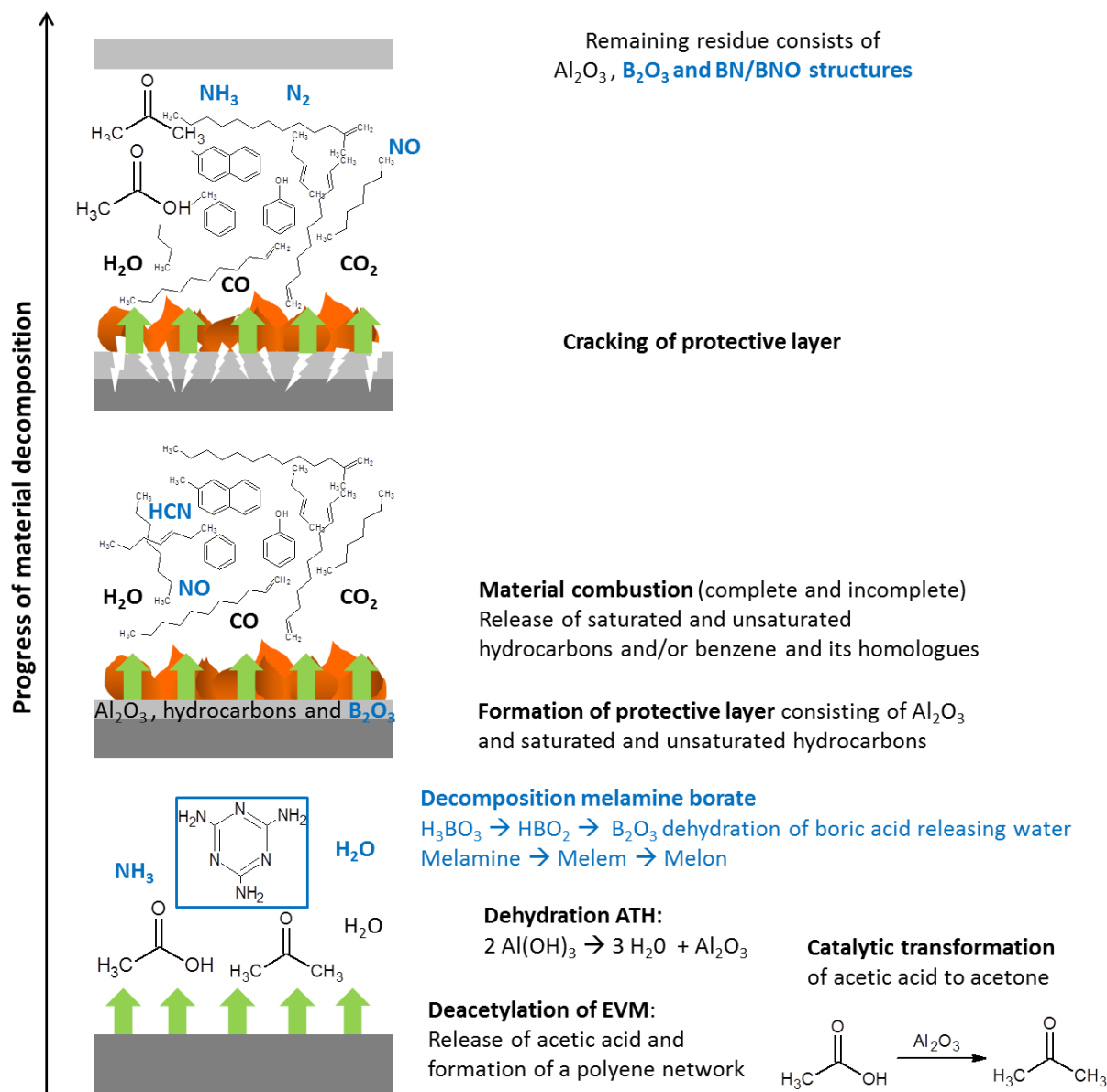
Figure 90: Decomposition mechanism of EVM-ATH-MB

Comparison of the decomposition of EVM-ATH-MB to that of EVM-ATH-MEL shows that firstly decomposition mechanisms for both materials are similar. Both are protected by a gas phase (dilution of fuel) and a condensed phase (formation of protection layer) mechanism. Nevertheless, one of the advantages of EVM-ATH-MB is its ignition at longer times in comparison the EVM-ATH-MEL. Longer TTI of EVM-ATH-MB is due to higher thermal conductivity induced through the presence of boron oxide in the matrix. Moreover, it was

shown that EVM-ATH-MB does not release hydrogen cyanide into the gas phase in a fire scenario. Due to the fact that in most cases, fires develop in the presence of oxygen, the absence of the toxic gas hydrogen cyanide is important for fire risk assessment for EVM-ATH materials containing melamine and its derivatives. Quantity of carbon monoxide evolved during material decomposition is an important factor as well. It was found that EVM-ATH-MB releases more carbon monoxide than EVM-ATH-MEL. Nevertheless, it has to be noted that carbon monoxide is mainly evolved at the end of the decomposition process.

The decomposition mechanism of an EVM material containing ATH in combination with melamine phosphate (MP), at the same ratio as ATH-MEL and ATH-MB, was also studied and is presented in **Appendix 2** [172] (**page 216**). This study investigated the fire retardant mechanism of EVM-ATH-MP using the same approaches as used for EVM-ATH, EVM-ATH-MEL and EVM-ATH-MB. It is shown that EVM-ATH-MP ignites at shorter time than EVM-ATH due to higher amount of flammable gases (ammonia from MP decomposition) in the gas phase. Moreover, it was evidenced that presence of phosphate in the condensed phase leads to the formation of aluminum phosphate improving stability and insulative properties of the char layer. For EVM-ATH-MP, $pHRR_2$ is reduced in comparison to the other materials. Even if EVM-ATH-MP forms a char with better insulative properties during decomposition, it has to be noted that this material contains phosphorous. In the targeted industrial applications, researchers prefer to use phosphorous-free materials. Indeed, phosphorous compounds are for example known to reduce stability of the material during hydrothermal aging.

4. Influence of the VA-content on material properties of EVM-ATH-MB materials

In this study, it was shown that the combination of ATH and MB in EVM having a vinyl acetate (VA) content of 60 %, leads to materials presenting good mechanical properties, high fire retardancy and low smoke release when compared to the virgin polymer. As it was discussed in Chapter I (**page 18**), material properties of ethylene vinyl acetate (EVA) polymers depend on VA content [6-8]. In this part, efficiency of the combination of ATH and MB regarding mechanical properties, fire retardancy and smoke release in EVA having different VA contents is investigated. Therefore, VA contents of 18, 28, 40, 50, 65 and 70 % are tested. It has to be noted that the material EVA(VA 60)-ATH-MB which was already characterized Chapter III (**page 83**) was processed a second time for the study. It is found that results presented in Chapter III are comparable to those found in this part. This shows that the results in this study are repeatable and reproducible.

4.1. Mechanical properties

The mechanical properties of EVA-ATH-MB materials having different VA contents are presented in **Table 32**. In general, EVA polymers are known to have thermoplastic properties up to 40 % VA content and above 80 % VA content. In between, from a VA content of 40 to 80 %, EVA polymers are elastomers.

As it is seen, hardness of the tested materials decreases with increasing VA content. It is known that VA units form the soft part of the polymer, whereas ethylene is the hard one. Increased VA content in the polymer therefore decreases hardness. Hardness decreases from 97 Shore A for the material having a VA content of 18 % to 77 Shore A for that having a VA content of 70 %. As observed for the hardness, tensile strength (TS) decreases with increasing VA content whereas it decreases from 9.6 MPa for the material having a VA content of 18 % to 6.1 for that having a VA content of 70 %. A tendency between elongation-at-break (EAB) and VA content in the polymer is not found. EVA(VA 18)-ATH-MB has a EAB of 183 %. Increasing VA to 28 % leads to increased EAB value of 344 % (the highest value observed). Afterwards, with increasing VA content, EAB decreases constantly to a value of

128 % for EVA(VA 70)-ATH-MB. Exception is EVA(VA 65)-ATH-MB having an EAB value of 245 %.

Table 32: EAB, TS and HSA of materials EVM-ATH-MB materials having different VA contents

	EAB [%]	TS [MPa]	HSA [Shore A]
EVA(VA 18)-ATH-MB	183	9.6	97
EVA(VA 28)-ATH-MB	344	8.7	93
EVA(VA 40)-ATH-MB	298	7.6	83
EVA(VA 50)-ATH-MB	224	8.2	80
EVA(VA 60)-ATH-MB	163	7.9	79
EVA(VA 65)-ATH-MB	245	6.5	79
EVA(VA 70)-ATH-MB	128	6.1	77

4.2. Fire retardancy and smoke release

Fire retardant properties are evaluated using MLC, LOI and UL-94 (**Table 33**). EVA-ATH-MB – materials having different VA contents do not show significant differences in MLC experiments. All materials exhibit comparable $pHRR_1$, ML and THR values. $PHRR_2$ is decreased with increasing VA content. Regarding TTI of tested materials, it is seen that increasing VA content in the material leads to longer TTI. TTI is raised from around 150 s for low VA contents (18 – 40 %) to around 200 s for materials containing high VA contents (60 – 70 %).

Table 33: Fire retardant properties of materials containing EVM (with different VA grades), ATH and MB; 35 kW/m²

	$pHRR_1$ [kW/m²]	$pHRR_2$ [kW/m²]	THR [MJ/m²]	TTI [s]	ML [%]	UL-94	LOI [vol%O_2]
EVA(VA 18)-ATH-MB	110	108	71	154	57	NC	31
EVA(VA 28)-ATH-MB	114	103	68	155	59	V-0	32
EVA(VA 40)-ATH-MB	109	68	51	148	60	V-0	31
EVA(VA 50)-ATH-MB	118	87	56	161	62	V-0	34
EVA(VA 60)-ATH-MB	117	94	65	201	63	V-0	35
EVA(VA 65)-ATH-MB	110	80	52	169	63	V-0	35
EVA(VA 70)-ATH-MB	106	70	54	208	63	V-0	38

Increased VA content in the material leads to higher release of acetic acid due to deacetylation of the polymer at the beginning of the material combustion. Moreover, increasing VA content leads to decreasing amount of ethylene in the polymer and therefore amount of polyene network formed during deacetylation is smaller. During analysis of the

gas phase mechanism it was shown that decomposition of polyene network starts during deacetylation. Therefore, acetic acid and hydrocarbons are present in the gas phase at the same time whereas ratio of acetic acid to hydrocarbons increases with increasing VA content. It is supposed that with increasing amount of acetic acid and decreasing amount of hydrocarbons in the gas phase, the flammability of the fuel decreases. Flammability of molecules is predicted using the so called F-Number which depends on the lower and upper flammability limit of each substance (**Equation 13**) [219]. The F-number increases with increasing flammability of the compound.

$$F = 1 - \sqrt{\frac{Lower\ flammability\ limit}{Upper\ flammability\ limit}}$$

Equation 13: Calculation of F-number (flammability)

Some examples F-numbers of selected molecules are shown in **Table 34**. As it is seen, acetic acid has a lower F-number, i.e. 0.552 than that observed for hydrocarbons (except in the case of methane and ethane), whereas F-number of hydrocarbons increases with increasing chain length and for some molecules with increasing number of double bonds. Butane, for example has a F-number of 0.564, decane of 0.615 and naphthalene of 0.609. Hypothesis postulated before that with increasing VA content the flammability of the fuel decreases can be validated by looking at the flammability of decomposition gases. The amount of hydrocarbons (having higher flammability than acetic acid) in the gas phase decreases with increasing VA content resulting in lower flammability of the fuel which leads to longer TTI.

Table 34: F-numbers of different molecules

Molecule	F-number	Molecule	F-number
Acetic acid	0.552	Hexane	0.617
Acetone	0.561	Benzene	0.594
Methane	0.423	Decane	0.615
Ethane	0.510	Xylene	0.604
Ethylene	0.726	Styrene	0.604
Butane	0.564	Naphthalene	0.609
1-Butene	0.600	Biphenyl	0.678

Concerning UL-94 test, all EVA-ATH-MB materials except of EVA(VA 18)-ATH-MB (not classified) reach V-0 classification. LOI values increase with increasing VA content in the materials. The LOI increases from 31 vol%O_2 for EVA(VA 18)-ATH-MB to 38 vol%O_2 for

EVA(VA 70)-ATH-MB. This corresponds to results reported in literature [9]: LOI increases with increasing VA content. As discussed for increasing TTI observed using MLC experiment with increasing VA content, increased LOI could be reasonably attributed to lower flammability of the fuel with increasing VA content in the polymer.

Smoke release values obtained for EVA-ATH-MB materials are presented in **Table 35**. As for fire retardant properties, smoke release, i.e. OD_{total}, VOF4 and the D_s values are comparable for the different VA contents. Exceptions are the OD_{total} of EVA(50)-ATH-MB, which is the lowest of the observed values (OD_{total} = 29) and D_s1 values of 0.4 of EVA(65)-ATH-MB and EVA(70)-ATH-MB which are increased in comparison to the other observed values. It is supposed that increased D_s1 values found for materials having high VA contents are in correlation with the higher amount of acetic acid which is released into the gas phase. Regarding TTI, it is seen that with increasing VA content TTI increases (as observed in MLC experiment).

Table 35: Data obtained by smoke test for materials containing EVM (containing different VA grades), ATH and MB

	OD_{total}	VOF 4	D_s4	D_s1	D_s2	TTI
EVA(18)-ATH-MB	44	10	0.2	0.2	0.1	183
EVA(28)-ATH-MB	41	8	0.2	0.2	0.1	191
EVA(40)-ATH-MB	41	7	0.2	0.1	0.1	220
EVA(50)-ATH-MB	29	10	0.1	0.1	0.1	200
EVA(60)-ATH-MB	40	11	0.3	0.2	0.1	227
EVA(65)-ATH-MB	33	11	0.1	0.4	0.1	351
EVA(70)-ATH-MB	38	8	0.1	0.4	0.1	270

4.3. Conclusion of influence of the VA content

In this part dedicated to the study of the influence of the VA content in EVA-ATH-MB materials, it was shown that as expected mechanical properties change with increasing VA content. Despite the fact that TTI increases with increasing VA content, the combination of ATH and MB in EVA is suitable as fire retardant and smoke suppressant for VA contents of 28 to 70 %. The lowest VA content of 18 % is excluded due to the fact that the material fails in UL-94 test. In general, material properties depending on flammability of gases, i.e. TTI and LOI are enhanced with increasing VA content due to lower flammability of the fuel.

Therefore, it is recommended to rather use the combination of ATH and MB as fire retardant and smoke suppressant in EVA for VA contents higher than 40 %. This assures longer TTI and high LOI which in case of fire gives more time to escape the fire source.

5. Conclusion of comprehensive study of EVM-ATH-MB

In Chapter V, a comprehensive study on the material EVM-ATH-MB was conducted. At first, it was found that both additives are well dispersed in the polymeric matrix. Afterwards, hydrothermal aging in distilled and sea water showed that EVM-ATH-MB has a higher resistance against the attack of distilled water than EVM-ATH and EVM-ATH-MEL. Immersion in sea water at the opposite leads to comparable results for the three materials. Differences between EVM-ATH-MEL and EVM-ATH-MB are explained by the higher solubility of MB leading to higher ionic strength of the medium which again limits penetration of water in the material.

In the second part, decomposition mechanism of MB and EVM-ATH-MB was investigated in pyrolytic and thermo-oxidative conditions. A detailed mechanism for MB taking into account condensed and gas phase was presented showing that decomposition of MB is similar in pyrolytic and thermo-oxidative conditions except at high temperature. During decomposition, orthoboric acid is dehydrated into metaboric acid and boron oxide. At the same time, melamine sublimates partially, whereas some of the molecules condensate forming melem and melon. At the end, melamine and its condensates are decomposed totally. Furthermore, presence of boron nitride (BN), boron oxide (B_2O_3) and BNO structures at the end of decomposition was evidenced, whereas concentrations of these compounds in the residue are different in pyrolytic and thermo-oxidative conditions.

Decomposition mechanism of EVM-ATH-MB was found to be similar to that of EVM-ATH-MEL. EVM is first deacetylated evolving acetic acid and acetone whereas a polyene network is formed. The polyene network is then degraded evolving hydrocarbons whereas their structure depends on applied heating ramp. At the same time, ATH and orthoboric acid are dehydrated evolving water in the gas phase. Moreover, melamine combined with MB sublimates partially, whereas the other part condensates to melem and melon which decompose later. In the condensed phase, EVM-ATH-MB is protected by a char layer consisting of alumina, boron oxide, boron nitride, BNO structures and hydrocarbons.

The third part of this study was dedicated to the influence of the VA content in EVA materials containing ATH and MB on their mechanical properties, fire retardancy and smoke release. It was found that with increasing VA content in the material, TTI and LOI increase

due to lower flammability of released gases. Consequently, the combination of ATH and MB was found to be more suitable for EVA materials having a VA content higher than 40 %.

General conclusion

This study was dedicated to the development of a new fire retarded ethylene vinyl acetate (EVM) materials with low smoke emission. Literature review revealed that combining aluminum trihydroxide (ATH) with melamine or different melamine derivatives could lead to EVM materials exhibiting high fire retardancy and low smoke release in case of fire. Screening of different formulations showed that partial replacement of ATH by melamine (ratio 5:1) reduces smoke release during combustion but leads to shorter ignition than the reference material (EVM-ATH). Replacing melamine by melamine borate (MB) maintains low smoke release as well as fire retardancy of EVM-ATH-MEL but ignites at longer time.

The goal was to understand the fire retardant mechanism of EVM-ATH-MEL in particular regarding the influence of melamine on shorter ignition and reduction of smoke. Hence, decomposition reactions of EVM-ATH and EVM-ATH-MEL were investigated in the condensed and gas phase using amongst others, new approaches such as pyrolysis-gas chromatography-mass spectrometry (py-GCMS) and mass loss calorimeter coupled with Fourier transform infra-red spectroscopy (MLC-FTIR). It was evidenced that shorter ignition of EVM-ATH-MEL is due to higher quantity of flammable gases, especially ammonia and hydrogen cyanide, released from melamine decomposition. Moreover, it was demonstrated that the protective layer consisting of hydrocarbons and alumina has better barrier properties for EVM-ATH-MEL than for EVM-ATH explaining the decreased smoke release during combustion of EVM-ATH-MEL. In addition, hydrothermal aging in distilled and sea water was carried out for EVM-ATH and EVM-ATH-MEL. Stability in sea water was found to higher than that in distilled water. Investigation of the decomposition mechanism of EVM-ATH-MB revealed that replacement of melamine by MB results in higher thermal conductivity of the material due to presence of boron oxide formed during MB decomposition. The fire retardant mechanisms of EVM-ATH-MEL and EVM-ATH-MB are not reported in literature up to now. Besides, the decomposition of MB in pyrolytic and thermo-oxidative conditions was examined and it was possible revisiting the mechanism proposed by Costa et al. [193] in the 90's. It was further demonstrated that EVM-ATH-MB exhibits higher stability in hydrothermal aging in distilled water than EVM-ATH-MEL. Additionally, it was evidenced that combination of ATH and MB is suitable for EVA materials having a vinyl acetate (VA) content of 40 % or higher.

In summary, the goal of finding a new material suitable for the cable and wire industry was reached. The combination of ATH and MB in EVM exhibits excellent fire retardant properties and low smoke release in case of fire. Moreover, high stability in hydrothermal aging in distilled and sea water was found.

Outlook

It was shown that combination of a mineral filler, i.e. ATH, with melamine or its derivatives (MB or MP) in EVM leads to materials with promising mechanical properties, high fire retardancy and reduced smoke release in comparison to the virgin polymer as well as to EVM-ATH. However, material properties were evaluated on "basic materials" to avoid interactions of fire retardants and/or polymer with processing additives which can change fire retardant mechanism drastically. Basic materials contained the polymer, the fire retardant additives and the vulcanization agents. Due to the fact that this work was carried out in cooperation with an industrial partner, LANXESS, one of the goals besides screening of new formulations and the understanding of their fire retardant mechanism, was to provide commercially suitable EVM-materials. For this purpose, ATH and the combination of ATH with MB as fire retardant additives are evaluated in a complete EVM-material. Their mechanical and fire retardant properties as well as smoke release are determined. Complete materials (**Table 36**) contain additionally to the fire retardants and the vulcanization agents, compounds acting as plasticizer (Disflamoll TOF, Edenor C18-98/100 and Aflux 18), anti-aging compounds (Vulkanox HS/LG) or additional smoke suppressants (zinc borate).

Table 36: Composition of complete materials

Compound	Loading (phr)
Levapren 600	100
FR additives	130
Zinc borate	10
Disflamoll TOF	20
Vulkanox HS/LG	1
Edenor C18-98/100	1.5
Aflux 18	1.5
Rhenofit TAC/S	1
Perkadox 14-40	6

Fire retardancy and smoke release of EVM-ATH$_{complete}$ and EVM-ATH-MB$_{complete}$ is investigated using MLC, LOI, UL-94 and smoke test. Fire retardancy results are shown in **Table 41** and **Figure 91**. Generally, fire retardancy is decreased for the complete materials. It is seen that pHRR$_1$ and THR have comparable values for basic and complete materials. However, regarding TTI, complete materials ignite significantly at shorter time than basic ones. TTI of complete materials is around 70 s which is at the same time as virgin polymer. Furthermore, pHRR$_2$ is obviously decreased for complete materials. It is supposed that early ignition of the complete materials avoids formation of a char layer (consisting of aromatic

carbons and alumina) as it was the case for basic materials. At this stage, ATH dehydration forming alumina is not completed leading to less alumina in the condensed phase and therefore less shielding of the protective layer. Regarding LOI values and UL-94 classification of complete materials, it is seen that both complete materials are classified V-0. LOI values are slightly decreased in comparison to the basic materials. EVM-ATH$_{complete}$ has a LOI of 31 vol%O$_2$ and EVM-ATH-MB$_{complete}$ of 32 vol%O$_2$.
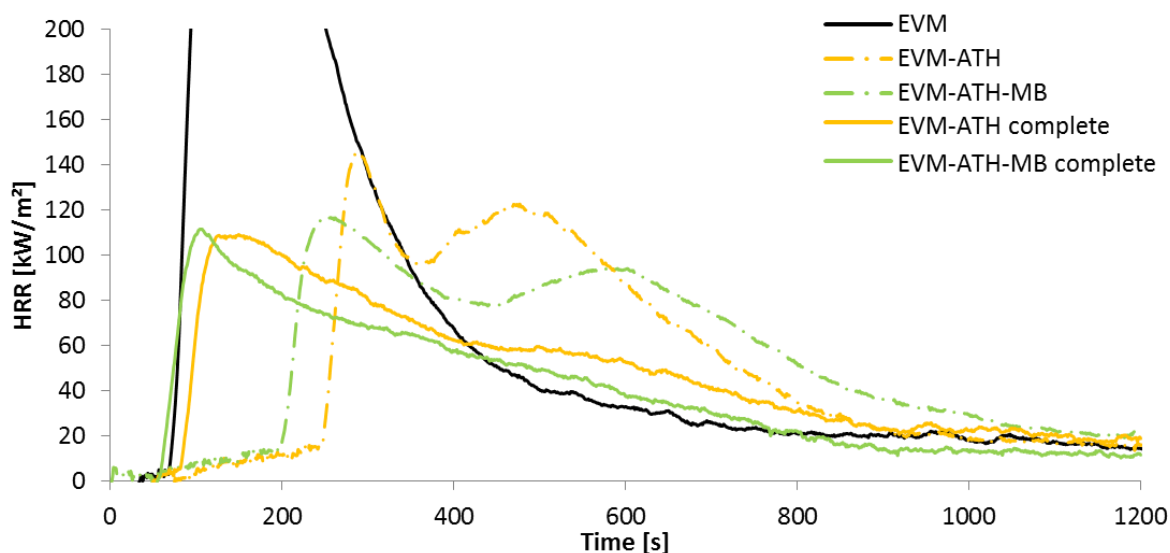
Figure 91: HRR curves for complete materials (35 kW/m²)

Table 37: Fire retardant values for complete materials

	pHRR$_1$ [kW/m²]	pHRR$_2$ [kW/m²]	THR [MJ/m²]	TTI [s]	UL-94	LOI [vol%O$_2$]
EVM	510	-	97	67	NC	19
EVM-ATH	146	123	60	245	V-0	33
EVM-ATH-MB	117	94	65	195	V-0	35
EVM-ATH$_{complete}$	110	-	56	84	V-0	31
EVM-ATH-MB$_{complete}$	112	-	48	58	V-0	32

Concerning smoke release of complete materials (**Table 38**), it is found that EVM-ATH-MB$_{complete}$ ignites at shorter time (at the same time as the virgin polymer) than the corresponding basic material. This corresponds to results obtained by MLC test. In the case of EVM-ATH, TTI of complete and basic material are comparable. VOF4 as well as D$_s$4 and D$_s$1 values for complete and basic materials are comparable, except of VOF4 for EVM-ATH and EVM-ATH$_{complete}$. Concerning OD$_{total}$, EVM-ATH$_{complete}$ and EVM-ATH-MB$_{complete}$ have comparable values to their basic materials.

Table 38: Smoke release values for complete materials

	OD_{total}	VOF 4	D_s4	D_s1	TTI [s]
EVM	114	87	1.1	1.1	86
EVM-ATH	67	9	0.3	0.4	176
EVM-ATH-MB	58	14	0.2	0.2	302
EVM-ATH$_{complete}$	71	20	0.3	0.3	171
EVM-ATH-MB$_{complete}$	65	19	0.3	0.3	73

Results obtained for complete materials concerning fire retardancy and smoke release did not show expected results. Addition of different plasticizers and an anti-aging compound results in shorter ignition of the materials and decrease of the LOI values. Nevertheless, other fire retardant and smoke release values are comparable to those obtained for the corresponding basic materials. Thus, the main disadvantage of the complete materials is their early ignition.

To overcome the disadvantages of early ignition it has to be understood why complete materials ignite at shorter times that the basic ones. Shorter ignition on the one hand could be due to higher amount of flammable gases in the gas phase. On the other hand, change of thermal conductivity of the material could be an explanation, too. Moreover, combination of both phenomena could be a possibility as well.

A first step could be the reduction of amount of plasticizer of 22.5 phr in total to around 10 to 15 phr. In general, plasticizers are added to the materials to facilitate processing and to decrease hardness. Analysis of the mechanical properties of the compete materials (**Table 39**) shows that even with decreased amount of plasticizer, the materials should be soft enough. Moreover, after discussion with the industrial partner, it is decided that a decreased amount of plasticizer still assures easy processing of the complete materials.

Table 39: Mechanical properties of complete materials

	EAB [%]	TS [MPa]	Hardness [Shore A]
EVA-ATH$_{complete}$	539	8.4	52
EVA-ATH-MB$_{complete}$	530	6.4	49

Afterwards, the influence of each compound has to be investigated. It is proposed to start with the basic material EVM-ATH-MB and to add at first only one additional compound.

Then, fire retardancy and smoke release should be tested using the same methods mentioned above. Moreover, additionally experiments should be carried out to evaluate thermal conductivity and to analyze gases evolved during decomposition of the material. It is proposed to analyze the gas phase using py-GCMS and MLC-FTIR. Thermal conductivity for example can be evaluated using a Hot Disk thermal constants analyzer (TPS2500) from Thermoconcept. This method allows measuring the thermal conductivity of materials as function of the temperature.

The described protocol should be applied first on each compound in the EVM-ATH-MB basic formulation and then with different combinations to find the source of early ignition and lower LOI value of the complete materials. After identification of the troublemaker, it should be replaced by another compound having the same function such as anti-aging or processing additive. Of course, the new compound should not exhibit the same negative influence on the TTI or on the LOI

List of tables, figures, equations and references

List of figures

List of tables

List of equations

References

1. *Overall Fire Death Rates and Relative Risk (2001-2010).* **cited 2013**; Available from: http://www.usfa.fema.gov/statistics/estimates/trend_overall.shtm.

2. marketsandmarkets, *Flame Retardant Chemicals Market by Type, Application & Geography – Market Estimates up to 2017* **(2012)**.

3. Perrin, M.W., Fawcett, E.W., Paton, J.G.and Williams, E.G., *Improvements in or relating to the interpolymerisation of ethylene with other organic compounds*, **1938**, C08F2/00 ; C08F10/00 ; C08F2/00 ; C08F10/00,

4. Meisenheimer, H. and Zens, A., *Ethylene Vinylacetate Elastomers (EVM)*, in *Handbook of Specialty Elastomers*, Klingender, R.C., Editor **2008**, CRC Press.

5. Henderson, A.M., *Ethylene-vinyl acetate (EVA) copolymers: a general review.* Electrical Insulation Magazine, IEEE, **1993**, 9(1): p. 30-38.

6. Seeger, A., Freitag, D., Freidel, F.and Luft, G., *Melting point of polymers under high pressure: Part I: Influence of the polymer properties.* Thermochimica Acta, **2004**, 424(1-2): p. 175-181.

7. Domininghaus, H., Elsner, P., Eyerer, P.and Hirth, T., *Kunststoffe - Eigenschaften und Anwendungen,* **2008**, SpringerLink.

8. Wang, L. and Jiang, P.K., *Thermal and flame retardant properties of ethylene-vinyl acetate copolymer/modified multiwalled carbon nanotube composites.* Journal of Applied Polymer Science, **2011**, 119(5): p. 2974-2983.

9. www.lanxess.com.

10. Perrin, M.W., *Interpolymerization of ethylene*, **1940**, United States, US2,200,429,

11. Roedel, M., *Ethylene/vinyl actetate polymerisation process*, **1955**, United States,

12. Schellenberg, W.-D., *Process for the continous preparation of ethylene/vinyal acetate copolymers using serially arranged reaction zones* **1967**, Germany,

13. Bartl, H., *Process for Production of Copolymers of Ethylene*, **1960**, Germany,

14. Tanaka, J. and Matsumoto, K., *Process for continuous production of ethylene-vinyl acetate copolymer*, **1987**, 4657994,

15. Jenkins, W.L., Hodge, D.T.and Sampson, K.J., *Process for preparing copolymers of ethylene and vinyl acetate*, **1987**, 4649186,

16. Yatsu, T., Moriuchi, S.and Fujii, H., *Copolymerization of Ethylene with Vinyl Acetate by Trialkylaluminum-Lewis Base-Peroxide Catalyst.* Macromolecules, **1977**, 10(2): p. 249-253.

17. Saegusa, T., Yatsu, T., Miyaji, S.and Fujii, H., *Dual Site Character of AlEt$_3$-ZnCl$_2$-CCl$_4$ Catalyst in the Copolymerization of Ethylene with Vinyl Acetate.* Polymer Journal, **1969**, 1(1): p. 7-12.

18. Röthemeyer, F. and Sommer, F., *Kautschuk Technologie (Werkstoffe-Verarbeitung-Produkte),* **2006**, Munich, Carl Hanser Verlag.

19. German, A.L., *The Copolymerisation of ethylene and vinylacetate at low pressure*, **1970**,

20. Guo, J., Choi, K.Y.and Schork, F.J., *Miniemulsion Copolymerization of Ethylene and Vinyl Acetate.* Macromolecular Reaction Engineering, **2009**, 3(7): p. 412-418.

21. Gheysari, D. and Behjat, A., *The effect of high-energy electron beam irradiation and content of ATH upon mechanical and thermal properties of EVA copolymer.* European Polymer Journal, **2002**, 38(6): p. 1087-1093.

22. Bunschoten, E., *Die Vulkanisation ohne Schwefel nach Ostromyslenski.* Kolloid-Zeitschrift, **1918**, 23(1): p. 25-31.

23. Mark, J.E., Erman, B.and Eirich, F.R., *The Science and Technology of RUBBER,* Press, E.A.**2005**, USA.

24. Loan, L.D., *Peroxide crosslinking reactions of polymers.* Pure Appl. Chem., **1972**, 30(Copyright (C) 2014 American Chemical Society (ACS). All Rights Reserved.): p. 173-80.

25. White, J.R. and De, S.K., *Rubber Technologist's Handbook,* **2001**, UK, Rapra Technology Limited.

26. Cérin, O., Duquesne, S., Fontaine, G., Roos, A.and Bourbigot, S., *Thermal degradation of elastomeric vulcanized poly(ethylene-co-vinyl acetate) (EVM): Chemical and kinetic investigations.* Polymer Degradation and Stability, **2011**, 96(10): p. 1812-1820.

27. Rimez, B., Rahier, H., Van Assche, G., Artoos, T., Biesemans, M.and Van Mele, B., *The thermal degradation of poly(vinyl acetate) and poly(ethylene-co-vinyl acetate), Part I: Experimental study of the degradation mechanism.* Polymer Degradation and Stability, **2008**, 93(4): p. 800-810.

28. McGarry, K., Zilberman, J., Hull, T.R.and Woolley, W.D., *Decomposition and combustion of EVA and LDPE alone and when fire retarded with ATH.* Polymer International, **2000**, 49(10): p. 1193-1198.

29. Allen, N.S., Edge, M., Rodriguez, M., Liauw, C.M.and Fontan, E., *Aspects of the thermal oxidation, yellowing and stabilisation of ethylene vinyl acetate copolymer.* Polymer Degradation and Stability, **2000**, 71(1): p. 1-14.

30. Allen, N.S., Edge, M., Rodriguez, M., Liauw, C.M.and Fontan, E., *Aspects of the thermal oxidation of ethylene vinyl acetate copolymer.* Polymer Degradation and Stability, **2000**, 68(3): p. 363-371.

31. Cai, X. and Shen, H., *Apparent Activation Energies of the Non-isothermal Degradation of EVA Copolymer.* Journal of Thermal Analysis and Calorimetry, **1999**, 55(1): p. 67-76.

32. Soudais, Y., Moga, L., Blazek, J.and Lemort, F., *Coupled DTA–TGA–FT-IR investigation of pyrolytic decomposition of EVA, PVC and cellulose.* Journal of Analytical and Applied Pyrolysis, **2007**, 78(1): p. 46-57.

33. Hull, T.R., Price, D., Liu, Y., Wills, C.L.and Brady, J., *An investigation into the decomposition and burning behaviour of Ethylene-vinyl acetate copolymer nanocomposite materials.* Polymer Degradation and Stability, **2003**, 82(2): p. 365-371.

34. Šimon, P., *Polymer degradation by elimination of small molecules.* Die Angewandte Makromolekulare Chemie, **1994**, 216(1): p. 187-203.

35. Roos, A. and La Rosa, M. *Halogen free flame retardant (HFFR) compounding with EVM and EVM/HNBR*. **2010**. American Chemical Society, Rubber Division.

36. Roos, A. and La Rosa, M. *High performance elastomers in cables for offshore and arctic regions*. **2010**. Smithers Rapra Technology Ltd.

37. Luks, A. *Halogen free and flame retardant compounds with submicron sized fillers*. **2010**. Smithers Rapra Technology Ltd.

38. Luks, A. and Sauerwein, R., *Halogen free and flame retardant elastomeric cable compounds with submicron sized fillers.* Proc. Int. Wire Cable Symp., **2008**, 57th: p. 134-137.

39. Meisenheimer, H., *Ethylene/vinyl acetate elastomers (EVM) for environmentally friendly cable applications.* Kautschuk und Gummi, Kunststoffe, **1995**, 48: p. 281-6.

40. Shen, K., Feng, J., Tu, H.and Wang, J. *The effect of $Al(OH)_3/Mg(OH)_2$ on flame retardance of EVA copolymers*. **1993**. Geol. Publ. House.

41. Price, D., Pyrah, K., Hull, T.R., Milnes, G.J., Ebdon, J.R., Hunt, B.J.and Joseph, P., *Flame retardance of poly(methyl methacrylate) modified with phosphorus-containing compounds.* Polymer Degradation and Stability, **2002**, 77(2): p. 227-233.

42. Wang, H., Wang, Q., Huang, Z.and Shi, W., *Synthesis and thermal degradation behaviors of hyperbranched polyphosphate.* Polymer Degradation and Stability, **2007**, 92(10): p. 1788-1794.

43. Lammers, M., Klop, E.A., Northolt, M.G.and Sikkema, D.J., *Mechanical properties and structural transitions in the new rigid-rod polymer fibre PIPD (`M5') during the manufacturing process.* Polymer, **1998**, 39(24): p. 5999-6005.

44. Cheng, T.W. and Chiu, J.P., *Fire-resistant geopolymer produced by granulated blast furnace slag.* Minerals Engineering, **2003**, 16(3): p. 205-210.

45. Wang, G. and Yang, J., *Influences of expandable graphite modified by polyethylene glycol on fire protection of waterborne intumescent fire resistive coating.* Surface and Coatings Technology, **2010**, 204(21-22): p. 3599-3605.

46.   Wang, Z., Han, E.and Ke, W., *An investigation into fire protection and water resistance of intumescent nano-coatings.* Surface and Coatings Technology, **2006**, 201(3-4): p. 1528-1535.

47.   Duquesne, S., Magnet, S., Jama, C.and Delobel, R., *Intumescent paints: fire protective coatings for metallic substrates.* Surface and Coatings Technology, **2004**, 180-181(0): p. 302-307.

48.   Gardelle, B., Duquesne, S., Vandereecken, P., Bellayer, S.and Bourbigot, S., *Resistance to fire of curable silicone/expandable graphite based coating: Effect of the catalyst.* European Polymer Journal, **2013**, 49(8): p. 2031-2041.

49.   Morgan, A.B. and Wilkie, C.A., *Fire Retardancy of Polymeric Materials,* **2010**, CRC Press, Taylor & Francis Group.

50.   Troitzsch, J., *Plastics Flammability Handbook,* **2004**, Munich, Carl Hanser Verlag Munich.

51.   Troitzsch, J.H., *Overview of flame retardants.* Chim. Oggi, **1998**, 16: p. 18-24.

52.   Weil, E.D. and Levchik, S.V., *Flame retardants in commercial use or development for polyolefins.* J. Fire Sci., **2008**, 26: p. 5-43.

53.   Yang, C.-P. and Chen, W.-T., *Effects of brominated flame retardants and crosslinking agents on the flame retardancy of rubbers.* Journal of Applied Polymer Science, **1988**, 36(4): p. 963-978.

54.   Zhang, X., Guo, F., Chen, J., Wang, G.and Liu, H., *Investigation of interfacial modification for flame retardant ethylene vinyl acetate copolymer/alumina trihydrate nanocomposites.* Polymer Degradation and Stability, **2005**, 87(3): p. 411-418.

55.   Basfar, A.A. and Bae, H.J., *Influence of magnesium hydroxide and huntite hydromagnesite on mechanical properties of ethylene vinyl acetate compounds cross-linked by DiCumyl peroxide and ionizing radiation.* Journal of Fire Sciences, **2010**, 28: p. 161-180.

56.   Hull, T.R., Witkowski, A.and Hollingbery, L., *Fire retardant action of mineral fillers.* Polymer Degradation and Stability, **2011**, 96(8): p. 1462-1469.

57.   Du, L., Qu, B.and Xu, Z., *Flammability characteristics and synergistic effect of hydrotalcite with microencapsulated red phosphorus in halogen-free flame retardant EVA composite.* Polymer Degradation and Stability, **2006**, 91(5): p. 995-1001.

58.   Basfar, A.A. and Bae, H.J., *Influence of Magnesium Hydroxide and Huntite Hydromagnesite on Mechanical Properties of Ethylene Vinyl Acetate Compounds Cross-linked by DiCumyl Peroxide and Ionizing Radiation.* Journal of Fire Sciences, **2010**, 28(2): p. 161-180.

59.   Morgan, A.B., Cogen, J.M., Opperman, R.S.and Harris, J.D., *The effectiveness of magnesium carbonate-based flame retardants for poly(ethylene-co-vinyl acetate) and poly(ethylene-co-ethyl acrylate).* Fire and Materials, **2007**, 31(6): p. 387-410.

60.   Laoutid, F., Lorgouilloux, M., Lesueur, D., Bonnaud, L.and Dubois, P., *Calcium-based hydrated minerals: Promising halogen-free flame retardant and fire resistant additives for polyethylene and ethylene vinyl acetate copolymers.* Polymer Degradation and Stability, **2013**, 98(9): p. 1617-1625.

61.   Huang, H., Tian, M., Liu, L., Liang, W.and Zhang, L., *Effect of particle size on flame retardancy of Mg(OH)$_2$-filled ethylene vinyl acetate copolymer composites.* Journal of Applied Polymer Science, **2006**, 100(6): p. 4461-4469.

62.   Camino, G., Maffezzoli, A., Braglia, M., De Lazzaro, M.and Zammarano, M., *Effect of hydroxides and hydroxycarbonate structure on fire retardant effectiveness and mechanical properties in ethylene-vinyl acetate copolymer.* Polymer Degradation and Stability, **2001**, 74(3): p. 457-464.

63.   Fernández, A.I., Haurie, L., Formosa, J., Chimenos, J.M., Antunes, M.and Velasco, J.I., *Characterization of poly(ethylene-co-vinyl acetate) (EVA) filled with low grade magnesium hydroxide.* Polymer Degradation and Stability, **2009**, 94(1): p. 57-60.

64.   Qiu, L., Xie, R., Ding, P.and Qu, B., *Preparation and characterization of Mg(OH)2 nanoparticles and flame-retardant property of its nanocomposites with EVA.* Composite Structures, **2003**, 62(3–4): p. 391-395.

65.   Jiao, C.M., Wang, Z.Z., Ye, Z., Hu, Y.and Fan, W.C., *Flame retardation of ethylene-vinyl acetate copolymer using nano magnesium hydroxide and nano hydrotalcite.* Journal of Fire Sciences, **2006**, 24(1): p. 47-64.

66.   Hornsby, P.R., Cusack, P.A., Cross, M., Toth, A., Zelei, B.and Marosi, G., *Zinc hydroxystannate-coated metal hydroxide fire retardants: Fire performance and substrate-coating interactions.* Journal of Materials Science, **2003**, 38(13): p. 2893-2899.

67.   Haurie, L., Fernandez, A.I., Velasco, J.I., Chimenos, J.M., Lopez Cuesta, J.and Espiell, F., *Synthetic hydromagnesite as flame retardant. Evaluation of the flame behaviour in a polyethylene matrix.* Polymer Degradation and Stability, **2006**, 91(5): p. 989-994.

68.   Huang, G., Fei, Z., Chen, X., Qiu, F., Wang, X.and Gao, J., *Functionalization of layered double hydroxides by intumescent flame retardant: Preparation, characterization, and application in ethylene vinyl acetate copolymer.* Applied Surface Science, **2012**, 258(24): p. 10115-10122.

69.   Wang, L., Li, B., Zhang, X., Chen, C.and Zhang, F., *Effect of intercalated anions on the performance of Ni–Al LDH nanofiller of ethylene vinyl acetate composites.* Applied Clay Science, **2012**, 56: p. 110-119.

70.   Wang, L., Li, B., Hu, Z.and Cao, J., *Effect of nickel on the properties of composites composed of layered double hydroxides and ethylene vinyl acetate copolymer.* Applied Clay Science, **2013**, 72: p. 138-146.

71.   Wang, L., Li, B., Yang, M., Chen, C.and Liu, Y., *Effect of Ni cations and microwave hydrothermal treatment on the related properties of layered double hydroxide–ethylene vinyl acetate copolymer composites.* Journal of Colloid and Interface Science, **2011**, 356(2): p. 519-525.

72.   Wang, L., Li, B., Zhao, X., Chen, C.and Cao, J., *Effect of Rare Earth Ions on the Properties of Composites Composed of Ethylene Vinyl Acetate Copolymer and Layered Double Hydroxides.* PLoS ONE, **2012**, 7(6): p. e37781.

73.   Nyambo, C. and Wilkie, C.A., *Layered double hydroxides intercalated with borate anions: Fire and thermal properties in ethylene vinyl acetate copolymer.* Polymer Degradation and Stability, **2009**, 94(4): p. 506-512.

74.   Nyambo, C., Kandare, E.and Wilkie, C.A., *Thermal stability and flammability characteristics of ethylene vinyl acetate (EVA) composites blended with a phenyl phosphonate-intercalated layered double hydroxide (LDH), melamine polyphosphate and/or boric acid.* Polymer Degradation and Stability, **2009**, 94(4): p. 513-520.

75.   Ye, L. and Qu, B., *Flammability characteristics and flame retardant mechanism of phosphate-intercalated hydrotalcite in halogen-free flame retardant EVA blends.* Polymer Degradation and Stability, **2008**, 93(5): p. 918-924.

76.   Ye, L., Ding, P., Zhang, M.and Qu, B., *Synergistic effects of exfoliated LDH with some halogen-free flame retardants in LDPE/EVA/HFMH/LDH nanocomposites.* Journal of Applied Polymer Science, **2008**, 107(6): p. 3694-3701.

77.   Alongi, J. and Frache, A., *Flame retardancy properties of α-zirconium phosphate based composites.* Polymer Degradation and Stability, **2010**, 95(9): p. 1928-1933.

78.   Gui, H., Zhang, X., Dong, W., Wang, Q., Gao, J., Song, Z., Lai, J., Liu, Y., Huang, F.and Qiao, J., *Flame retardant synergism of rubber and Mg(OH)$_2$ in EVA composites.* Polymer, **2007**, 48(9): p. 2537-2541.

79.   Zhang, G., Ding, P., Zhang, M.and Qu, B., *Synergistic effects of layered double hydroxide with hyperfine magnesium hydroxide in halogen-free flame retardant EVA/HFMH/LDH nanocomposites.* Polymer Degradation and Stability, **2007**, 92(9): p. 1715-1720.

80.   Li, L., Qian, Y.and Jiao, C., *Synergistic flame retardant effect of melamine in ethylene–vinyl acetate/layered double hydroxides composites.* Journal of Thermal Analysis and Calorimetry, **2013**, 114(1): p. 45-55.

81.   Chen, X., Jiao, C.and Zhang, J., *Thermal and combustion behavior of ethylene-vinyl acetate/aluminum trihydroxide/Fe-montmorillonite composites.* Polymer Engineering & Science, **2012**, 52(2): p. 414-419.

82. Yen, Y.-Y., Wang, H.-T.and Guo, W.-J., *Synergistic flame retardant effect of metal hydroxide and nanoclay in EVA composites.* Polymer Degradation and Stability, **2012**, 97(6): p. 863-869.

83. Sabet, M., Hassan, A.and Ratnam, C.T., *Effect of zinc borate on flammability/thermal properties of ethylene vinyl acetate filled with metal hydroxides.* Journal of Reinforced Plastics and Composites, **2013**, 32(15): p. 1122-1128.

84. Wang, L., Wang, G.and Jiang, P., *Research on the related properties of EVM/Al(OH)$_3$/SiO$_2$ composites applied for halogen-free flame retardant cable insulation and jacket.* Journal of Applied Polymer Science, **2011**, 120(1): p. 368-378.

85. Ramírez-Vargas, E., Sánchez-Valdes, S., Parra-Tabla, O., Castañeda-Gutiérrez, S., Méndez-Nonell, J., Francisco Ramos-deValle, L., López-León, A.and Lujan-Acosta, R., *Structural characterization of LDPE/EVA blends containing nanoclay-flame retardant combinations.* Journal of Applied Polymer Science, **2012**, 123(2): p. 1125-1136.

86. Cérin, O., *Development and charaterization of a novel flame retardant EVM-based formulation: investigation and comprehension of the flame retardant mechnisms*, **2010**, PhD thesis, University of Lille 1 - Sciences and Technologies, France

87. Fu, M. and Qu, B., *Synergistic flame retardant mechanism of fumed silica in ethylene-vinyl acetate/magnesium hydroxide blends.* Polymer Degradation and Stability, **2004**, 85(1): p. 633-639.

88. Cardelli, A., Ruggeri, G., Calderisi, M., Lednev, O., Cardelli, C.and Tombari, E., *Effects of poly(dimethylsiloxane) and inorganic fillers in halogen free flame retardant poly(ethylene-co-vinyl acetate) compound: A chemometric approach.* Polymer Degradation and Stability, **2012**, 97(12): p. 2536-2544.

89. Huang, H., Tian, M., Liu, L., He, Z., Chen, Z.and Zhang, L., *Effects of silicon additive as synergists of Mg(OH)$_2$ on the flammability of ethylene vinyl acetate copolymer.* Journal of Applied Polymer Science, **2006**, 99(6): p. 3203-3209.

90. Ye, L., Miao, Y., Yan, H., Li, Z., Zhou, Y., Liu, J.and Liu, H., *The synergistic effects of boroxo siloxanes with magnesium hydroxide in halogen-free flame retardant EVA/MH blends.* Polymer Degradation and Stability, **2013**, 98(4): p. 868-874.

91. Ye, L., Wu, Q.and Qu, B., *Synergistic effects and mechanism of multiwalled carbon nanotubes with magnesium hydroxide in halogen-free flame retardant EVA/MH/MWNT nanocomposites.* Polymer Degradation and Stability, **2009**, 94(5): p. 751-756.

92. Carpentier, F., Bourbigot, S., Le Bras, M., Delobel, R.and Foulon, M., *Charring of fire retarded ethylene vinyl acetate copolymer — magnesium hydroxide/zinc borate formulations.* Polymer Degradation and Stability, **2000**, 69(1): p. 83-92.

93. Huang, N.H., Chen, Z.J., Yi, C.H.and Wang, J.Q., *Synergistic flame retardant effects between sepiolite and magnesium hydroxide in ethylene-vinyl acetate (EVA) matrix.* eXPRESS Polym. Lett., **2010**, 4(4): p. 227-233.

94. Durin-France, A., Ferry, L., Lopez Cuesta, J.M.and Crespy, A., *Magnesium hydroxide/zinc borate/talc compositions as flame-retardants in EVA copolymer.* Polymer International, **2000**, 49(10): p. 1101-1105.

95. Clerc, L., Ferry, L., Leroy, E.and Lopez-Cuesta, J.-M., *Influence of talc physical properties on the fire retarding behaviour of (ethylene–vinyl acetate copolymer/magnesium hydroxide/talc) composites.* Polymer Degradation and Stability, **2005**, 88(3): p. 504-511.

96. Laoutid, F., Gaudon, P., Taulemesse, J.M., Lopez Cuesta, J.M., Velasco, J.I.and Piechaczyk, A., *Study of hydromagnesite and magnesium hydroxide based fire retardant systems for ethylene–vinyl acetate containing organo-modified montmorillonite.* Polymer Degradation and Stability, **2006**, 91(12): p. 3074-3082.

97. Szép, A., Szabó, A., Tóth, N., Anna, P.and Marosi, G., *Role of montmorillonite in flame retardancy of ethylene–vinyl acetate copolymer.* Polymer Degradation and Stability, **2006**, 91(3): p. 593-599.

98. Ahamad, A., Patil, C.B., Mahulikar, P.P., Hundiwale, D.G.and Gite, V.V., *Studies on the flame retardant, mechanical and thermal properties of ternary magnesium hydroxide/clay/EVA nanocomposites.* Journal of Elastomers and Plastics, **2012**, 44(3): p. 251-261.

99. Ducrocq, P., Duquesne, S., Magnet, S., Bourbigot, S.and Delobel, R., *Interactions between chlorinated paraffins and melamine in intumescent paint—investing a way to suppress chlorinated paraffins from the formulations.* Progress in Organic Coatings, **2006**, 57(4): p. 430-438.

100. Wang, Z., Lv, P., Hu, Y.and Hu, K., *Thermal degradation study of intumescent flame retardants by TG and FTIR: Melamine phosphate and its mixture with pentaerythritol.* Journal of Analytical and Applied Pyrolysis, **2009**, 86(1): p. 207-214.

101. Zilberman, J., Hull, T.R., Price, D., Milnes, G.J.and Keen, F., *Flame retardancy of some ethylene–vinyl acetate copolymer-based formulations.* Fire and Materials, **2000**, 24(3): p. 159-164.

102. Rybiński, P., Janowska, G., Dobrzyńska, R.and Kucharska, A., *Effect of halogenless flame retardants on the thermal properties, flammability, and fire hazard of cross-linked EVM/NBR rubber blends.* Journal of Thermal Analysis and Calorimetry, **2014**, 115(1): p. 771-782.

103. van der Veen, I. and de Boer, J., *Phosphorus flame retardants: Properties, production, environmental occurrence, toxicity and analysis.* Chemosphere, **2012**, 88(10): p. 1119-1153.

104. Nguyen, C., Lee, M.and Kim, J., *Relationship between structures of phosphorus compounds and flame retardancies of the mixtures with acrylonitrile–butadiene–styrene and ethylene–vinyl acetate copolymer.* Polymers for Advanced Technologies, **2009**, 22(5): p. 512-519.

105. Twarowski, A., *The influence of phosphorus oxides and acids on the rate of H + OH recombination.* Combustion and Flame, **1993**, 94(1–2): p. 91-107.

106. Twarowski, A., *Reduction of a phosphorus oxide and acid reaction set.* Combustion and Flame, **1995**, 102(1–2): p. 41-54.

107. Twarowski, A., *The temperature dependence of H + OH recombination in phosphorus oxide containing post-combustion gases.* Combustion and Flame, **1996**, 105(3): p. 407-413.

108. Jayaweera, T.M., Melius, C.F., Pitz, W.J., Westbrook, C.K., Korobeinichev, O.P., Shvartsberg, V.M., Shmakov, A.G., Rybitskaya, I.V.and Curran, H.J., *Flame inhibition by phosphorus-containing compounds over a range of equivalence ratios.* Combustion and Flame, **2005**, 140(1–2): p. 103-115.

109. MacDonald, M.A., Gouldin, F.C.and Fisher, E.M., *Temperature dependence of phosphorus-based flame inhibition.* Combustion and Flame, **2001**, 124(4): p. 668-683.

110. Wu, K., Shen, M.-M.and Hu, Y., *Combustion Behavior and Thermal Oxidative Degradation of EVA Containing Intumescent Flame Retardant.* Polymer-Plastics Technology and Engineering, **2010**, 49(15): p. 1527-1533.

111. Wang, B., Tang, Q., Hong, N., Song, L., Wang, L., Shi, Y.and Hu, Y., *Effect of Cellulose Acetate Butyrate Microencapsulated Ammonium Polyphosphate on the Flame Retardancy, Mechanical, Electrical, and Thermal Properties of Intumescent Flame-Retardant Ethylene–Vinyl Acetate Copolymer/Microencapsulated Ammonium Polyphosphate/Polyamide-6 Blends.* Applied Materials & Interfaces, **2011**, 3(9): p. 3754-3761.

112. Wang, D.-Y., Cai, X.-X., Qu, M.-H., Liu, Y., Wang, J.-S.and Wang, Y.-Z., *Preparation and flammability of a novel intumescent flame-retardant poly(ethylene-co-vinyl acetate) system.* Polymer Degradation and Stability, **2008**, 93(12): p. 2186-2192.

113. Zhang, Y., Lu, Y., Guo, F., Peng, C., Li, M.and Xu, W., *Preparation of microencapsulated ammonium polyphosphate with montmorillonite-melamine formaldehyde resin and its flame retardancy in EVM.* Polymers for Advanced Technologies, **2012**, 23(2): p. 166-170.

114. Wang, B., Wang, X., Tang, G., Shi, Y., Hu, W., Lu, H., Song, L.and Hu, Y., *Preparation of silane precursor microencapsulated intumescent flame retardant and its enhancement on the properties of ethylene–vinyl acetate copolymer cable.* Composites Science and Technology, **2012**, 72(9): p. 1042-1048.

115.   Wang, B., Hu, S., Zhao, K., Lu, H., Song, L.and Hu, Y., *Preparation of Polyurethane Microencapsulated Expandable Graphite, and Its Application in Ethylene Vinyl Acetate Copolymer Containing Silica-Gel Microencapsulated Ammonium Polyphosphate.* Industrial & Engineering Chemistry Research, **2011**, 50(20): p. 11476-11484.

116.   Burns, M., Wagenknecht, U., Kretzschmar, B.and Focke, W.W., *Effect of hydrated fillers and red phosphorus on the limiting oxygen index of poly(ethylene-co-vinyl actate)-poly(vinyl butyral) and low density polyethylene-poly(ethylene-co-vinyl alcohol) blends.* Journal of Vinyl and Additive Technology, **2008**, 14(3): p. 113-119.

117.   Alongi, J., Pošković, M., Frache, A.and Trotta, F., *Novel flame retardants containing cyclodextrin nanosponges and phosphorus compounds to enhance EVA combustion properties.* Polymer Degradation and Stability, **2010**, 95(10): p. 2093-2100.

118.   Jiao, C., Wang, Z., Chen, X., Yu, B.and Hu, Y., *Irradiation crosslinking and halogen-free flame retardation of EVA using hydrotalcite and red phosphorus.* Radiation Physics and Chemistry, **2006**, 75(5): p. 557-563.

119.   Li, L., Qian, Y.and Jiao, C., *Influence of red phosphorus on the flame-retardant properties of ethylene vinyl acetate/layered double hydroxides composites.* Iranian Polymer Journal, **2012**, 21(9): p. 557-568.

120.   Le Bras, M., Bourbigot, S.and Revel, B., *Comprehensive study of the degradation of an intumescent EVA-based material during combustion.* Journal of Materials Science, **1999**, 34(23): p. 5777-5782.

121.   Zaharri, N.D., Othman, N.and Ishak, Z.A.M., *Thermal and Mechanical Properties of Zeolite Filled Ethylene Vinyl Acetate Composites.* Procedia Chemistry, **2012**, 4: p. 95-100.

122.   Wang, L., Yang, W., Wang, B., Wu, Y., Hu, Y., Song, L.and Yuen, R.K.K., *The Impact of Metal Oxides on the Combustion Behavior of Ethylene−Vinyl Acetate Coploymers Containing an Intumescent Flame Retardant.* Industrial & Engineering Chemistry Research, **2012**, 51(23): p. 7884-7890.

123.   Zhou, K., Wang, B., Jiang, S., Yuan, H., Song, L.and Hu, Y., *Facile Preparation of Nickel Phosphide ($Ni_{12}P_5$) and Synergistic Effect with Intumescent Flame Retardants in Ethylene−Vinyl Acetate Copolymer.* Industrial & Engineering Chemistry Research, **2013**, 52(19): p. 6303-6310.

124.   Wang, L., Hu, Y., Song, L.and Yuen, R.K.K., *Investigation of Thermal and Combustion Properties for Intumescent Flame-Retardant Ethylene−Viny Acetate Composites Containing Ferrous Disulfide.* Industrial & Engineering Chemistry Research, **2012**, 51(46): p. 15082-15088.

125.   Wang, B., Zhou, K., Wang, L., Song, L., Hu, Y.and Hu, S., *Enhancement on physical properties of flame retarded ethylene-vinyl acetate copolymer/ferric pyrophosphate composites through electron beam irradiation.* Composites Part B: Engineering, **2012**, 43(2): p. 641-646.

126.   Riva, A., Camino, G., Fomperie, L.and Amigouët, P., *Fire retardant mechanism in intumescent ethylene vinyl acetate compositions.* Polymer Degradation and Stability, **2003**, 82(2): p. 341-346.

127.   Wang, L., Jiang, J., Jiang, P.and Yu, J., *Synthesis, characteristic of a novel flame retardant containing phosphorus and its application in poly(ethylene-co-vinyl acetate).* Fire and Materials, **2011**, 35(4): p. 193-207.

128.   Zhu, W., Weil, E.D.and Mukhopadhyay, S., *Intumescent flame-retardant system of phosphates and 5,5,5',5',5",5"-hexamethyltris (1,3,2-dioxaphosphorinanemethan)amine 2,2',2"- trioxide for polyolefins.* Journal of Applied Polymer Science, **1996**, 62(13): p. 2267-2280.

129.   Camino, G., Sgobbi, R., Zaopo, A., Colombier, S.and Scelza, C., *Investigation of flame retardancy in EVA.* Fire and Materials, **2000**, 24(2): p. 85-90.

130.   Nguyen, C. and Kim, J., *Synthesis of a Novel Nitrogen-Phosphorus Flame Retardant Based on Phosphoramidate and Its Application to PC, PBT, EVA and ABS.* Macromolecular Research, **2008**, 16(7): p. 620-625.

131. Wang, L., Wu, X., Wu, C., Yu, J., Wang, G.and Jiang, P., *Study on the flame retardancy of EVM/magnesium hydroxide composites optimized with a flame retardant containing phosphorus and silicon.* Journal of Applied Polymer Science, **2011**, 121(1): p. 68-77.

132. Lichun, W., Jinhong, Y., Zongliu, T.and Pingkai, J., *Synthesis, characteristic, and flammability of modified carbon nanotube/poly(ethylene-co-vinyl acetate) nanocomposites containing phosphorus and silicon.* Journal of Material Science, **2010**, 45: p. 6668–6676.

133. Bonnet, J., Bounor-Legaré, V., Boisson, F., Melis, F., Camino, G.and Cassagnau, P., *Phosphorus based organic–inorganic hybrid materials prepared by reactive processing for EVA fire retardancy.* Polymer Degradation and Stability, **2012**, 97(4): p. 513-522.

134. Wu, Q., Qu, B.and Sun, M., *Photocrosslinking of halogen-free flame-retarded ethylene-vinyl acetate copolymer by phosphorous-nitrogen compound NP28.* Journal of Applied Polymer Science, **2009**, 114(1): p. 562-569.

135. Liu, Y., Zhang, Y., Cao, Z.and Fang, Z., *Synthesis of Three Novel Intumescent Flame Retardants Having Azomethine Linkages and Their Applications in EVA Copolymer.* Industrial & Engineering Chemistry Research, **2012**, 51(34): p. 11059-11065.

136. Liu, H., Xiong, Y., Xu, W., Zhang, Y.and Pan, S., *Synthesis of a novel intumescent flame retardant and its application in EVM.* Journal of Applied Polymer Science, **2012**, 125(2): p. 1544-1551.

137. Liu, Y., Zhang, Y., Cao, Z., Peng, M.and Fang, Z., *Synthesis of novel poly(aminophosphonate ester)s flame retardants and their applications in EVA copolymer.* Polymers for Advanced Technologies, **2013**, 24(2): p. 197-203.

138. Gross, D., Loftus, J.J.and Robertson, A.F., *Method for Measuring Smoke from Burning Materials*, in *Fire Test Methods, Restraint and Smoke***1966**, American Society for Testing and Materials. p. 166-204.

139. Fitzgerald, K.T. and Flood, A.A., *Smoke Inhalation.* Clinical Techniques in Small Animal Practice, **2006**, 21(4): p. 205-214.

140. Leisewitz, A., Kruse, H.and Schramm, E., *Substituting Environmentally Relevant Flame Retardants: Assessment Fundamentals*, **2000**, German Federal Environmental Agency (Umweltbundesamt): Germany.

141. Gann, R.G., Babrauskas, V., Grayson, S.J.and Marsh, N.D., *Hazards of combustion products: Toxicity, opacity, corrosivity, and heat release: The experts' views on capability and issues.* Fire and Materials, **2011**, 35(2): p. 115-127.

142. Weil, E.D. and Choudhary, V., *Flame-Retarding Plastics and Elastomers with Melamine.* Journal of Fire Sciences, **1995**, 13(2): p. 104-126.

143. Stec, A.A. and Rhodes, J., *Smoke and hydrocarbon yields from fire retarded polymer nanocomposites.* Polymer Degradation and Stability, **2011**, 96(3): p. 295-300.

144. Rhodes, J., Smith, C.and Stec, A.A., *Characterisation of soot particulates from fire retarded and nanocomposite materials, and their toxicological impact.* Polymer Degradation and Stability, **2011**, 96(3): p. 277-284.

145. Shi, L., Li, D., Li, S., Wang, J., Evans, D.and Duan, X., *Structure, flame retarding and smoke suppressing properties of Zn-Mg-Al-CO3 layered double hydroxides.* Chinese Science Bulletin, **2005**, 50(11): p. 1101-1104.

146. Bourbigot, S., Le Bras, M., Leeuwendal, R., Shen, K.K.and Schubert, D., *Recent advances in the use of zinc borates in flame retardancy of EVA.* Polymer Degradation and Stability, **1999**, 64(3): p. 419-425.

147. Hull, T.R., Quinn, R.E., Areri, I.G.and Purser, D.A., *Combustion toxicity of fire retarded EVA.* Polymer Degradation and Stability, **2002**, 77(2): p. 235-242.

148. Cross, M.S., Cusack, P.A.and Hornsby, P.R., *Effects of tin additives on the flammability and smoke emission characteristics of halogen-free ethylene-vinyl acetate copolymer.* Polymer Degradation and Stability, **2003**, 79(2): p. 309-318.

149. Bugajny, M., Bourbigot, S., Le Bras, M.and Delobel, R., *The origin and nature of flame retardance in ethylene-vinyl acetate copolymers containing hostaflam AP 750.* Polymer International, **1999**, 48(4): p. 264-270.

150. Wu, X., Wang, L., Wu, C., Yu, J., Xie, L., Wang, G.and Jiang, P., *Influence of char residues on flammability of EVA/EG, EVA/NG and EVA/GO composites.* Polymer Degradation and Stability, **2011**, 97(1): p. 54-63.

151. Massiot, D., *Dmfit*, **Dmfit, 2011**.

152. Gustafsson, S.E., *Transient plane source techniques for thermal conductivity and thermal diffusivity measurements of solid materials.* Review of Scientific Instruments, **1991**, 62(3): p. 797-804.

153. Ahmed, K., Nizami, S.S.and Riza, N.Z., *Reinforcement of natural rubber hybrid composites based on marble sludge/Silica and marble sludge/rice husk derived silica.* Journal of Advanced Research, **2014**, 5(2): p. 165-173.

154. Enescu, D., Frache, A., Lavaselli, M., Monticelli, O.and Marino, F., *Novel phosphorous– nitrogen intumescent flame retardant system. Its effects on flame retardancy and thermal properties of polypropylene.* Polymer Degradation and Stability, **2013**, 98(1): p. 297-305.

155. Schartel, B., Weiß, A., Mohr, F., Kleemeier, M., Hartwig, A.and Braun, U., *Flame retarded epoxy resins by adding layered silicate in combination with the conventional protection-layer-building flame retardants melamine borate and ammonium polyphosphate.* Journal of Applied Polymer Science, **2010**, 118(2): p. 1134-1143.

156. Lazko, J., Landercy, N., Laoutid, F., Dangreau, L., Huguet, M.H.and Talon, O., *Flame retardant treatments of insulating agro-materials from flax short fibres.* Polymer Degradation and Stability, **2013**, 98(5): p. 1043-1051.

157. Unlu, S.M., Dogan, S.D.and Dogan, M., *Comparative study of boron compounds and aluminum trihydroxide as flame retardant additives in epoxy resin.* Polymers for Advanced Technologies, **2014**, published online.

158. Bodzay, B., Marosfoi, B.B., Igricz, T., Bocz, K.and Marosi, G., *Polymer degradation studies using laser pyrolysis-FTIR microanalysis.* Journal of Analytical and Applied Pyrolysis, **2009**, 85(1–2): p. 313-320.

159. Levchik, S.V., Balabanovich, A.I., Levchik, G.F.and Costa, L., *Effect of melamine and its salts on combustion and thermal decomposition of polyamide 6.* Fire and Materials, **1997**, 21(2): p. 75-83.

160. Casu, A., Camino, G., De Giorgi, M., Flath, D., Morone, V.and Zenoni, R., *Fire-retardant mechanistic aspects of melamine cyanurate in polyamide copolymer.* Polymer Degradation and Stability, **1997**, 58(3): p. 297-302.

161. Gijsman, P., Steenbakkers, R., Fürst, C.and Kersjes, J., *Differences in the flame retardant mechanism of melamine cyanurate in polyamide 6 and polyamide 66.* Polymer Degradation and Stability, **2002**, 78(2): p. 219-224.

162. Naik, A.D., Fontaine, G., Samyn, F., Delva, X., Bourgeois, Y.and Bourbigot, S., *Melamine integrated metal phosphates as non-halogenated flame retardants: Synergism with aluminium phosphinate for flame retardancy in glass fiber reinforced polyamide 66.* Polymer Degradation and Stability, **2013**, 98(12): p. 2653-2662.

163. Hoffendahl, C., Fontaine, G., Duquesne, S., Taschner, F., Mezger, M.and Bourbigot, S., *Fire retardant mechanism of ethylene vinyl acetate elastomer (EVM) containing aluminium trihydroxide and melamine phosphate.* RSC Advances, **2014**, submitted.

164. Guermazi, N., Elleuch, K., Ayedi, H.F.and Kapsa, P., *Aging effect on thermal, mechanical and tribological behaviour of polymeric coatings used for pipeline application.* Journal of Materials Processing Technology, **2008**, 203(1–3): p. 404-410.

165. Chapman, R.P., Averell, P.R.and Harris, R.R., *Solubility of Melamine in Water.* Industrial & Engineering Chemistry, **1943**, 35(2): p. 137-138.

166. Bretti, C., De Stefano, C., Lando, G.and Sammartano, S., *Thermodynamic properties of melamine (2,4,6-triamino-1,3,5-triazine) in aqueous solution. Effect of ionic medium, ionic*

strength and temperature on the solubility and acid–base properties. Fluid Phase Equilibria, **2013**, 355: p. 104-113.

167. Beg, M.D.H. and Pickering, K.L., *Reprocessing of wood fibre reinforced polypropylene composites. Part II: Hygrothermal ageing and its effects.* Composites Part A: Applied Science and Manufacturing, **2008**, 39(9): p. 1565-1571.

168. Bubb, D.M., McGill, R.A., Horwitz, J.S., Fitz-Gerald, J.M., Houser, E.J., Stroud, R.M., Wu, P.W., Ringeisen, B.R., Piqué, A.and Chrisey, D.B., *Laser-based processing of polymer nanocomposites for chemical sensing applications.* Journal of Applied Physics, **2001**, 89(10): p. 5739-5746.

169. Costa, L. and Camino, G., *Thermal behaviour of melamine.* Journal of Thermal Analysis and Calorimetry, **1988**, 34(2): p. 423-429.

170. Balabanovich, A.I., *The effect of melamine on the combustion and thermal decomposition behaviour of poly(butylene terephthalate).* Polymer Degradation and Stability, **2004**, 84(3): p. 451-458.

171. Camino, G., Maffezzoli, A., Braglia, M., De, L.M.and Zammarano, M., *Effect of hydroxides and hydroxycarbonate structure on fire retardant effectiveness and mechanical properties in ethylene-vinyl acetate copolymer.* Polymer Degradadation and Stability, **2001**, 74: p. 457-464.

172. Hoffendahl, C., Fontaine, G., Duquesne, S., Taschner, F., Mezger, M.and Bourbigot, S., *Fire retardant mechanism of ethylene vinyl acetate elastomer (EVM) containing aluminium trihydroxide and melamine phosphate.* RSC Advances, **2014**, 4(39): p. 20185-20199.

173. Witkowski, A., Stec, A.A.and Richard Hull, T., *The influence of metal hydroxide fire retardants and nanoclay on the thermal decomposition of EVA.* Polymer Degradation and Stability, **2012**, 97(11): p. 2231-2240.

174. Bredael, P., *Pyrolysis of 1,7-octadiene.* Journal of Analytical and Applied Pyrolysis, **1982**, 4(3): p. 205-210.

175. Morikawa, T., *Evolution of Soot and Polycyclic Aromatic Hydrocarbons from Combustion and Pyrolysis of Polymers and Low Molecular Weight Hydrocarbons.* Fire Science and Technology, **1984**, 4(1): p. 27-35.

176. Cypres, R., *Aromatic hydrocarbons formation during coal pyrolysis.* Fuel Processing Technology, **1987**, 15: p. 1-15.

177. Poddar, N.B., Thomas, S.and Wornat, M.J., *Polycyclic aromatic hydrocarbons from the co-pyrolysis of 1,3-butadiene and propyne.* Proceedings of the Combustion Institute, **2013**, 34(1): p. 1775-1783.

178. Ngohang, F.E., Fontaine, G., Gay, L.and Bourbigot, S., *Revisited investigation of fire behavior of ethylene vinyl acetate/aluminum trihydroxide using a combination of mass loss cone, Fourier transform infrared spectroscopy and electrical low pressure impactor.* Polymer Degradation and Stability, **2014**, in press.

179. Grcar, J.F., Glarborg, P., Bell, J.B., Day, M.S., Loren, A.and Jensen, A.D., *Effects of mixing on ammonia oxidation in combustion environments at intermediate temperatures.* Proceedings of the Combustion Institute, **2005**, 30(1): p. 1193-1200.

180. Holleman, A. and Wiberg, E., *Lehrbuch der Anorganischen Chemie*. Vol. 102, **2007**, Walter de Gruyter & Co.

181. MacDonald, J.L., Werner-Zwanziger, U., Chen, B., Zwanziger, J.W.and Forgeron, D., *A 43Ca and 13C NMR study of the chemical interaction between poly(ethylene–vinyl acetate) and white cement during hydration.* Solid State Nuclear Magnetic Resonance, **2011**, 40(2): p. 78-83.

182. Stael, G.C. and Tavares, M.I.B., *NMR carbon-13 high resolution study of poly(ethylene-co-vinyl acetate).* Polymer Testing, **1997**, 16(2): p. 193-198.

183. Pécoul, N., Bourbigot, S.and Revel, B., *^{13}C, ^{25}Mg and ^{11}B solid-state NMR study of a fire retarded ethylene-vinyl acetate copolymer.* Macromolecular Symposia, **1997**, 119(1): p. 309-315.

184. Rottstegge, J., Arnold, M., Herschke, L., Glasser, G., Wilhelm, M., Spiess, H.W.and Hergeth, W.D., *Solid state NMR and LVSEM studies on the hardening of latex modified tile mortar systems.* Cement and Concrete Research, **2005**, 35(12): p. 2233-2243.

185. de Souza, C.M.G. and Tavares, M.I.B., *NMR study of commercial poly(ethylene-co-vinyl acetate).* Polymer Testing, **1998**, 17(8): p. 533-541.

186. Carpentier, F., Bourbigot, S., Le Bras, M., Delobel, R.and Foulon, M., *Charring of fire retarded ethylene vinyl acetate copolymer - magnesium hydroxide/zinc borate formulations.* Polymer Degradation and Stability, **2000**, 69(1): p. 83-92.

187. Delfini, M., Segre, A.L.and Conti, F., *Sequence Distributions in Ethylene-Vinyl Acetate Copolymers. I. 13C Nuclear Magnetic Resonance Studies.* Macromolecules, **1973**, 6(3): p. 456-459.

188. Bourbigot, S., Bras, M.L.and Delobel, R., *Carbonization mechanisms resulting from intumescence association with the ammonium polyphosphate-pentaerythritol fire retardant system.* Carbon, **1993**, 31(8): p. 1219-1230.

189. Sanz, J. and Serratosa, J.M., *Distinction of Tetrahedrally and Octahedrally Coordinated Al in Phyllosilicates by NMR Spectroscopy.* Clay Minerals, **1984**, 19: p. 113-115.

190. Slade, R.C.T., Southern, J.C.and Thompson, I.M., *^{27}Al nuclear magnetic resonance spectroscopy investigation of thermal transformation sequences of alumina hydrates. Part 1.-Gibbsite, [gamma]-Al(OH)$_3$.* Journal of Materials Chemistry, **1991**, 1(4): p. 563-568.

191. Ingram-Jones, V.J., Slade, R.C.T., Davies, T.W., Southern, J.C.and Salvador, S., *Dehydroxylation sequences of gibbsite and boehmite: study of differences between soak and flash calcination and of particle-size effects.* Journal of Materials Chemistry, **1996**, 6(1): p. 73-79.

192. Jahromi, S., Gabriëlse, W.and Braam, A., *Effect of melamine polyphosphate on thermal degradation of polyamides: a combined X-ray diffraction and solid-state NMR study.* Polymer, **2003**, 44(1): p. 25-37.

193. Costa, L., Camino, G.and Luda, d.C.M.P., *Mechanism of thermal degradation of fire-retardant melamine salts.* ACS Symp. Ser., **1990**, 425: p. 211-38.

194. Kandola, B.K., Horrocks, R.A.and Horrocks, S., *Char Formation in Flame-Retarded Fibre–Intumescent Combinations. Part V. Exploring Different Fibre/Intumescent Combinations.* Fire and Materials, **2001**, 25(4): p. 153-160.

195. Jimenez, M., Duquesne, S.and Bourbigot, S., *Intumescent fire protective coating: Toward a better understanding of their mechanism of action.* Thermochimica Acta, **2006**, 449(1–2): p. 16-26.

196. Damodaran, K., Sanjayan, G.J., Rajamohanan, P.R., Ganapathy, S.and Ganesh, K.N., *Solid State NMR of a Molecular Self-Assembly: Multinuclear Approach to the Cyanuric Acid-Melamine System.* Organic Letters, **2001**, 3(12): p. 1921-1924.

197. Jürgens, B., Irran, E., Senker, J., Kroll, P., Müller, H.and Schnick, W., *Melem (2,5,8-Triamino-tri-s-triazine), an Important Intermediate during Condensation of Melamine Rings to Graphitic Carbon Nitride:Synthesis, Structure Determination by X-ray Powder Diffractometry, Solid-State NMR, and Theoretical Studies.* Journal of the American Chemical Society, **2003**, 125(34): p. 10288-10300.

198. Lotsch, B.V. and Schnick, W., *New Light on an Old Story: Formation of Melam during Thermal Condensation of Melamine.* Chemistry – A European Journal, **2007**, 13(17): p. 4956-4968.

199. Lotsch, B.V., Döblinger, M., Sehnert, J., Seyfarth, L., Senker, J., Oeckler, O.and Schnick, W., *Unmasking Melon by a Complementary Approach Employing Electron Diffraction, Solid-State NMR Spectroscopy, and Theoretical Calculations—Structural Characterization of a Carbon Nitride Polymer.* Chemistry – A European Journal, **2007**, 13(17): p. 4969-4980.

200. Lucena, M.d.C.C., V. de Alencar, A.E., Mazzeto, S.E.and Soares, S.d.A., *The effect of additives on the thermal degradation of cellulose acetate.* Polymer Degradation and Stability, **2003**, 80(1): p. 149-155.

201. Jimenez, M., Duquesne, S.and Bourbigot, S., *Characterization of the performance of an intumescent fire protective coating.* Surface and Coatings Technology, **2006**, 201(3–4): p. 979-987.

202. Brauer, G. and Editor, *Handbook of Preparative Inorganic Chemistry in Three Volumes, Vol. 1. 3rd Ed,* **1975**, Enke. 608 pp.

203. Kline, D., Bray, P.J.and Kriz, H.M., *Structure of Crystalline Boron Oxide.* The Journal of Chemical Physics, **1968**, 48(11): p. 5277-5278.

204. Berger, S.V., *The crystal structure of boron oxide.* Acta Chem. Scand., **1953**, 7: p. 611-22.

205. Neiner, D., Luedtke, A., Karkamkar, A., Shaw, W., Wang, J., Browning, N.D., Autrey, T.and Kauzlarich, S.M., *Decomposition Pathway of Ammonia Borane on the Surface of Nano-BN.* The Journal of Physical Chemistry C, **2010**, 114(32): p. 13935-13941.

206. Li, J., Bernard, S., Salles, V., Gervais, C.and Miele, P., *Preparation of Polyborazylene-Derived Bulk Boron Nitride with Tunable Properties by Warm-Pressing and Pressureless Pyrolysis.* Chemistry of Materials, **2010**, 22(6): p. 2010-2019.

207. Gervais, C., Framery, E., Duriez, C., Maquet, J., Vaultier, M.and Babonneau, F., *11B and 15N solid state NMR investigation of a boron nitride preceramic polymer prepared by ammonolysis of borazine.* Journal of the European Ceramic Society, **2005**, 25(2–3): p. 129-135.

208. Berger, F., Müller, A., Aldinger, F.and Müller, K., *Solid-state NMR Investigations on Si-B-C-N Ceramics derived from Boron-Modified Poly(allylmethylsilazane).* Zeitschrift für anorganische und allgemeine Chemie, **2005**, 631(2-3): p. 355-363.

209. Feng, D., Zhou, Z.and Bo, M., *An investigation of the thermal degradation of melamine phosphonite by XPS and thermal analysis techniques.* Polymer Degradation and Stability, **1995**, 50(1): p. 65-70.

210. Thomas, A., Fischer, A., Goettmann, F., Antonietti, M., Muller, J.-O., Schlogl, R.and Carlsson, J.M., *Graphitic carbon nitride materials: variation of structure and morphology and their use as metal-free catalysts.* Journal of Materials Chemistry, **2008**, 18(41): p. 4893-4908.

211. Trehan, R., Lifshitz, Y.and Rabalais, J.W., *Auger and x-ray electron spectroscopy studies of hBN, cBN, and N+2 ion irradiation of boron and boron nitride.* Journal of Vacuum Science & Technology A, **1990**, 8(6): p. 4026-4032.

212. Franke, R., Bender, S., Arzberger, I., Hormes, J., Jansen, M., Jüngermann, H.and Löffelholz, J., *The determination of local structural units in amorphous SiBN3C by means of X-ray photoelectron and X-ray absorption spectroscopy.* Fresenius' Journal of Analytical Chemistry, **1996**, 354(7-8): p. 874-878.

213. Uddin, M.N., Shimoyama, I., Baba, Y., Sekiguchi, T., Nath, K.G.and Nagano, M., *B–C–N hybrid synthesis by high-temperature ion implantation.* Applied Surface Science, **2005**, 241(1–2): p. 246-249.

214. Gouin, X., Grange, P., Bois, L., L'Haridon, P.and Laurent, Y., *Characterization of the nitridation process of boric acid.* Journal of Alloys and Compounds, **1995**, 224(1): p. 22-28.

215. X-ray Photoelectron Spectroscopy Database *National Institute of Standards and Technology (NIST)*, **2012**, version 4.1

216. Ju, S.-S., Han, C.-C., Wu, C.-J., Mebel, A.M.and Chen, Y.-T., *The Fragmentation of Melamine: A Study via Electron-Impact Ionization, Laser-Desorption Ionization, Collision-Induced Dissociation, and Density Functional Calculations of Potential Energy Surface.* The Journal of Physical Chemistry B, **1998**, 103(3): p. 582-596.

217. Ghoneim, N.A. and Halawa, M.M., *Effect of boron oxide on the thermal conductivity of some sodium silicate glasses.* Thermochimica Acta, **1985**, 83(2): p. 341-345.

218. Wypych, G., *Handbook of Polymers,* **2012**, ChemTec Publishing.

219. Kondo, S., Urano, Y., Tokuhashi, K., Takahashi, A.and Tanaka, K., *Prediction of flammability of gases by using F-number analysis.* Journal of Hazardous Materials, **2001**, 82(2): p. 113-128.

Appendix

Appendix 1: Comparison of different mineral fillers as fire retardant additive in EVM

In this part of the study four different fillers are compared according their influence on mechanical properties, fire retardancy and smoke release of EVM materials containing 130 phr of additive. The following mineral fillers are tested (**Table 40**): aluminum trihydroxide (ATH), magnesium dihydroxide (MDH), huntite (H) and hydromagnesite (HM).

Table 40: Different mineral fillers as fire retardant additive in EVM

	ATH	MDH	H	HM
Formula	$Al(OH)_3$	$Mg(OH)_2$	$Mg_3Ca(CO_3)_4$	$Mg_5(CO_3)_4(OH)_2·4H_2O$
Product name	Apyral 120E	Magnifin H-10	Ultracarb 1250	Ultracarb LH3
Supplier	Nabaltec	Albermarle	Minelco	Minelco
$T_{decomposition}$ [°C]	180-200	300-320	450-800	220-250
Decomposition reaction	$Al(OH)_3$ $\rightarrow Al_2O_3 + 3H_2O$	$Mg(OH)_2$ $\rightarrow MgO + H_2O$	$Mg_3Ca(CO_3)_4$ $\rightarrow 3MgO + CaO + 4CO_2$	$Mg_5(CO_3)4(OH)_2·4H_2O$ $\rightarrow 5MgO + 4CO_2 + 5H_2O$

It is found that mechanical properties are comparable for tested materials, i.e. EVM-ATH, EVM-MDH, EVM-H and EVM-HM. Therefore mechanical properties are not presented. Concerning flame retardant properties (**Table 41**), all materials exhibit improved fire retardancy in comparison to the virgin polymer, whereas $pHRR_1$, THR and ML have comparable values.

Table 41: Fire retardant properties of EVM materials containing different mineral fillers

	$pHRR_1$ [kw/m²]	$pHRR_2$ [kw/m²]	THR [MJ/M²]	TTI [s]	ML [%]	LOI [vol%O_2]	UL-94
EVM	510	-	97	67	96	19	NC
EVM-ATH	146	123	60	245	61	33	V-0
EVM-MDH	117	61	54	151	56	40	V-0
EVM-H	130	90	61	111	61	34	V-0
EVM-HM	143	111	61	161	68	34	V-0

Furthermore, it is observed that $pHRR_2$ is different for tested materials: EVM-ATH has the highest (123 kW/m²) and EVM-MDH the lowest value (61 kW/m²). Regarding TTI, it appears that with increasing decomposition temperature of the mineral filler, TTI decreases. EVM-

ATH has therefore the longest TTI of 245 s and EVM-H the earliest (111 s). Concerning results obtained by LOI and UL-94 test, it is found that all tested materials are classified V-0. Highest LOI, of 40 vol%O_2 is obtained for EVM-MDH; LOI of other tested materials is 33 and 34 vol%O_2 respectively.

The comparison of the four materials concerning smoke release (**Table 42**), it is observed that smoke release is decreased in comparison to the virgin polymer. First it is found that EVM-ATH, EVM-MDH and EVM-HM have comparable OD_{total} values of around 65. EVM-H instead has an OD_{total} of only 49. Regarding VOF4, the lowest value of 9 is obtained for EVM-ATH. Regarding Ds values it appears that EVM-ATH and EVM-MDH have higher values than EVM-H and EVM-HM. Like it was observed during MLC experiment, tendency of TTI of tested materials is increase of TTI with decreasing decomposition temperature of the mineral filler.

Table 42: Smoke release of EVM materials containing different mineral fillers

	OD_{total}	VOF 4	D_s4	D_s1	D_s2	TTI [s]
EVM	114	87	1.1	1.1	-	86
EVM-ATH	67	9	0.3	0.3	0.4	176
EVM-MDH	63	36	0.4	0.4	0.1	141
EVM-H	49	17	0.2	0.2	0.1	72
EVM-HM	61	13	0.1	0.1	0.2	91

Investigation of mechanical and fire retardant properties as well as smoke release of EVM materials containing different mineral fillers showed that most material properties depend on decomposition temperature of the mineral filler. Considering TTI as an important parameter in fire risk assessment, ATH can be considered as the most promising mineral filler in EVM among the tested ones.

Appendix 2: Fire retardant mechanism of ethylene vinyl acetate elastomer (EVM) containing aluminium trihydroxide and melamine phosphate

Fire retardant mechanism of ethylene vinyl acetate elastomer (EVM) containing aluminium trihydroxide and melamine phosphate

C. Hoffendahl,[a] G. Fontaine,[a] S. Duquesne,[a] F. Taschner,[b] M. Mezger,[b] S. Bourbigot[a]

Fire retardancy and smoke release of ethylene vinyl acetate (vinyl acetate content of 60 %, EVM) with aluminium trihydroxide (ATH) and melamine phosphate (MP) are evaluated by cone calorimetry, limiting oxygen index (LOI), UL-94 and a home-made smoke test. It was found that EVM-ATH has better fire retardant properties and lower smoke emission than the virgin polymer. Partial substitution of ATH by MP led to further increase in LOI but earlier ignition of the material measured by cone calorimetry. Moreover, less smoke is released for EVM-ATH-MP than for EVM-ATH. Fire retardant mechanism was investigated for EVM-ATH and EVM-ATH-MP to evaluate the role of MP in the material. The dispersion of the additives was examined by scanning electron microscopy (SEM) showing that all additives are homogenously dispersed in the matrix. Further the thermal decomposition, the condensed and the gas phase mechanism of both materials was investigated using thermogravimetric analysis (TGA), mass loss calorimeter coupled with a Fourier transform infrared spectrometer (MLC-FTIR), pyrolysis-gas chromatography-mass spectrometry (py-GCMS), and solid state nuclear magnetic resonance (NMR) of ^{13}C, ^{27}Al and ^{31}P. It was shown that both materials are protected by a gas and condensed phase mechanism. The endothermic decomposition of ATH has a cooling effect and dilutes the fuel through release of water. In the condensed phase, it was found that both materials are protected through formation of a physical barrier. It is evidenced that the barrier formed for EVM-ATH-MP exhibits higher insulative properties than in the case for EVM-ATH.

1 Introduction

Polymers are quantitatively the most important products of the chemical industry used worldwide in everyday live. Polymers are used in medicine, in textiles, for packaging, in building industry etc. One of the main drawbacks of polymeric materials is their high flammability. Therefore, it is necessary to flame retard materials for many of the previously cited applications. In the last decade, it was already possible to decrease the total number of fire deaths thanks to concentrated use of fire retarded materials. The number of fire death was decreased in the USA from 4013 persons in 2001 to 3445 persons in 2010 [1]. In this paper fire retardancy of ethylene vinyl acetate with a vinyl acetate content of 60 % (EVM) is discussed. EVM has a huge range of applications: electronic devices, electrical engineering, wire and cables, buildings, transportation (aircraft, cars), photovoltaic etc. For many of these applications, it is required to fire retard EVM to meet the regulation. The most common method to enhance flammability properties of EVM based materials is the incorporation of mineral fillers, e.g. aluminium trihydroxide (ATH) or magnesium dihydroxide (MDH) [2]. However, high loadings of this type of filler (higher than 50 wt%) are required to enhance fire retardancy of EVM leading to dramatically change of the mechanical properties of the material [3,4]. To overcome this disadvantage, mineral fillers can be incorporated in combination with other conventional flame retardants. In literature, mineral fillers are often combined with phosphorous compounds [5-7], nitrogen containing additives [8], silicone compounds [87, 90] or nanoadditives [82, 91, 95-98] to improve fire retardant properties and to decrease smoke release in some cases. Zilberman et al. [8] showed that the incorporation of ATH in combination with melamine enhances the fire retardant properties of ethylene vinyl acetate but also increases the smoke release in comparison to the virgin polymer. To overcome an increase in the smoke production maintaining the

improved fire retardant properties, ATH will be combined with melamine phosphate (MP) in this study. As far as we know, up to now nothing is reported in literature about the combination of ATH and MP in EVM-materials.

In the first part of this paper fire retardancy and smoke release of EVM-materials containing ATH and MP will be investigated. Afterwards the dispersion of the additives in the polymeric matrix will be analysed via scanning electron microscopy (SEM). The decomposition mechanism of EVM-materials containing ATH in combination with MP will be finally investigated using thermogravimetric analysis (TGA), solid state nuclear magnetic resonance (NMR) (^{13}C, ^{27}Al and ^{31}P), pyrolysis-gas chromatography-mass spectrometry (py-GSMS) and mass loss calorimeter coupled with a Fourier transform infrared spectrometer (MLC-FTIR).

2 Experimental

2.1 Materials

Levapren®600 (hereafter called EVM), an ethylene-vinyl acetate with 60 wt% vinyl acetate, was supplied by LANXESS. Aluminium trihydroxide (hereafter called ATH) was supplied in powder from Nabaltec as Apyral 120E (BET = 11 m²/g). Melagard MP, melamine phosphate (hereafter called MP) was received in powder from Italmatch Chemicals. Rhenofit TAC/S (triallyl cyanurate) was supplied by LANXESS in powder. Perkadox 14-40B-PD (Bis(tert-butyldioxyisopropyl) was received from Akzo Nobel in powder.

2.2 Processing of materials

Samples were prepared following an upside down process in an internal mixer GK 1.5L from Werner & Pfleiderer. Mixing was performed at 20 °C with a rotation speed of 40 rpm for 4 min. Additives were added into the mixing chamber before the polymer. After mixing, materials were further dispersed on an open two roll mill at 20 °C.

Table 43: Composition and name of the formulations EVM/ATH/MP

Formulation Name	EVM [phr]	FR [phr]	ATH [phr]	MP [phr]
EVM	100	0	0	0
EVM-ATH	100	130	130	0
EVM-ATH-MP	100	130	108	22

Vulcanization agents, Perkadox TAC/s (6 phr) and Rhenofit (1 phr), were added afterwards on the two roll mill. After batch off and 24h relaxation time, materials were treated a second time with the two roll mill. Later the compounds were pressed into plates and vulcanized at 180 °C for 12 min. Composition and name of the prepared formulations are gathered in Table 1.

2.3 Fire testing

Fire Testing Technology (FTT) Mass Loss Calorimeter was used to perform measurements on samples following the procedure defined according to ASTM E 906. The equipment is identical to that used in oxygen consumption cone calorimetry (ASTM E-1354-90), except that a thermopile in the chimney is used to obtain heat release rate (HRR) rather than employing the oxygen consumption principle. Our procedure involved exposing plates (100 x 100 x 3 mm³) in horizontal orientation. Samples are covered by a grid to prevent swelling. Samples were then wrapped in aluminium foil leaving the upper surface exposed to the heater (external heat flux = 35 kW/m²) and placed on a ceramic backing board at a distance of 25 mm from cone base. The mass loss calorimeter is used to determine the following principal fire properties: heat release rate (HRR) as a function of time, time to ignition (TTI) and total heat release (THR). When measured at 35 kW/m², HRR, THR and TTI values are reproducible to within ±10%.

To investigate the gases released during MLC experiment, MLC was connected to a Fourier transform infra-red spectrometer (MLC-FTIR). Using this device released gases are analysed online quantitatively and qualitatively. Gas picking pistol and transfer line were provided by M&C Tech Group; FTIR, Antaris™ Industrial Gas System, was provided by ThermoFisher. The transfer line between MLC and FTIR is 2 m long and was heated up to 200 °C. To assure constant temperature of the transfer line, two temperature controllers were installed. Before analysing the gases by FTIR, soot particles were filtered off by two different heated filters (2 and 0.1 µm). Filters consist of glass fibres and ceramic respectively. The FTIR gas cell was set to 185 °C and 652 Torr. The optical pathway is 2 m long and the chamber of the spectrometer is filled with dry air. FTIR spectra obtained using MLC-FTIR were treated using OMNIC software. To quantify gases, spectra have to be recorded at different concentrations for targeted gases and a quantification method has to be created using TQ Analyst. To create a method, representative regions in the spectra of the selected gas have to be chosen and interactions with other gases have to be taken into account. Using MLC-FTIR the following gases can be quantified: water, carbon monoxide, carbon dioxide, acetic acid, ammonia, methane, nitrogen monoxide, nitrogen dioxide, hydrogen cyanide. Quantification is reproducible within ± 10%.

Limiting Oxygen Index (LOI = minimum oxygen concentration to support candle-like combustion of plastics) was measured using a Fire Testing Technology (FTT) instrument on sheets (100 x 10 x 3 mm³) according to the standard 'oxygen index' test (ISO4589). It measures the minimum concentration of oxygen in a nitrogen/oxygen mixture required to just support combustion of a test sample under specified test

conditions in a vertical position (the top of the test sample is ignited with a burner).

UL-94 tests were performed according to IEC 60695-11-10 on samples 127 x 13 x 15 mm³. It describes the tendency of a material to extinguish or to spread the flame after ignition of the material. It classifies specimens from V-0, V-1 to V-2, where V-0 is the best rating.

2.4 Smoke opacity test

Smoke opacity test used in this study is a homemade test developed to evaluate the smoke release during combustion (Fig. 1). The structure is similar to that of the mass loss calorimeter. An external heat flux of 35 kW/m² produced by a conical heater was applied on a horizontal sample (100 x 100 x 3 mm³). The distance between the heating element and the sample was fixed at 35 mm (instead of 25 mm for MLC) which permits to work without grid on the sample surface. Samples were ignited by a spark igniter. The generated smoke was measured at the top of the chimney with a smoke density analyser TRDA 302 from Taurus Instrument. A light source (halogen point light source) emits light (intensity I_0) and the transmitted light (intensity I) was measured by a light sensor. Curves of optical density (OD = -log I/I_0) versus time present smoke release during combustion. The following values were determined using smoke opacity test: total optical density (OD_{total}), VOF4, i.e. the summation of the optical density (OD) over the first four minutes, maximum optical density during the experiment (D_s1 for the first local maximum and D_s2 for the second local maximum of the curve) and the maximum optical density during the first four minutes (D_s4).
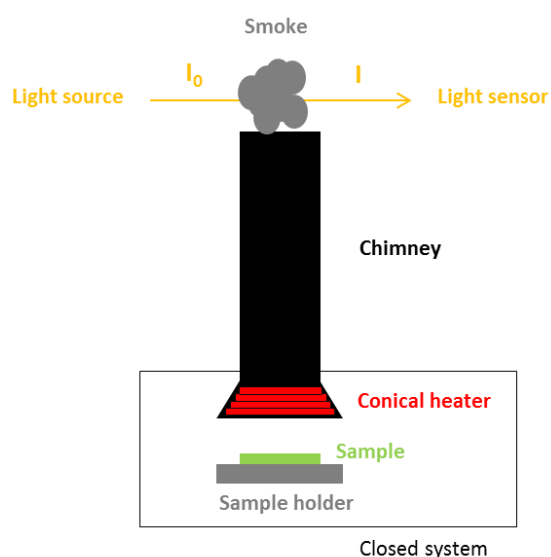

Fig. 1: Schematic presentation of smoke test device

2.5 Microscopy

Scanning electron microscopy (SEM) images were taken at various levels of magnification using a Hitachi S4700 SEM at 6 kV. All samples were ultra microtomed with a diamond knife on a Leica UltraCut microtome at cryo temperature (−120◦C) to obtain smooth surfaces.

2.6 Thermal analysis

Thermogravimetric analysis was carried out on a TA Instrument (TGA Q5000IR). The balance purge flow was set to 15 mL/min and the sample purge flow (nitrogen) to 100 mL/min. The powdered samples put in open alumina pan underwent a heating from 50 to 800 °C with a heating rate of 10 °C/min.

2.7 Pyrolysis GCMS (py-GCMS)

Pyrolysis-Gas chromatography-mass spectrometry (py-GCMS) analyses were performed on a device provided by Shimadzu. The device consists of a micro-furnace pyrolyzer (Frontier Lab PY-2020iD) coupled with a GCMS device (Shimadzu GCMS QP2010 SE). Experiments are performed under inert conditions using helium. Sample size is about 200 μg. Tests were performed using the desorption mode, i.e. the samples (in a stainless steel cup) are heated up in the furnace to the desired temperature with a chosen heating rate (10 °C/min or infinite). This heating rate was chosen to mimic the TGA-FTIR experiment and to get more information about gases evolved during pyrolytic decomposition. After the desorption process, evolved gases were introduced into the GCMS system whereas a part of the gases was split to avoid blockage in the column or saturation of the detector. Released decomposition gases were separated using a 30 m long fused silica capillary column. The temperature of the column was set at 35 °C during the desorption process. The column was then heated up to 300 °C with a heating rate of 10 °C/min followed by an isotherm at 300 °C for 30 min. The linear velocity of the carrier gas (helium) was set at 40 cm/s. The separated gases and fragments were then analysed with the quadrupole mass spectrometer with an Electron-Impact (IE) ionization source. The IE spectra were recorded at 70 eV with a mass scan of 2 scans per second. The interface between the pyrolyzer and the GC was heated up to 320 °C; the interface GC-MS to 280 °C. The ion source had a temperature of 230 °C. Obtained chromatograms were treated using F-Search (Frontier Lab) whereas NIST mass spectral database was used for identification of molecules.

2.8 Solid State NMR

^{13}C solid state NMR spectra were recorded at 100.6 MHz (B_0 = 9.4 T) on Bruker Avance II 400 using a 4 mm standard probe. The conditions were cross-polarization (CP) ^{1}H-^{13}C (contact time of 1 ms) with dipolar decoupling (DD) and magic angle spinning (MAS) at 10 kHz. The recycle delay between two pulses was 5 s. The number of scans was 1024 and ^{13}C chemical shifts were referenced to tetramethylsilane (TMS).

^{27}Al NMR measurements were carried out at a frequency of 24.5 MHz on a Bruker Avance II 400 ($B_0 = 9.4$ T) with a probe head of 4 mm using MAS at 12.5 kHz. The repetition time was fixed at 1 s for all samples. The number of scans was fixed to 128. The reference used was 1 M solution of aluminium nitrate.

^{31}P NMR measurements were obtained at a frequency of 40.1 MHz on a Bruker Avance II 400 ($B_0 = 9.4$ T) with a probe head of 4 mm using MAS at 12.5 kHz. Phosphoric acid was used as reference. Number of scans was set to 16 and repetition time was fixed at 120 s to ensure complete signal relaxation.

3 Results and discussion

3.1 Microscopy

The dispersion of ATH and MP in EVM-ATH and EVM-ATH-MP was examined using SEM. Fig. 2 (a) shows a SEM image of the ATH particles in EVM-ATH. ATH particles are well dispersed in the polymeric matrix exhibiting a size lying between 0.5 and 1 μm. This consists with data indicated by the supplier for the particle size of ATH

Dispersion of ATH and MP particles in EVM-ATH-MP is presented in Fig. 2 (b, c). The dispersion of ATH in EVM-ATH-MP is similar to that observed for EVM-ATH.

In the case of MP particles two different types of agglomerates are observed: agglomerates formed with needle-like particles (circled straight line) and particle agglomerates (circled dotted line). Both sorts of agglomerates are due to the presence of MP in the polymeric matrix. The crystal-like agglomerates have a size of around 16 to 33 μm, whereas it is possible that they are even bigger due to the fact that only a cross-section of the material is presented. In the case of the agglomerates consisting of needle-like structures, the size of single needles is up to 20 μm, whereas their thickness/diameter varies between 0.1 and 0.5 μm.

3.2 Fire retardancy and smoke release

Fig. 3 shows HRR curves for the tested materials. The corresponding values, i.e. peak of heat release rate (pHRR), reduction in pHRR in comparison to the virgin polymer, THR, TTI and the mass loss during combustion as well as the LOI values and UL-94 classification of the tested materials are presented in Table 2.

The virgin polymer has a pHRR of 510 kW/m², a THR of 97 MJ/m², a TTI of 67 s. After the combustion nearly no material remains in the aluminium foil. Incorporation of 130 phr of ATH leads to a decrease of pHRR by 71 % in comparison to the virgin polymer (146 kW/m²) and a THR of 60 MJ/m² which corresponds to a reduction of 38 % in comparison to the virgin polymer. EVM-ATH has a mass loss of 61 % and a TTI of 245 s.

It is noteworthy that in the case of EVM-ATH-MP, pHHR2 (78 kW/m²) is significantly smaller than that of EVM-ATH (123 kW/m²). EVM-ATH-MP has a TTI of 167 s which is increased in comparison to the virgin polymer but decreased in comparison to EVM-ATH.

The LOI value increases from 19 vol%O_2 for the virgin polymer to a value of 33 vol%O_2 for EVM-ATH and to 38 vol%O_2 in the case of EVM-ATH-MP. Both materials, EVM-ATH and EVM-ATH-MP reach V-0 classification in UL-94 test, whereas the virgin polymer is non-classified.
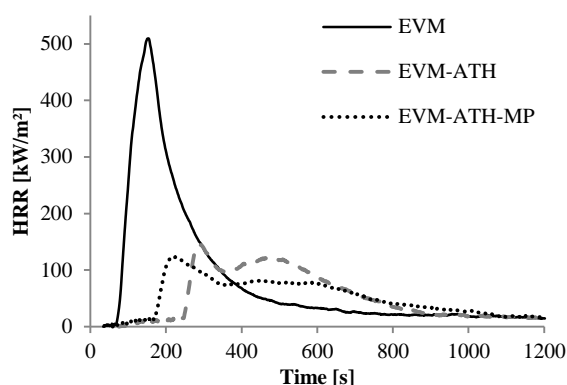
Fig. 3: Heat release rate (HRR) curves at 35 kW/m2

Optical density curves measured during combustion of the tested materials and corresponding values are presented in Fig. 4 and Table 2.
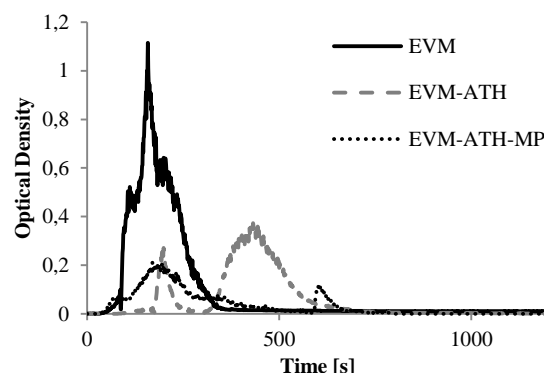
Fig. 4: Optical density (OD) curves at 35 kW/m² of EVM-ATH-MP formulations

The virgin polymer, EVM, has an OD_{total} of 114, a VOF4 value of 87 and a D_S4 as well as D_S1 of 1.1. Incorporation of 130 phr of ATH leads to a decrease of smoke release. OD_{total} of EVM-ATH is decreased to a value of 67 and VOF4 is decreased to 9. EVM-ATH has further a D_s4 and D_s1 of 0.3 and a D_s2 value of 0.4. Combination of ATH and MP in EVM (EVM-ATH-MP) further reduces the total optical density observed during the experiment. EVM-ATH-MP has an OD_{total} value of 48, which corresponds to a decrease by 60 % in comparison to the virgin polymer. D_s4 and D_s1 are 0.2; D_s2 is 0.1. D_s2 peak in the smoke curved of EVM-ATH-MP is due to extinguishment of the material. D_s values are all decreased in comparison to EVM and EVM-ATH.

Appendix 2: Fire retardant mechanism of ethylene vinyl acetate elastomer (EVM) containing aluminium trihydroxide and melamine phosphate

Fig. 2: SEM image EVM-ATH (a) and EVM-ATH-MP (b,c)

Table 2: Fire retardant properties and smoke release of EVM, EVM-ATH and EVM-ATH-MP

Material	pHRR [kW/m²]	pHRR reduction [%]	THR [MJ/m²]	THR reduction [%]	TTI [s]	ML [%]	LOI [vol%O$_2$]	UL-94	OD$_{total}$	VOF 4	D$_s$4	D$_s$1	D$_s$2
EVM	510	-	97	-	67	96	19	NC	114	87	1.1	1.1	-
EVM-ATH	146	71	60	38	245	61	33	V-0	67	9	0.3	0.3	0.4
EVM-ATH-MP	124	76	60	38	167	64	38	V-0	48	23	0.2	0.2	0.1

Regarding VOF4 it appears that EVM-ATH-MP has a value of 23 which corresponds to an increase in comparison to EVM- ATH but a significant decrease in comparison to the virgin polymer. The high VOF4 value is explained by the fact 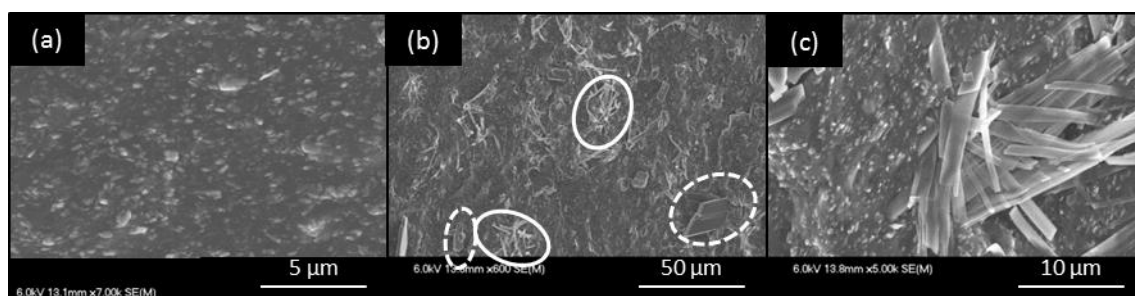that EVM-ATH-MP releases smoke during the first 400 s whereas nearly no smoke is evolved from 400 to 1200s. For EVM-ATH more smoke is evolved from 400 to 1200 s than from 0 to 400 s

3.3 Decomposition mechanism

The decomposition mechanism of EVM-ATH and EVM-ATH-MP is investigated in the following part. First thermal decomposition of the additives and of the materials are discussed. Then, the gas and condensed phase for both materials are analysed.

3.3.1 THERMAL ANALYSIS

TG curves in nitrogen and air of individual compounds, i.e. EVM, ATH and MP are presented in Fig. 5. The decomposition of EVM is already reported in literature [17]. The pyrolytic decomposition of EVM shows three steps. The first step occurs between 250 and 390 °C (T$_{max}$ = 350 °C, 42 wt% mass loss). This step corresponds to the deacetylation of the polymer. During this step acetic acid is evolved and the polymer is decomposed into linear polyenes. The second step is observed between 390 and 510 °C (T$_{max}$ = 470 °C, 54 wt% mass loss) and is attributed to the decomposition of the polyenes that were formed before. The third step occurs between 600 and 680 °C (T$_{max}$ = 650 °C) with a mass loss of 1 wt%. This step is due to the presence of Perkadox (Bis(tert-butyldioxyisopropyl) benzene) which is used for vulcanization of the material. At the end of the pyrolytic decomposition of EVM a residue of 2wt% is left. The thermo-oxidative decomposition of the EVM is more complex than that under inert conditions; it is a five step process. The first one occurs from 200 to 220 °C (1 wt% mass loss), the second one is observed between 220 and 410 °C (T$_{max}$ = 335 °C, 56 wt% mass loss), the third one from 410 to 480 °C (T$_{max}$ = 445 °C, 23 wt% mass loss), the fourth one from 480 to 570 °C (T$_{max}$ = 510 °C, 16 wt% mass loss) and the fifth step occurs between 570 and 670 °C (T$_{max}$ = 645 °C, 1 wt% mass loss). At the end of the thermo-oxidative decomposition a residue of 2.5 wt % is left. Concerning the thermal decomposition of ATH it can be seen that the thermo-oxidative as well as the pyrolytic decomposition of ATH are similar. It has two steps, one between 160 and 200 °C (mass loss 1 wt%) and the second one from 200 to 315 °C (T$_{max}$ = 270 °C, mass loss 30 wt%). The first small step can be attributed to the partial decomposition of gibbsite (Al(OH)$_3$) into boehmite (AlO(OH)) [18]. The second step between 200 and 315 °C is due to the complete dehydration of the hydroxide into oxide (Al$_2$O$_3$) [171]. At the end of the pyrolytic as well as the thermo-oxidative decomposition a residue of 63 wt% is left. The data found for decomposition of MP, corresponds to that already reported in literature [19-22]. It can be seen that MP has a comparable thermal decomposition in air and nitrogen. The first step occurs from 200 to 285 °C (T$_{max}$ = 275 °C, 5 wt% mass loss) and the second one from 285 to 330 °C (T$_{max}$ = 310 °C, 5 wt% mass loss). These two steps are attributed to dehydration processes. In the first step melamine phosphate condensates to melamine pyrophosphate which is transformed into melamine polyphosphate in the second dehydration step. The third step takes place from 330 to 420 °C (T$_{max}$ = 390 °C, 13 wt% mass loss). During this step the melamine polyphosphate degrades to melam ultraphosphate evolving water, ammonia and melamine. The fourth step

takes place from 420 to 530 °C (5 wt% mass loss). The fifth step differs depending on the conditions. In air the fifth decomposition step occurs from 530 to 690 °C (T_{max} = 560 °C, 27 wt% mass loss); in nitrogen from 530 to 705 °C (T_{max} = 560 °C, 21 wt% mass loss). From 420 to around 700 °C the melam ultraphosphate is degraded leaving a residual mass of 25 (in air) and 29 wt % (in nitrogen) respectively.
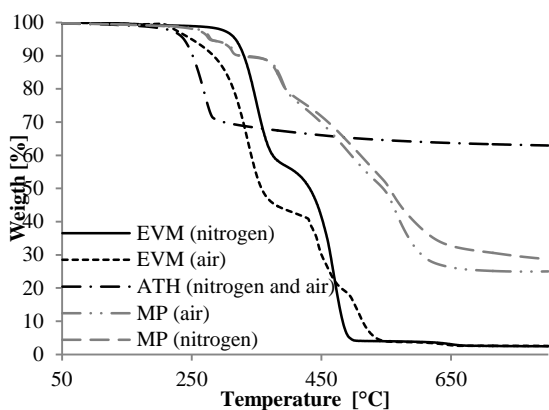

Fig. 5: TG curves of EVM-ATH and EVM-ATH-MB (10°C/min, under nitrogen and air)

TG curves of the materials, EVM-ATH and EVM-ATH-MP are presented in Fig. 6. Thermal decomposition of ethylene vinyl acetate materials containing ATH is already reported in literature [23]. Therefore the observed decomposition steps in pyrolytic and thermo-oxidative conditions for EVM-ATH can be discussed in details. Pyrolytic decomposition of EVM-ATH is a four step process. The first step occurs from 180 to 315 °C (T_{max} = 265 °C). The weight loss during this step is 17 wt% which corresponds to the mass lost during dehydration of ATH. The second step is obtained from 315 to 400 °C (T_{max} = 350 °C, 16 % weight loss). This step can be attributed to the deacetylation reaction of EVM. The third pyrolytic decomposition step takes place from 400 to 540 °C with a mass loss of 27 wt% (T_{max} = 470 °C). This step can be attributed to the decomposition of the polyenes that were formed during the deacetylation of the polymer. This could be due to the formation of a char residue which results in a less important mass loss. The last decomposition step occurs from 625 up to 700 °C with a maximum weight loss at 660 °C and a weight loss of 1 wt%. This step can be attributed to the presence of vulcanization agents in the material and its decomposition. At the end of the pyrolytic decomposition a residue of 37 wt% is left.

In the case of the thermo-oxidative decomposition of EVM-ATH (100-130) a five-step-process is obtained. The first decomposition under thermo-oxidative conditions is similar to that of the pyrolytic decomposition, it takes place from 180 to 315 °C (T_{max} = 290 °C, 21 % weight loss) and is attributed to the decomposition of ATH. During the second step (315 – 410 °C, T_{max} = 335 °C) a mass loss of 18 wt% is

observed. The third decomposition step occurs from 410 to 480 °C (T_{max} = 450 °C) with a corresponding mass loss of 15 wt%. From 480 to 580 °C a fourth step takes place (T_{max} = 500 °C, 9 % weight loss). The last step in thermo-oxidative conditions occurs between 580 and 675 °C. A residue of 35 wt% is left at the end of the decomposition process.
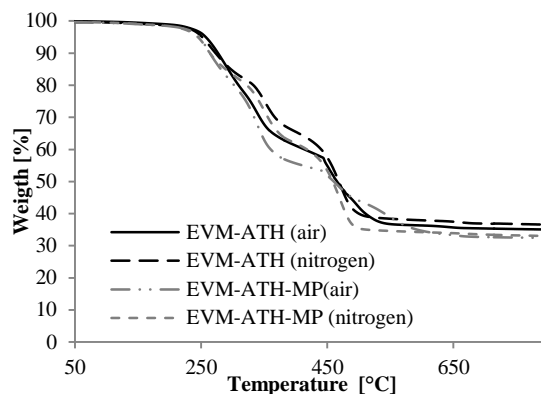

Fig. 6: TG curves of EVM-ATH and EVM-ATH-MP (10°C/min, under nitrogen and air)

In contrast to the thermal decomposition of EVM-ATH, the decomposition of EVM-ATH-MP is not reported in literature. The pyrolytic decomposition of EVM-ATH-MP is a three-step process. The first step of EVM-ATH-MP occurs from 180 to 305 °C (T_{max} = 250 °C, 16 % weight loss), the second one from 305 to 390 °C (T_{max} = 350 °C, 20 % weight loss) and the third one from 390 to 520 °C (T_{max} = 470 °C, 27 % weight loss). At the end of the pyrolytic decomposition process a residue of 33 wt% is left. The thermo-oxidative decomposition of EVM-ATH-MP takes places in five steps. The first one takes place from 180 to 300 °C (T_{max} = 260 °C, 18 % weight loss), the second one from 300 to 430 (T_{max} = 340 °C, 27 % weight loss), the third one from 430 to 500 °C (T_{max} = 450 °C, 10 % weight loss), the fourth one from 500 to 640 °C (T_{max} = 540 °C, 10 % weight loss) and the fifth one from 640 to 700 °C (T_{max} = 660 °C, 1 % weight loss). The third step has two local maxima whereas the highest decomposition rate is obtained at 540 °C. At the end of the thermo-oxidative decomposition of EVM-ATH-MP (100-108-22) a residue of 33 wt% is left.

3.3.2 GAS PHASE ANALYSIS

In this part, gases released during decomposition of EVM-ATH and EVM-ATH-MP are analysed. Investigation of gases released during decomposition of EVM-ATH is already reported in literature [23]. In this study, gases are analysed using simultaneous thermal analysis with evolved gas analysis (STA-FTIR). To go further in the comprehension of gas phase, two other methods are used in our study: py-GCMS and MLC-FTIR. First gases released during pyrolytic decomposition of EVM-ATH and EVM-ATH-MP are detected using py-GCMS. This method is based on thermal decomposition investigated by TGA; released gases are analysed after each decomposition step. Then

decomposition in thermo-oxidative conditions is further investigated using MLC-FTIR. Released gases are detected quantitatively during experiment.

EVM-ATH

Fig. 7 presents the chromatograms obtained by py-GCMS in inert conditions for EVM-ATH. First of all, it has to be mentioned that the peak (air) present in the mass spectra corresponds to air that is left in the interfaces and which is evolved into the column after heating ramp of the material. From 50 to 315 °C, the following gases are detected: water (1) coming from the decomposition of ATH, acetic acid (2) evolved during deacetylation of the polymer and different molecules (3) due to the presence of vulcanization agents in the material. The chromatogram between 315 and 400 °C shows the presence of hydrocarbons (5), whereas saturated and monounsaturated hydrocarbon structures from C8 to C34 are found. Moreover, a big peak at early retention times is detected (4). This peak can be attributed to the presence of acetic acid and acetone. The formation of acetone is explained through transformation of acetic acid into acetone. This reaction is possible due to the presence of alumina formed by decomposition of ATH in the condensed phase, which has a catalytic effect on the formation reaction of acetone [173, 178]. These latter studies reported that during decomposition of the EVA-ATH materials no acetic acid was detected in the gas phase; instead acetone was found. However, these studies were performed on EVA-materials having low VA contents. The content of VA in this study is more than two times higher than in the studies reported in literature. It is supposed that the high quantity of VA and therefore the resulting high quantity of acetic acid released during decomposition lead to the fact that not all acetic acid molecules are transformed into acetone by catalytic reaction through alumina. Moreover, conditions used in this study are different: Witkowski et al. [23] analysed gases evolved during decomposition using simultaneous thermal analysis with evolved gas analysis (STA-FTIR) with controlled heating ramp.

Regarding gases present in the gas phase from 315 to 400 °C it can be said that in this temperature range the deacetylation of the polymer is complete. Moreover, polyenes formed during deacetylation also start to degrade in this temperature range.

From 400 to 540 °C, peaks indicating the presence of hydrocarbon structures are found. The structures of the hydrocarbons are equal to those obtained before, from 315 to 400 °C. In this temperature range the decomposition of polyenes formed during deacetylation of the polymer takes place. Between 540 and 800 °C peaks corresponding to Perkadox (Bis(tert-butyldioxyisopropyl) benzene), a vulcanization agent, are detected. Moreover, unsaturated hydrocarbons containing 18 to 49 carbon atoms are found. Looking at the analysis of the gas phase in inert conditions (low heating ramp) using py-GCMS, it can be said that EVM-

ATH is first protected by dilution of the fuel. Fuel is diluted through water coming from the endothermic decomposition of ATH. During the first decomposition step of EVM-ATH the deacetylation of the polymer forming a polyene residue takes place. The formed polyenes start to degrade during deacetylation and are fully degraded afterwards.
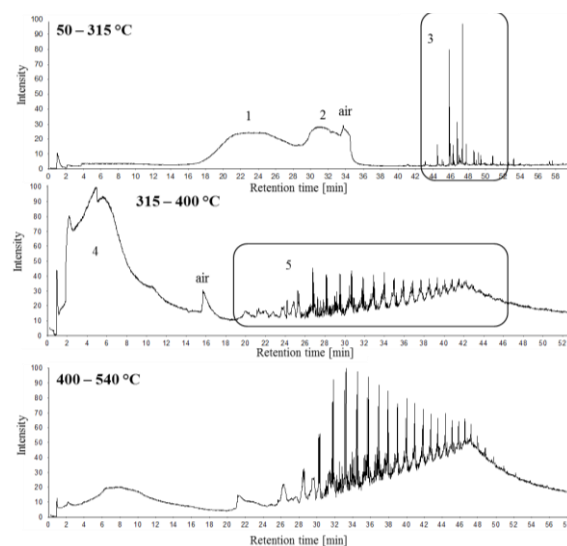
Fig. 7: Chromatograms of EVM-ATH, 10°C/min

Changing the heating ramp from 10 °C/min to an infinite heating ramp, the decomposition gases change completely. Fig. 8 presents the chromatogram obtained at infinite heating ramp. This process leads to detection of the following molecules: water (1), butadiene (2), acetone (3), cyclopentadiene (4), cyclopentene (5), 1-hexene (6), acetic acid (7), benzene (8), 1,3-cyclohexadiene (9), toluene (10), ethylbenzene (11), xylene (12), styrene (13), 1,8-nonadiene (13), 1-nonene (13), isopropylbenzene (14), ethyltoluene (14), 1-decene (14), methylstyrene (14), 1-propenylbenzene (15), indane (15), indene (16), 1-methylindene (17), ethylstyrene (17), 1-undecene (17), tetrahydronaphthalene (18), naphthalene (19), 1-methylnaphthalene (20), 2-methylnaphthalene (21), 3,3-dimethyl-1-indanone (22).

Fig. 8: Chromatogram of EVM-ATH, heating ramp infinite

Thus, this indicates that decomposition of ATH evolves water like it is the case for low heating ramps. Concerning the polymer decomposition, deacetylation

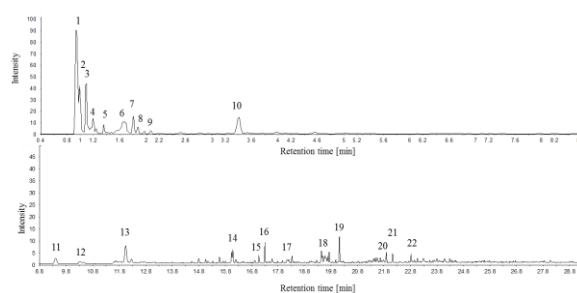takes place like at low heating ramp – acetic acid and acetone are evolved. However, decomposition of the polyene structure formed during deacetylation is different for high heating ramps. Instead of saturated and monounsaturated hydrocarbons in the case of low heating ramps, benzene and its homologues are formed. It is assumed that at high heating rates, formation of benzene and its homologues is thermodynamically favoured over formation of linear hydrocarbons.

The gas phase in thermo-oxidative conditions was analysed using MLC-FTIR. MLC-FTIR is a powerful tool to understand reactions going on during MLC experiment. Evolution of gases as a function of time is detected directly during experiment (Fig. 9 and Table 3).
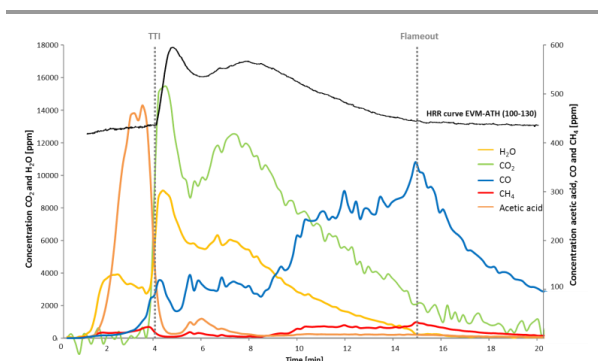

Fig. 9: Spectra obtained by MLC-FTIR for EVM-ATH

Table 3: Quantification of released gases during MLC-FTIR experiment for EVM-ATH

Gas	Total quantity released [ppm]	Released before ignition [ppm]	Released before ignition [%]
H2O	303888	46229	15
CO2	592951	12257	2
CO	18368	208	1
CH4	1581	186	12
Acetic acid	5194	3796	73

Before ignition of the material three main gases are released: acetic acid, water and methane. Before ignition 3796 ppm of acetic acid are detected; this corresponds to 73 % of total release. This indicates that deacetylation of the polymer is almost completed before ignition of EVM-ATH. Moreover it can be seen that release of acetic acid decreases already before ignition. Decrease of the concentration of acetic acid is therefore not due to ignition. This observation supports the assumption that deacetylation process is almost complete before ignition. Late ignition of the material, despite presence of flammable acetic acid, is explained by the presence of water (released during ATH decomposition) diluting the fuel. Moreover a small quantity of methane (186 ppm, 12% of total release) is also detected in the gas phase before ignition. The presence (or absence) of acetone in the gas phase cannot be confirmed regarding FTIR spectra.

Once the material starts to burn, a rapid increase of the concentration of carbon dioxide and water is observed.

Carbon dioxide reaches a maximum concentration of 15432 ppm and water of 9045 ppm after ignition whereas concentration decreases afterwards. The presence of these two gases indicates complete combustion of the material. Besides carbon dioxide and water, carbon monoxide is detected in low quantity (100 ppm) indicating that also incomplete combustion is taking place but it has to be noted that complete combustion dominates the incomplete one. In the ongoing combustion process the quantity of methane released is comparable; the quantity never exceeds 50 ppm. At around 360 s an additional increase of concentration of carbon dioxide and water is found. Moreover, the concentration of acetic acid increases as well. At the same time, the HRR increases. Due to increase of quantity of gases in the gas phase between $pHRR_1$ and $pHRR_2$, it is supposed that a protective layer is formed on the material surface after ignition which is broken at around 360 s. This leads to a more important release of fuel into the flame and a therefore results in an increase of water and carbon dioxide in the gas phase. Until flameout and end of the combustion the concentration of carbon dioxide and water decreases constantly. In the case of carbon monoxide, the concentration increases up to 360 ppm until flameout at around 900 s. After flameout, concentration of carbon monoxide decreases. The same phenomenon is obtained for methane: after flameout the concentration decreases slightly. Over the whole experiment complete combustion dominates incomplete one whereas incomplete one is getting more important at the end of combustion. It is known that incomplete combustion leads to increased production of soot particles. The increased production of smoke in the second part of the combustion process in MLC experiment can therefore be explained by this fact.

The analysis of the gas phase action of EVM-ATH by py-GCMS and MLC-FTIR showed that the material is first protected through the presence of ATH in the material. ATH decomposes endothermically releasing water which dilutes the fuel. The polymer starts to degrade at the same time. First the deacetylation takes place. During this step a polyene network is formed which is then degraded evolving hydrocarbons. Structure of hydrocarbons depends on the chosen heating rate: low heating rates lead to saturated and mono unsaturated linear hydrocarbons, whereas high heating ramps lead mainly to formation of benzene and its homologues.

EVM-ATH-MP

Analysis of the gas phase under inert conditions (py-GCMS) of EVM-ATH-MP (Fig. 10) showed that up to 180 °C gases due to the presence of vulcanization agents (1) in the material are observed. Moreover, a small quantity of melamine (2) coming from the melamine phosphate was detected. Between 180 and 305 °C, water (3), melamine (5) and acetic acid (4) are detected in the gas phase. Additionally to these peaks, molecules due to

the presence of the vulcanization agents are still detected (6). The presence of water indicates the decomposition of ATH into alumina, which is known to take place in this temperature range [2]. The presence of melamine proves the decomposition of MP. Moreover, it can be assumed that the deacetylation of the polymer starts in this temperature range (presence of acetic acid).
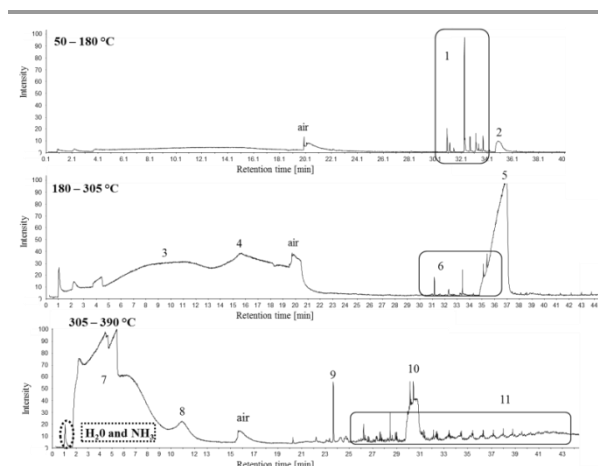

Fig. 10: Chromatograms of EVM-ATH-MP, 10°C/min

Between 305 and 390 °C, peaks corresponding to acetic acid (7), acetone (8), 3,5,5-trimethylcyclohex-2-enone (9) and melamine (10) are detected. Additionally peaks corresponding to saturated and monounsaturated hydrocarbons from C8 to C34 (11) are detected. As in the case of EVM-ATH, the presence of acetone is explained by the catalytic effect of alumina in the condensed phase. The presence of melamine corresponds to thermal decomposition of MP as reported in literature [22]. In this temperature range, melamine phosphate degrades to melam ultraphosphate evolving water, ammonia and melamine. The peak corresponding to ammonia and water is also detected. From 390 to 520 °C and from 520 to 800 °C, gases detected in the gas phase of EVM-ATH-MP are similar to those obtained for EVM-ATH from 400 to 540 °C and from 540 to 800°C. Molecules containing phosphorous were not detected. It is therefore assumed that phosphorus acts in the condensed phase (it will be discussed in the following).

Gases evolved during pyrolytic decomposition of EVM-ATH-MP at high heating rate change completely compared to those obtained at low heating rate (Fig. 11).
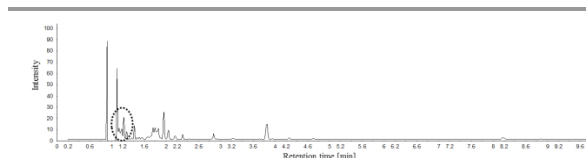

Fig. 11: Chromatogram of EVM-ATH-MP, heating ramp infinite

Chemical nature of released gases evolved from EVM-ATH-MP are similar to those obtained for EVM-ATH at high heating rate except of one peak that can be assigned to hydrogen isocyanate and isocyanic acid. Due to the fact that these gases are not detected for EVM-ATH it is assumed that their presence is due to MP in the material, whereas these gases were not detected during decomposition of EVM-ATH-MP at low heating ramps. As for the decomposition at low heating rate, molecules containing phosphorous are not detected in the gas phase.

As for EVM-ATH, the gas phase in thermo-oxidative conditions for EVM-ATH-MP was analysed using MLC-FTIR (Fig 12 and Table 4). Before ignition of the material, mainly water (17830 ppm), acetic acid (1738 ppm) and ammonia (867 ppm) are evolved whereas concentration of ammonia and acetic acid increase constantly until ignition of the material. As it was discussed for EVM-ATH, the presence of acetic acid indicates deacetylation of the polymer and presence of water proves that decomposition of ATH is taking place. Presence of ammonia in the gas phase is due to decomposition of MP [22].
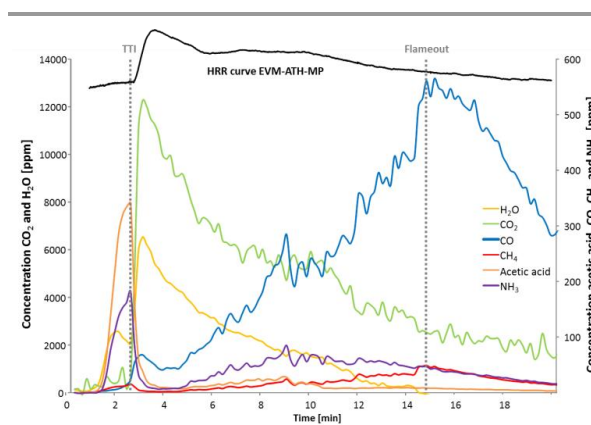
Fig. 12: Spectra obtained by MLC-FTIR for EVM-ATH-MP

Table 4: Quantification of released gases during MLC-FTIR experiment for EVM-ATH

Gas	Total quantity released [ppm]	Released before ignition [ppm]	Released before ignition [%]
H_2O	169 302	17 830	11
CO_2	517 772	5 912	1
CO	30 477	74	0
CH_4	2 259	87	4
NH_3	5 104	867	17
HCN	632	6	1
NO	1460	40	3
Acetic acid	3 126	1 738	56

Before, it was shown that EVM-ATH-MP ignites 78 s earlier than EVM-ATH. The earlier ignition can be explained through the presence of ammonia in the gas phase. Due to presence of ammonia and acetic acid more flammable gases are present in the gas phase than it is the case for the material without MP. At room temperature ammonia is known to ignite at 630 °C whereas its flammability range lies between 15 and 28 % in air. At the same time the amount of ATH in EVM-ATH-MP is smaller than in EVM-ATH and the dilution effect of water (coming from ATH decomposition) is

smaller. As a consequence, the fuel consists of more flammable gases than it is the case for EVM-ATH. Concentration of released water is not high enough to dilute the fuel sufficiently to prevent ignition. When material ignites, the concentrations of acetic acid and ammonia decrease abruptly due to the fact that they are burning. After ignition, nitrogen oxide is detected (not presented in Fig. 10) due to combustion of ammonia. A maximum quantity of nitrogen oxide of 59 ppm is detected just after ignition; afterwards the concentration decreases constantly until flameout. In total, 1460 ppm of nitrogen oxide are released. Nitrogen dioxide was not detected in the gas phase which is explained by the combustion reaction of ammonia [25]:

$$2\ NH_3\ +\ 4\ O_2\ \rightarrow\ 2\ NO\ +\ 3\ H_2O$$
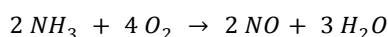
Moreover, after ignition, concentration of water and carbon dioxide increases sharply due to complete combustion of the material. Both gases reach maximum concentration before $pHRR_1$: 6543 ppm in the case of water and 12261 ppm for carbon dioxide. Afterwards concentrations decrease constantly until the end of the experiment. The concentration of carbon monoxide, indicating incomplete combustion, increases constantly from the ignition of the material until the flameout. At the flame out, a maximum of 565 ppm release is observed at the flame out; then concentration of carbon monoxide decreases until end of experiment.

Concerning release of acetic acid, ammonia and methane, it can be seen that the three gases show the same profile after ignition: After ignition concentration decreased until $pHRR_1$. Then, concentrations increase until $pHRR_2$. Afterwards concentration decreases until the end of experiment. The increase of concentration of acetic acid, ammonia and methane before $pHRR_2$ suggests that a protective layer is formed at the beginning of the experiment which cracks after $pHRR_1$ and releases gases trapped under the layer formed before (as for EVM-ATH). Whereas it can be clearly seen that increase of gas concentration is significantly lower than for EVM-ATH. It can therefore be assumed that the protective layer formed at the material surface is more stable and accordingly more effective in the case of EVM-ATH-MP than it is the case for EVM-ATH. A more effective protective layer explains reduced $pHRR_2$ for EVM-ATH-MP.

Regarding the total quantities of gases released during experiment it appears that in the case of EVM-ATH-MP, 30604 ppm of carbon monoxide is evolved during combustion process which is nearly two times higher than in the case of EVM-ATH (18368 ppm). It is concluded that incomplete combustion is more likely when MP is present in the material. An evidence for the presence of acetone in the gas phase during MLC-FTIR experiment was not found.

As a short conclusion for the analysis of the gas phase of EVM-ATH-MP (py-GCMS, MLC-FTIR), it can be said that the material is protected through endothermic decomposition of ATH and the resulting release of

water. However, presence of MP leads to earlier ignition due to ammonia released from MP decomposition. Moreover, presence of MP leads to higher release of carbon monoxide than it is the case for EVM-ATH. Concerning gases released during thermo-oxidative and pyrolytic decomposition, it was found that the polymer degrades following the pathway described for EVM-ATH: deacetylation of the polymer forming polyenes which are then degraded. At low heating rates saturated and mono unsaturated linear hydrocarbons are formed; high heating ramps lead to favoured formation of benzene and its homologues.

3.3.3 CONDENSED PHASE ANALYSIS

The condensed phase was analysed using a method in which the combustion process is stopped at characteristic times during the cone calorimeter experiment. Samples were removed from the external heat source and flames were quenched immediately to prevent further decomposition. The resulting materials afterwards were analysed by solid state NMR (^{13}P, ^{13}C and ^{27}Al). The top of the resting plates, i.e. the char and the bottom, i.e. the protected plate under the char were analysed separately.

EVM-ATH

For EVM-ATH the combustion was stopped at six characteristic points: before the ignition (230 s), during increase (245 s), at the $pHRR_1$ (275 s), at the $pHRR_2$ (444 s), during decrease (700 s) and at the end of combustion (1200 s). The residues (Fig. 13) were analysed by ^{13}C and ^{27}Al solid state NMR.

^{13}C spectra obtained at the different stages of combustion are presented in Fig. 14. The spectrum of the unburned material (a) shows several peaks (attribution of observed chemical shifts presented in Table 5). The spectrum corresponds to data reported already in literature for pure EVM [17,26-30][26, 181-185]. The peak at 20.8 ppm corresponds to CH_3-group of the acetic acid functionality of the polymer [183]. Those at 25.1, 29.8 and 34.5 ppm are attributed to CH_2–groups in the polymer backbone [182, 186]. The multiplicity of the peaks is due to the fact that when VA monomer copolymerizes with ethylene, a random copolymer is obtained leading to several different monomer sequences in the chain. According to Delfini et al. [32], the chemical shift depends on the position of the carbon in a monomer.
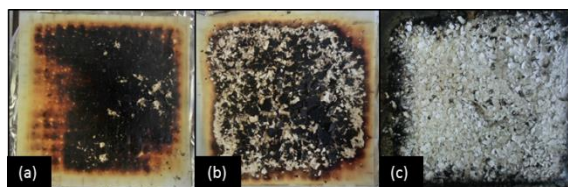

Fig 13: Residues of EVM-ATH (a) after ignition (b) at $pHRR_1$ (c) at end of combustion

However, this work was carried out in liquid state NMR, and thus does not take into account structural effects, but, since all the reported bands are present on our solid

state NMR spectrum, it can be assumed that the assignments are transposable. Peaks assigned to CH are detected around 70 ppm. The multiplicity of the CH chemical shift is also explained by the sequence distribution of pentads in the polymer [32].
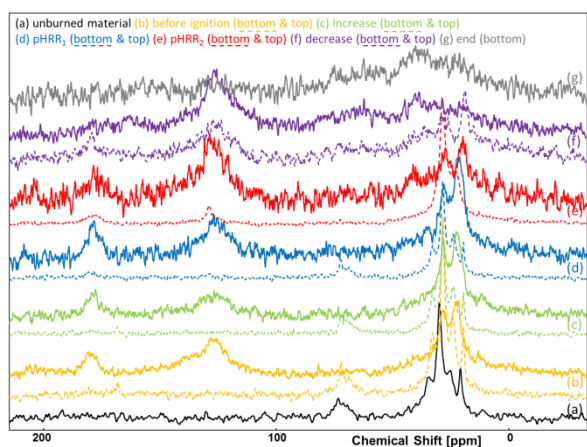

Fig 14: ^{13}C spectra obtained for different stages of combustion of EVM-ATH

Table 5: Attribution of chemical shifts obtained for EVM-ATH and EVM-ATH-MP

Chemical Shift [ppm]	Attribution
20.8	CH$_3$
25.1, 29.8, 34.5 and ~ 42	CH$_2$
69.3, 71.2 and 73.4, 76.1	CH
129.5	Unsaturated hydrocarbons
169.4	C=O in acetate/C=N in melamine
182.0, 180.9, 180 and 178.7	C=O (carbonyl)

The chemical shift at 170 ppm corresponding to C=O in the acetate group is not observed for the virgin polymer. Due to the fact that this peak is obtained for the virgin polymer (Fig. 15) it can be said that the absence of the C=O peak in unburnt EVM-ATH is due to the large anisotropy of the chemical shift tensor of C=O [33].

The spectra of samples taken before ignition of the materials show changes in comparison to the virgin polymer. The sample taken at the bottom of the plate exhibits an additional peak at 169 ppm. This peak is assigned to C=O in the carbonyl function in acetic acid. The spectrum of the top of the sample taken before ignition shows a peak corresponding to aliphatic hydrocarbons. Additionally, a broad peak around 130 ppm, appears signalizing the formation of unsaturated hydrocarbon structures (char). Moreover, a multiple peak around 180 ppm (182.0, 180.9, 180.0 and 178.7 ppm) is observed in the residue taken before the ignition (top of plate). This peak is attributed to carbonyl (C=O) indicating that oxidized unsaturated hydrocarbons are present in the residue. Spectra recorded after ignition, at the increase of the curve (top and bottom) are identical to those obtained before the ignition. At the pHRR$_1$, the spectrum recorded for the bottom of the plate is similar to that obtained before the ignition at the bottom. This

observation indicates that the material under the char layer is still protected. At the top of the plate and at the pHRR$_1$ a change of the spectra in comparison to before ignition is observed: the chemical shift attributed to methyl of acetic acid group has disappeared. It can therefore be said that at the top of the plate the deacetylation process of the polymer is completed. Nevertheless, peaks around 180 ppm indicate that molecules containing carbonyls are still present in the condensed phase.
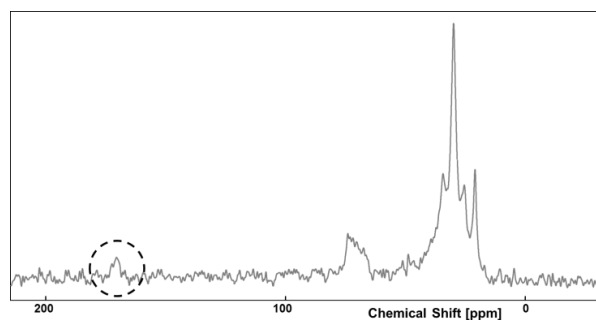

Fig 15: ^{13}C spectra obtained for unburnt EVM

At the pHRR$_2$, the spectrum of the residue taken at the bottom of the plate changes. Peaks corresponding to CH$_2$ (29.6 and 24.8 ppm), unsaturated hydrocarbons (130 ppm) and carbonyls (180 ppm) are observed. At the pHRR$_2$, the deacetylation of the polymer is completed in the whole material and saturated and unsaturated hydrocarbons are present in the residue. At the same time the broad peak corresponding to carbonyl functions indicating presence of oxidation of the char structure is still present. The top of the plate at the pHRR$_2$, as well as the bottom of the plate at the decrease show exactly the same chemical shifts as described for the bottom of the plate taken at pHRR$_2$. The top of the plate taken at the decrease only shows chemical shifts assigned to saturated (CH$_2$) and unsaturated hydrocarbons. At the end of the combustion only the spectrum of the bottom of the sample was recorded. The top of the residue did not show any results even after accumulation of the spectra for a longer time. The reduction of the resolution of the ^{13}C signal is related to the anisotropy of the paramagnetic susceptibility of the aromatic compounds present in the residue. In the case of paramagnetic materials, this anisotropy is large and, consequently, leads to disappearance of the ^{13}C signal.

^{27}Al spectra of the residues of EVM-ATH are presented in Fig 16. The unburnt material exhibits a peak at 8 ppm corresponding to octahedral coordinated aluminium [34]. An additional site is observed at -2.9 ppm. The recorded spectrum corresponds to the spectrum for gibbsite (Al(OH)$_3$) found in literature [35,36]. In gibbsite hydroxyl ions are hexagonal close packed with aluminium ions in octahedral co-ordination. The bottom of the sample taken before ignition of the material has the same spectrum like the unburnt material. The spectrum recorded at the top of the plate shows an additional

chemical shift at 65.0 ppm attributed to tetrahedral coordinated aluminium. The appearance of this peak indicates the thermal decomposition of ATH releasing water and leading to the formation of alumina consisting of a close packed oxygen lattice where Al^{3+} occupies tetrahedral and octahedral holes. The ratio of AlO_4 to AlO_6 (simulated using Dmfit [37]) is 1:4. As mentioned during analysis of the thermal decomposition of ATH, it is known that ATH (gibbsite form) degrades forming alumina (Al_2O_3). It is known that boehmite and corundum consist of only octahedral coordinated Al-ions, whereas several crystal structures of alumina are possible [35,36]. The most commonly form of alumina is α-alumina which consists of only octahedral coordinated Al-ions. The same is true for boehmite, formed during dehydration of gibbsite, only octahedral coordinated Al-ions are present. Due to the fact that in our case tetrahedral and octahedral coordinated Al-ions are present in the condensed phase it can be concluded that also η- or θ-alumina (consisting of both tetrahedral and octahedral sites) is formed. Nevertheless it can be said that the alumina consisting of only octahedral coordinated Al-ions, i.e. boehmite and alumina, are mainly formed due to the ratio of AlO_4 to AlO_6 of 1:4. Moreover, it can be seen that the peak corresponding to octahedral coordinated Al is getting broader with progressed combustion time. Widening of the peak is explained by decreasing of crystallinity of the formed product.
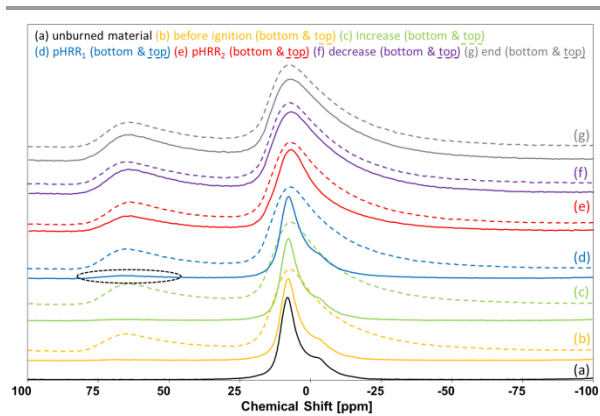

Fig 16: ^{27}Al spectra obtained for different stages of combustion of EVM-ATH

Regarding the spectra recorded for the other stages of combustion it can be seen, that the bottom of the sample taken at the increase exhibits the same spectra as the unburnt material. This observation shows that the underlying material is still protected and that not all of ATH present in the material is degraded. First change of the spectrum of the underlying material is obtained at the $pHRR_1$, where a small peak corresponding to tetrahedral coordinated Al is found (ratio AlO_4/AlO_6 = 7/100). It can therefore be concluded that only a small part of ATH is degraded at this stage of the combustion. Concerning top of the samples taken at the different stages of combustion it can be seen that all spectra

exhibit the same chemical shifts, corresponding to tetrahedral and octahedral coordinated Al-ions. Moreover the ratio AlO_4/AlO_6 is the same for all other samples (1:4).

It has further to be noted that water detected after ignition of EVM-ATH during MLC-FTIR experiment, is not only due to complete combustion but also to the dehydration of ATH occurring until the $pHRR_1$. Presence of a char protecting the material at its surface can be evidenced through the fact that ^{27}Al NMR showed that ATH is not fully degraded until $pHRR_1$, the underlying material is protected through a layer formed at the sample surface consisting of alumina and saturated and unsaturated hydrocarbons. This result is different to the results found in earlier studies [38]. In this study, an ethylene vinyl acetate polymer having a VA content of 24 % is studied. It is shown that when 65 wt% ATH are incorporated into the polymeric matrix, ATH is completely degraded into alumina oxide before ignition of the material. The difference between the results found in this study and in our actual study is explained by the different conditions used. First, the VA content of the polymer in our study is much higher. Secondly, residues were obtained stopping MLC experiment carried at 50 kW/m², whereas 35 kW/m² is used in our case.

EVM-ATH-MP

Combustion of EVM-ATH-MP was stopped at six characteristic points: before the ignition (120 s), during increase (175 s), at the $pHRR_1$ (190 s), at the $pHRR_2$ (425 s), during decrease (700 s) and at the end of combustion (1200 s). Residues (Fig. 17) were analysed by ^{13}C, ^{27}Al and ^{31}P solid state NMR.
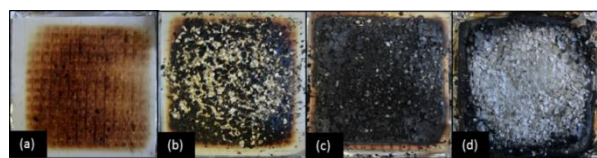

Fig 17: Residues of EVM-ATH-MP (a) after ignition (b) at $pHRR_1$ (c) at $pHRR_2$ (d) at end of combustion

^{13}C NMR spectra of the residues at different stages of combustion are presented in Fig. 18. The unburnt material exhibits the same chemical shift as unburnt EVM-ATH. Peaks attributed to CH_3 (20.8 ppm), CH_2 (25.5, 29.8 and 33.9 ppm), and CH (73.4 ppm) are observed. Additionally, two peaks at 157.3 and 165. 4 ppm attributed to MP (melamine ring) are present [39,40]. These chemical shifts could also be due to the quaternary C atom connecting the vinyl acetate groups to the polymer backbone. Nevertheless, this possibility is excluded due to the fact that the peak is not present in unburnt EVM-ATH.

Before ignition of the material, at the bottom of the plate, only the chemical shift at 157 ppm is present. It is known that condensation products of melamine exhibit chemical shifts around 156 and 164 ppm. Due to the fact

that the peak corresponding to MP is not shifted to these resonances it is concluded that melamine is present in its non-condensed form. Moreover a peak at 180 ppm corresponding to carbonyl structures (C=O) in carboxylic acids is observed. Peaks corresponding to CH, CH_2 and CH_3 are still present. At the top of the plate taken before ignition, the intensity of the peak corresponding to the methyl group of vinyl acetate decreases and additional peaks at 130 ppm (unsaturated hydrocarbons) and 180 ppm (carbonyl) are observed. These peaks indicate the presence of an oxidized, aromatic char. The spectrum of the bottom of the sample taken at the increase is equal to the one obtained before ignition (bottom). The top of the plate at this stage of the combustion process exhibits chemical shifts corresponding to CH_2-groups, unsaturated hydrocarbons (130 ppm) and 182.1 ppm corresponding to carbonyl functions. A peak at 167 ppm attributed to melamine [40] can be suspected whereas its intensity is very low. At the same time, this chemical shift can also be attributed to the carbonyl function present in the acetate group of the polymer.
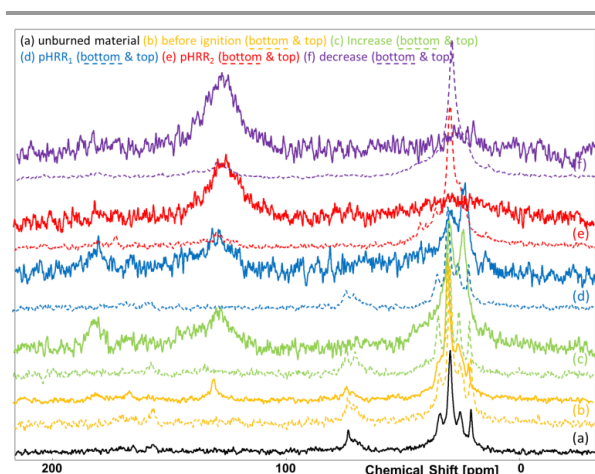

Fig 18: [13]C spectra obtained for different stages of combustion of EVM-ATH-MP

At pHRR$_1$, the spectrum of the bottom of the plate is similar to that obtained at the increase which indicates that the bulk material under the protective layer is protected until the pHRR$_1$. Peaks corresponding to methyl in the vinyl acetate group are still present. For the top of the plate taken at the pHRR$_1$, peaks corresponding to CH_2-groups (23.3 and 29.6 ppm), unsaturated hydrocarbons (130 ppm) and carbonyl functions (180 ppm) are observed.

Spectra of the bottom of the plate at the pHRR$_2$ consists of chemical shifts corresponding to CH_2-groups (29.8 ppm) and unsaturated hydrocarbon structures (130 ppm) as well as a chemical shift assigned to carbonyl functions (oxidation of the char) are obtained (180 ppm). The residues of the top of the plate taken at pHHR$_2$ only exhibit chemical shift at 130 ppm indicating the presence of unsaturated hydrocarbon structures (charring peak). The same is true for the spectrum taken of the top of the plate at the decrease. The bottom of the plate at the decrease shows the same peaks as the spectrum taken at the bottom of pHRR$_2$ whereas the peak corresponding to carbonyl is found at 181 ppm. Spectra of the residues left at the end of the experiment give no signal due to low content (or possible absence) of carbon atoms in the residues. Reduction of the resolution of the ^{13}C signal is due to increased anisotropy of paramagnetic susceptibility of carbon atoms present in the residue.

^{27}Al NMR spectra of the residues are presented in Fig. 19. The spectrum obtained for unburnt EVM-ATH-MP is similar to that obtained for unburnt EVM-ATH. The chemical shift at 7.9 ppm with a small shoulder at -2.0 ppm is attributed to octahedral coordinated Al^{3+} [34].
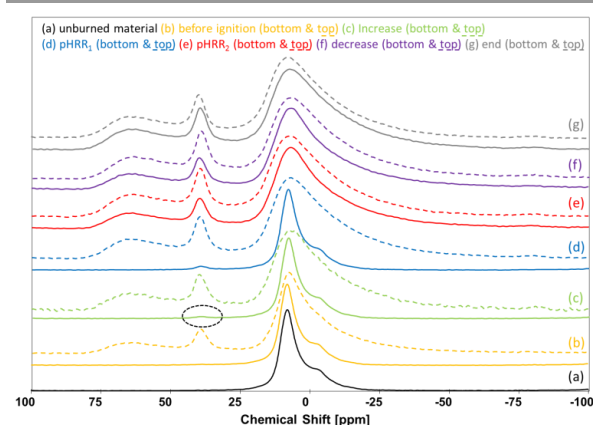

Fig 19: [27]Al spectra obtained for different stages of combustion of EVM-ATH-MP

At the top of the plate taken before the ignition a peak assigned to tetrahedral coordination of aluminium indicating the dehydration of ATH forming an aluminium oxide is detected (65 ppm). The underlying material (bottom of the plates) has the same spectra like unburnt EVM-ATH-MP until pHRR$_1$. Top of the plates always show chemical shifts corresponding to tetrahedral and octahedral coordinated aluminium. As for EVM-ATH, the peak corresponding to octahedral coordinated Al is getting broader with progressed combustion process. It is assumed that a char layer consisting of unsaturated hydrocarbons and aluminium oxide is formed protecting the material against heat. This indicates that decomposition of ATH is completed after pHRR$_1$. Hence the material is protected through endothermic dehydration of ATH and the resulting release of water until pHRR$_1$.

Moreover, an additional peak is observed at around 39.5 ppm assigned to aluminium phosphate (AlO_4), whereas Al^{3+} has a tetrahedral coordination (AlO_4) [41,42]. This peak is observed in all spectra of samples taken at the top of the plates. Concerning the bottom of the plates, $AlPO_4$ is observed for the first time at the increase.

It can be seen that phosphate present in MP coordinates with Al present in the condensed phase to form aluminium phosphate when melamine is evolved due to

decomposition of MP (corresponds to ^{13}C NMR results of EVM-ATH-MP). The peak assigned to aluminium phosphate is present in all residues taken at the top of samples for each step of the combustion process. Bourbigot et al. [33] showed that formation of orthophosphates in intumescent systems improves stability the protective layer. They proposed that formed char layer consisting of aromatic and aliphatic molecules is bridged by the phosphates leading to improved properties of the protective char layer. These results are in agreement with those found in this study. During MLC experiment, it was found that $pHRR_2$ is lower for EVM-ATH-MP than it is for EVM-ATH. It is therefore supposed that formation of aluminium phosphate during decomposition of EVM-ATH-MP leads to formation of a protective layer at the material surface exhibiting higher insulative properties. It is assumed that phosphates formed during decomposition of EVM-ATH-MP bridge the aromatic char system developed during combustion to form a more stable protective char layer. The formation of aluminium phosphate improving the efficiency of the char layer supports the assumption postulated in discussion of MLC-FTIR results. It was supposed that the gas flow at $pHRR_2$ is lower for EVM-ATH-MP due to formation of a more insulative protective layer.

The formation of aluminium phosphate is confirmed by analysis of the residues by ^{31}P NMR (Fig. 20). It can be seen that the peak corresponding to aluminium phosphate (-30 ppm) is observed in all samples taken at the bottom of the plate and in samples taken at the bottom from the increase to the end of the combustion. The unburnt material exhibits a peak at 1.3 ppm having a shoulder at -1 ppm corresponding to orthophosphate. The presence of these two peaks indicates different structures of the orthophosphates. The orthophosphate species have either one or two neighbour aluminium atoms . It can be seen that the chemical shift corresponding to orthophosphate changes a little bit before ignition of the material (bottom of the plate): the shoulder at -1 ppm is getting more important than the signal at 1.3 ppm. This change is explained through structure changes taking place due to decomposition of MP which is known to evolve melamine.
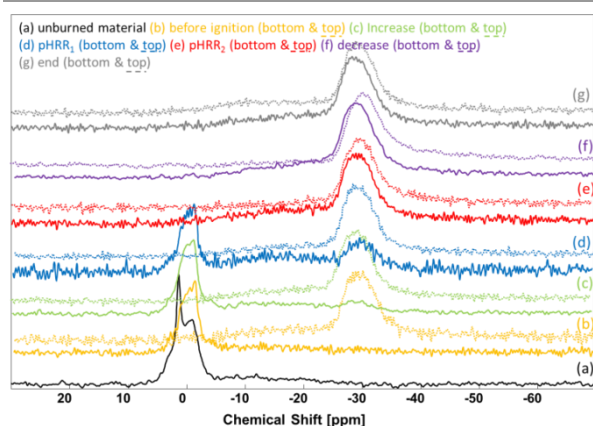

Fig 20: ^{31}P spectra obtained for different stages of combustion of EVM-ATH-MP

All together it can be said that the phosphate present in MP is degraded to $AlPO_4$ during decomposition. It is supposed that this compound has a role in the formation of a protective surface layer which protects the material against the attack of fire and improved properties of this layer.

Protection mechanism for the EVM-ATH and EVM-ATH-MP

It was found that EVM-ATH is protected through a gas phase and a condensed phase mechanism. In the condensed phase, ATH degrades forming alumina. Decomposition of the polymer results in formation of a protective layer. The developed layer protects the material against the attack of fire. At the same time, water coming from the dehydration of ATH dilutes the fuel and prevents early igniton reinforced by the endothermic dehydration of ATH. Concerning decomposition of the polymer, it was found that deacetylation of EVM evolving acetic acid takes place before ignition. Linear polyenes formed during deacetylation are degraded afterwards whereas the nature of released gases depends on the heating rate. Low heating rates lead to formation of linear saturated and mono unsaturated hydrocarbons whereas high heating rates lead to formation to benzene and its homologues and small linear unsaturated hydrocarbons (mono and di unsaturated). In the case of EVM-ATH-MP, ATH exhibits the same action in the gas phase and in the condensed phase as it was found for EVM-ATH. Analysis of the role of MP in the system showed that release of ammonia (from MP decomposition) leads to earlier ignition of the material. At the same time, phosphates remaining in the condensed phase after decomposition of MP form aluminum phosphates. The formed aluminum phosphates connected aliphatic and aromatic molecules which are present in the protective layer at the material surface. The protective layer of EVM-ATH-MP improves the barrier effect of the protective layer. Due to improved efficiency of the char layer, release of heat, decomposition gases and smoke in the second part of the combustion process is reduced in comparison to EVM-ATH.

Conclusions

Flame retardant properties and smoke release of EVM materials were investigated using ATH and MP as fire retardant additives. It was found that partial replacement of ATH by MP leads to earlier ignition of the material and reduction of $pHRR_2$. To understand the role of MP in the system both materials, i.e. EVM-ATH and EVM-ATH-MP were further analysed. It was found that all additives are well dispersed in the polymeric matrix. Decomposition mechanism of both materials was investigated. It was detected that both materials are

protected by a gas phase mechanism: decomposition of ATH evolves water diluting the fuel. At the same time ATH has a cooling effect due to its endothermic decomposition. Early ignition of EVM-ATH-MP was explained by presence of more flammable gases, i.e. ammonia, coming from decomposition of MP. It was also found that structure of released gases depend on the used heating ramp. Condensed phase mechanism was analysed for both materials: a physical barrier is formed during combustion protecting the material against external heat. The presence of MP leads formation of aluminium phosphate in the condensed phase improving stability and insulative properties of the char layer.

Acknowledgements

Notes and references

[a] R₂Fire group/UMET – UMR CNRS 8207, Ecole Nationale Supérieure de Chimie de Lille (ENSCL), University of Lille, 59652 Villeneuve d'Ascq, France

[b] LANXESS Deutschland GmbH, 50569 Köln, Germany

1. Overall Fire Death Rates and Relative Risk (2001-2010), http://www.usfa.fema.gov/statistics/estimates/trend_overall.shtm, 2013.

2. G. Camino, A. Maffezzoli, M. Braglia, L. M. De and M. Zammarano, *Polymer Degradadation and Stability*, 2001, **74**, 457-464.

3. X. Zhang, F. Guo, J. Chen, G. Wang and H. Liu, *Polymer Degradation and Stability*, 2005, **87**, 411-418.

4. A. A. Basfar and H. J. Bae, *Journal of Fire Sciences*, 2010, **28**, 161-180.

5. C. Jiao, Z. Wang, X. Chen, B. Yu and Y. Hu, *Radiation Physics and Chemistry*, 2006, **75**, 557-563.

6. A. Riva, G. Camino, L. Fomperie and P. Amigouët, *Polymer Degradation and Stability*, 2003, **82**, 341-346.

7. L. Du, B. Qu and Z. Xu, *Polymer Degradation and Stability*, 2006, **91**, 995-1001.

8. J. Zilberman, T. R. Hull, D. Price, G. J. Milnes and F. Keen, *Fire and Materials*, 2000, **24**, 159-164.

9. M. Fu and B. Qu, *Polymer Degradation and Stability*, 2004, **85**, 633-639.

10. L. Ye, Y. Miao, H. Yan, Z. Li, Y. Zhou, J. Liu and H. Liu, *Polymer Degradation and Stability*, 2013, **98**, 868-874.

11. L. Clerc, L. Ferry, E. Leroy and J.-M. Lopez-Cuesta, *Polymer Degradation and Stability*, 2005, **88**, 504-511.

12. F. Laoutid, P. Gaudon, J. M. Taulemesse, J. M. Lopez Cuesta, J. I. Velasco and A. Piechaczyk, *Polymer Degradation and Stability*, 2006, **91**, 3074-3082.

13. A. Szép, A. Szabó, N. Tóth, P. Anna and G. Marosi, *Polymer Degradation and Stability*, 2006, **91**, 593-599.

14. A. Ahamad, C. B. Patil, P. P. Mahulikar, D. G. Hundiwale and V. V. Gite, *Journal of Elastomers and Plastics*, 2012, **44**, 251-261

15. Y.-Y. Yen, H.-T. Wang and W.-J. Guo, *Polymer Degradation and Stability*, 2012, **97**, 863-869.

16. L. Ye, Q. Wu and B. Qu, *Polymer Degradation and Stability*, 2009, **94**, 751-756.

17. O. Cérin, S. Duquesne, G. Fontaine, A. Roos and S. Bourbigot, *Polymer Degradation and Stability*, 2011, **96**, 1812-1820.

18. O. Cérin, University of Lille 1 - Sciences and Technologies, France, 2010.

19. W. Xing, L. Song, H. Lu, Y. Hu and S. Zhou, *Polymers for Advanced Technologies*, 2009, **20**, 696-702.

20. Z. Wang, P. Lv, Y. Hu and K. Hu, *Journal of Analytical and Applied Pyrolysis*, 2009, **86**, 207-214.

21. S. Zhou, Z. Wang, Z. Gui and Y. Hu, *Fire and Materials*, 2008, **32**, 307-319.

22. L. Costa, G. Camino and d. C. M. P. Luda, *ACS Symp. Ser.*, 1990, **425**, 211-238.

23. A. Witkowski, A. A. Stec and T. Richard Hull, *Polymer Degradation and Stability*, 2012, **97**, 2231-2240.

24. F. E. Ngohang, G. Fontaine, L. Gay and S. Bourbigot, *Polymer Degradation and Stability*, 2014, **in press**.

25. J. F. Grcar, P. Glarborg, J. B. Bell, M. S. Day, A. Loren and A. D. Jensen, *Proceedings of the Combustion Institute*, 2005, **30**, 1193-1200.

26. J. L. MacDonald, U. Werner-Zwanziger, B. Chen, J. W. Zwanziger and D. Forgeron, *Solid State Nuclear Magnetic Resonance.*, 2011, **40**, 78-83.

27. G. C. Stael and M. I. B. Tavares, *Polymer Testing*, 1997, **16**, 193-198.

28. N. Pécoul, S. Bourbigot and B. Revel, *Macromolecular Symposia*, 1997, **119**, 309-315.

29. J. Rottstegge, M. Arnold, L. Herschke, G. Glasser, M. Wilhelm, H. W. Spiess and W. D. Hergeth, *Cem. Concr. Res.*, 2005, **35**, 2233-2243.

30. C. M. G. de Souza and M. I. B. Tavares, *Polym. Test.*, 1998, **17**, 533-541.

31. F. Carpentier, S. Bourbigot, M. Le Bras, R. Delobel and M. Foulon, *Polymer Degradation and Stability.*, 2000, 69, 83-92.

32. M. Delfini, A. L. Segre and F. Conti, *Macromolecules*, 1973, **6**, 456-459.

33. S. Bourbigot, M. L. Bras and R. Delobel, *Carbon*, 1993, **31**, 1219-1230.

34. J. Sanz and J. M. Serratosa, *Clay Minerals*, 1984, **19**, 113-115.

35. R. C. T. Slade, J. C. Southern and I. M. Thompson, *Journal of Materials Chemistry*, 1991, **1**, 563-568.

36. V. J. Ingram-Jones, R. C. T. Slade, T. W. Davies, J. C. Southern and S. Salvador, *Journal of Materials Chemistry*, 1996, **6**, 73-79.

37. D. Massiot, Dmfit, 2011.

38. S. Bourbigot, M. L. Bras, R. Leeuwendal, K. K. Shen and D. Schubert, *Polymer Degradation and Stability*, 1999, **64**, 419-425.

39. S. Jahromi, W. Gabriëlse and A. Braam, *Polymer*, 2003, **44**, 25-37.

40. P. Ducrocq, S. Duquesne, S. Magnet, S. Bourbigot and R. Delobel, *Progress in Organic Coatings*, 2006, 57, 430-438.

41. R. J. Kirkpatrick and R. K. Brow, *Solid State Nuclear Magnetic Resonance*, 1995, **5**, 9-21.

42. J. Quartararo, M. Guelton, M. Rigole, J.-P. Amoureux, C. Fernandez and J. Grimblot, *Journal of Materials Chemistry*, 1999, **9**, 2637-2646.

Flame retardancy of EVM-based polymers with low smoke emission

Summary:

This work deals with new elastomeric ethylene-vinyl acetate (EVM) materials containing aluminum trihydroxide (ATH) in combination with melamine or its derivatives are evaluated regarding mechanical properties, hydrothermal aging, fire retardancy and smoke release. The decomposition mechanism of EVM containing ATH and melamine borate (MB) (EVM-ATH-MB) is analyzed in details because of its high stability during hydrothermal aging and its low smoke release. Decomposition reactions EVM-ATH-MB are studies using amongst others new approaches such as pyrolysis-gas chromatography-mass spectrometry (py-GCMS) and mass loss calorimeter coupled with Fourier transform infra-red (MLC-FTIR). It is found that EVM-ATH-MB is mainly protected by the mode of action of ATH diluting the fuel and forming a protective layer that reduces mass and heat transfer.

Keywords: flame retardancy, ethylene vinyl acetate, elastomer, aluminum trihydroxide, melamine borate

Procédé de polymères EVM ignifugés à faible émission de fumées

Résumé:

Cette étude est dédiée aux matériaux élastomères à base d'éthylène acétate de vinyle (EVM) ignifugés à l'aide de trihydroxide d'aluminium (ATH) et de mélamine ou de ses dérivés. Les différents types de formulations sont testés concernant leurs propriétés mécaniques, vieillissement, ignifugation et libération de fumée. La combinaison d'ATH et borate de mélamine dans l'EVM (EVM-ATH-MB) présente une plus faible libération de fumées et une meilleure stabilité pendant les tests vieillissement. En conséquence les mécanismes de la décomposition sont étudiées en utilisant entre autres des nouvelles approches comme le pyrolyzeur chromatographie en phase gazeuse couplée à la spectrométrie de masse (py-GCMS) et calorimètre à cône couplé à la spectroscopie infrarouge à transformée de Fourier (MLC-FTIR). L'effet de refroidissement ainsi que la formation d'une couche protectrice à la surface protège le matériau principalement.

Mots clés :   ignifugation, éthylène-acétate de vinyle, élastomère, hydroxyde d'aluminium, borate de mélamine